Radiolabelled *Bacillus anthracis* toxin-based probes for molecular imaging of MMP activity in tumour models

Mary-Ann Elvina Xavier

Hertford College

Michaelmas 2018

Abstract

Radiolabelled *Bacillus anthracis* toxin-based probes for molecular imaging of MMP activity in tumour models

Thesis submitted as partial fulfilment for the degree of Doctor of Philosophy
Mary-Ann Elvina Xavier, Hertford College
Michaelmas 2018

Increased activity of matrix metalloproteinases (MMPs) is associated with poor prognosis and metastasis in different cancer types. To exploit this feature and target cancer cells, the protective antigen (PAWT) of the binary anthrax lethal toxin (LT) was modified to form pores in cell membranes only when cleaved by MMPs (PAL1). Anthrax lethal factor (LF) is then able to translocate through these pores into the cytosol of tumour cells. The aim of this work was to develop a novel non-invasive imaging agent for the detection of matrix metalloproteinase (MMP) activity based on engineered variants of LT. Here, ^{111}In-radiolabelled form of LF was used with the PAL1/LF system to allow non-invasive in vivo imaging and quantification of MMP activity in tumour tissue by SPECT.

Initially, PAL1 MMP-activation was tested in a cell free assay. Subsequently, the activation of PAL1 was evaluated by a cytotoxic assay in a range of cancer cell lines, with or without a broad spectrum MMP inhibitor. MMP2 and MMP9 activity in the different cancer cells was assessed by gelatin zymography. Expression levels of MMP14, and LT native receptors (TEM8 and CMG2) were evaluated by western blot analysis. LT components were radiolabelled with ^{111}In. Cell abundance of TEM8 and CMG2 was determined by saturation binding assays using ^{111}In-radiolabelled PAWT. After ^{111}In-radiolabelling non-toxic variants of LF, their cell uptake was evaluated in the presence or not of PAL1. Evaluation of the in vivo pharmacokinetics and biodistribution of ^{111}In-radiolabelled LT components was performed by SPECT/CT in naive mice or MMP-expressing MDA-MB-231 tumour-bearing mice.

PAL1 MMP-cleavage was confirmed in a cell free assay. Notably, PAL1 capacity to cause cytotoxicity in a panel of cancer cells correlated with anthrax toxin receptor and MMP14 expression. Additionally, in the presence of MMP inhibitors PAL1 mediated cytotoxicity was prevented. Selective delivery of ^{111}In-radiolabelled LF variants to MMP-expressing cells by PAL1 was demonstrated in vitro, and corroborated using confocal microscopy with fluorescently labelled variants of LF. Dynamic SPECT imaging demonstrated superior and

selective uptake of radiolabelled PAL1 in tumour tissue when compared to radiolabelled PAWT. Finally, a radiolabelled LF variant was selectively delivered to MMP-positive MDA-MB-231 tumour bearing mice by PAL1, presenting excellent target-to-background contrast.

Taken together, these results indicate that radiolabelled forms of mutated anthrax lethal toxin hold promise for non-invasive imaging of MMP activity in tumour tissue.

Acknowledgements

I would like to thank my supervisor, Professor Bart Cornelissen, for his continuous support, patience and guidance. I am and will remain grateful to him for giving me the unique opportunity to study for a DPhil in Oncology at Oxford University, and for everything he has done for me. I also would like to thank Professor Nicola Sibson for her invaluable support, during the first years of my DPhil study.

Special thanks goes to Dr Stephen Leppla for his constant help and support. A truly great person to make a collaboration with, he was always available to help, discuss and support this project. I thank Dr Shihui Liu, Dr Thomas Bugge and Dr Mahtab Moayeri for the helpful scientific discussion and input to this project. I also want to give a special thanks to Dr Rasem Fattah and Dr Kuang-Hua Chen for making this project possible.

A big thanks goes to my country for funding my scholarship. I would like to thank Professor Paulo Cesar de Morais and Dr Marcella Lemos Brettas for supporting me to pursue my dreams in Science. A special thanks goes to my Professor Zulmira Lacava that even though far, has always given me her friendship and support.

I want to thank all my colleagues in the RRI for making such a great environment to study. Thanks Ms Mio Shimazaki, Ms Anne-Marie Honeyman-Tafa, Dr Caroline Fitchett, Dr Katie Morrison, Dr Graham Brown, Dr Rhodri Wilson, Mr Mick Woodcock, Ms Penny Berry, Mr Andrew Mortimer, Dr Danny Allen, Dr Sean Smart, Ms Isabel Apolinario, Mr Euridice Apolinario and Ms Jiaqi Wu. A special thanks for Ms Karla Watson, Ms Magdalena Hutchins, Dr Sally Hill, Dr Ana-Gil Bernardes, Dr Veerle Kersemans, and Ms Sheena Wallington. I thank specially to the countless hours of discussions and the good time we spent together to Dr Zenobia D'costa, Ms Luisa Contreras Bravo, Ms Gleiskelen de Camargo, Dr Luiza Helana Maria Lourenco, Ms Irini Skaripa, Ms Sarah Able, Dr Martin Gil, Dr Nagma Khan, Dr Bas Bavelaar, Mr Javian Malcon, Dr Nadia Falzone, Ms Christina Simoglou Karali, Dr Vinton Cheng and my friend Dr Abul Azad.

Thanks to my lab group members for all their invaluable support, especially Dr Sofia Koustoulidou, the best desk-mate ever, Mr Mathew Veal, Dr Gemma Dias and Dr James Knight. A special thanks to Dr Julia Torres, Mr Michael Mosley and Dr Samantha Hopkins for their continuous support, patience and guidance during my DPhil study.

Special thanks go for Ms Jannet Penrose for welcoming me in her house in Oxford. And I would like to thanks my friend Ms Dhivina Gagoomal for always being there for me.

I want to thank my family, especially my parents, which even though far way, they have always been very close to me in spirit, supporting with their prayers and love. Last but not least I would like to thank to my husband, Joshua Owen, for his encouragement and unconditional love during the last years of my study. Obrigada Thuco.

Table of Content

List of Figures

List of Tables

Index List

A

ACPP: Activatable cell penetrating peptide

ADP: Adenosine diphosphate

AF488: Alexa Fluor 488

AMP: Adenosine monophosphate

ANOVA: Analysis of variance

ANTXR1: Anthrax toxin receptor 1

ANTXR2: Anthrax toxin receptor 2

AR: Autoradiography

ATP: Adenosine triphosphate

B

BCA: Bicinchoninic acid assay

B_{MAX}: receptor total density

BRAF: v-raf mitogen-activated protein kinase kinase

Brij-35: Dodecan-1-ol, ethoxylated

C

$CaCl_2$: Calcium Chloride

cAMP: cyclic AMP

CD44: cluster of differentiation 44

CD63: cluster of differentiation 63

CMG2: capillary morphogenesis gene 2

CO_2: Carbon dioxide

CPM: Counts per minute

CT: Computed tomography

Cy: Cyanine

D

Da: Dalton

DAPI: 4',6-diamidino-2-phenylindole

dH_2O: deionised H2O

DMEM: Dulbecco's Modified Eagle Medium

DMSO: Dimethyl sulfoxide

DNA: Deoxyribonucleic acid

DPX: Distyrene, plasticiser, and xylene

DTPA: diethylenetriamine pentaacetate

E

EC50: Half maximal effective concentration

E-cadherin: Calcium dependent adhesion molecule

ECM: Extracellular matrix

EDTA: Ethylenediaminetetraacetic acid

eEF2: eukaryotic Elongation factor 2

EF: Edema Factor

EGFR: Epidermal growth factor receptors

EMT: Epithelial-to-mesenchymal transition

EPR: Enhanced permeability retention

ERK: Extracellular signal regulated kinase

ET: Edema Toxin

F

FBS: Fetal Bovine Serum

FP59: fusion toxin

FRET: Forster Resonance Energy Transfer

G

^{68}Ga: Gallium-68

GAPO: growth retardation, alopecia, pseudoanodontia and progressive optic atrophy

GM6001: (R)-N'-Hydroxy-N-[(S)-2-indol-3-yl-1-(methylcarbamoyl)ethyl]-2-isobutylsuccinamide

H

H&E: haematoxylin and eosin

H/L: heavy and light chain

H_2O: dihydrogen monoxide

HEPES: 4-(2-hydroxyethyl)-1-piperazineethanesulfonic acid

HRP: Horseradish peroxidase

I

ICAM-1: Intercellular adhesion molecule-1

IgG: Immunoglobulin G

^{111}In: Indium-111

$^{111}In^{3+}$: ^{111}In ion

$^{111}InCl^{3}$: ^{111}In Chloride

^{123}I: Iodine-123

^{125}I: Iodine-125

IONPs: Iron oxide nanoparticles

iTLC: instant thin layer chromatography

J

JACoP: Just another Colocalisation plugin

JNK: c-Jun N-terminal kinase

K

K_D: Dissociation constant

KPC: LSL-Kras$^{G12D/+}$, LSL-Trp53$^{R172H/+}$, Pdx-1-Cre

L

LC-MS: Liquid chromatography-Mass Spectroscopy

LF: Lethal factor

LF^{E687A}: LF variant with a defective catalytic domain with a valine substitution

LFn: N-terminal truncated LF

LT: Lethal toxin

LTBP-1: Latent TGF-β binding protein 1

^{177}Lu: Lutetium-177

M

MAPK: Mitogen-Activated protein kinase

MEK: MAPK/ERK kinase

MES: 2-(N-morpholino)ethanesulfonic acid

$MgCl_2$: Magnesium Chloride

miRNA: Micro RNA

MMP: matrix metalloproteinase

MRI: Magnetic Resonance Imaging

mRNA: Messenger RNA

MTT: (3-(4, 5-dimethylthiazol-2-yl)-2,5-diphenyltetrazolium bromide)

MT-MMP: transmembrane MMP

MW: Molecular Weight

N

NaCl: Sodium Chloride

NaOH: Sodium hydroxide

NHS: succinimidyl ester

NIR: Near-infrared

P

PA: Protective antigen

PA_{20}: 20 kDa N-terminal PA fragment

PA_{63}: 63 kDa C-terminal PA fragment

PA_{83}: PA full-length

PAGL9: PA variant MMP14-cleavable

PAHL9: PA variant MMP14-cleavable

PAL1: PA variant MMP-cleavable

$PAL1_{20}$: 20 kDa N-terminal PAL1 fragment

$PAL1_{63}$: 63 kDa C-terminal PAL1 fragment

$PAL1_{83}$: PAL1 full-length

PANL12: PA variant MMP14-cleavable

PANL8: PA variant MMP14-cleavable

PASSSR: PA variant uncleavable

PAU7: PA variant uncleavable

$PAU7_{83}$: PAU7 full-length

PAWT: PA wild type furin-cleavable

$PAWT^{K563C}$: PA variant with a cysteine substitution

PBS: Phosphate-buffered saline

PCA: Proteinase-modulated contrast agent

PEG: polyethylene glycol

PET: Positron Emission Tomography

pH: power of hydrogen

Pro-MMP14: proform MMP14

Pro-MMP2: proform MMP2

p-SCN-Bn-DTPA: isothiocyanatobenzyl-DTPA

R

RCP: Radiochemical purity

RCY: Radiochemical yield

R*f*: Retention fraction

RIPA: Radioimmunoprecipitation assay

RNA: Ribonucleic acid

rpm: rotations per minute

RTK: Receptor tyrosine kinases

S

scFv: single chain variable fragment

SCID: Severe combined immunodeficiency

SDS: sodium dodecyl sulphate

SDS-PAGE: SDS polyacrylamide gel electrophoresis

S*f*: Solvent front

SIP: Small immuno protein

S*p*: Starting point

SPECT: Single Photon Emission Computed Tomography

Src: Sarcoma

T

TAC: Time activity curve

TBS: Tris-buffered saline

^{99m}Tc: Technetium-99m (metastable)

TEM8: tumour endothelial marker 8

TGF-β: transforming growth factor-β

THP: triple helical peptide

3D: three dimensional

TIMP: Tissue Inhibitor of MMP

TMR: tetramethylrhodamine

Tris: 2-Amino-2(hydroxymethyl)propane-1,3-diol

V

V: Volume

VEGF: Vascular endothelial growth factor

VOI: Volume of interest

vWA: von Willebrand A

W

Wnt: wingless-type mouse mammary tumour virus integration site

Z

ZBG: Zinc binding group

$ZnSO_4$: Zinc Sulphate

^{89}Zr: Zirconium-89

Zn^{2+}: Zinc ion

Chapter 1

1. Chapter 1: Introduction

1.1. Opportunities and challenges

In this thesis, a modified version of anthrax toxin was used to image matrix metalloproteinase (MMP) activity in tumour models using molecular imaging. At first, the characteristics of MMPs that make them attractive imaging targets in cancer, as well as the challenges to the development of an MMP imaging agent are described. Subsequently, the most relevant imaging agents developed for molecular imaging of MMPs in cancer are examined. Then, a detailed description of the *Bacillus anthracis* lethal toxin system is given. Finally, the therapeutic effect of engineered variants of the toxin that target MMP activity is discussed.

1.2. Characteristics and classification of the MMP family

The matrixins or matrix metalloproteinases (MMPs) is a family of proteases that is part of the larger metzincin superfamily, characterised by the presence of a zinc ion (Zn^{2+}) protease binding motif [1]. The MMP family comprises 23 MMP proteins. The defining activity of these enzymes, also known as peptidases, is the hydrolysis of peptide bonds within proteins and peptides. All MMPs present a latent form called zymogen, can be inhibited by a tissue inhibitor of MMP (TIMP), and have an ability to hydrolyse components of the extracellular matrix (ECM) [2]. Therefore, the main physiological roles of MMPs are linked to matrix remodelling processes such as, wound healing, tissue development and inflammation [1].

MMPs are present in multicellular eukaryotes and may have evolved from a single-domain protein to the multidomain architecture observed in the MMPs expressed in humans. The most simple version of an MMP contains (1) a signal sequence, that direct them to the secretory pathway, followed by the propeptide domain containing a conserved cysteine

which interacts with, and inactivates the catalytic domain of the zymogen [3]. The MMP prototype built also contains a hinge region, followed by a hemopexin-like domain that is involved in substrate recognition and protein-protein interactions [4, 5]. Only MMP 2 and 9 present a gelatin-binding domain (fibronectin type II motif) within their catalytic region, which plays a role in substrate recognition [6] (see Figure 1.1).

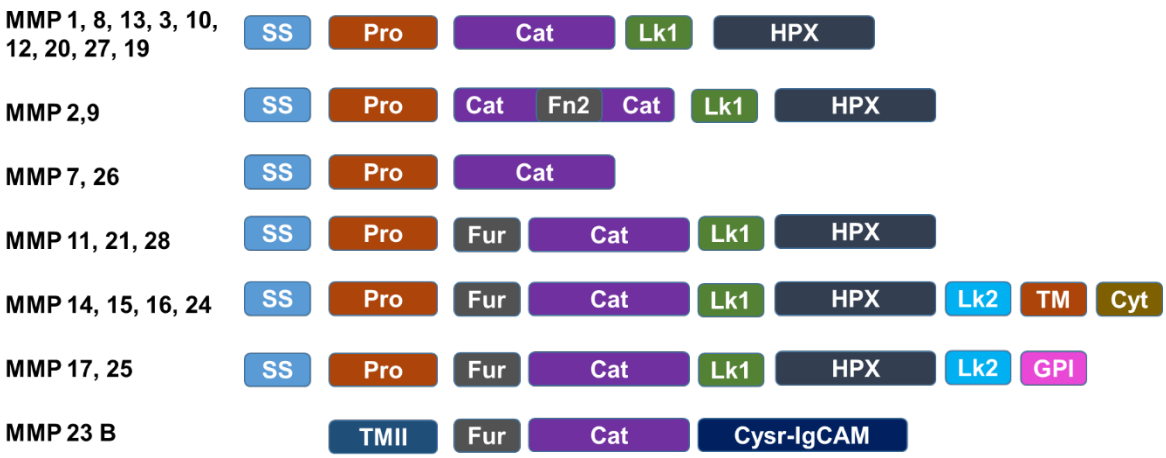

Figure 1.1 Domain composition of human MMPs.
Abbreviation: SS, signal sequence; Pro, propeptide; Fur, furin cleavage site; Cat, catalytic domain; Fn2, fibronectin type II motif; Lk1, Linker domain type I; HPX, hemopexin-like domain; Lk2, linker domain type 2; TM, transmembrane domain type II, GPI, glycosylphosphatidylinositol anchor; Cyt, cytoplasmic domain; Cysr-IgCAM, cysteine rich and Ig-like domain cell adhesion domain (based references [1, 7])

Six members of the MMP family have a unique capacity to anchor to the plasma membrane instead of being secreted extracellularly. The structural difference of these MMPs is either an additional transmembrane domain or a glycosylphosphatidylinositol (GPI) modification on the C-terminal of the hemopexin domain [8]. In addition to this architectural feature these transmembrane MMPs (MT-MMPs) also present a cytoplasmic tail that governors their internalisation and turnover of these enzymes on the cell surface [9]. These anchored MMPs, together with four secreted MMPs (11, 21, 28 and 23B), present a furin recognition sequence between the propeptide and the catalytic domains (see Figure 1.1).

MMP 23B is the most atypical MMP. Its N-terminal contains a type-II transmembrane domain followed by a furin recognition sequence, and a cysteine-rich IgG-like cell adhesion domain (see Figure 1.1). Given the lack of a signal-sequence and a propeptide domain, the type-II transmembrane domain acts as both, hence both activation and secretion of this MMP happen simultaneously when cleaved [7, 10].

Based on their domain organisation and substrate preference [11], MMPs can be grouped into 6 categories: collagenases (MMP1, MMP8, MMP13), gelatinases (MMP2 and MMP9), stromelysins (MMP3 and MMP10), matrilysins (MMP 7 and MMP 26), MT-MMPs which can be membrane anchored (MMP14/ MT1-MMP, MMP15/ MT2-MMP, MMP16/ MT3-MMP and MMP24 / MT5-MMP) or GPI anchored proteins (MMP17/ MT4-MMP and MMP 25/ MT6-MMP), and others grouping, the 8 remaining MMPs (MMP11, MMP12, MMP19, MMP20, MMP21, MMP 23 B, MMP27 and MMP28) [1].

Notably, due to their broad overlap in substrate recognition, MMPs cannot be classified effectively according to their substrate preference. Unsurprisingly, MMPs cleave various substrates with similar catalytic efficiency due to the high degree of homology in their catalytic domains. An alternative way of classifying MMPs is based on phylogenetic relationships, which affords a more general insight on the properties of MMP family members. Bioinformatics alignment of the primary catalytic domain sequences showed that MMPs can be grouped in four major phylogenetic branches: (1) transmembrane, (2) GPI-anchored, (3) gelatinase and (4) non-furin regulated MMPs [11-13]. Studies correlating MMP cleavage patterns in a synthetic peptide library, demonstrated that the differences in MMP substrate preference mirror the sequence phylogeny classification [12, 14].

1.3. Substrate recognition by MMPs

Several attempts have been made over the past decade to systematically determine cleavage motif preferences for individual MMPs. This understanding is fundamental for the design of specific MMP activity assays, the development of small molecule inhibitors, prodrugs, imaging agents and the prediction of yet unknown physiological substrates. Studies using methodologies such as a series of synthetic peptides [15, 16], substrate phage display libraries [17-20], and protease-generated peptide libraries [21, 22] were performed to elucidate the preferential sequence surrounding the scissile bond in MMP substrates. At least some of this emerging information has been compiled in databases such as MEROPS [23], the Human Protein Reference Database [24], and UniProt [25].

Similar to other proteases, MMPs substrate specificity is guided by positional preferences of the residues on both N-terminal and C-terminal from the scissile bond here represented as (↓). The substrate of MMPs contain a canonical P-X-X-↓L motif [15]. Depending on the nature of the other amino acids, the resulting sequence can be cleaved by all MMPs or show a preference for some individual MMPs or groups. This high level of substrate cleavage redundancy explains the functional overlap observed among members of the MMP family. In fact, the majority of MMP-knockout mouse models, with exception of MMP14 and MMP20 [26], only present a mild phenotype, indicating the existence of proteolytic redundancy and enzymatic compensation [27, 28].

The development of proteomics and bioinformatics fields demonstrated that certain residue positions contribute to substrate recognition and specificity more than others [29]. Nevertheless, there are still many difficulties in studying MMPs substrate preference. It was demonstrated that MMP substrates that were designed as linear single-strand peptides, such as those used in the majority of peptide libraries, do not translate to the three-dimensional

context of protein substrate structure. Neither do these libraries consider any substrate recognition sites outside of the MMP catalytic domain (also known as exosites) [30, 31]. Additionally, none of the libraries evaluate the impact of residues which are beyond the substrate with 10-mer around the scissile bond. It is known that collagen, a normal substrate of MMPs, interacts with subsites outside this range of the scissile bond. These limitations can prevent the prediction of MMPs physiological substrates. Altogether, the design of substrate sequences that are specifically targeted by MMP activity is still a challenge.

1.4. Regulation of MMP activity

MMPs can degrade virtually all components of the ECM and cleave proteins related to cell growth, proliferation, and inflammation [32]. Hence, MMPs play a central role as regulators of homeostasis, presenting a low basal expression in physiological conditions. Uncontrolled MMP activity has the potential to result in pathological effects and diseases. Therefore, complex mechanisms are in place to tightly control MMP proteolytic activity via (1) gene expression, (2) pro-domain removal and activation, (3) endogenous inhibition, and (4) localisation in cell compartments.

Transcription of MMP genes is mainly constitutive, except for when matrix remodelling events occur, such as ovulation, wound healing, and organ development. Growth factors, cytokines, hormones, hyperglycemia, oxidized low-density lipoprotein, bio-products of ECM, and prostaglandins can all modulate MMP transcriptional activation [32-34]. The majority of MMP promoters are similar, and share several cis-elements which can be co-regulated or co-supressed by its trans-activators [35]. Stabilising factors such as the multifunctional cytokine transforming growth factor-β (TGF-β) prolongs MMP9 mRNA half-life in the cytoplasm and thus promotes protein expression. Recently, other post-

transcriptional events based on miRNA and epigenetic modifications have been described as modulators of MMP gene expression [34].

Following gene transcription, all MMPs are translated as inactive precursors called zymogens or pro-MMPs. To become active, MMP zymogens have their prodomain removed, either proteolytically or by a specific chemical modification. MMP members with a furin domain can be activated intracellularly within the trans-Golgi network before being secreted in the pericellular environment [36]. In the extracellular environment, proteolytic activation of MMPs is regulated by various classes of enzymes, including, plasmin or other MMPs. Interestingly, once activated, MMPs themselves can degrade plasminogen, modulating conversion to active plasmin, which can in turn activate more MMPs. A well-described example of cooperative activation of MMP is that of pro-MMP2, which forms a complex with TIMP2 and MMP14 on the cell surface, allowing removal of its prodomain by a second active MMP14 molecule [37].

Even after activation, MMP proteolysis can still be halted by interaction with their natural physiological inhibitor TIMPs, or the pan anti-proteinase α2-macroglobulin. There are four different TIMP molecules (TIMP1, 2, 3 4), which are secreted by different cells and act as broad spectrum inhibitors, chelating the zinc ion from the MMP catalytic site through their N-terminal domain [38]. TIMPs also possess non-inhibitory functions. For example, in the context of wound-healing, TIMP1 interaction with CD63 membrane protein present in endothelial cells results in protection against apoptosis signalling in this cytokine-rich environment [39]. In the blood stream, α2-macroglobulin is able to interact with MMPs, resulting in a complex that can be scavenged by specific cell receptors present in the liver [40].

One way of evading these natural inhibitors and thereby increasing MMP activity is by interacting with specific cell surface proteins [1]. This can potentiate MMP activity by increasing the local concentration in a specific microdomain of the plasma membrane, by protecting MMPs from their inhibitors or proteolysis [41]. For instance, the binding of MMP2 to $\alpha_v\beta_3$ integrin via their hemopexin-like domain is essential to allow cell invasion activity [42, 43]. MMP9 docking with $\alpha_4\beta_1$-integrin, observed in chronic B-cell lymphocytic leukaemia, is associated with localisation of proteolytically active MMP9 and malignant cell invasion [44, 45]. In addition to all aforementioned regulatory mechanisms, an increasing amount of evidence suggests that the degradation products of ECM can also result in peptides able to promote or inhibit MMP activity, serving as positive or negative feedback signalling mechanisms [32]. It is therefore clear that multilevel regulation of MMPs is essential for tissue homeostasis. The full extent of this is yet to be elucidated.

1.5. Physiological roles of MMPs

The development of MMP knockout mice allowed the identification of some of its substrates in vivo, and a better understanding of the role of these enzymes in physiological processes. At present, 19 MMP knockout models have been generated, with an overall benign phenotype. The main phenotypical changes are observed after challenging stimuli, such as bone fracture, wound promotion or tumour implantation [28, 46-49]. The experiments performed with these models allowed the establishment of a direct relationship between MMP activity and different physiological processes mentioned bellow.

Certain MMP knockout mouse models show a phenotype related with the same process demonstrating that several MMPs are required for certain biological events to happen. Conversely, knockout of one MMP can lead to an impact on different physiological processes. This is well exemplified in the case of bone formation defects observed in MMP9

and 13 knockout mice. In both cases, bone development is hindered to a small degree causing long bone shortening, while the double knockout leads to a severe bone shortening. The results suggest that MMP9 and 13 cooperate in collagen cleavage within the ECM of long bones, which is essential for correct development [50]. In addition, MMP9-null mice show modifications in innate and adaptive immune responses, since this enzyme participates in immune cell recruitment showing pro and anti-inflammatory effects [51, 52].

MMP2 and 14 activity is also relevant for bone growth and modelling, yet the knockout models present phenotypes distinct from the ones described above. MMP14 gene ablation resulted in a remarkably severe spontaneous phenotype with skeletal deformations including craniofacial dysmorphia, dwarfism and fibrosis on the soft tissues, as well as development of vasculature defects. This highlights the central role of MMP14 in collagen turn over [53], and its contribution to vessel sprouting through degradation of type I collagen and release of proangiogenic factors [54, 55]. On the other hand, MMP2 gene ablation has been found to result in reduced angiogenesis and in skull deformations [56, 57]. The double knockout for MMP2 and MMP14 presents an additive effect compared to the single knockout models, suggesting functional overlap in mice between the two MMPs with distinct molecular natures [58].

In summary, dysregulation of MMP activity leads to unwanted activity, and a variety of disorders. In particular MMP2 and MMP9 and membrane-anchored MMP14 have been implicated heavily in tumorigenesis, and as such have been proposed as therapeutic targets and as potential biomarkers linked to cancer aggressiveness and progression [59]. Apart from their role in cancer, MMPs are also implicated in cardiovascular conditions and neurodegenerative disorders, such as Alzheimer's disease, Parkinson's disease and autoimmune disorders [60], as well as several pulmonary and oral pathologies. In the next section, the diverse roles of MMPs in cancer progression and metastasis will be discussed.

1.6. MMPs and tumour progression

Elevated MMP expression is frequently associated with poor prognosis for cancer patients [61]. The human protein atlas data base report that over expression of MMP14 and MMP9 is classified as unfavourable prognostic markers for renal, hepatic and ovarian cancer [62, 63]. Mouse gene knockout models confirmed that MMPs are involved in tumorigenesis, corroborating initial studies dating from the early 1980s [56, 64, 65]. Interestingly, MMPs can promote tumour progression but they can also have a tumour-suppressor role for MMP3, 8, 9, 11, 12 and 19 (see review [66]). At first, the involvement of MMPs in tumour progression was attributed only to their capacity to cleave ECM, removing and remodelling it to allow cell invasion and tumour expansion. However, mounting evidence showed that MMPs act through a broader range of substrates, involved in multiple signalling pathways, thus modulating the tumour biology in a complex manner that is yet to be fully elucidated.

In cancer, signalling pathways controlling fundamental cellular processes such as growth, proliferation, differentiation, migration and apoptosis are dysregulated. Mitogen-activated protein kinase (MAPK) pathways are evolutionarily conserved kinase modules. Extracellular stimuli can interact with receptor tyrosine kinase (RTK) and activate the MAPK signalling pathway, modulating the machinery that controls these important cellular processes.

Epidermal growth factor receptor (EGFR) is a RTK, who activation by ligand binding (e.g. epidermal growth factor, epiregulin, transforming growth factor-α) contributes to cancer cell proliferation, invasion, and metastasis. EGFR activation and signalling are leading causes of malignancy in many types of cancer such as breast, lung, metastatic colorectal, head and neck, ovarian, and brain cancers. Activation of EGFR in tumour cells results in upregulation of MMP2, MMP9 and MMP14 [67]. Moreover, non-tumour cells associated to the tumour

microenvironment, additionally to infiltrating leukocytes are also stimulated to produce these MMPs (see Figure 1.2) [68, 69].

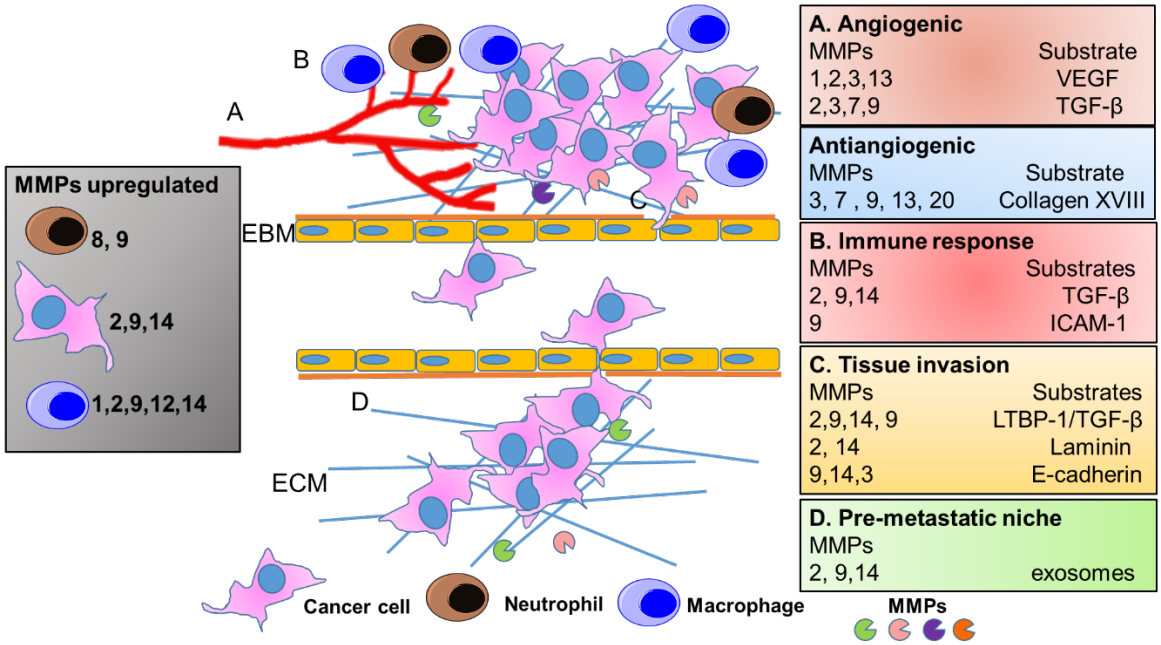

Figure 1.2 MMP multiple functions in the tumour microenvironment

The formation of new blood vessels (A. angiogenesis) can be triggered by the release of vascular endothelial growth factor (VEGF) and also tumour growth factor-β (TGF-β). Differently it can be supressed (Antiangiogenic) by the release of Collagen XVIII fragments (endostatin). The conversion of latent pro-TGF-β or latent TFG-β binding protein 1 (LTBP-1) can cause evasion of the immune surveillance (B. immune response) increasing invasion and metastasis and also leads to stimulation of neutrophils to produce more MMP9. Tissue invasion (C. tissue invasion) of the tumour and cancer metastasis require ECM (extracellular matrix) remodelling and down regulation of cell adhesion. MMPs can degrade cell surface molecules that mediate cellular adhesion, such as CD44 and E-cadherin. The high proteolytic activity in the tumour microenvironment releases cytokines, growth factors, and exosomes containing MMPS that can prepare distal tumour sites for tumour cells colonization and survival (D. pre-metastatic niche).

MMP9 can be compartmentalised on the cell surface by docking with CD44, a cell surface adhesion receptor. This result in increased MMP9-mediated TGF-β activation, which in turn causes stromal cells to evade immune surveillance leading to increased invasion by non-tumour cells [70]. Another way that these MMPs (2, 9 and 14), can modulate the bioactivity of TGF-β is by cleaving latent TGF-β binding protein 1 (LTBP-1), an important ECM

component [71, 72]. This increase of soluble TGF-β can induce cancer promotion and trigger invasion and metastasis (see Figure 1.2) [73].

Another MMP9 substrate involved in tumour progression is the intercellular adhesion molecule 1 (ICAM-1), a cell surface glycoprotein that is implicated in cellular interactions with immune cells. Shedding of ICAM-1 by MMP9 cleavage halts cell-cell communication and confers resistance to cell-mediated immune responses [74]. MMP9 and MMP14 proteolytic activity also affects the cell-cell interaction governed by E-cadherin. Its cleavage leads to increased proliferation in ovarian cancer, detachment of primary tumour cells from the ovarian surface and metastases [75]. MMP3 overactivity can also degrade E-cadherin, thereby promoting epithelial-to-mesenchymal transition (EMT) and tumorigenicity in mammary cells through a process that involves increased expression of Rac1b, a protein that stimulates alterations in cytoskeletal structure [76-78].

Angiogenesis is an enabling characteristic of the tumour progression, and it is considered a hallmark of cancer being called the "angiogenic switch". Interestingly, it became established that the critical factor is the vascular endothelial growth factor (VEGF) and its proteolytic release from the ECM by MMPs. Additionally, inhibition of MMP2, 9 and 14 activity resulted in reduced angiogenesis in a lung cancer mouse model [79]. E.g. in pancreatic islet tumours, MMP9 activates VEGF by cleaving an insoluble precursor anchored in the ECM, which can then interact with its receptors and promote angiogenesis [80, 81]. Additionally, MMP14 activity induces transcription of VEGF through activation of Src-tyrosine kinases [82]. Interestingly, MMPs not only promote angiogenesis but also cause anti-angiogenic effects. It has been described that MMP3, 7, 9, 12, 13 and 20 can generate the anti-angiogenic factor endostatin by processing type XVIII collagens in vitro [83].

Notably, in vitro experiments have demonstrated that MMP2, 9 and 14 activity can lead to the promotion of lymphangiogenesis [84]. In cancer, lymphatic vasculature promotion is related to increased metastatic process [85]. A lung cancer mouse model confirmed this correlation: fewer lymph node metastases were observed after inhibition of MMP activity when compared to control mice [79]. In a more recent report, using an MMP14-knockout mouse model, it was shown that MMP14 gene ablation lead to a lymphangiogenic effect in the corneas. It was observed that MMP14 cleaves the lymphatic vessel endothelial hyaluronic receptor-1, present on the surface of lymphatic endothelial cells, thus restricting the lymphangiogenic potential [86].

MMP activity in cancer is linked to the metastatic process which is the lethal outcome of the vast majority of cancers [87]. It was described that MMP2, 9 and 14 in exosomes are important for the initiation of the pre-metastatic niche formation in distal organs [88, 89]. Growth factors and cytokines released from the primary tumour site as a result of MMP activity, can create a receptive niche in organs such as the lungs, liver and bones, where tumour cells would be able to engraft and grow into secondary lesions [90].

With mounting evidence, the central role of MMP activity in tumour progression became clear. As a result, a number of clinical trials treating late-stage cancer patients with MMP inhibitors were started by major pharmaceutical companies in the early 1980s [91]. However, the results of these trials turned out to be unsatisfactory, as the treatment failed to improve the survival rate of cancer patients while presenting severe side effects such as musculoskeletal syndrome impairing patient life quality [92]. In summary, MMP function is more complex than originally thought, and better experimental designs associated with more specific molecules are required. Moreover, a better understanding about the physical location and dynamics of MMP enzymatic activity are fundamental to further elucidate the physiological role of these enzymes in tumour progression.

1.7. Studying MMPs in vivo

As laid out above, MMPs can affect many of the central processes involved in tumorigenesis and metastasis. Thus, their value as a cancer biomarker has been studied extensively [93, 94]. A plethora of methodologies have been used to determine MMP expression in vivo, at transcriptional and protein level, and to correlate this to staging or prognosis. Despite the value of the information produced by these methods, expression levels of MMPs are less relevant to disease status than their proteolytic activity, and these two parameters do not necessarily correlate. Hence, it is challenging to draw conclusions using mRNA or protein expression measurements only, as these methods disregard the post-translational regulation of MMP activity. Moreover, these methods are based on ex vivo or liquid biopsy samples, which interfere with MMPs interaction with their inhibitors and promoting molecules.

Another attempt to use MMPs as a prognostic marker originates from cancer patients' studies, which demonstrated that in their body fluids MMPs are at increased levels. Therefore, MMP profiling was performed in blood, urine, or saliva, trying to elucidate whether this could be used as a diagnostic tool, or predictor factor for cancer outcome [95-97]. Notably, the levels of MMP in body fluids allowed the differentiation between patients with cancer from healthy control individuals [98, 99]. However, inflammation process and benign tumours were also detected as false positives results. Probably because increased levels of MMPs can be associated with inflammatory reaction in tumour progression. Additionally, different cancer types originate the same upregulated MMPs in body fluids. Moreover, this test does not give spatial information about the cancer lesion, hence, it cannot be considered as definite diagnostic tool.

A non-invasive technological approach aiming to address these problems should utilise molecular imaging probes, which are capable of delineating MMP-specific activity in vivo.

Molecular imaging modalities have the ability to target molecules associated with cancer biology with high affinity and specificity, thus can provide very specific information which can have a decisive influence on patient management [100]. Despite the challenges associated with imaging MMPs, these enzymes are secreted and activated in the extracellular environment, avoiding the need to transfer the probe to intracellular compartments. Moreover, they are active at physiological pH, and perhaps most importantly, their activity is catalytic and thus provides an opportunity for signal amplification not found with targets that bind in a 1:1 fashion. Therefore, a molecular imaging agent capable of measuring MMP activity may be a useful clinical tool to detect early-stage cancerous lesions with increased sensitivity, identify tumours that might benefit from the use of MMP inhibitors as chemotherapy drugs, assess the efficacy of inhibitory MMP molecules in vivo, and determine cancer patient prognosis. As mentioned above, MMP activity is involved in different pathologies and in fact, imaging agents for these other diseases were also developed but will not be mentioned here (for review [101-103]).

Several non-invasive technological approaches have been developed to address these questions using different molecular imaging modalities. All are based on natural or synthetic MMP inhibitors, peptides, antibodies, cell-penetrating peptides or substrates [101]. The imaging agents used so far for MMP measurement in oncological models are optical imaging probes, radiolabelled imaging agents for either positron emission tomography (PET) or single photon emission computed tomography (SPECT) and magnetic resonance imaging (MRI) probes [104]. Below, a more detailed overview of the most relevant MMP imaging agents developed so far is provided.

1.7.1. Molecular optical imaging

Molecular optical imaging is based on a targeting agent presenting a fluorophore attached to, or incorporated in its structure. This fluorophore can be excited by a specific wavelength provided by an external light source, and emit a photon with lower energy [105]. There are two ways for fluorescently labelled probes to present the contrast necessary to be an imaging agent. One possibility is via accumulation of the fluorophores through affinity of the targeting moiety to a binding site, or thorough leakage in the tumour abnormal vasculature. Alternatively, a substrate containing an acceptor and a donor fluorophore can be designed to present Förster Resonance Energy Transfer (FRET), in which the fluorescent signal is quenched until the two fluorophore moieties are separated through cleavage of this substrate [106].

To image MMP2 activity and also assess MMP inhibition in vivo, Bremer et al. developed a probe using a peptide [107] based on MMP's substrate attached to a Cy5 fluorophore. The emission photons of this fluorophore are within the near-infrared (NIR) region and this particular probe was quenched by an acceptor group present in the structure [108]. MMP activity in a fibrosarcoma mouse tumour model was detected using this probe and after treatment with a broad spectrum MMP inhibitor, the emission of the fluorescence signal was reduced [109].

Another version of a probe that was designed to detect MMP activity was developed by Tsien et al., dubbed 'activatable cell penetrating peptide' [110, 111]. This peptide contained a sequence labile to MMPs, linking a fluorescently labelled cell-penetrating polyarginine-based oligopeptide and a neutralising polyanionic peptide composed of glutamic acid residues. Upon MMP activity, this hairpin-shaped peptide splits into two moieties, allowing the polycationic domain to adhere to the negatively charged cell surface and be subsequently

internalised. This strategy allowed selective accumulation of the fluorigenic probe within the tumour cells. Another version using the same ACPP but containing two fluorophores resulting in quenching by FRET, was shown to detect metastasis in the liver of a fibrosarcoma tumour mouse model which presented MMP activity [112]. The capacity to report MMP14 activity in tumour-bearing mice was also exploited using an MMP14 substrate containing a NIR dye-quencher pair, which showed an efficient boost in fluorescence upon cleavage [113].

Another strategy based on FRET and substrates for MMPs was based on a self-assembling homotrimeric triple helical peptide (THP), incorporating segments of type V collagen, with high specificity for MMP2 and MMP9 proteolysis. This strategy has the advantage of mimicking the topology of the substrate, possibly increasing specificity. Although, in vivo, THP showed a low fluorescence enhancement in the fibrosarcoma tumour model upon MMP cleavage, the signal was reduced when mice were treated with a broad spectrum MMP inhibitor prior to THP injections. This result indicates that the observed tumour fluorescence was indeed enzyme mediated [114].

A different scaffold based on a small immuno protein (SIP) targeting the catalytic domain of human MMP2 was fluorescently labelled with Cy5 and utilised as an optical imaging agent. In this study, MMP2 knockout mice were used to evaluate the specificity of the uptake. Indeed, the presence of MMP2 activity correlated with the uptake of the fluorescently labelled SIP. Therefore this approach can be a potential non-invasive imaging biomarker for the evaluation of MMP2 activity in tumours [115].

A number of approaches were developed using nanotechnological devices as platforms incorporating fluorophores in a peptidic substrate labile to MMP activity. One example is based on a polymer fluorogenic dendrimer containing a substrate sequence labile to MMP7.

In this particular case, fluorophores were quenched by FRET and upon MMP7 activity the fluorescent signal would be generated. This strategy was sensitive enough to detect benign lesions of one millimetre radius in mouse models bearing colorectal cancer [116].

Despite the fact that optical imaging is a sensitive technique, with high resolution and relatively low cost, it cannot be used to detect cancer lesions within deep tissues in the body. As aforementioned, the fluorophores do not emit photons spontaneously, hence, there is a need for them to be externally excited. Secondly, the NIR emission photons penetrate at best two centimetres in tissue, limiting the ability for visualisation of the majority of cancer types. Nevertheless, this strategy has great potential in oncological surgery because it can highlight where the small lesions are, and help to define the resection margin of the tumour [117].

1.7.2. MRI

Magnetic resonance imaging (MRI) has become widely available in the clinic and is a commonly utilised modality of cancer imaging which offers soft tissue contrast of high spatial resolution with excellent tissue penetration. This imaging modality is based on the absorption and emission of radio frequency energy by certain atomic nuclei being hydrogen atoms the most often used. Pulses of radio waves excite the nuclear spin energy transition, and magnetic field gradients localise the signal in space. By varying the parameters of the pulse sequence, different contrasts may be generated between tissues based on the relaxation properties of the hydrogen atoms therein.

Specific morphological features of tumours can be better visualised by gadolinium-based or iron oxide nanoparticles (IONPs) enhancement agents. These enhancement agents disturb the magnetic relaxivity of the surrounding protons, increasing or decreasing the MRI signal resulting in image contrast [118]. However, they do not possess targeting characteristics,

making it necessary to associate these metals with elements which will confer the specificity to molecular markers in tumour tissue.

A novel proteinase-modulated contrast agent (PCA) containing gadolinium was developed to detect the MMP2 activity in vivo by MRI. The PCA agent incorporates a solubility switch system, whereupon cleavage of a peptide substrate by MMP2 causes the water solubility to decrease leading to aggregation [119]. Evidence suggests that this leads to an accumulation of cleaved PCA in MMP2-positive mammary carcinoma tumour-xenograft in mice, which can be visualised by MRI. In addition, PCA accumulation in a MMP2 knockdown tumour model, in vivo, was reduced. Additionally, a scrambled peptide sequence inserted into the PCA agent did not accumulate in MMP2-positive tumour bearing mice.

Another MMP-sensing agent was developed by Long et al. using self-aggregating IONPs. In this study, the authors used a bispecific nanoparticle presenting a peptide to target a chemokine receptor overexpressed in cancer cells, and a polyethylene glycol layer, linked to the surface of IONPs through an MMP-labile sequence. Upon MMP cleavage, these nanoparticles aggregated, thereby enhancing MRI signal in a glioblastoma tumour model [120]. To confirm if the aggregation observed was dependent on MMP activity, inhibitors were injected and the accumulation of IONPs in the tumour site was reduced, reaching the same levels as the control group consisting of IONPs with a scrambled sequence not specific for MMP2 activity [121]. Although the development of magnetic MRI probes have high resolution with no requirement for the use of radiation, the biggest limitation is their low sensitivity and the relatively large quantity of probe required to achieve good image contrast, which may hinder its clinical application.

1.7.3. SPECT/PET

The nuclear imaging modalities PET and SPECT are a very attractive alternative for MMP imaging as they present comparable sensitivity as optical imaging. Additionally, these techniques rely on γ–emissions which can pass largely unimpeded through tissues. Consequently, PET and SPECT are routinely used to track biochemical, physiological and pharmacological processes in a non-invasive manner in the clinic [100]. These imaging modalities require the use of radionuclides that will generate γ–emissions as a result of radioactive decay. SPECT radionuclides generate the γ-rays directly, while PET radionuclides emit a positron. The latter has the same mass as an electron but an opposite charge. When this positron meets its anti-particle, an electron, an annihilation event takes place, producing a pair of 511 keV γ-rays [122].

Different scaffolds were used for the development of SPECT or PET MMP imaging agents [101]. For example, inhibitors first developed for cancer treatment were radiolabelled to be tested as MMP imaging agents These are synthetic small molecules classified on the basis of the zinc binding group (ZBG), which chelate the zinc ion in the catalytic site, rendering an inactive MMP [123]. Some of these molecules derive from the sequences of the amino acids of the MMP's endogenous substrates called peptidomimetic. For instance, Marimastat, a hydroxamate peptidic broad-spectrum MMP inhibitor which was tested in the clinic [124], was labelled with the PET radionuclide Fluorine-18 (^{18}F). The resulting molecule [^{18}F]marimastat, was injected intravenously in mice bearing MMP-expressing murine breast cancer cells, resulting in rather low tumour uptake. Nonetheless, the specificity of the tracer distribution was confirmed by a blocking experiment in control animals first loaded with 10-fold excess unlabelled Marimastat [125].

Another MMP inhibitor originally developed for cancer therapy [126, 127] was used as a scaffold for the development of a PET tracer, more MMP2 and 9 selective, by Furumuto et al. The imaging agent had a carboxylic acid as ZBG, conferring higher selectivity but lower binding affinity when compared to hydroxamate-based inhibitors [128]. ^{18}F-labelled inhibitor, [^{18}F]SAV03, accumulated in xenografts mice bearing breast cancer with tumour-to-blood ratios of uptake equivalent to 2.72 ± 0.27. Whole-body autoradiography also indicated tumour accumulation of the radiotracer but no other controls were included in this work [129].

Another attempt of imaging MMP using small inhibitors as PET tracers was developed using cyclic inhibitory peptides: a decapeptide ring containing the HWGF motif, designed to confer additional selectivity towards MMP2 and 9 [130]. The peptide scaffold was radiolabelled with two different PET radionuclides, either ^{18}F or Gallium-68 (^{68}Ga) and injected in tumour-bearing mice [131, 132]. For both tracers, ex vivo biodistribution studies revealed low tumour accumulation which was below or similar to the concentration of the radiotracer in blood. In the case of the ^{18}F-labeled cyclic peptide, a blocking experiment was performed using an excess of cold, unlabelled cyclic peptide pre-injected in the mice, which resulted in reduced uptake of the radiotracer, demonstrating the binding specificity of the inhibitor to its targets.

The natural MMP inhibitor, TIMP, also has been used as a platform to develop SPECT tracers. TIMPs' N-terminal domain present high affinities to the MMPs' catalytic domain establishing a non-covalent interaction. The first TIMP-based radiotracer was comprised of the N-terminal domain of recombinant human TIMP2, radiolabelled with the radionuclide Indium-111 (^{111}In) [133]. Imaging studies were performed with this radiotracer which was injected in Kaposi sarcoma patients. Unfortunately, the tracer distribution was

predominantly in the kidneys and did not localise in other tissues and no Kaposi sarcoma lesions could be identified [134].

TIMP2 was also radiolabelled using Iodine-123 (^{123}I) to allow MMP14 imaging [135]. The rationale is that the TIMP2's C-terminal binds to the hemopexin-like domain of MMP14, which is tethered in the plasma membrane of cancer cells possibly reducing background noise due to secreted MMPs present in the body fluids. However, high blood uptake and a low tumour uptake were observed, possibly caused by shedding of MMP14 to the blood stream [136].

Radiolabelled antibodies are an obvious choice to target protein biomarkers in cancer imaging. Temma et al. developed a Technetium-99m (^{99m}Tc) labelled anti-MMP14 monoclonal antibody and evaluated its ex-vivo biodistribution in studies using three rodent models of breast cancer [137]. Tumour-to-blood ratio of the radiolabelled antibody were only 1:1, possibly due to the presence of MMP14 in the blood stream. Additionally, no imaging study was performed. Pfaffen et al. also used an antibody-based imaging probe to target MMPs. In the study they developed a radiolabelled SIP with Iodine-125 (I^{125}). This SIP was based on the covalent dimerization of the single chain variable fragment presenting a total molecular weight of 75 kDa. From the three different SIPs developed to target MMP1, 2 and 3, only the MMP3-targeting variant demonstrated specific tumour uptake in teratocarcinoma lesions in mouse. Again, no imaging study was performed with this approach [138].

Recently, Morcillo et al. developed two radiotracers: (1) using an antibody against MMP14 radiolabelled with Zirconium-89 (^{89}Zr), and (2) a MMP14 binding peptide ^{68}Ga-radiolabelled. Both probes were evaluated in a mouse pancreatic tumour model and presented different characteristics. ^{89}Zr-anti-MMP14 antibody presented a better tumour-to-

blood ratio (1.44 ± 0.43) when compared to the ^{68}Ga-MMP14-binding peptide (0.5), as well as a better image contrast [139].

Even though SPECT and PET are nuclear imaging modalities that present remarkable sensitivity, all of the aforementioned inhibitor-based or antibody imaging agents, which bind to the catalytic domain in a 1:1 fashion, do not generate the desired contrast. What is more, they suffer from increased background signal, given the presence of MMPs in the blood stream. Yet another disadvantage of this approach is that these agents indiscriminately bind to both the active and latent form of the proteases. Therefore, the development of a probe for MMP activity using PET/SPECT imaging is far more desirable to improve cancer patient management.

Duijnhoven et al. aimed to address these issues by radiolabelling a version of the ACPP developed by Tsien with Lutetium-177 (^{177}Lu) and Iodine-125 (^{125}I) to enable monitoring of MMP2/9 activity in pre-clinical models of fibrosarcoma tumours by SPECT [140]. While no imaging experiments were performed, ex vivo biodistribution analysis revealed that radiolabelled ACPP exhibited only very minor accumulation in tumour tissue and this was attributed to activation of the probe in the vascular compartment.

An interesting PET imaging agent for MMP activity was developed by Chuang et al. [141]. The probe, containing a tetramethylrhodamine (TMR) group and a PEGylated MMP peptide substrate, was ^{18}F-labelled forming a PEG-peptide-^{18}F-TMR probe. Upon MMP cleavage, the hydrophobic ^{18}F-TMR was released and preferentially accumulated in MMP-expressing tumours as shown by PET imaging.

Table 1.1 MMP targetting probes for PET and SPECT

year	Cancer model	[1]T/B Ratio	Imaging	[2]MMPs	Scaffold	Isotope	[3]Ref
2010	Mammary	--	yes	Broad Spectrum	Marimastat	^{18}F	[125]
2015	Ovarian/ Prostrate	0.77±0.12 0.48±0.14	yes	2, 9	Cyclic peptide inhibitor	^{18}F/^{68}Ga	[131, 132]
2010	Pulmonary	0.89±0.14	yes	Broad Spectrum	Marimastat	^{123}I	[136]
2009	Mammary	1.54±0.17	no	14	Antibody	^{99m}Tc	[137]
2010	Teratocarcinoma	5.5±0.9	no	3	Small immuno conjugates	^{125}I	[138]
2018	Pancreatic	1.44±0.43 ~ 0.50	yes	14	Antibody/ Non-substrate peptide	^{89}Zr/^{68}Ga	[139]
2011	Fibrosarcoma	--	no	2,9	[4]ACPP	^{177}Lu/^{125}I	[140]
2012	Fibrosarcoma	2.5±0.9	yes	7, 9, 12, 13	[5]TMR-PEG-Peptide	^{18}F	[141]
2010	Melanoma	0.9±0.03	yes	9	Binding Peptide	^{68}Ga	[142]

[1]T/B: tumour-to-blood ratio ex-vivo biodistribution; [2]MMP: Matrix Metalloproteinase targeted; [3]Ref: Bibliographic reference; [4]ACPP: Activatable cell-penetrating peptide; [5]TMR: tetramethylrhodamine.

The above table summarises key information about the different probes developed for preclinical SPECT or PET imaging. A large number of strategies have been developed to image MMPs. Nevertheless, there is room for improvement and novel platforms for imaging agents targeting MMP activity in cancer should be explored. Here, we used a modified anthrax lethal toxin to probe MMP activity by SPECT imaging. In the next section, the biology of the anthrax toxin will be explained in detail. The feasibility of such a novel approach to detect MMP activity using SPECT or PET imaging modality will be discussed.

1.8. Anthrax lethal toxin mechanism

1.8.1. Background

Bacillus anthracis is a gram-positive bacterium and the causative agent of anthrax disease. Anthrax is a zoonotic disease associated with domestic animals and soil, in its spore resistant form [143]. In rare occasions, *Bacillus anthracis* can infect humans by cutaneous, gastrointestinal, or respiratory entry, the latter being the more hazardous route. In pulmonary or inhalational anthrax, the spores are carried by macrophages from the lungs to adjacent lymph nodes. In this favourable environment, the spores can germinate and multiply. If left untreated for 48 h after the onset of the acute phase symptoms, death occurs in almost 100% of the cases [144].

The *Bacillus anthracis* bacteria is considered one of the most significant weapons in biological warfare due to its high pathogenicity and its relative ease of preparation and dissemination of its spores, which present great resistance to elimination [145]. Sadly, in 2001 *Bacillus anthracis* spores were used in the United States in a bioterrorism attack increasing the attention given to the understanding of this disease and effort to improve vaccines and treatment for this bacteria [146].

Bacillus anthracis present two major virulence factors encoded by two different plasmids, the poly-gamma-D-glutamic acid capsule and the tripartite anthrax toxin [147, 148]. The largest plasmid (pXO1) contains the genes for the anthrax toxin while, the pXO2 plasmid codes for the capsule which it lays outside of the cell wall and protects the bacteria against phagocytosis, or degradation by defensive cells from its host's immune system [149].

Without the pXO2 plasmid, the bacteria can be phagocytised and destroyed. However, anthrax toxin is the major virulent factor and it is responsible for the extensive edema and

organ failure seen in anthrax patients [150-152]. This toxin is composed of three polypeptides which are individually non-toxic, namely, protective antigen (PA), lethal factor (LF) and edema factor (EF). Interestingly, these names were given after the isolation of the three components and the understanding that anthrax toxin is a A-B type or binary toxin [153]. Therefore, it needs a binary combination of the correct components in order to present any toxic effects. In fact, PA+LF injected into rats lead to sudden death when injected in rats and was named lethal toxin (LT) [154, 155]. In contrast, the binary combination of PA+EF was called edema toxin (ET) because it led to skin edema when injected intradermally in rats or guinea pigs.

Both the EF and the LF of the anthrax toxin correspond to the "A" components, and PA corresponds to the "B" component. PA attaches to host cell receptors, tumour endothelial marker 8 (TEM8) [156] or capillary morphogenesis gene 2 (CMG2) [157], and forms a pre-pore that allows interaction and endosomal escape of EF and LF reaching the cytosol.

1.8.2. The protective antigen: PA

The PA, part B of the anthrax toxin, was named as such because of its ability to promote a protective immune response against anthrax disease [158]. The mechanism of intoxication of the anthrax toxin has been extensively investigated over the last decades and is possibly one of the best described bacterial toxin mechanisms (see Figure 1.3) [159]. PA attaches to host cell receptors, TEM8 [156] or CMG2 [157], and forms a pore that allows interaction and endosomal escape of EF and LF reaching the cytosol. The mature PA protein has 735 amino acids (PA_{83}) with a molecular weight of 82,684 Da [160]. The first crystal structure of the PA_{83} monomer revealed that the molecule is folded into four functional domains that play a unique role during the intoxication process.

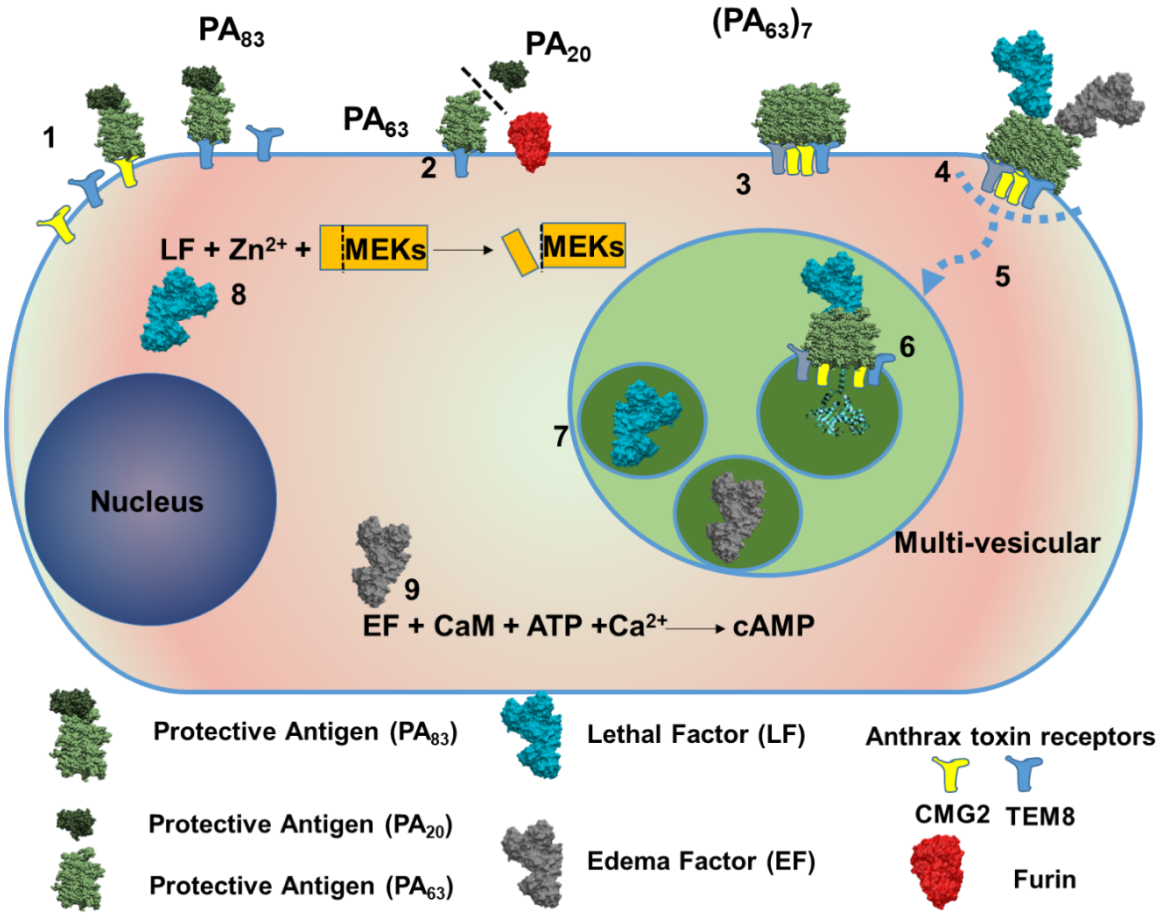

Figure 1.3 Anthrax toxin mechanism of cell intoxication

1. PA binds to cell anthrax receptors tumour endothelial marker 8 (TEM8) or capillary morphogenesis gene 2 (CMG2); 2. PA is cleaved by furin like proteases with PA_{63} remaining bound to the receptor. 3. Clustering of anthrax toxin receptors and forming of a heptameric pre-pore $(PA_{63})_7$ creates the binding sites for (4) LF and EF resulting in lethal toxin (LT) and edema toxin (ET) respectively. 5. Endocytosis of LT and ET along with receptors. 6. Translocation of EF and LF through PA pore under acidic conditions. 7. Release of LF and EF to the cytoplasm. 8. LF cleavage of MEKs (MAPK/ERK kinase) in the presence of zinc ion (Zn^{2+}). 9. EF adenylate cyclase activity transforming of ATP to cAMP using calmodulin (CaM) and calcium ions (Ca^{2+}) as cofactors.

Domain 1 comprises the first 249 residues (PA_{20}, 20 kDa) and contains the region ($RKKR_{167}$) which is cleaved upon proteolytic action of furin or furin-like proteases. The remaining 82 residues of this domain forms the binding site for EF and LF [161-163], which spans two adjacent C-terminal fragments (PA_{63}, 63 kDa) [164]. Removing the steric hindrance by

proteolysis allows seven or eight PA_{63} to self-assemble into a ring-shaped formation on the cell surface, a structure called a pre-pore [165, 166]. Each pre-pore can interact with 2 or 3 molecules of EF and/or LF, forming stable complexes [167] on the cell surface before being endocytosed [164]. In contrast, if not cleaved, PA_{83} persists on the cell surface while the heptamer or octamer of PA_{63} is endocytosed via a receptor mediated clathrin-dependent process [168, 169].

Subsequently, the complex is delivered to early endosomes, where it associates with intraluminal vesicles [170]. In the multi-vesicular endosome environment, the PA pre-pores undergoes an acid-triggered conformational rearrangement, becoming a pore that mediates the translocation of LF to the lumen of a late endocytic compartment, which in turn can be released to the cytoplasm through a process of back-fusion of endosomes [171].

The rearrangement of PA residues 250 to 487, Domain 2, allows the formation of the lumen of the pore [172]. Under acidic conditions, similar to those encountered in the endosomes, the pre-pore undergoes conformational changes and converts to a mushroom-shape pore forming a channel through the plasma membrane [173, 174]. This is a narrow lumen (15 Å) requiring that the catalytic factors, LF and EF, unfold in order to translocate through this channel [175].

Mutagenic experiments identified residues 488–594 (Domain 3) as being relevant to protein–protein interactions during the oligomerisation of PA_{63}. Domain 3 is the smallest of the four domains but it has a hydrophobic region that directs the formation of the pre-pore [176]. The C-terminal residues 595–735 comprises the receptor-binding Domain 4, which has limited contact with other domains. Monoclonal antibodies against the epitope formed by residues 671-721 blocked the interaction of radiolabelled PA with cells [177]. Amino acid

substitution corroborated that within this region, residues 679-693 are critical for receptor binding [178, 179].

1.8.3. Lethal factor (LF) and Edema factor (EF)

Translocation of LF and EF through the PA pore into the cytosol triggers a cascade of cellular metabolic changes leading to cytotoxicity, and potentially cell death. Arora et al. engineered a potent fusion toxin (FP59) by fusing the truncated N-terminal region of LF (1-254 residues, LFn) to the domain III of exotoxin A produced by *Pseudomonas aeruginosa*, which was capable of killing cells that were resistant to the wild type LT. These experiments demonstrated that LFn is the domain of LF responsible for the interaction with PA_{63} oligomers, and their translocation through the pore channel [180]. The remaining C-terminal domains of both LF and EF contains distinct enzymatic regions.

EF polypeptide contains 767 residues (89 kDa) and it was the first of the two enzymatic polypeptides of anthrax toxin to be characterised [181]. Leppla demonstrated that EF was an adenylate cyclase enzyme, able to convert intracellular adenosine triphosphate (ATP) into cyclic adenosine monophosphate (cAMP) [182]. The catalytic activity of EF requires the binding of calmodulin and calcium as cofactors. In fact, the presence of EF triggers the influx of calcium into the infected cells [183]. The resulting increase in cAMP levels has been shown to alter cellular chemotaxis, and ultimately, EF activity impairs the antimicrobial response of the immune system (extensively reviewed in [184]).

Aside from causing rapid mortality in vivo, LT can lyse cultured macrophages through an oxidative burst action [185-187]. LF is a protease (776 amino acid; 90 kDa) and contains a zinc-binding motif spanning residues 686-690, which is characteristic of the metzincin superfamily [188]. It was demonstrated that LF cleaves within the N-terminal region near the kinase domain of MEKs (MAPK/ERK kinase) [189, 190], thus removing a region

involved in protein–protein interaction. MEKs are enzymes that are involved in MAPK pathway, thus modulating intracellular signalling pathways through phosphorylation cascade. LF is able to cleave and inactivate all of the MEKs, with the exception of MEK5, and thus it can inhibit the ERK1/2, JNK, and p38 branches of the MAPK pathway [191]. In fact, consistent with its inhibitory effects on MEK function, LT suppresses the inflammatory response and the production of inflammatory cytokines by immune cells, which permits growth and diffusion of *Bacillus anthracis* [192-194].

1.8.4. Anthrax toxin native receptors

The first step of anthrax toxin entry into host cells is the interaction of PA to its cognate receptor on the surface [195]. Bradley et al. demonstrated that cells with mutations in the TEM8 gene (ANTXR1) were resistant to PA/FP59 treatment, and when the functional gene was restored, the cells were able once again to bind to PA, and were sensitive to treatment [156]. As CMG2 shares 40% amino acid identity with TEM8, it seemed obvious to test it as a possible second anthrax toxin receptor (ANTXR2) [157]. After demonstrating that CMG2 is another anthrax toxin, Scobie et al. used a soluble version of the receptor that interacted with PA in the blood stream, protecting rats injected with LT [196]. CMG2 presents four different isoforms resulting from alternative splicing. The two larger isoforms are predicted to be anchored in the plasma membrane and thus able to interact with and internalise PA. Similarly, TEM8 presents 3 different isoforms resultant from alternative splicing, the two larger ones have transmembrane domains and can also act as PA receptors.

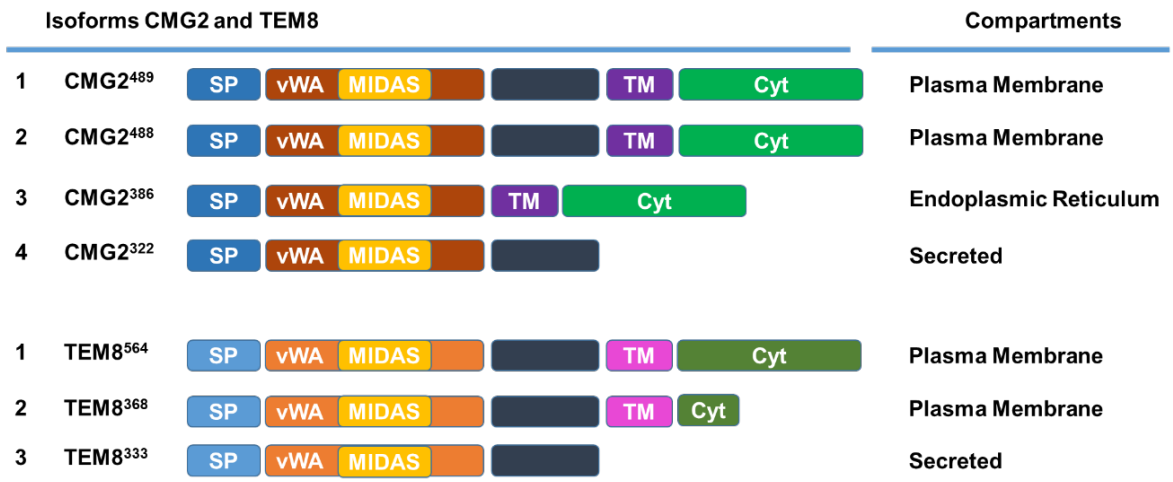

Figure 1.4 Schematic representation of Anthrax toxin receptors isoforms

The different isoforms of capillary morphogenesis gene 2 (CMG2) and tumour endothelial marker 8 (TEM8) are presented with their correspondent fate within a cell comportment or secreted. Abbreviation: SP = signal peptide; vWA = von Willebrand Domain; MIDAS = metal ion dependent adhesion site; TM, transmembrane domain type I; Cyt = cytoplasmic domain; (based on references [157, 197]).

Both TEM8 and CMG2 are a single-pass type I transmembrane glycoproteins [198] comprising of different isoforms with distinct domains (see Figure 1.4) [157, 199]. The N-terminal is the extracellular region characterised by a von Willebrand factor-A (vWA) domain, which contains the metal ion adhesion site (MIDAs) that binds to divalent ions allowing the interaction with PA molecules. Even though they present homology in the vWA domain, TEM8 and CMG2 bind with different affinities to PA. Liu et al. have demonstrated in cytotoxic experiments that the PA/CMG2 complex interacts with a 10 times stronger affinity than PA/TEM8 complex [200]. Moreover, CMG2 gene ablation confers resistance to mice challenged with lethal doses of LT while TEM8 null mice do not present resistance, demonstrating that CMG2 is the major receptor for anthrax toxin [201]. The C-terminal, cytoplasmic tail, is relevant for internalisation, requiring a post-translational modification with a saturated fatty acid molecule (palmitate) [202]. This palmitoylation of the receptors in the cytoplasmic tail secures the correct transport of PA_{63} molecules to micro-domains of

the plasma membrane and correct oligomerisation of the PA_{63} pre-pore [169]. Another important feature of this domain is the presence of tyrosine residues. Abrami et al. has demonstrated that replacement of these residues delays toxin uptake due to hindrance of Src-dependent phosphorylation for its subsequent ubiquitination, which is required for clathrin-mediated endocytosis [203].

The physiological role of these receptors is still being determined, nevertheless, in vitro data demonstrated that TEM8 and CMG2 interacts with the ECM through its extracellular vWA domain, and both receptors are involved in cell adhesion, migration, and modulation of the ECM itself [204]. Moreover, the cytoplasmic tails of both TEM8 and CMG2 link to the actin cell cytoskeleton allowing a physical interaction that is necessary for cell migration and angiogenesis. CMG2 binds to laminin, collagen IV and VI [205, 206], being responsible for the modulation of the latter and maintenance of the ECM homeostasis. In contrast,TEM8 ligands include domain C5 of collagen VI and collagen I [207] which are both pro-angiogenic extracellular matrix components.

In vivo, deletion of TEM8 in knockout mice resulted in leaky vessels in the skin due to a thinner endothelial basal membrane. In contrast, the fibroblasts in these mice presented an increase in fibre-forming collagens, resulting in fibrosis in the skin and internal organs [208, 209]. This phenotype is equivalent to the human recessive genetic disease named GAPO, where the TEM8 gene is mutated, resulting in extracellular-matrix-homeostasis defects and deposition of ECM in different organs [210].

The initial studies of TEM8 and CMG2 expression demonstrated their presence in endothelial cells present in cancer or tubule formation during angiogenesis, respectively [205, 211]. However, later studies made clear that both receptors are more widely expressed. In mouse tissue both were detected by Western Blot analysis in lung, skin and small

intestines, with the association of TEM8 with the epithelial lining in these organs confirmed by immunohistochemistry [197]. Similarly, CMG2 was detected in a variety of cell types within lungs, intestine, and skin organ [212].

The discovery of the involvement of TEM8 and CMG2 in angiogenesis has resulted in targeted treatment for antiangiogenic therapy [213]. In breast cancer, higher expression levels of TEM8 have been linked to metastasis and cancer progression. Additionally, The Human Protein Atlas reports TEM8 as an unfavourable prognostic marker for thyroid and cervical cancer [214]. In a lung cancer model, Gong et al. demonstrated that TEM8 is involved in proliferation, migration and cell survival [215]. In fact, in preclinical experiments using different tumour models, antibodies against TEM8 inhibited cancer growth due to their antiangiogenic effect [216, 217]. Similarly, Rogers et al., demonstrated that a PA mutant that remains bound to CMG2 and TEM8 (named PASSSR), prevents them from interacting with their physiological substrates, leading to inhibition of angiogenesis and tumour growth in mice [218]. A recent study performed with human patients showed that CMG2 was highly expressed in gastric cancer tissues and the expression levels were associated with invasion depth and lymph node metastasis, and inversely correlated with survival [219]. Further characterisation demonstrated that the phenotype of the stem-like cancer cells was dependent on CMG2 expression and activation of Wnt/β-catenin pathway through the co-receptor lipoprotein-receptor-related protein 6 [219, 220]. Thus, CMG2 and TEM8 appear relevant receptors in cancer progression and a better understanding in their biology would be advantageous.

1.8.5. Variants of anthrax toxin for cancer therapy

Anthrax toxin has a unique cell entry mechanism that could be adapted for cancer therapy. Changing the furin-cleavable sequence in PA, making it more labile to tumour-associated

proteases would result in a preferential tumour-cell killing anthrax toxin [221]. With this in mind, our collaborators, Leppla et al. engineered and produced anthrax toxin variants. The MMP proteases were investigated because their increased activity in different cancer types is linked to cancer aggressiveness and poor prognosis for cancer patients, as explained above [68]. Our collaborators have developed mutated PA proteins, PAL1 and PAL2, in which the furin recognition site was replaced by sequences susceptible to MMP2, MMP9, MMP14 and possibly other MMPs. These two sequences were modelled after the MMP cleavage site in the α1 chain of type I collagen, but contain substitutions that enhance cleavage by MMP2 and MMP9, based on previous work by Netzel-Arnett el al. [222]. When combined with the fusion toxin FP59, these PA proteins showed selective killing of MMP-overexpressing human tumour cell lines while sparing non-tumour cells when grown together in a co-culture model, indicating that PAL1 activation and delivery of FP59 occurred on the tumour cell surface [223].

In combination with LF, PAL1 exhibited anti-tumour efficacy in tumour xenografts [224]. MMP-activated LT had higher specificity to human tumour xenografts and a much lower toxicity to mice than the wild-type LT [225]. Surprisingly, cell lines which were resistant to PAL1/LF treatment in vitro became sensitive after being engrafted in the mouse, resulting in necrosis and reduction of tumour vasculature [226]. These initial findings were further investigated and the LF-mediated anti-angiogenic effects were attributed to inhibition of ERK1/2, JNK and p38 MAPK activation, which are linked to endothelial invasion and neovasculature formation [227]. Moreover, when injected into the blood stream PAL1 displayed lower immunogenicity when compared with the wild-type toxin [226], possibly due to its increased resistance to proteolysis by enzymes present in the serum when compared to PA wild type [228].

1.9. Outline and aims of the thesis

Engineered LT variants targeting MMP activity have previously presented therapeutic effect in cancer models [225]. The mechanism of cell-entry of LT toxin requires that both LT components are on the cell surface in order to allow PAL1 pore formation and delivery of LF [223], thus, giving an opportunity to evade targeting MMPs present in the body fluids [99]. Hence, in the present work, the experimental hypothesis tested is that radiolabelled engineered anthrax toxin can detect MMP activity in cancer models by SPECT, a previously unexplored strategy (see Figure 1.5).

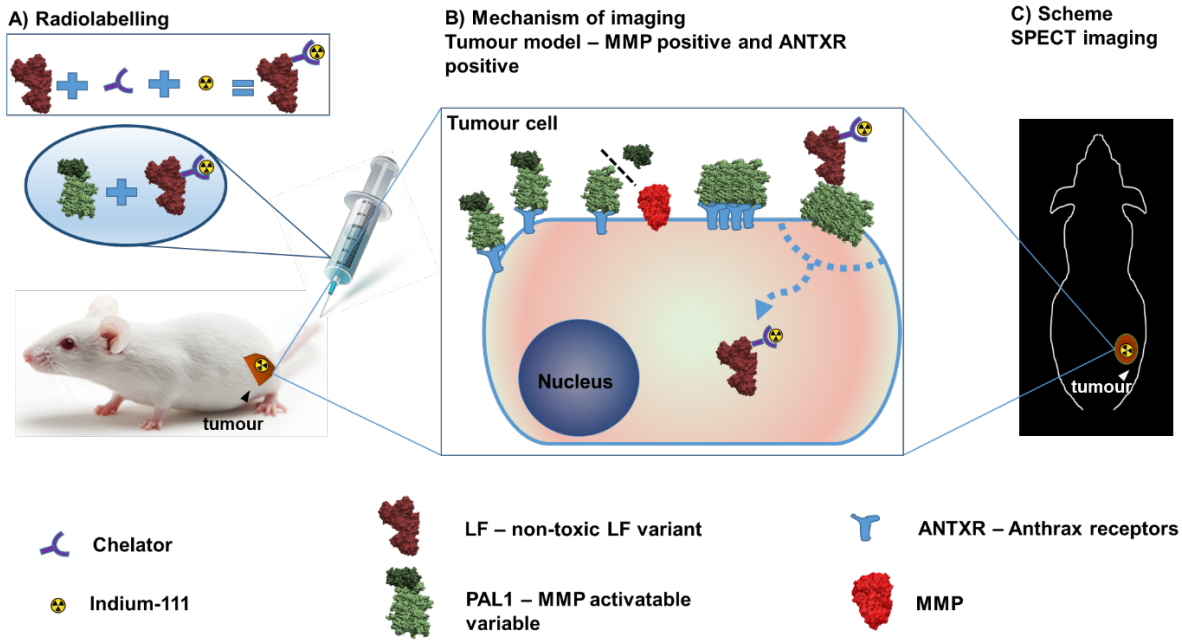

Figure 1.5 Project outline

Schematic representation of the thesis. A) Simplified radiolabelling reaction of non-toxic variants of Lethal Factor (LF) and in vivo experimentation in tumour models with the engineered variants of anthrax toxin. B) Mechanism of matrix metalloproteinases (MMP) activation of PAL1 and pore formation allowing radioactive delivery to tumour cells of radiolabelled LF variants. C) Imaging of tumour by SPECT based on radiolabelled probes of anthrax toxin targeting MMP activity and anthrax receptors (ANTXR).

The aim of the present thesis was to develop a novel way to non-invasively image MMP activity in tumour tissue. We used a radiolabelled engineered non-toxic anthrax toxin version

(PAL1/LF^{E687A}) in combination with SPECT/CT imaging. **Chapter 1**, this chapter, lays out the importance of MMP proteolytic activity in tumour biology. The relevance of assessing MMP activity was examined because of its central role in tumour progression, aggressiveness and metastasis. The challenges of using MMP activity as a tumour biomarker were highlighted, namely structural similarities among the different MMPs resulting in overlap of substrate recognition and its presence in the blood stream. Highly relevant to the present thesis, the different strategies developed to date to image MMPs using different imaging modalities were described. The opportunities and drawbacks of each modality were discussed, and the necessity to pursue novel strategies was emphasized, considering the complex biology of MMPs. A unique cell-entry mechanism of the A-B type anthrax toxin was modified by our collaborators to target MMP activity and two relevant cell receptors, CMG2 and TEM8, on the surface of tumour cells. In the next chapter, **Chapter 2,** the experimental methods and the materials used to the development of this project are described.

The validation of anthrax toxin as an MMP activity targeting system are examined in **Chapter 3**. Cell free assays, exposing different variants of PAs to MMP2, MMP14 or furin were performed to elucidate the cleavage susceptibilities of the different PA variants. A panel of cancer cell lines was characterised for the different components relevant for the toxin delivery system. Cell viability assays were performed with or without MMP inhibitors to determine the dependence of engineered anthrax toxin to MMP activity. Fluorescently labelled versions of the engineered toxin were investigated in cell uptake experiments by confocal microscopy. Additionally, the cellular co-distribution of MMP14 and CMG2 was investigated. **Chapter 4** describes the development of radiolabelled anthrax toxin variants and their evaluation in a variety of cell-based assays to elucidate the impact of the radiolabelling reaction in binding affinity, specificity, cytotoxicity and stability. The

abundance of CMG2 and TEM8 receptors present in the cell membrane was assessed using radiolabelled PA in the tumour cell line panel. In **Chapter 5**, in vivo experiments are described using radiolabelled LT components. The pharmacokinetic parameters of radiolabelled anthrax toxin were evaluated by SPECT/CT image analysis. The variant which presented optimal pharmacokinetics for the binary imaging system was used in subsequent experiments to analyse MMP activity in tumour bearing mice. In **Chapter 6**, the findings of the preclinical study are summarised, highlighting and discussing the limitations of the anthrax toxin-based MMP imaging agent. To conclude, possible future avenues derived from the current work are proposed and discussed.

Chapter 2

2. Chapter 2: Materials and Methods

2.1. Lethal toxin variants

All components of *Bacillus anthracis* lethal toxin (LT) were expressed and purified by our collaborators from the National Institute of Health (NIH, United States) and were kindly provided by Dr Leppla [229]. Briefly, proteins secreted by the non-virulent *B. anthracis* strain BH500 were adsorbed to Phenyl-Sepharose by addition of solid ammonium sulphate, eluted with low salt, and then submitted to chromatographic purification using Q-Sepharose and hydroxyapatite columns [230]. Fractions containing the desired proteins were combined, dialysed, and evaluated for purity using SDS-PAGE and frozen. Samples were shipped on dry ice and stored at -80°C until further use. All protein batches were analysed by liquid chromatography mass spectrometry analysis and SDS-PAGE to confirm purity.

Wild type protective antigen (PAWT; 83 kDa) is cleavable by furin and other furin-like enzymes [231]. Here, we also used a PAWT variant containing an engineered cysteine ($PAWT^{K563C}$; 83 kDa) [232]. PAL1 has the furin cleavage site replaced by a sequence targeted by matrix metalloproteinases (MMP) such as MMP2, 9 or 14 (PAL1; 83 kDa) [233], whereas in PAU7 an uncleavable sequence was inserted (PAU7; 83 kDa) [234]. Lethal factor (LF) variants included the fusion toxin of the N-terminal translocation domain of LF (LFn, LF amino acids 1–254) and *Pseudomonas aeruginosa* exotoxin A domain III (FP59; 53 kDa) [234], LFn modified with a cysteine residue at the C-terminus (LFn; 30 kDa) [235] and full length mutant LF^{E687A} (90 kDa) containing a defective catalytic domain [236].

2.2. In vitro cleavage assay

To evaluate the susceptibility to enzymatic cleavage of the different PA variants ten µg of PAs were incubated with 50 nM of active human recombinant MMP2 (62 kDa, Sigma, Dorset, UK), furin (64 kDa, Abcam, Cambridge, UK) or furin pre activated proMMP14 (34

kDa, R&D systems, Abingdon, UK) in 50 µL of assay buffer below. The reaction was incubated for 16 h at 500 rpm at 37°C ThermoMixer C (Eppendorf, Stevenage, UK). Ten µL aliquots of each sample was prepared with SDS loading sample buffer (containing 10 mM Dithiothreitol), denatured by heating (10 min at 70°C) before loading gel. Sample aliquots were separated by SDS-PAGE using 4–12% gradient Tris-glycine gel (Novex, San Diego, CA). Additionally, PAL1 and PAU7 cleavage was analysed by intact protein Mass spectrometry.

Table 2.1 Cell-free cleavage assay buffers for PA samples.

Buffer	Composition	Enzyme
Activation	50 mM Tris (pH 9.0), 1 mM $CaCl_2$, 0.5% [v/v] Brij-35, 0.86 µg/mL furin; 1 h 30 min; at 37 °C; 500 rpm	Pro-MMP14
Assay	50 mM Tris (pH 8.5), 3 mM $CaCl_2$, 1 µM $ZnCl_2$	MMP14
Assay	50 mm HEPES (pH 7.5), 150 mm NaCl, 0.2 mm EDTA, 0.2, 100 µg/ml ovoalbumin, 1.0 mm $CaCl_2$, and 1.0 mm $MgCl_2$	MMP2 & Furin

2.3. Intact protein LC-MS

LT components were submitted to intact protein mass spectrometry analysis in order to test purity, cleavage or protein modifications. Dr Georgina Berridge (Targeted Discovery Institute, Oxford University, UK) performed these analyses. Reverse-phase chromatography was performed in-line prior to mass spectrometry using an Agilent 1290 HPLC system equipped with a Zorbax 300SB-C3 column (4.6x150 mm), using 0.1% formic acid in ultrahigh purity water (solvent A) and 0.1% formic acid in methanol (solvent B) as the mobile phase, using gradient elution as follows: 95% A and 5% B and a flow rate of 0.6 ml/min for 2 min followed by a linear gradient 95% B over 5 min. Protein intact mass was determined using Jetstream electrospray ionisation into an Agilent 6550 IMQTof

operated in positive-ion mode. The ion source was operated with the capillary voltage at 4000 V, nebulizer pressure at 20 psig, drying gas at 150°C, and drying gas flow rate at 5 L/min and sheath gas 12 L/min. Data analysis was performed using the Mass Hunter Qualitative Analysis Version B.07.00 Agilent software. The deconvoluted mass for each protein was compared with the theoretical mass of the proteins.

2.4. Cells and cell culture

Breast (MCF7; MDA-MB-231), pancreatic adenocarcinoma (CAPAN1) and fibrosarcoma (HT1080) human cancer cell lines were obtained from American Type Culture Collection (ATCC). KPC-mouse-derived B8484 cells were provided by Professor Owen Sansom at the CRUK Beatson Institute, Glasgow, UK [237]. Cells were cultured in complete Dulbecco's Modified Eagle Medium (DMEM; Sigma, Dorset, UK) supplemented with 10% fetal bovine serum (FBS; ThermoFisher Scientific, Paisley, UK), 2 mM L-Glutamine, 50,000 units of penicillin and 0.1 mg/mL streptomycin (Sigma, Dorset, UK), and incubated at 37°C, 5% CO_2. Chinese Hamster Ovarian (CHO) cells were genetically modified to overexpress either of anthrax toxin's natural receptors CMG2 or TEM8 as described [200] and were kindly provide by Dr Leppla (NIH, United States). Transfected CHO cells were cultured in Ham's F-12K Medium Kaighn's (Life Technologies) supplemented with 500 µg/mL hygromycin-B (Insight Biotechnology, Wembley, UK), 10% FBS, 2 mM L-Glutamine, 50,000 units of penicillin and 0.1 mg/mL streptomycin (Sigma, Dorset, UK). All cells were authenticated by their supplier, and cultured no longer than 20 passages after resuscitation from liquid nitrogen storage.

2.4.1. Cytotoxicity assay

The ability of the different PA variants to permit intoxication of the panel of cancer cell lines was determined by MTT assay (3-(4,5-dimethylthiazol-2-yl)-2,5-diphenyltetrazolium

bromide) after exposure of cells to PAWT, PAL1, or PAU7 in combination with the potent fusion toxin FP59 [238]. Cells were harvested using trypsin (Sigma, Dorset, UK) and seeded in 96-well plate (3,000 – 5,000 cells/200 µL) and incubated in humid cell incubator 37ºC and 5% CO_2. At 80% confluence, 100 µL of the conditioned media was replaced with PAWT, PAL1 or PAU7 at different concentrations combined with FP59. At different time points MTT (3-(4, 5-dimethylthiazol-2-yl)-2, 5 diphenyltetrazolium bromide, Sigma, Dorset, UK) was added to a final concentration of 0.5 mg/mL and incubated for 2 h at 37°C. The insoluble reduced MTT salt was dissolved by dimethyl sulfoxide (DMSO, Sigma) after removal of cell cultured media. Absorbance at 495 nm was measured at plate reader Infinite-proM200 (Tecan, Männedorf, CH) and considered as a signal of cell viability.

To investigate PA activation by MMP hydrolysis, cells were washed three times with serum free media and pre-incubated with the broad spectrum MMP inhibitor GM6001 (Abcam, Cambridge, UK) for 30 min prior to adding LT components. After 6 h of incubation at 37°C, cells were washed three times and a fresh supplemented cell culture media was added. After 48 h of incubation at 37°C cell viability was determined by the MTT assay.

2.4.2. Gelatin zymography

To determine the levels of MMP2 (62 kDa) and MMP9 (82 kDa) secreted in the cultured media (named conditioned media) cells were seeded into 6-well plates (250,000 cells/well) and incubated overnight at 37°C, 5% CO_2. At 70-80% confluence cells were washed twice with serum-free culture media and incubated at 37°C overnight. Subsequently, conditioned media was harvested and any cell debris was removed by centrifugation at 8,800 x *g* for 10 min at 4°C. Enzymes secreted in the conditioned media were concentrated using centrifugal filters (Millipore) with a 10 kDa cut-off at 17,300 x *g*, 4°C for 10 min. After this step samples were either used immediately, or stored at -80°C until use. Aliquots of five microliters of

concentrated sample were mixed with Tris-Glycine SDS sample buffer (Novex, San Diego, CA) and loaded in a 10% gelatin gel (Novex, San Diego, CA). After electrophoresis, the gel was washed in dH_2O and incubated with renaturing buffer (Novex, San Diego, CA) for 30 min at room temperature under gentle agitation. Subsequently, developing buffer (Novex, San Diego, CA) was used to equilibrate the gel for 30 min, after which the gel was incubated at 37°C for 30 h with fresh developing buffer. In control experiments, the broad-spectrum MMP inhibitor GM6001 (30 μM; Abcam, Cambridge, UK) was added in the developing buffer. Gels were stained with SimplyBlue SafeStain solution (Thermo Scientific) for 3 h to visualise digested gelatin as non-stained bands in the gel.

2.4.3. Cell lysates and immunoblotting

Cells were cultured in T-175 cm^2 cultured flasks at 80% confluence were washed twice with ice cold PBS before being harvested (10 mL PBS). Cells were placed in pre-chilled tubes on ice and centrifuged at 500 x *g*, 5 min at 4°C to remove any excess of PBS. Total cell lysates were prepared incubating packed cell volume 1:1 [v/v] for 30 min on ice using radioimmunoprecipitation assay buffer (RIPA; 50 mM Tris-HCl, pH 8.0, 150 mM NaCl, 1% Triton X-100, 0.5% sodium deoxycholate; Sigma, Dorset, UK) prepared with EDTA free protease inhibitor cocktail (Roche, Germany). Cell suspensions were sonicated three times at 50% amplitude using a 30 sec on/ 10 sec off cycle. Homogenised cell lysates were cleared by centrifugation at 16,500 x *g* at 4°C for 20 min. Protein concentration of the supernatant was determined using the colorimetric bicinchoninic acid assay (BCA) (Sigma, Dorset, UK).

To prepare samples enriched with proteins present in the plasma membrane, a separation of subcellular compartments of protein extracts was performed. To achieve that after harvesting cells and preparing the packed cell volume the subcellular protein fractionation kit for cultured cells (Thermo Fisher Scientific, Catalogue number 78840) was used according to

manufacturer's guidelines with all buffer and protein inhibitors provided. Membrane fraction was further homogenised and cleared as described above, and protein concentration of the supernatant was determined by BCA assay.

Protein samples were separated in a denaturant pre-cast SDS-PAGE gel (Thermo Fisher Scientific, Paisley, UK). Protein was transferred to polyvinylidene difluoride membrane using a tank blotting system (Bio-Rad, Watford, UK). Membranes were blocked using TBS buffer (Santa Cruz Biotechnology, Wembley, UK) with 0.5% [v/v] Tween-20 and 5% [w/v] skim milk (both supplied by Sigma, Dorset, UK). Blots were incubated with appropriate primary antibodies in blocking solution overnight at 4°C (Table below). Next day, blots were washed three times for 10 min each in TBS with 0.5% [v/v] Tween-20 and incubated with the appropriate secondary horseradish peroxidase conjugated antibodies for 1 h at room temperature. Subsequently, blots were washed and then incubated for 5 min in enhanced chemiluminescence reagents (Thermo Fisher Scientific, Paisley, UK) and exposed to X-ray film (Kodak, New York, UK).

Table 2.2 Antibodies used for immunoblotting or immunofluorescence experiments

Antibodies	Species	Supplier	Dilution	Molecular Weight
[1]MMP14[EP1264Y]	Rabbit	Abcam, UK	1:2,000	66 kDa
[2]TEM8[AB21270]	Rabbit	Abcam, UK	1:2,000	All isoforms (45 kDa)
[3]CMG2[AF2940]	Goat	R & D systems	1:2,000	All isoforms 55 kDa
Furin[SC-133142]	Mouse	Santa Cruz Biotechnology, UK	1:100	60 kDa
Protective Antigen [BAP0105]	Mouse	Abcam, UK	1:2,000	83 and 63 kDa
β-Actin [AB8227]	Rabbit	Abcam, UK	1:10,000	42 kDa
Goat anti-Mouse [4]IgG [5](H/L) [6]HRP	Mouse	Bio-Rad, UK	1:3,000	Not applicable
Goat anti-Rabbit IgG (H/L) HRP	Rabbit	Invitrogen, UK	1:3,000	Not applicable
Rabbit anti-Goat IgG (H/L) HRP	Goat	Abcam, UK	1:3,000	Not applicable

[1]MMP: Matrix Metalloproteinases, [2]TEM8: Tumour endothelial marker 8; [3]CMG2: Capillary morphogenesis gene 2; [4]IgG: Immunoglobulin; [5](H/L):heavy and light chain; [6]HRP: Horseradish peroxidase,

2.5. Fluorescent labelling of LF^{E687A} and LFn

To allow subcellular visualisation of LF variants two distinct fluorophores presenting non-overlapping excitation and emission spectra were selected. Cyanine3 (Cy3) NHS ester (GE Healthcare, Amersham, UK) was conjugated to LF^{E687A} and LFn molecules were labelled with Alexa Fluor® 488-NHS (Life Technologies, UK). The bioconjugation reaction was performed according to the manufacturer instruction using 200 µg of protein and a 10-fold molar excess of the dye in sodium carbonate buffer (pH 9.5). The reaction mixture was incubated at 25°C for 2 h under continuous agitation at 550 rpm using a ThermoMixer C (Eppendorf, Stevenage, UK). Molecules of non-conjugated dye were separated from

fluorescently labelled protein (Cy3-LF^{E687A} or AF488-LFn) by gel filtration chromatography using Sephadex G–25 resin (LFn) or Sephadex G-50 (Sigma, Dorset, UK) in mini-columns (height 90.0 x diameter 5.0 mm). Protein samples were eluted using 100 μL PBS for each fraction. The absorbance of these fractions was measured at 280 nm wavelength, to determine protein concentration, and at wavelengths of 550 nm for samples containing Cy3 or 495 nm for samples labelled with AF488 using nanodrop system (Thermo Fisher Scientific, Paisley, UK). The number of dye molecules conjugated was determined according to the manufacturer.

2.5.1. Cell uptake of Cy3-LF^{E687A} or AF488-LFn

Confocal microscopy was used to visualise the subcellular localization of AF488-LFn or Cy3-LF^{E687A} in HT1080 and MCF7 cells. Sterile round glass coverslips (ThermoFisher Scientific, Paisley, UK) were dipped in 70% ethanol and placed in the bottom of 24-well plates. Aliquots of 50,000 cells/mL were seeded and left overnight to allow cell adherence. Conditioned media prepared with 300 ng/mL AF488-LFn or Cy3-LF^{E687A} in the presence or absence of 1200 ng/mL PAWT or PAL1 was incubated for 2 h at 37°C. After treatment the cells were washed 3 times with cold PBS and fixed for 10 min at room temperature with 4 % [v/v] paraformaldehyde (Sigma, Dorset, UK) in PBS. Coverslips were gently placed on glass slides (Thermo Fisher Scientific, Paisley, UK) containing VECTASHIELD mounting media and DAPI (Vector Laboratories, Peterborough, UK) for visualisation of cell nuclei. The slides were imaged with 63x oil objective using a Leica TCS SP8 (Leica, Milton Keynes, UK) laser scanning confocal microscope.

2.5.2. Live cell imaging

To allow subcellular visualisation of LT components simultaneously in live cell imaging analysis, two distinct fluorophores presenting distinct excitation and emission spectra were

selected. Cy3-NHS (GE Healthcare, Amersham, UK) was conjugated to PAL1 or PAWT molecules, whereas LF^{E687A} and LFn where labelled with Alexa Fluor® 488-NHS.

Live cell imaging microscopy was performed with CAPAN1 and MCF7 cells exposed to fluorescently labelled LT components. Cells were seeded in 35 mm imaging dishes (IBIDI, Uddingston, Glawgow) using Opti-MEM™ media without phenol red supplemented with 10% FBS (both provided by Thermo Fisher Scientific, Paisley, UK), 2 mM L-Glutamine, 50,000 units of penicillin and 0.1 mg/mL streptomycin (Sigma, Dorset, UK) – and incubated at 37°C, 5% CO_2 overnight.

Before imaging cells, nuclei were stained using 1 µg/mL Hoechst 333442 (Thermo Fisher Scientific, Paisley, UK) in PBS for 10 min at room temperature. Conditioned media prepared with 300 ng/mL AF488–LFn or AF488–LF^{E687A} in the presence or absence of 1200 ng/mL Cy3-PAWT or Cy3-PAL1 was added to the cells. Images were acquired using a confocal microscope (LSM 780 microscope, Zeiss, Cambridge, UK).

2.6. Immunocytochemistry

To visualise the localization of MMP14 and CMG2 on cell surfaces simultaneously, cells were seeded on gelatin-coated coverslips in 24 well plates and left overnight to adhere. Cells were washed twice with ice-cold PBS and stained with rabbit anti-MMP14 (Abcam, ab51074, EP1264Y, 1:200) and goat anti-CMG2 (R&D, AF2940, 1:200) for 1 h at 4°C. The cells were then washed three times with ice-cold PBS and fixed in 4% PFA for 10 min at room temperature, incubated in PBS containing 5% donkey serum (Sigma, Dorset, UK) for 1 h at room temperature, and then stained with donkey anti-goat IgG Alexa Fluor 488 (Life Technologies, 1:2000) and donkey anti-rabbit IgG Alexa fluor 594 (Life Technologies, 1:2000) for 1 h at room temperature. Following three washes with PBS, coverslips were mounted using VECTASHIELD containing DAPI (Vectorlabs). The slides were imaged

using a 63X oil objective on a Leica TCS SP8 (Leica, Milton Keynes, UK) laser scanning confocal microscope. Then, Pearson coefficients were calculated using the JACoP plug-in for Image J (methods of Manders for spatial intensity correlation analysis with Costes method for automatic thresholding).

2.7. Radiolabelling of LT components

All radiolabelling was performed using Chelex 100 (Bio-Rad, Watford, UK) treated nanopure water to generate buffers. Diethylenetriaminepentaacetic acid maleimide (maleimide-DTPA, CheMatech, Dijon, FR) was conjugated to LFn or $PAWT^{K563C}$ and isothiocyanatobenzyl-diethylenetriamine-pentaacetic acid (*p*-SCN-Bn-DTPA, Macrocyclics, Texas, USA) was used to modify PAL1 or LF^{E687A}. A tenfold molar excess of chelator was used to modify 200 µg of protein in 100 µL PBS buffer (pH 7.4; maleimide reactions) or 100 µL Sodium Carbonate buffer (pH 9.5; isothiocyanate reactions). The reaction mixtures were incubated for 2 h under agitation (550 rpm) at 25°C in a Thermomixer C (Eppendorf, Stevenage, UK). Free chelator molecules were removed from protein-bound DTPA by size exclusion chromatography using a mini-column (90 x 5.0 mm) with Sephadex G–25 resin (only LFn) or Sephadex G–50 (Sigma, Dorset, UK) eluted with PBS. Absorbance at 280 nm was determined for each fraction eluted using nanodrop system (Thermo Fisher Scientific, Paisley, UK). Pooled fractions of DTPA bound to protein was concentrated to 2 mg/mL. PBS was exchanged to 0.5 M MES Buffer pH 5.5 using centrifugal filters (Millipore, Watford, UK) with three centrifugation steps at 17,500 x g (4°C).

Radioactivity was measured using a dose calibrator (Capintec, New Jersey, USA). Radiolabelling was performed with 20 MBq or 10 MBq of indium-111 (^{111}In) chloride (0.02 M HCl, Mallinckrodt) buffered (0.5 M MES Buffer pH 5.5) added to 20 µg of Bn-DTPA-LF^{E687A}, Bn-DTPA-PAL1, DTPA-$PAWT^{K563C}$ or DTPA-LF. The reaction mixture was incubated at room temperature for 2 h. The radiolabelling purity of [^{111}In]In-DTPA-LF^{E687A},

[^{111}In]In-DTPA-PAL1, [^{111}In]In-DTPA-PAWT^{K563C} or [^{111}In]In-DTPA-LFn, samples was determined by instant thin-layer chromatography (iTLC) using 0.1 M Citrate Buffer at pH 5.5 (Sigma, Dorset, UK) as the mobile phase and strips of glass microfiber chromatography paper (Agilent, USA) impregnated with silicic acid as the stationary phase using a radio-TLC AR-2000 imaging scanner (Eckert & Ziegler, Germany).

2.7.1. Stability of radiolabelled LT components

To mimic tracer stability in vivo, all LT radiolabelled components were incubated with commercially available mouse serum (Sigma, Dorset, UK). After radiolabelling reaction, compounds (1 MBq in 10 µL) were incubated in 500 µL of mouse serum at 37°C under agitation (300 rpm, Eppendorf, UK). At each time point, 5 µL of the mixture was removed, added to sample buffer (without denaturing agent), and heated (10 min, 70°C) before being analysed by SDS-PAGE. Samples were onto a 4-12% Bis-Tris protein gel (170 V, 40 min). The gel was then exposed to Super Resolution Phosphor screens (Type SR, PerkinElmer) and developed on the Cyclone Plus Storage Phosphor system (Perkim Elmer). For reference, the gel was stained with coomassie stain (SimplyBlue^{TM}) to correlate each radioactive band to specific protein weights. To evaluate in vitro stability mimicking cell-based assays, tracer stability was also analysed in 500 µL of PBS and incubated at 37°C (at 300 rpm) and analysed by iTLC as described above.

2.7.2. Saturation binding assay

Radioligand saturation cell binding experiments were carried out to determine the apparent affinity constant (K_D) and maximum number of binding sites (B_{MAX}) on cancer cells for ^{111}In-[^{111}In]In-DTPA-PAL1 or [^{111}In]In-DTPA-PAWT^{K563C} and membrane anthrax receptors. Briefly, 50,000 cells/well were plated and incubated overnight in a 24 well plate at 37°C, 5% CO_2. Adherent cells were then washed twice with PBS and fixed for 10 min at

room temperature with 4 % [v/v] paraformaldehyde (Sigma, Dorset, UK) in PBS. The fixative agent was removed and cells were washed two times with PBS and incubated with blocking buffer consisting of 10 % FBS (ThermoFisher Scientific, Paisley, UK) in PBS for 1 h at room temperature. The total number of cells was determined from a different plate that was not fixed. After trypsinisation live cells were counted using an automated cell counter *Countess II* and trypan blue solution 0.4% [w/v] (both provided by ThermoFisher Scientific, Paisley, UK). Saturation binding assays were performed with increasing concentrations (0–50 nM) of radiotracer in blocking buffer (10 % FBS in PBS) in a total volume of 300 µL for 3 h at room temperature. Cells were then washed twice with ice-cold PBS to remove unbound radioactivity and subsequently dissolved in 2 M NaOH and measured in an automated gamma counter 2489 WIZARD^2 (PerkinElmer). K_D and B_{MAX} values were obtained using non-linear regression using a one-site saturation binding model assuming that the amount of nonspecific binding was proportional to the concentration of radioligand added, using GraphPad Prism.

2.7.3. Cell internalisation of radiolabelled LF^{E687A} and LFn

Cell internalisation assays with either 25 nM of [^{111}In]In-DTPA-LF^{E687A} or [^{111}In]In-DTPA-LFn was performed to evaluate their capacity to interact with PA pores and be delivered to cells after the radiolabelling reaction. First, 50,000 cells were seeded in 24-well plates and incubated for 48 h at 37°C, 5% CO_2. Cells were exposed to either [^{111}In]In-DTPA-LF^{E687A} or [^{111}In]In-DTPA-LFn in the presence or absence of 80 nM of different PA variants for 3 h at 37°C using 300 µL of conditioned cell media. Blocking experiment with an excess of unlabelled LFn or LF^{E687A} was achieved with a pre-incubation of a 10-fold excess for 30 min prior to addition of radiotracer and 80 nM PAs. Cells were then washed twice with ice-cold PBS to remove unbound radioactivity and subsequently dissolved in 0.1 M NaOH. Cell lysates were placed in gamma counting tubes and had their radioactivity detected by

automated gamma counter 2470 WIZARD^2 (PerkinElmer). The amount of radioactivity was normalised by the protein content determined by BCA (Sigma, Dorset, UK) assay and used to normalize the values of radioactivity associated with cells.

2.7.4. Stability of radiolabelled LF^{E687A} interaction with PA pre-pores

To assess the affinity of [^{111}In]In-DTPA-LF^{E687A} to PA (pre)pores, CHO-CMG2 cells were plated at a density of 250,000 cells/well in 24-well culture plates. After complete cell adhesion the medium was replaced with DMEM containing saturating concentrations (80 nM) of purified PAU7, PAL1 or PAWT and plates were placed at 4°C for 16 h to allow the cleavage but not the internalisation of PA pre-pores. The medium was removed by aspiration, and the cells were washed gently 3 times with ice cold PBS. DMEM containing various concentrations of [^{111}In]In-DTPA-LF^{E687A} in 300 µL was placed on the plates well. Plates were incubated at 4°C for 2 h. The medium was aspirated, and the monolayers were washed twice with ice cold PBS to remove unbound proteins. Cells were solubilized with 0.1 M NaOH and transferred to individual tubes. The radioactive content of [^{111}In]In-DTPA-LF^{E687A} associated with the cells was measured using an automated gamma counter (Perkin Elmer). To confirm the formation of PA cleaved pre-pores bound to CHO-CMG2 cell receptors, Western blot analysis were performed according to section 2.7 (described above) against PA protein using cells that were incubated with either PAU7, PAL1 or PAWT for 16 h at 4°C to ensure that PA fragments (PA_{63}, 63 kDa) would remain on the cell surface.

2.8. In vivo experiments

All animal procedures were performed in accordance with the UK Animals (Scientific Procedures) Act 1986 and with local ethical committee approval. Mice were housed in individually ventilated cages in sex-matched groups of up to 6 per cage in an artificial day-

night cycle facility with ad libitum access to food and water. No animals were euthanised for welfare reasons.

2.8.1. Pharmacokinetic of radiolabelled LF variants in naïve mice

To measure plasma clearance of the heart, dynamic SPECT/CT chest gated (2 bed positions; 30 s per bed position) imaging was performed after intravenous administration, through a cannula inserted in the tail vein, of [^{111}In]In-DTPA-LFn (3 µg, 3 MBq; 100 µL) or [^{111}In]In-DTPA-LF^{E687A} (10 µg, 10 MBq; 100 µL) in tumour naïve female 8-9 weeks old C.B-17 SCID (Charles Rivers, Harlow, UK) mice (n = 3). During cannula implantation and imaging session mice were anaesthetised by isoflurane inhalation 2.5 % [v/v].

2.8.2. Xenograft tumour models

Tumour xenografts were generated by subcutaneous injection of MDA-MB-231 (5×10^6 cells/ 100 µL 1:1 matrigel, PBS), CAPAN1 (5×10^6 cells/ 100 µL PBS) or HT1080 (1×10^6 cells 100 µL PBS) cell suspensions in the hind flank of SCID animals. A single tumour was implanted per animal. Tumour growth were determined with manual calliper measurements using the following equation $V = (a \times b \times c)/2$, where *a* is the width of the tumour, *b* is the length and *c* the height of the tumour. Animals were used for further studies when tumour volume exceeded 0.2 mL, as measured by calliper, after randomisation into groups.

2.8.3. Pharmacokinetic of radiolabelled PA variants in tumour bearing-mice

To determine the pharmacokinetics of PA variants in vivo, dynamic whole-body SPECT images (10 bed positions; 30 s per bed position) were acquired in tumour-bearing mice over 3 h after intravenous injection of [^{111}In]In-DTPA-PAL1 or [^{111}In]In-DTPA-PAWT^{K563C} (10 MBq, 20 µg, 100 µL). Subsequently whole-body CT images were acquired. Data was reconstructed and analysed as section. Three mice were used per group.

2.8.4. Imaging of radiolabelled LF^{E687A}

MMP-activatable, PAL1-mediated uptake of radiolabelled LF was evaluated in a pre-targeting-inspired setup. MDA-MB-231 tumour xenograft-bearing mice were administered with [^{111}In]In-DTPA-LF^{E687A} (10 MBq, 10 µg, 50 µL) by intravenous injection, together with PAL1 (20 µg, 50 µL). To determine the PAL1 selectivity of tumour uptake, and thus of MMP-mediated uptake, groups of control animals were administered [^{111}In]In-DTPA-LF^{E687A} alone, or in combination with PAWT (20 µg, 50 µL), PAU7 (20 µg, 50 µL), or with PAL1 and an excess of unlabelled LF^{E687A} (1 mg, 100 µL). Whole Body list mode acquisition SPECT imaging (10 bed position; 30 s per bed position; 5 min) was performed 3 h and 24 h after administration of [^{111}In]In-DTPA-LF^{E687A}/PA combinations. Three mice were used per group.

2.8.5. SPECT/CT imaging and reconstruction

SPECT/CT images were acquired using a VECTor^{4}CT scanner (MILabs, Utrecht, the Netherlands) equipped with a HE-UHR-RM collimator containing pinhole apertures of 1.8 mm diameter. Data were acquired in list mode (photo peak collection 0-1200 keV) using MILabs acquisition software v7.15. Triple-energy-window based scatter correction was applied for a photon peak window (140-200 keV). All images were reconstructed with MILabs reconstruction software v3.24 on 0.8 mm isotropic 3D voxel grids using dual matrix similarity regulated ordered-subset expectation maximization (dual matrix SROSEM). Dynamic scans were reconstructed into 2-min time bins, considering energy widow set over the 173 keV and 247 keV peaks. Subsequently whole-body CT images were acquired at 50 kV and 0.24 mA using continuous rotation (40 degrees/s). After reconstruction, the SPECT and corresponding CT data were co-registered and re-sampled to equivalent 200 µm voxel sizes. CT based attenuation correction was applied.

2.8.6. Image reconstruction and analysis

Reconstructed images were viewed and analysed using PMOD v.3.37 (PMOD Technologies, Zurich, Switzerland). A standard 3D Gaussian filter was applied (1.0 mm full width at half maximum). Using the fusion tool to analyse time activity curves in dynamic scans, SPECT images frames were registered to corresponding CT images and volume of interest (VOI) was defined manually using fixed-volume sphere (radius of 1.5 mm) around the most intense voxel for quantification of activity in tumour or heart. VOI was expressed as %ID/mL by dividing the sum of activity within the VOI expressed as MBq/mL by the total injected activity and normalised to the VOI volume under the assumption that density of the tissue was 1 g/mL.

2.8.7. Ex vivo biodistribution

After the last (24 h) imaging session after radiotracer injection, mice were euthanised by cervical dislocation and selected organs, tissues and blood were removed. The samples were immediately transferred into pre-weighed tubes. After weighing the organs, the amount of radioactivity in each tube was measured using a 2489 WIZARD^2 (PerkinElmer). Counts per minute were converted into radioactivity units (MBq) using calibration curves generated from known standards. These values were decay-corrected to the time of injection, and the percentage of the injected dose per gram (%ID/g) of each tissue was calculated. Tumour tissue was stored in 30% sucrose overnight and flash-frozen using dry ice and stored at -80°C until required for further processing.

2.8.8. Ex vivo autoradiography and H&E

To obtain a microscopic distribution of the different radiotracer in the tumour tissue sections were analysed by autoradiography. Firstly, frozen tumour tissue (8 µm thick) was cut using a cryostat microtome (OTF5000, Bright Instruments Ltd, UK) and mounted on slides

(Thermo Fisher Scientific) which were mounted on glass slides. Tumour tissue sections were exposed to a Super Resolution Phosphor screen (Type SR, PerkinElmer) in autoradiography cassettes for 48 h at 4°C. The screen was then digitally developed using the Cyclone Plus Storage Phosphor system (PerkinElmer).

The same tissue sections were stained with hematoxylin and eosin (H&E) to characterise tissue morphology, staining for the nuclei and cytoplasm respectively. Briefly, tissue sections were first washed under running water for 5 min and subsequently stained with filtered Mayer's hematoxylin (Sigma-Aldrich) for 2 min. Slides were rinsed in PBS for 20 min prior to staining with 1% eosin [v/v] for 10 s. Finally, sections were dehydrated in increasing concentrations of ethanol (70%, 95%, and 100% [v/v] in dH_2O; Fisher Scientific) and cleared in xylene (Fisher Scientific). Slides were mounted using DPX (distyrene, plasticiser, and xylene) mounting medium (Fisher Scientific) and scanned at 20× magnification with the ScanScope CS system (Aperio, USA). Adjacent sections were also stained for CMG2 and MMP14 with an aim to acquire immunofluorescence micrographs, using a protocol based on immunocytochemistry, as above. H&E and immunofluorescence micrographs were co-registered with autoradiography images using MATLAB-based software developed in-house (MathWorks, UK) with manually chosen landmarks.

2.8.9. Immunofluorescence on tissue sections

Adjacent tumour tissue sections from the one stained by H&E were rehydrated in PBS for 10 min. Subsequently they were fixed with 4% PFA for 10 min at 4°C, followed by three washes in PBS for 5 min at room temperature. Samples were incubated in blocking buffer (5% [v/v] donkey serum in PBS) for 1 h at room temperature. Subsequently, slides were incubated with goat anti-CMG2 (R&D, AF2940, 1:50) overnight at 4°C. In the following day after being washed (3 times PBS), slides were incubated for 1 hour with donkey anti-

goat IgG Alexa fluor 488 (Life Technologies, 1:500) at room temperature. Finally, slides were counterstained with DAPI (1:1,000 in PBS) to visualise nuclei and mounted using cover-slips and Vectashield mounting medium for fluorescence microscopy (Vector Laboratories). The slides were imaged using 63× oil objective using a Leica TCS SP8 (Leica, Milton Keynes, UK) laser scanning confocal microscope.

2.9. Statistical analysis

All statistical and regression analyses were performed using GraphPad Prism v7 (GraphPad Software, San Diego, CA, USA). Means were compared using a t-test with Welch's correction for non-equal variances to compare two groups. One-way ANOVA tests followed by Dunnet's post-tests were used to compare multiple groups. Two-way ANOVA tests were used to analyse grouped data. All results are reported as mean ± standard deviation (SD).

Chapter 3

3. Chapter 3: MMP targeting by engineered Lethal Toxin in tumour cells

3.1. Introduction

Matrix metalloproteinases (MMPs) are a family of proteases that degrade a wide range of substrates. Basal expression of MMPs in physiological conditions are usually low with some exception such as in wound healing and in the ovulation process. In cancer, increased MMP activity has been associated with tumour growth, angiogenesis and metastasis and is linked to poorer patient prognosis [61, 239, 240]. In particular, the overexpression of the secreted gelatinases, MMP2, MMP9 and the membrane bound MMP14 [241] is linked to cancer progression. Several drugs were developed based on the inhibition of MMP activity, aiming to achieve a therapeutic effect reducing tumour progression and metastasis [242].

A completely different therapeutic approach targeting MMP activity on the surface of cancerous cells was developed by exploiting the intoxication mechanism of the *Bacillus anthracis* AB-type Lethal Toxin (LT). This toxin uses two different molecules in order to enter the host-cells. First, the cell binding moiety, protective antigen (PA; 83 kDa, PA_{83}) interacts with its native receptors on the cell surface: tumour endothelial marker-8 (TEM8) or capillary morphogenesis gene 2 (CMG2). Subsequently, PA_{83} is cleaved/activated by the ubiquitous furin enzyme or other furin-like proteases into 2 fragments: PA_{20} (20 kDa), corresponding to the N-terminal, and PA_{63} (63 kDa), corresponding to the C-terminal [161]. PA_{63} can oligomerise and form a heptameric or octameric ring-shaped structure (also referred to as a pre-pore) which contains the binding site for the catalytic lethal factor (LF; 90 kDa). The PA/LF complex is then endocytosed and LF escapes from the late endosome by translocating into the cytosol through the PA_{63} pore. Finally, the proteolytic activity of LF causes cleavage and inactivation of different MEKs (MAPK/ERK kinase), and thus

inhibition of the mitogen-activated protein kinase (MAPK) pathway, resulting in cell cytotoxicity [243].

Interestingly, CMG2 and TEM8, PA native receptors, have been implicated in tumour angiogenesis and therefore have been considered potential targets for cancer therapy [213, 244]. Our collaborators, Leppla et al., have modified PA aiming to produce a tumour-selective toxin targeting the MMP activity present in cancer tissues. The cleavage site spans amino acids 161-171, forming a disordered loop in the crystal structure of PA molecule (see Figure 3.1.A). They replaced the amino acid sequence recognised by furin ($_{164}$RKKR) in the wild type PA_{83} (PAWT), to an MMP-labile sequence ($_{164}$GPLGMLSQ) resulting in PAL1 variant (see Figure 3.1.B). This PA variant is described to be susceptible to the hydrolysis of MMP2, 9 and 14 and probably others MMPs [223].

In the current chapter, PAL1 susceptibility to MMP activity was tested and compared with other PA variants. Moreover, a panel of cancer cell lines was characterised for the different phenotypic characteristics required for PAL1-driven cell intoxication of LF (CMG2, TEM8, MMP2 and 14). In addition, cytotoxicity caused by LT treatment in vitro was examined and contrasted with their cell profiling to determine the most and least responsive cell lines. The translocation domain of LF (LFn, 1-254 residues, N-terminal) is sufficient to interact with PA pores on the cell surface and be endocytosed [180]. Therefore, the capacity of PA to deliver two non-toxic variants of fluorescently labelled LF presenting different molecular weights, LFn (30 kDa) and LF^{E687A} (90 kDa, LF with a defective catalytic domain) were evaluated in vitro because both are the variants used here to develop the imaging tool proposed in this thesis in association with PAL1. Notably, Reeves et al. has described that CMG2 physiological role partially correlates with MMP14 and CMG2 is a positive regulator of MMP14 activity [245]. Therefore, analysis of the localisation of MMP14 and CMG2 in

vitro was also examined because the physical proximity of the two components further corroborates the efficiency of these approaches to target cancer cells.

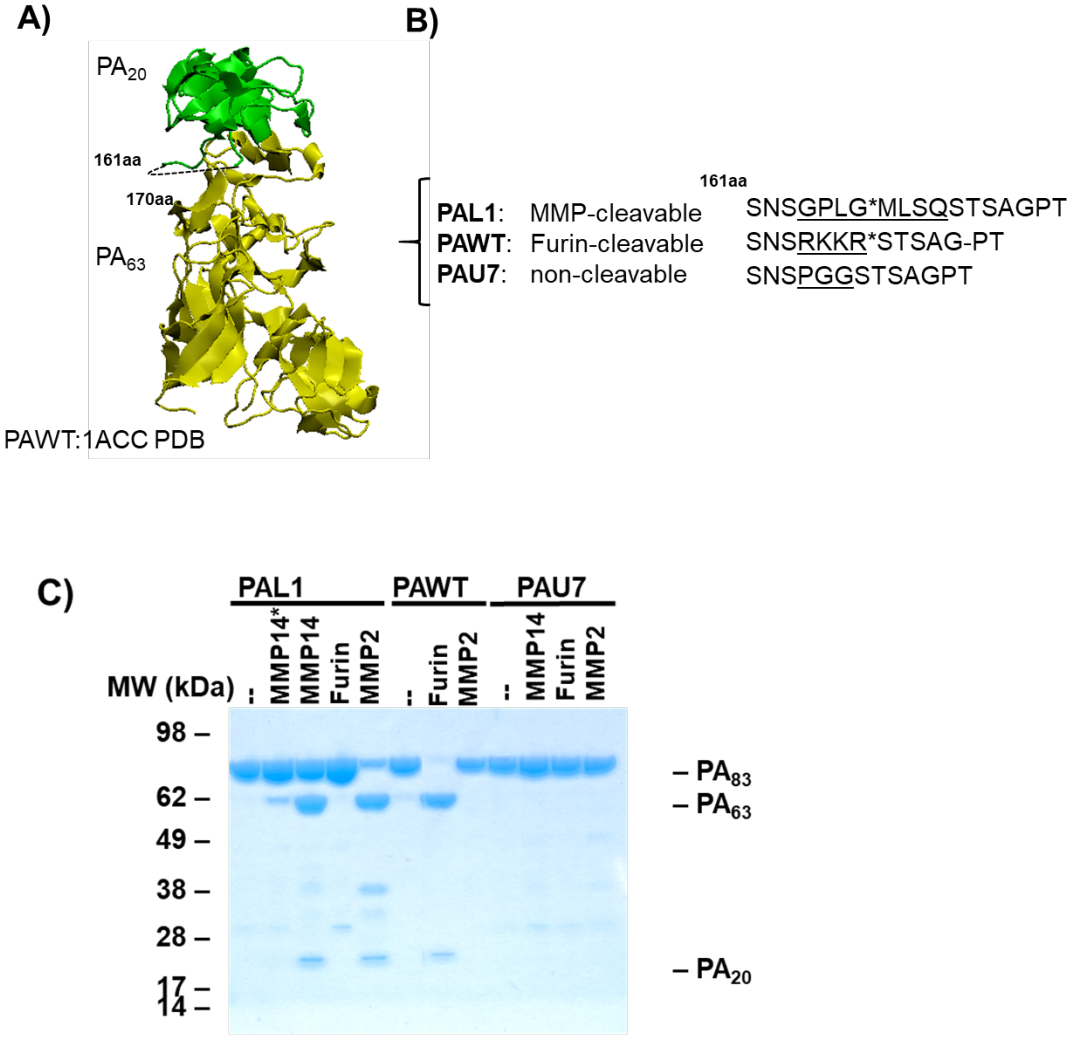

Figure 3.1 Engineered PAs present different susceptibility to furin and MMPs activity

A) Crystal structure of PA_{83} (83 kDa) and the disordered loop, depicted as a dotted line in the structure, where the amino acids of the cleavage site links between the N-terminal PA_{20} (20 kDa) and the C-terminal PA_{63} (63 kDa). B) Aligned amino acid sequence of furin cleavage site (*) of PAWT and the mutants PAL1 and PAU7. C) SDS-PAGE of PA prepared with furin or MMPs in a cell-free assay after incubation for 16 h at 37ºC. pro-MMP14 not pre-activated with furin (MMP14*) was used as a control to evaluate the presence of MMP14 bands in the gel.

3.2. Results

Firstly the effects of either MMP2, MMP14 or furin on cleavage, and therefore activation, of PAL1, PAWT and PAU7 [246] (an uncleavable version) were evaluated (see Figure 3.1.B). Samples of the pure protein PA variants were incubated with the respective enzyme for 16 h at 37ºC, under agitation in the reaction buffer. Subsequently, a small aliquot of the reaction mixture was evaluated by SDS-PAGE, where a differential fragmentation pattern was observed (Figure 3.1.C).

3.2.1. PAL1, PAWT and PAU7 cleavage assay

Two different variants of PA (PAL1 and PAU7) were compared with the wild type molecule (PAWT). As expected, PAL1 was cleaved by MMP14 and MMP2, but not by furin, whereas PAWT was cleaved by furin only (Figure 3.1.C). Besides confirming that PAL1 sequence confers MMP susceptibility, PAU7 variant also presented the expected behaviour, and was not cleavable by furin or MMPs, and can thus be used as a negative control in future experiments (Figure 3.1.C). Surprisingly, a small fragment correspondent to a faint band with 32 kDa was observed in all PAL1 samples, possibly due to molecules cleaved non-specifically throughout the purification process. This band was more evident when a larger quantity of protein was loaded, such as in the lane correspondent to furin + PAL1 condition.

To further test whether the cleavage site for PAL1 corresponded to the one designed, the reaction mixture was analysed by Intact Protein Mass-Spectrometry (see Appendix, Figure A. 3, page 174). As demonstrated in the table below (Table 3.1) the fragments resulting from the MMP2 or MMP14 cleavage were confirmed (predicted masses derived from (www.expasy.org). PAU7 analysis confirmed the resistance of this variant to MMP cleavage: no peak other than that corresponding to the full-length protein was observed (see Appendix, Figure A. 4, page 174).

Table 3.1 LC-MS analysis and theoretical mass of PA variants cleaved by MMPs

Protein fragment	[1]MMPs	[2]Expected MW (Da)	[3]Measured MW (Da)
$PAL1_{20}$	2	19000.2	19002.46
$PAL1_{63}$	2	63908.4	63914.11
$PAL1_{20}$	14	19000.2	19002.46
$PAL1_{63}$	14	63908.4	63914.81
$PAU7_{83}$	2	82464.8	82414.20
$PAU7_{83}$	14	82464.8	82415.20

[1]Matrix metalloproteinases. [2] Molecular weight (MW) based on the sequence and calculated by Expasy Bioinformatics tool (www.expasy.org). [3]Major peaks from Intact protein mass-spectrometry after liquid chromatography are given.

3.2.2. Characterisation of cancer cells for LT delivery system components

A panel of cancer cell lines was characterised for the various elements required in the *Bacillus anthracis* MMP-activatable LT system. Whole cell lysates of breast (MCF7 and MDA-MB-231), pancreatic (B8484 and CAPAN1) and fibrosarcoma (HT1080) cancer cells were analysed by Western blot for the expression levels of CMG2, TEM8, MMP14 and furin.

The CAPAN1, HT1080 and MDA-MB-231 cells presented high levels of CMG2, and MMP14 expression (see Figure 3.2.A-B). Broader bands observed for MMP14 and also CMG2 [198] can be attributed to heterogeneous glycosylation patterns reported in the literature [247]. All cell lines but HT1080 expressed relatively high levels of furin (Figure 3.2.C). B8484 was found to have less CMG2 and MMP14 expression, whereas levels in MCF7 cells were undetectable by this technique (Figure 3.2A-B). Gelatin zymography probing for MMP2 and MMP9 activity revealed high MMP2 levels in HT1080, with far lower activity levels in the other cell lines of the panel (Figure 3.2.D). In the presence of a broad spectrum MMP inhibitor, GM6001, no activity of MMPs present in the conditioned media was observed.

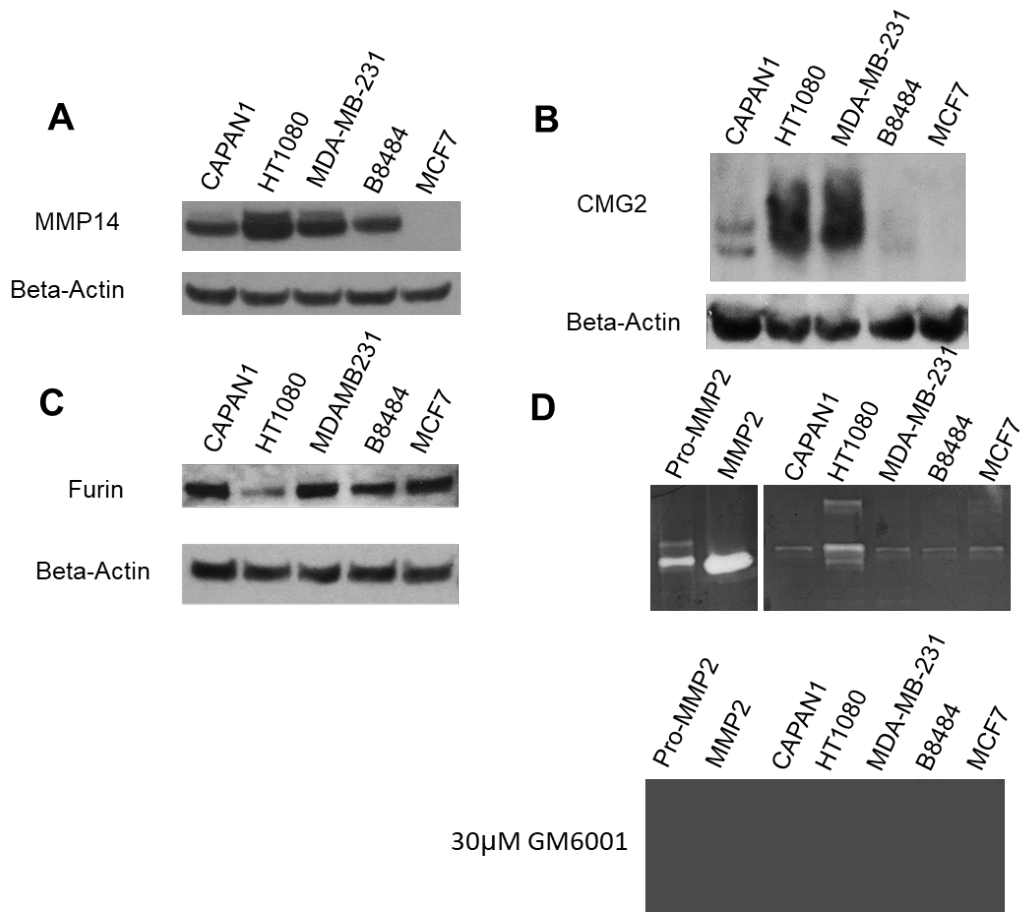

Figure 3.2 Characterisation of cancer cell panel for LT delivery system components

Protein expression levels of (A) matrix metalloproteinase (MMP) 14, (B) capillary morphogenesis gene 2 (CMG2) and (C) furin was analysed by SDS-PAGE and Western blotting of whole cell lysate samples. Beta-actin was used as the loading control. (D) Gelatin zymography gels with serum-free culture media which was incubated with cells overnight. Purified pro-MMP2, MMP2 was used as a reference for molecular weight in the first two lanes. GM6001 a broad spectrum MMP inhibitor demonstrates its inhibitory capacity.

The other native cell receptor for PA is TEM8, therefore, the level of protein expression was also evaluated in the panel of cancer cells. To validate the data obtained by this analysis, CHO cell lines presenting different phenotypes for anthrax receptors were also included in the assay [200]. CHO cells overexpressing either receptor, (CHO-TEM8) or (CHO-CMG2), were originated from a modified parental cell (CHO-PR230) that does not express either receptor ($CMG2^{-/-}$, $TEM8^{-/-}$). Whole cell lysates or membrane enriched protein extracts analysed for TEM8 expression presented no difference among the different CHO cell types

in the 45 kDa band expected (Figure 3.3.A-B). These results indicate that this particular TEM8 antibody is not suitable for probing the target.

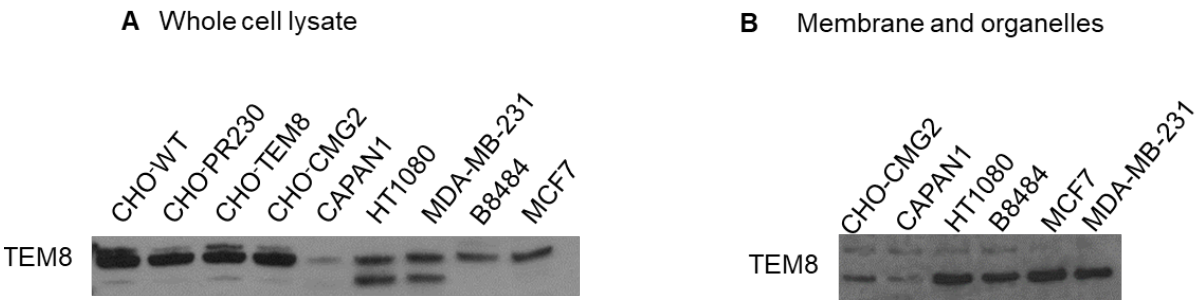

Figure 3.3 Validation of antibody probing for TEM8 anthrax receptor in cancer cells

Comparison of Western-blots between two different sample preparation and probing for TEM8.

3.2.3. Evaluation of LT delivery system using fusion toxin FP59 and PAs

To establish the integrity of LT delivery to tumour cells, in vitro cytotoxicity experiments were performed challenging the panel of cancer cells studied in this project. Since certain tumour cells can be resistant to LF [243] the potent fusion toxin FP59 was used instead. FP59 consists of the N-terminal translocation domain of LF (LFn, 1-254 residues) fused to *Pseudomonas aeruginosa* exotoxin-A catalytic domain [248]. This domain catalyses the transfer of the adenosine diphosphate (ADP)-ribosyl moiety of nicotinamide adenine dinucleotide to the eukaryotic polypeptide elongation factor (eEF2) and thus inactivates eEF2, resulting in inhibition of protein synthesis [249].

Treatments were more efficacious in CAPAN1, MDA-MB-231 and HT1080, compared to B8484 and MCF7 cells at 48 h after treatment. Moreover, PAWT/FP59 treatment was found out to be more efficient than PAL1/FP59 treatment for all the cells (see Figure 3.4).

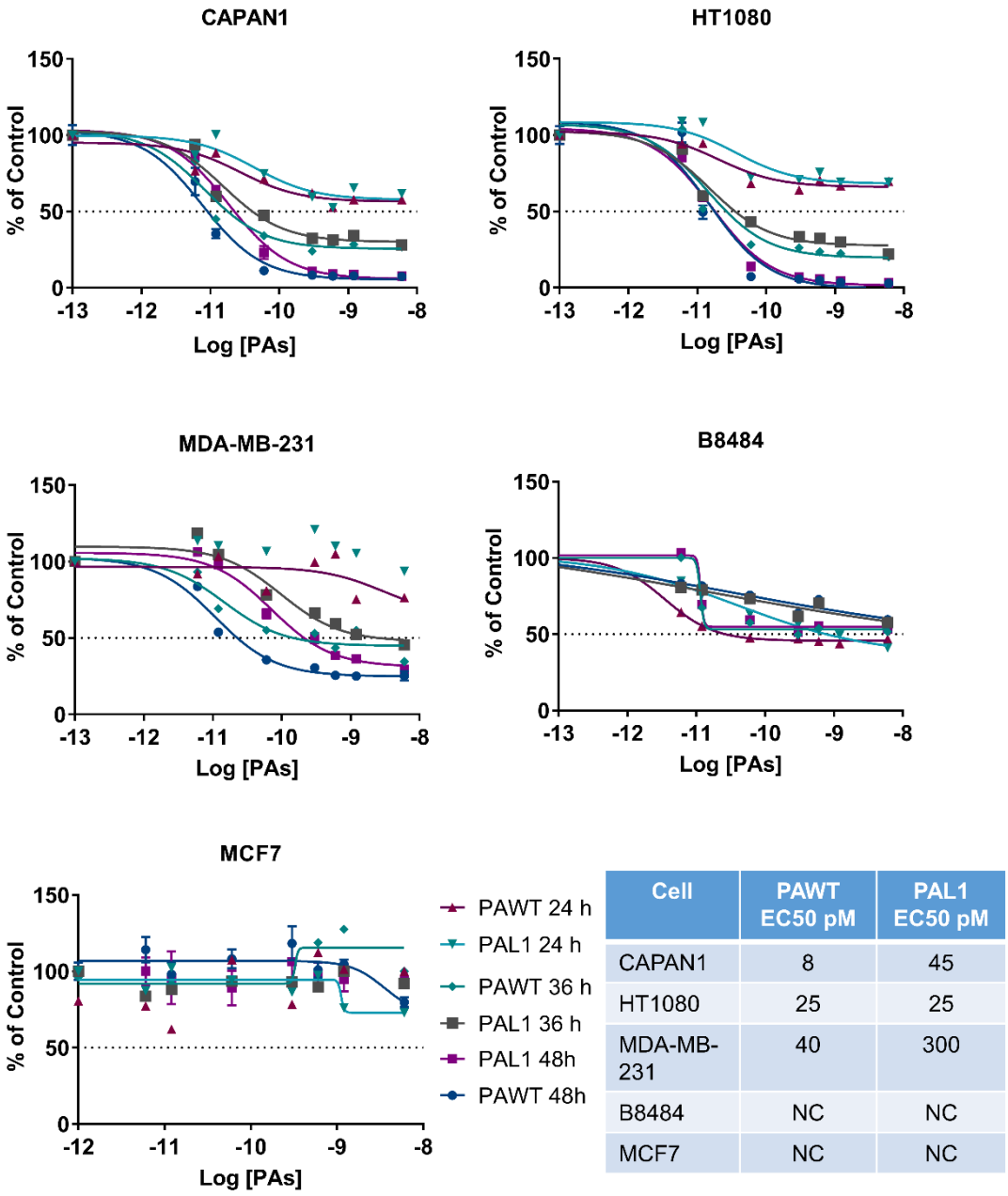

Cell	PAWT EC50 pM	PAL1 EC50 pM
CAPAN1	8	45
HT1080	25	25
MDA-MB-231	40	300
B8484	NC	NC
MCF7	NC	NC

Figure 3.4 Cytotoxicity promoted by PAs/FP59 treatment in cancer cells

Cancer panel present different sensitivity to protective antigen (PAs) and fusion toxin FP59 (0.25 nM) determined by MTT assay. Cells were incubated with PAWT/FP59 or PAL1/FP59 prior to MTT salt addition. Absorbance at 495 nm and the percentage of the control. Effective concentration (EC50) data on table for the different cells. Data are expressed as average ± standard deviation from experiments carried out in triplicate.

The potency of the treatments, represented by the PA concentration where 50% of the total viability is reached (EC50), confirms the differences between the cell lines. Concerning PAL1/FP59 treatment, cell sensitivity can be represented as HT1080>CAPAN1>MDA-MB-

231>>B8484>>MCF7. In comparison, for PAWT/FP59 treatment it can be represented as CAPAN1>HT1080>MDA-MB-231>>B8484>>MCF7. FP59 toxicity relies on the impairment of protein translation by ADP-ribosylation of the translation elongation factor 2 (eEF2) [249]. It is unlikely that the cell lines depend differently to this biogenic pathway, indicating, therefore, that the cytotoxic results may be at least partially explained by the amount of FP59 that reaches the cytosol of these cells delivered by PA pre-pores.

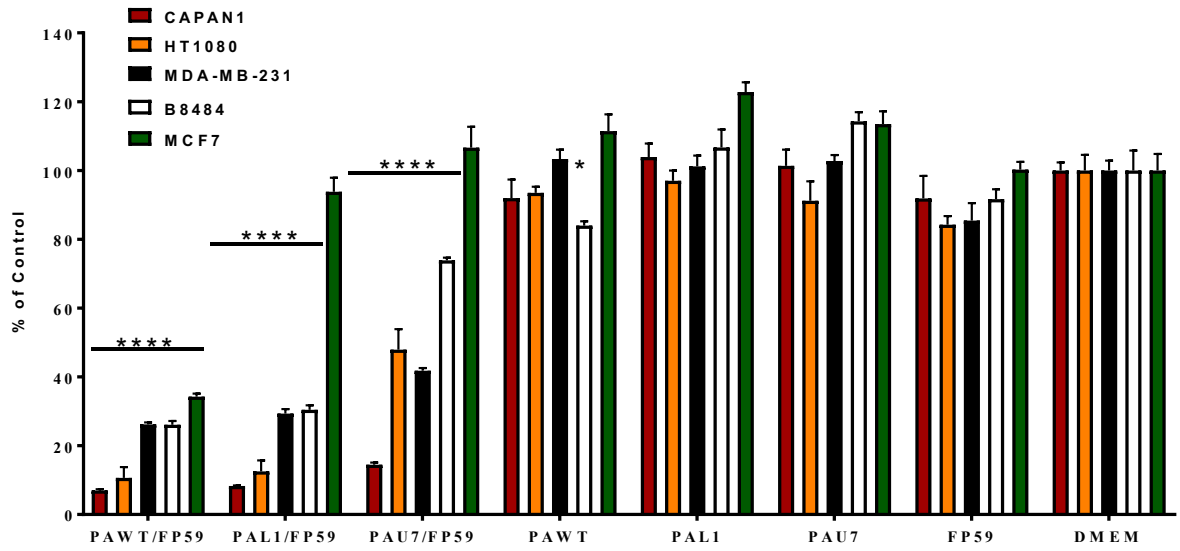

Figure 3.5 Cytotoxicity of LT variants to cancer cells

Cancer cell panel present different sensitivity to protective antigen 3.5 nM PAs and fusion toxin 0.5 nM FP59 determined by MTT assay. Cells were incubated with the different treatment prior to MTT salt addition 48 h after. Absorbance was measured at 495 nm and the percentage of the control was considered as viability. Data are expressed as average ± standard deviation from experiments carried out in triplicate.

Studies including uncleavable PAU7, or omitting either the PAs protein or FP59 toxin showed that the system is highly selective, and requires all components of the system to deliver its payload (see Figure 3.5).These findings are consistent with previous reports using this system on a different panel of cell lines [226]. Surprisingly, cells treated with PAU7/FP59, in this high concentration demonstrated at least some reduction in cell viability,

indicating that possibly PAU7 is being cleaved and able to form competent pre-pores that can translocate FP59.

3.3. Cleavage and activation of PAL1 by MMP activity

The next step was to evaluate whether PAL1 is activated by MMP activity only. To answer this question an MTT experiment was perform in the presence of GM6001 (Ilomastat), a broad-spectrum MMP inhibitor presenting a hydroxamic acid as zinc chelator group. For this experiment HT1080 cells were used, one of the most sensitive cells for PAL1/FP59 treatment which also express MMP2, 9 and 14 (section 3.2.2). After washing the cells, we added GM6001 to the cell and pre-incubated for 30 min before exposing to the different treatments. After 6 h of incubation all the media was removed and replaced with culture media supplemented with serum. After 48 h of incubation, MTT salt was added and the viability was considered as a percentage of the absorbance measured for the control condition.

As expected, in the presence of GM6001 cell viability was restored to the same levels of the one determined to the control condition ($P = 0.001$) (see Figure 3.6.A). Contrastingly, in the case of PAWT there was no increase in cell viability after exposure to GM6001, further confirming that the modified PAL1 sequence resulted in preferential susceptibility to MMP activity. To confirm the presence of MMP activity in the cell conditioned media, samples were collected over 6 h. At 2 h after the addition of fresh media, two bands correspondent to MMP2 and MMP9 were observed (Figure 3.6.B). Taken together, these results confirm the requirement of MMPs to activate PAL1 but not PAWT.

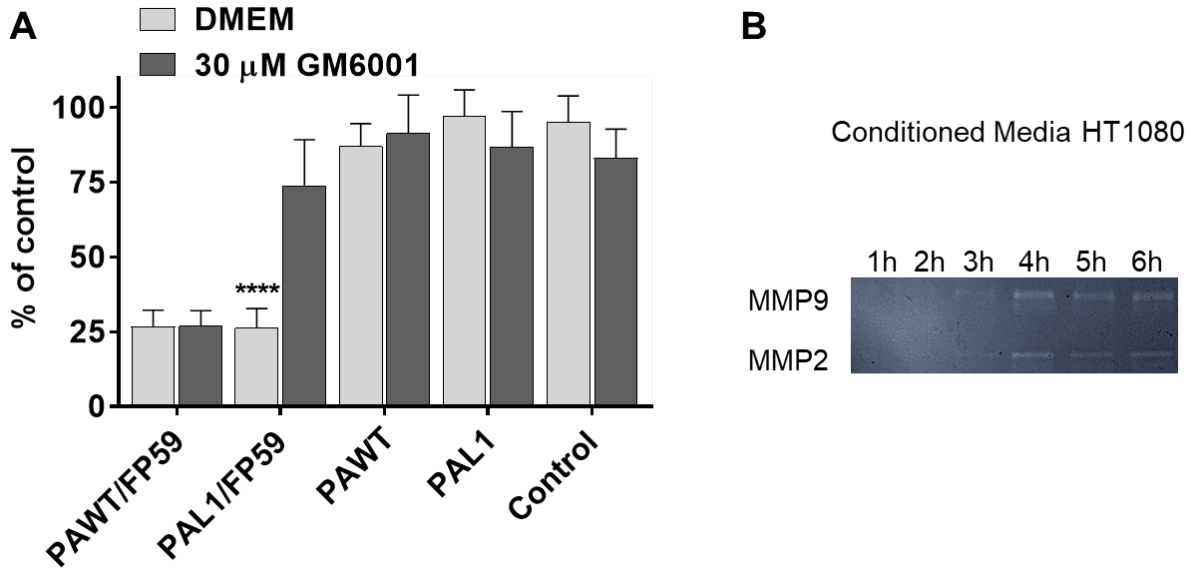

Figure 3.6. MMP inhibitor protects cells from MMP-targeted PA proteins

A) HT1080 cells were washed before pre-incubating with broad matrix metalloproteinase (MMP) inhibitor GM6001 for 30 min. Subsequently 3.5 nM of either PAWT or PAL1 was added in combination with 0.5 nM FP59 toxin. After 6 h, the medium containing the toxins and MMP inhibitors was removed, and fresh serum containing medium was added. 48 h after treatment, MTT salt was added to determine cell viability. B) Zymography gels demonstrating the presence of MMPs secreted in the cell culture media obtained from HT1080 cells starts as soon as 2 h after replacing the media for a serum-free type.

To evaluate if an engineered variant of PAWT containing one single cysteine residue substitution ($PAWT^{K563C}$) was still susceptible to furin proteolysis a cell-free cleavage assay was performed (section 3.2.1). The results demonstrate that the replacement of the cysteine does not hinder the enzymatic activity of furin against $PAWT^{K563C}$ and both fragments, presenting the expected molecular weight, were observed by SDS-PAGE analysis (see Figure 3.7.A).

Additionally, the capacity of $PAWT^{K563C}$ to form competent pre-pores and deliver the fusion toxin FP59 into CAPAN1 cells was assessed by MTT assay. After exposing cells to a variety of $PAWT^{K563C}$ concentrations combined with 0.5 nM FP59 for 48h, the cytotoxicity revealed by MMT assay was similar to cells treated with FP59/PAWT (Figure 3.7.B). In MCF7 cells,

no such effect was observed (see Figure 3.7.C). These results suggest that PAWT^{K563C} interacts with CMG2 and TEM8 in a similar way as PAWT, can be cleaved, oligomerise and form de novo binding sites for FP59 as PAWT molecules.

All these results together provide ample evidence that the mutated version of PA provided by our collaborators corresponds to the predicted resistance/susceptibility to enzymatic hydrolysis and can be used for further experiments with the advantage of having one cysteine residue.

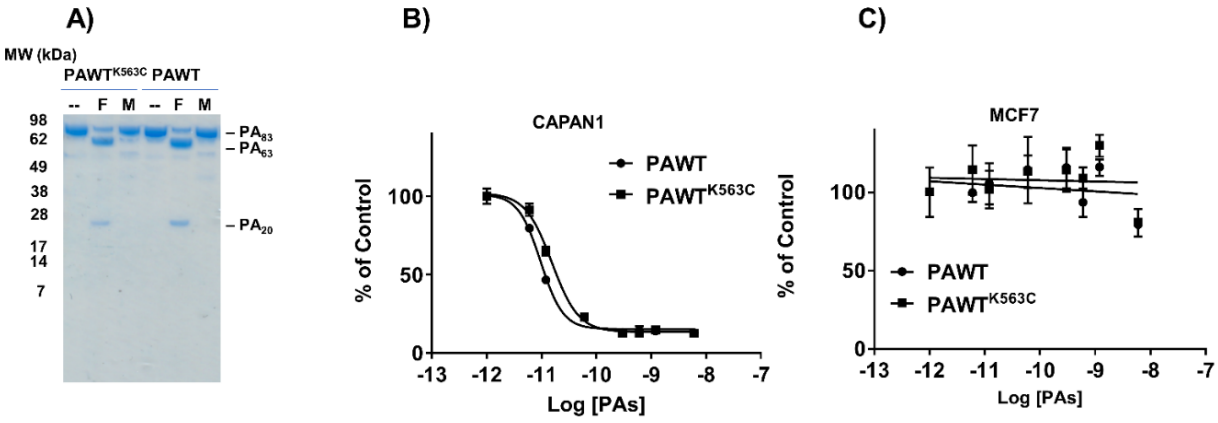

Figure 3.7 PAWT^{K563C} mutant presents the same characteristics as PAWT
Cell-free cleavage assay using purified Protective antigen (PA) variants incubated with different enzymes, analysed by SDS-PAGE. A) After incubation for 16 h at 37ºC of the different PAs in the presence or not of furin (F), Matrix Metalloproteinase 2. B-C) Cytotoxic assay using variable concentrations of PAs and 0.5 nM of FP59 fusion toxin.

3.4. Subcellular localisation of fluorescently labelled LT components in a cell-based assay by confocal microscopy

LFn (30 kDa) and LF^{E687A} (90 kDa) variants are non-toxic versions of LF and both were chosen to be tested for the development of MMP-activity imaging tool, in association with PAL1, in cancer models proposed for the current thesis. Therefore, the delivery of these variants by PA pores were tested in cell-based delivery assays. To visualise these molecules

under the microscope, they were fluorescently labelled and exposed to cells that have presented differential susceptibility to LT intoxication as described above (section 3.2.3).

It is important to state that for each ring-shaped pre-pore containing 7 or 8 cleaved PA_{63}, there are 2-3 binding sites that can be occupied by LF [167]. Hence, for the current experiments the concentrations used were based on this ratio of approximately 1:3-4 LF/PA molecules. Additionally, in a cell-based assay, processing of PA on the cell membrane (interaction with receptor, proteolytic cleavage, and oligomerisation) is the limiting step for LF interaction and endocytosis. In previous studies, Beauregard et al. have demonstrated that exposing macrophages to 12 nM PAWT and performing immunofluorescence in fixed non-permeabilised cells PAWT persisted in the cell membrane for 90 min [168]. They further demonstrated that PA bound to the membrane receptor stays accessible for 65 min to LF interaction and cell intoxication. The LT intoxication process is considerably slower when compared to other receptor mediated endocytosis, such as for epidermal growth factor receptor and transferrin [250, 251].

3.4.1. Confocal microscopy of fluorescently labelled LF^{E687A} and LFn

LF^{E687A} was fluorescently labelled using a Cy3-dye via a lysine-directed activated ester of Cy3, resulting in Cy3-LF^{E687A}. The identity of the resulting construct was determined via absorbance measurements, and the number of Cy3 moieties per molecule of LF^{E687A} was calculated to be 6:1. Cells were exposed to 14 nM of PA variants and 3.5 nM of Cy3-LF^{E687A} for 3 h at 37ºC before fixation and preparation for analysis under confocal microscope.

Cy3-LF^{E687A} was taken up by MMP-expressing cells when combined with the MMP-activatable PAL1, and when combined with furin-activatable PAWT. Negligible uptake was observed when no PA was added (Figure 3.8). Similarly, only little uptake was observed in MCF7 cells with a slight increase in the presence of PAWT, indistinguishable from Cy3-

LF^{E687A} non-specific uptake, potentially due to micropinocytosis [252]. Even though PAWT/FP59 treatment does present cytotoxic effects to MCF7 cells, as reported above (section 3.2.3) indicating that FP59 is translocated in these cells. This observation may be explained because the amount of FP59 molecules necessary to cause cytotoxicity after 48 h is much less than the uptake of Cy3-LF^{E687A} in these cells under these experimental conditions.

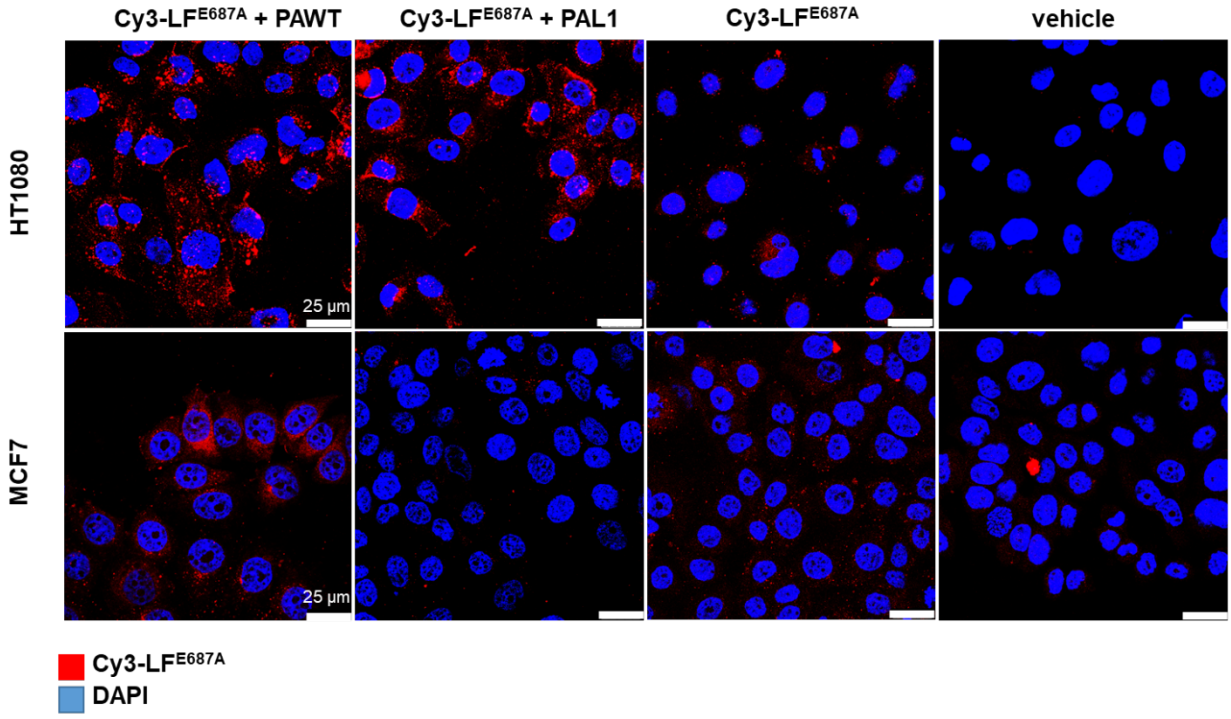

Figure 3.8 Cell uptake of Cy3-LF^{E687A} depends on PA variants and cell phenotype

Cells were treated with Cy3 fluorescently labelled 3.5 nM LF^{E687A} (Cy3- LF^{E687A}) and 14 nM PAs variants for 3 h at 37°C before fixation. Representative images of non-permeabilised cells imaged under a confocal microscope.

To study the cellular delivery of the smaller LF variant, the translocation domain LFn was modified with the fluorescent dye NHS-AlexaFluor488 (AF488). The identity of the resulting AF488-LFn was determined via absorbance measurements to determine the number of AF488 moieties per molecule of LFn as 4:1. Further analysis of the specific uptake and subcellular distribution of AF488 was performed using confocal microscopy

imaging of HT1080 and MCF7 cells in the presence or absence of PAL1 or PAWT (Figure 3.9). A higher amount of AF488-LFn was observed in HT1080 cells treated with PAL1 or PAWT when compared to cells treated with AF488-LFn alone. Contrarily, AF488-LFn was not taken up by MCF7 cells in the presence of PAL1 but it was internalized by MCF7 cells in the presence of PAWT. These results corroborate the cytotoxic assays presented previously in this chapter (section 3.2.3), confirming the delivery of AF488-LFn as PA dependent.

Differently from Cy3-LF^{E687A}, AF488-LFn reaches nuclei/nucleolus in HT1080 cells when combined with PAL1 or PAWT. One possible explanation for this difference is that proteins smaller than 40 kDa can diffuse through the nuclear pore complex [253], as is the case for AF488-LFn.

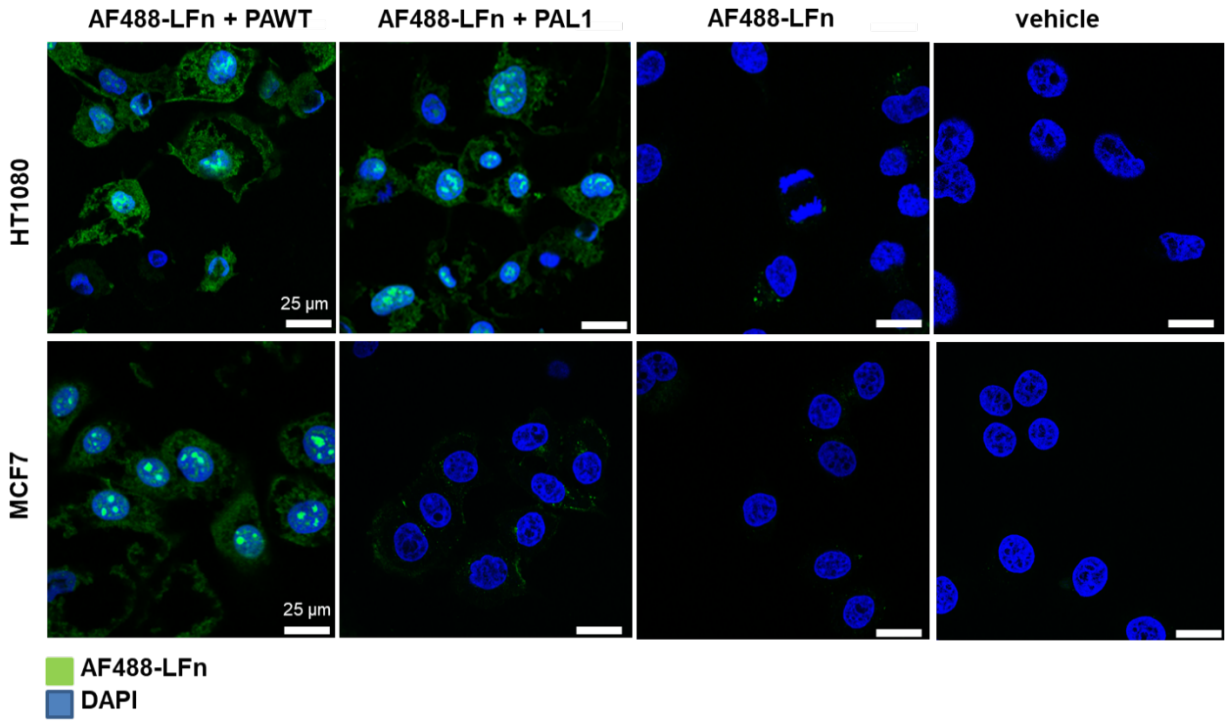

Figure 3.9 Subcellular distribution of AF488-LFn depends on PA variants and cell phenotype

HT1080 or MCF7 cells were treated with AF488 fluorescently labelled LFn (3.5 nM AF488-LFn) and 14 nM PAs variants for 3 h at 37°C before fixation. Representative images of non-permeabilised cells imaged under a confocal microscope.

3.4.2. Live cell imaging of LT fluorescently labelled

To further evaluate the cellular dynamics of LT uptake in cancer cells and to reduce potential artefacts due to fixation processes, live cell imaging was used with fluorescently labelled LT components. PA variants were fluorescently labelled with the Cy3 dye via lysine-directed reaction. The resulting molecules, Cy3-PAL1 and Cy3-PAWT, presented 10 moieties of dye per molecule according to absorbance measurements. LF^{E687A} and LFn molecules were labelled with AF488 dye as above. Cells were evaluated over 3 h after exposure to (3.5 nM AF488-LF variants; 14 nM Cy3-PAs) (Figure 3.10).

In CMG2-positive CAPAN1 cells, high uptake of Cy3-PAL1 was observed in the plasmatic membrane which increased overtime, possibly indicating the presence of its native receptors. This increase also correlated with the presence of either AF488-LF^{E687A} or AF488-LFn in the perinuclear region.

Differently from cells treated with AF488-LFn and PAs which were fixed, no AF488-LFn signal was associated with the nuclear region stained with Hoechst dye, indicating that LFn may not reach the nuclei and the subcellular distribution pattern observed in the experiment described above may be an artefact due to the chemical fixation. In a control condition where no Cy3-PAL1 was added, AF488-LF^{E687A} and AF488-LFn was also observed within the cell boundaries indicating that these molecules can be taken up by the cell non-specifically, probably through micropinocytosis characterised by vesicles presenting diameter below 100 nm [254].

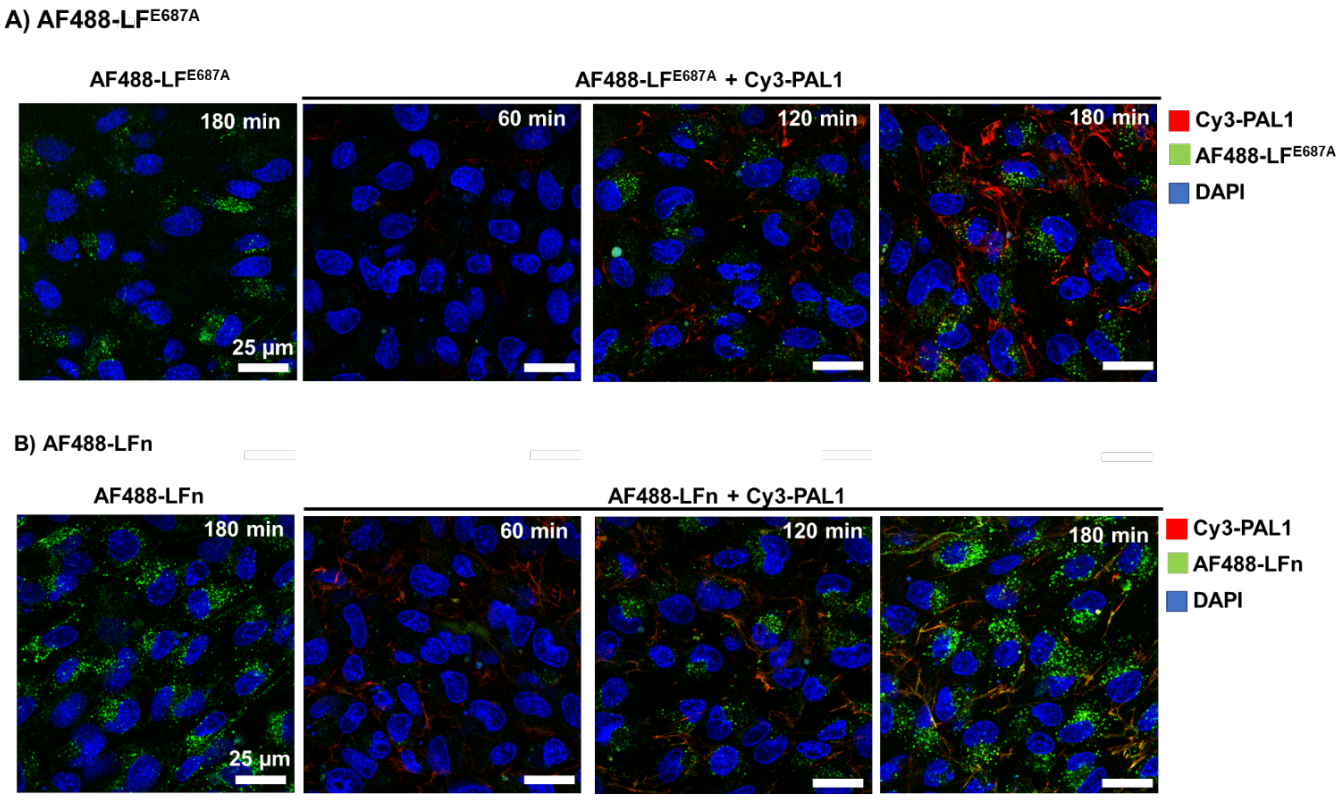

Figure 3.10 MMP-expressing cell line treated with fluorescently labelled LT

CAPAN1 cells were treated with AF488 fluorescently labelled LF variants (A) AF488-LF^{E687A} or (B) AF488-LFn) and Cy3 labelled PAL1 (Cy3-PAL1) for 180 min at 37°C. Images were acquired of live cells (not-fixed) under a confocal microscope.

Differently, MCF7 cells did not present Cy3-PAL1 associated with their plasma membrane, possibly indicating a lower number of anthrax receptors. However, an increasing amount over time of either AF488-LF^{E687A} or AF488-LFn was observed in the control condition where no PAL1 was added (Figure 3.11).

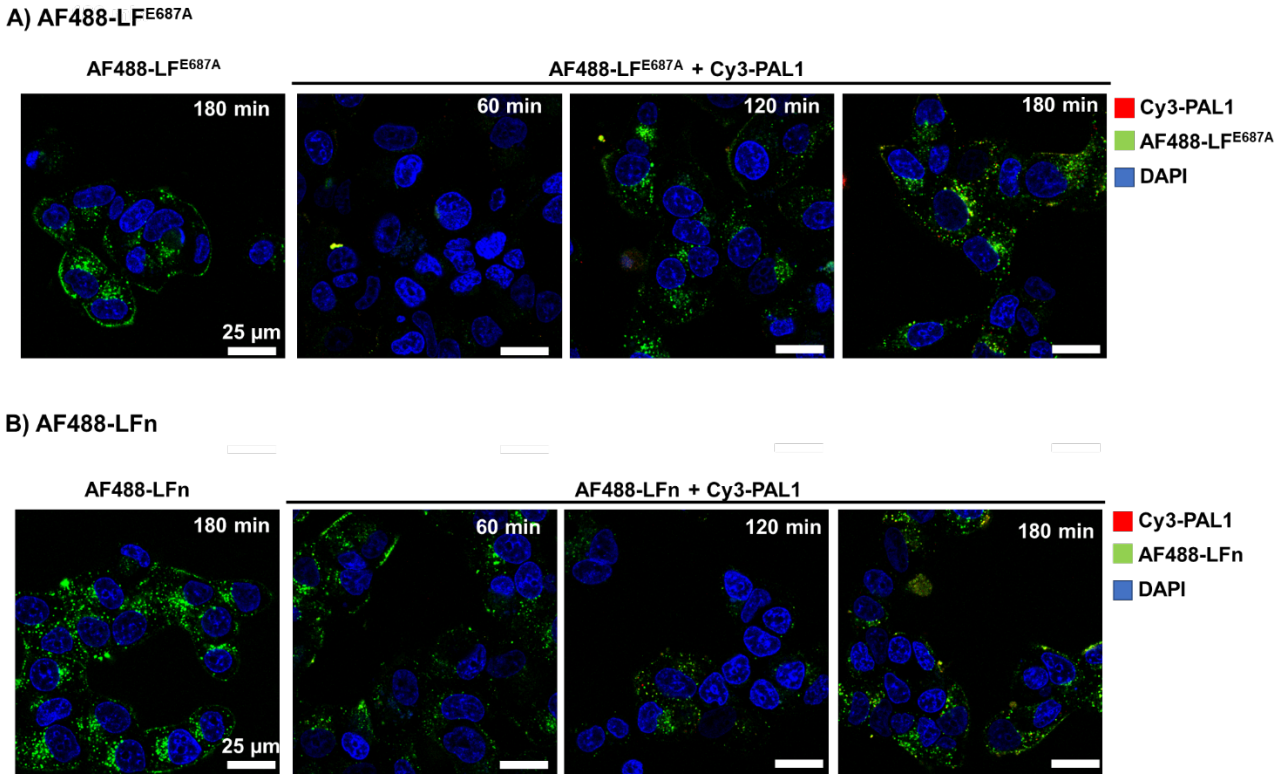

Figure 3.11 MMP-non-expressing cell line treated with fluorescently labelled LT

MCF7 cells were treated with 3.5 nM of AF488 fluorescently labelled LF variants (A) AF488-LF^{E687A} or (B) AF488-LFn) and Cy3 labelled PAL1 (Cy3-PAL1) for 180 min at 37°C. Images were acquired of live cells (not-fixed) under a confocal microscope.

3.5. Co-localisation of CMG2 and MMP14

Next, the distribution of MMP14 and CMG2 on the cell membrane was investigated by immunofluorescence of non-permeabilised fixed cells (see Figure 3.12) [255]. Previously MDA-MB-231 cells, presented expression of both MMP14 and CMG2 by Western blot analysis (section 3.2.2). Therefore, after performing immunocytochemistry for both protein, MDA-MB-231 cells were analysed by confocal microscopy and the resulting images were analysed using Image J software.

The Pearson's Correlation coefficient calculated for MMP14 signal and CMG2 was 0.90 in MDA-MB-231 cells. This indicates that these two molecules are codistributed in this cell line. Differently, in MCF7 cells no signal was observed for either MMP14 or CMG2.

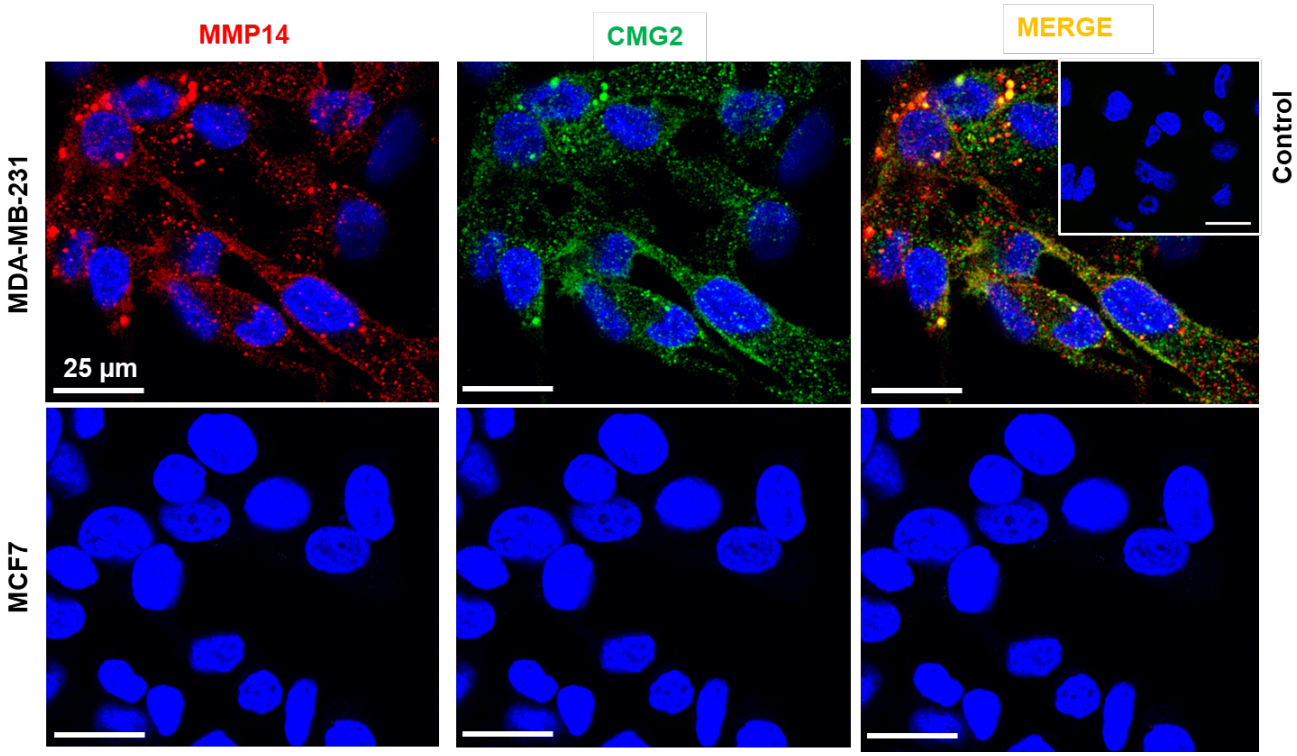

Figure 3.12 CMG2 and MMP14 co-localise

Immunofluorescence for MMP14 and CMG2 was performed in non-permeabilised cells. In merged images the yellow colour indicates that MMP14 and CMG2 colocalise on the cell surface. DAPI is used for nuclear staining as blue colour.

3.6. Discussion

Targeting MMP activity on the surface of cancerous cells by the intoxication mechanism of an engineered anthrax lethal toxin was previously developed by our collaborators [223]. They demonstrated that PAL1, an MMP-cleavable protective antigen variant, allows for selective delivery of lethal factor, LF, to tumour tissue in vivo, for therapeutic gain in pre-clinical experiments [225, 226, 256]. Here, this system is further tested and validated to the development of a molecular imaging system using a radiolabelled form of LF.

In a cell-free assay the engineered cell binding moiety of LT, PAL1, was susceptible to both MMP14 and MMP2 cleavage, but not to furin. The fragments resultant from the proteolysis were compatible with the designed labile bond. However, MMPs are a large family of proteases, with 23 members described in humans presenting high similarity of the catalytic

domain and also overlap in substrate targets [21]. As in the current work, PAL1 hydrolysis by other members of the MMP family was not tested systematically it is not possible to affirm that PAL1 cleavage sequence is specific towards MMP2 and MMP14 only.

To develop a tumour model to test our imaging approach a panel of cancer cell line was selected. A detailed characterisation for the different components required for the intoxication mechanism of LT was performed followed by cytotoxic assays of LT treatment. Initially, the effect of PAL1/FP59 treatment in cell viability was correlated with the presence of MMP2 activity, MMP14 or CMG2 expression. A correlation of 0.62 between MMP2 activity and cell sensitivity to PAL1/FP59 treatment was calculated, which indicates that there is no established correlation between these two variables (Figure 3.13.A). Even though MMP14 activity was not measured directly, its protein expression levels correlated statistically significantly with FP59 intoxication (R = 0.88; *P* = 0.02) (Figure 3.13.B).

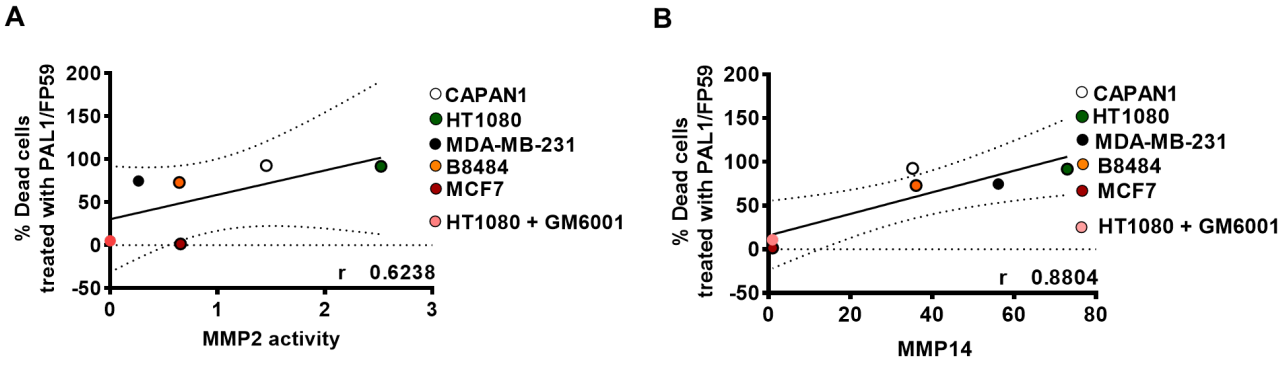

Figure 3.13 MMP14 expression confers sensitivity to PAL1/FP59 treatment in cancer cells

The Y axis is the percentage of dead cells calculated from MTT assays performed 48 h after treatment with 500 ng/mL PAL1 in addition to 12.5 ng/mL FP59. A) X axis is the signal obtained for MMP2 assessed by gelatin zymography. B) X axis is the relative optical density for MMP14 obtained from Western blot analysis of whole cell lysate and normalised by beta-actin signal.

As part of the characterisation of the LT system it was necessary to determine the presence and level of expression of anthrax receptors TEM8 and CMG2. However, in the current project only CMG2 expression levels could be determined reliably.

Notably, the sensitivity of the cells to FP59/PAL1 treatment did not correlate with the expression of CMG2 only, indicating that other factors might influence FP59 delivery (see Figure 3.14.B). Possibly, there is a contribution of TEM8 receptors to the cytotoxic effect that could not be determined here. Interestingly, MMP14, in contrast, did correlate with CMG2 expression ($R = 0.84$; $P = 0.035$) (see Figure 3.14.A). Additionally, immunofluorescence analysis of both CMG2 and MMP14, demonstrated that these two membrane proteins are codistributed on the cell. Similar results, corroborating the intimate relationship between MMP14 and CMG2, were described by Reeves et al. [245], who demonstrated that the presence of CMG2 enhances MMP14 activation. Contrastingly, a more recent publication casted doubt over this claim [206]. Goot et al., demonstrated that the activities of both MMP14 and MMP2 were in fact higher in the uterus of CMG2 null mice than in that of control mice. This demonstrates that more studies are necessary to better understand the physiological roles of CMG2.

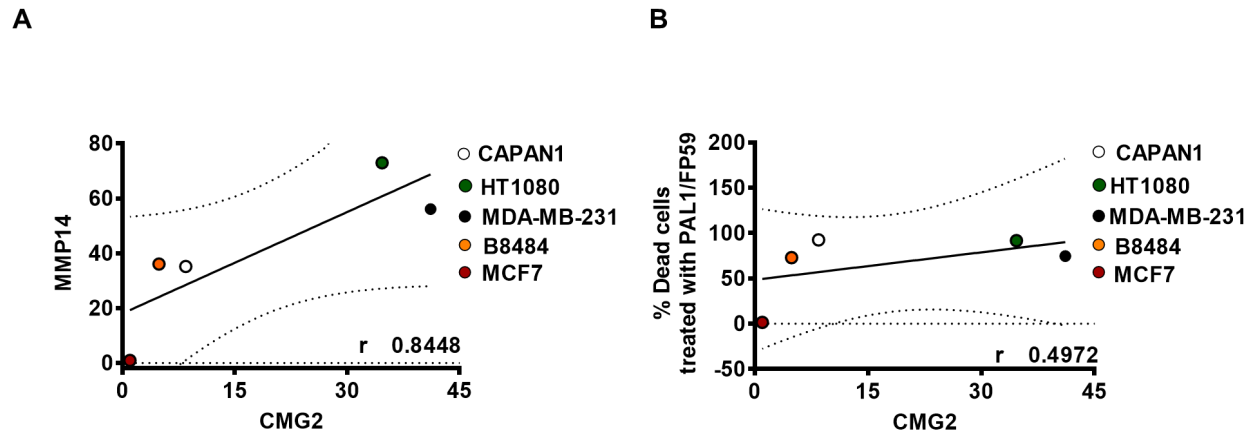

Figure 3.14 CMG2 expression and MMP14 correlates

X axis is the relative optical density for CMG2 obtained from Western blot analysis of whole cell lysates normalised by beta-actin signal. A). Y axis is the relative optical density for MMP14 obtained from Western blot analysis of whole cell lysate and normalised by beta-actin signal. B) Y axis is the percentage of dead cells calculated from MTT assay, performed 48 h after cell exposure to 500 ng/mL PAL1 in addition to 50 ng/mL FP59.

A fluorescently labelled version of LFn, (AF488-LFn) and LF^{E687A} (Cy3-LF^{E687A}) developed in the current work, further corroborates that these proteins depend on PAL1 presence to be delivered into the cytoplasm to cancer cells. Those cells presenting the higher levels of MMP14 and CMG2 were clearly more susceptible to the delivery of either LFn, (AF488-LFn) or LF^{E687A} (Cy3-LF^{E687A}) to their cytoplasm.

3.7. Conclusion

PAL1 is cleaved by MMP activity and is capable of delivering fluorescently labelled LF^{E687A} or LFn into the cell cytoplasm. CMG2 and MMP14 have similar distribution patterns on the cell surface, which can be exploited by PAL1/LF delivery system. Among the five different tumour cell lines tested here, CAPAN1, HT1080, and MDA-MB-231 are the ones which presented higher susceptible to intoxication by PAL1/FP59 or PAWT/FP59. Taken together the data presented here demonstrates that PAL1/LF^{E687A} or PAL1/LFn hold promise to be used as an imaging method targeting MMP activity in tumour cells.

Chapter 4

4. Chapter 4: In vitro evaluation of radiolabelled Lethal Toxin variants in tumour models

4.1. Introduction

Increased activity of matrix metalloproteinase (MMP) is associated with poor prognosis and metastasis in different cancer types [68]. To exploit this feature, the protective antigen (PA) of the binary anthrax lethal toxin (LT) was modified by our collaborators to form a pore in cell membranes only when cleaved by MMPs (PAL1) [223]. Anthrax lethal factor (LF) is then able to translocate through these pores into the cytosol of tumour cells. In the current chapter, radiolabelled LT components were developed to allow further characterisation of their interaction with cancer cells aiming to develop a novel radiotracer for non-invasive MMP activity imaging using Single Photon Emission Computed Tomography (SPECT) as the imaging modality.

Here, the chosen radionuclide to radiolabel the LT components was Indium-111 (^{111}In). Different protein based imaging molecules with similar characteristics as the LT components have been ^{111}In-radiolabelled because of its compatible physical properties (half-life of 2.8 days) and also the emission of two γ-rays (171 keV and 245 keV) which can be detected by SPECT [257]. Additionally, ^{111}In has a low-cost production and a well-established radiochemistry [122, 258]. To achieve ^{111}In-radiolabelling, firstly the LT components were modified to provide a suitable site for radiolabelling [258]. A novel radiotracer must undergo in vitro validation to assess target specificity, uptake and its impact on cellular survival [259, 260]. As PA serves as the delivery vehicle for translocation of LF into the cytosol of the cells, furin-cleavable PA variant with an engineered cysteine ($PAWT^{K563C}$) and MMP-cleavable PAL1 were used to study the interaction between PA and its native receptors in a panel of cancer cells. In addition, the specific interaction between $PAWT^{K563C}$ and its

receptors, capillary morphogenesis gene 2 (CMG2) and the tumour endothelial marker 8 (TEM8), was determined in radioligand binding assays. Additionally, it was also tested whether ^{111}In-radiolabelling of the two non-toxic LF variants used here, truncated LFn (1-254 residues, N-terminal) and full-length LF^{E687A} (presenting a defective catalytic domain) would impair their delivery by PAL1 pores to the panel of cancer cells. Finally, the stability of all the radiotracers developed here was tested in mimicking in vivo conditions.

4.2. Results

4.2.1. Site-specific or non-site-specific conjugation of LT components with different chelators

In order to develop ^{111}In-radiolabelled LT compounds, first these molecules were modified with a chelator. Bifunctional diethylenetriamine pentaacetate (DTPA) was the molecule of choice that presents the capacity to combine a radionuclide to a targeting construct, creating a single structure. DTPA is a widely used acyclic chelator, which is known to coordinate with In^{3+}, forming a thermodynamically stable complex suitable to radiolabel proteins and other biological molecules [122]. Additionally, the incorporation of In^{3+} to DTPA happens at mild temperatures, which is compatible with the radiolabelling of proteins as the LT components [258, 261].

Bioconjugation reactions were performed using two types of DTPA molecules, which differed by its functional group, responsible to covalently bind to LT structure. PAL1 and LF^{E687A} were conjugated with *p*-isothiocyanate-benzyl-DTPA (*p*-SCN-Bn-DTPA), which can form a covalent bond selectively with lysine side chains and N-terminal amines as shown in Figure 4.1.A. Conversely, as $PAWT^{K563C}$ and LFn present a single engineered cysteine residue, maleimide-DTPA was used to modify these molecules (see Figure 4.1.B). These two types of bifunctional DTPA molecules were selected because the reaction conditions are mild and compatible with LT proteic nature and also result in stable bioconjugates.

The different bioconjugates were separated from free, unreacted chelator molecules by size exclusion chromatography. Each fraction had its absorbance determined at 280 nm wavelength, and chromatograms were used to determine the fractions correspondent to the modified LT molecules, which eluted within the void volume of the column. Free *p*-SCN-Bn-DTPA molecules eluted in later fractions, as depicted in (Figure 4.1.A). The resulting conjugates were analysed by intact protein mass-spectrometry after liquid chromatography which demonstrated that PA variants, PAL1, $PAWT^{K563C}$ and the LF variants, LF^{E687A} and LFn, were successfully modified with their respective chelators.

As expected, $PAWT^{K563C}$ and LFn which were conjugated with maleimide-DTPA molecules displayed one chelator per molecule. On the other hand, LF^{E687A} and PAL1 modified with *p*-SCN-Bn-DTPA presented a varied number of molecules attached. A range of 4-8 chelator molecules were found to be conjugated with LF^{E687A}, while 1-2 chelator moieties were conjugated to PAL1.

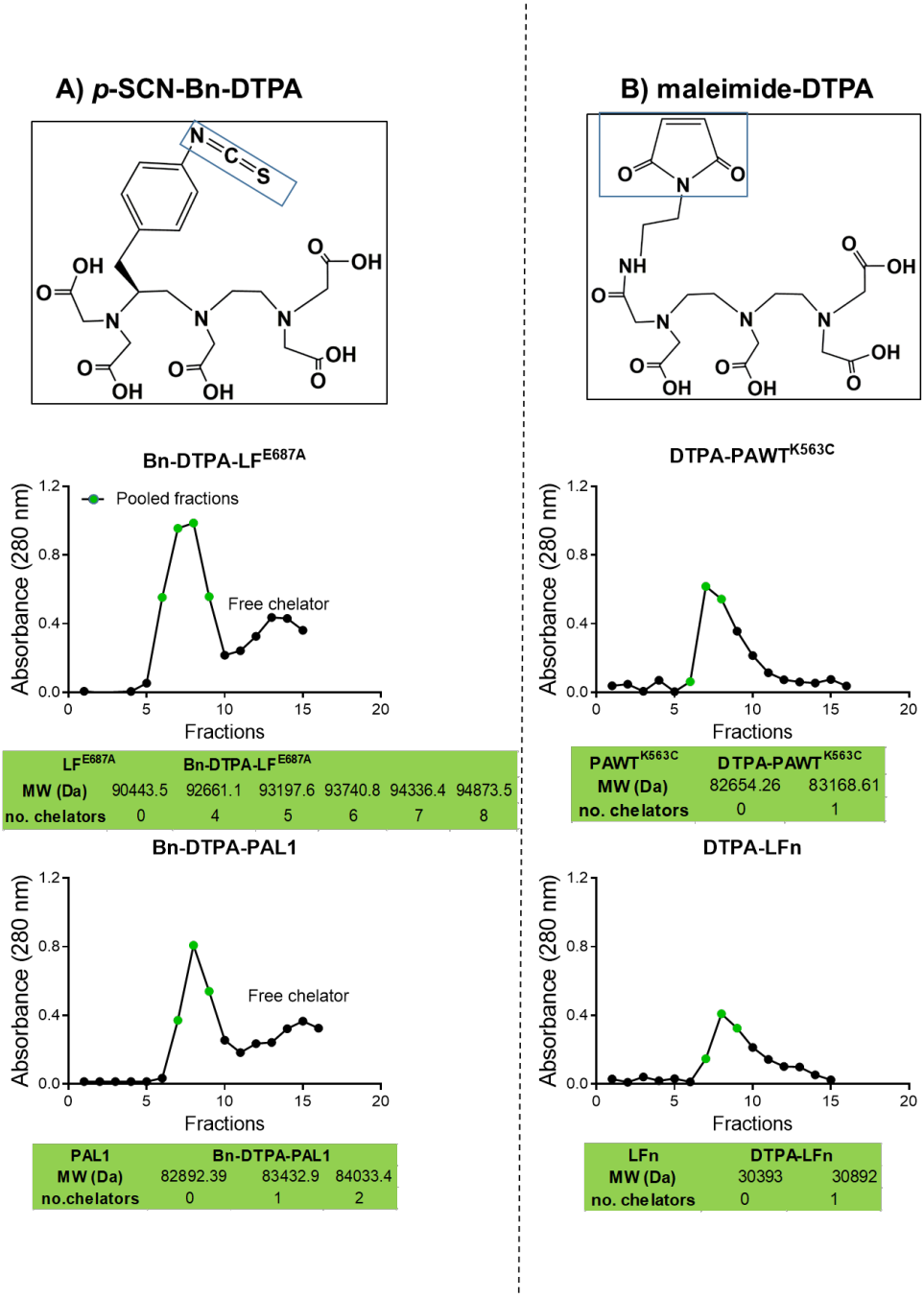

LF E687A	Bn-DTPA-LF E687A					
MW (Da)	90443.5	92661.1	93197.6	93740.8	94336.4	94873.5
no. chelators	0	4	5	6	7	8

PAWT K563C	DTPA-PAWT K563C	
MW (Da)	82654.26	83168.61
no. chelators	0	1

PAL1	Bn-DTPA-PAL1		
MW (Da)	82892.39	83432.9	84033.4
no.chelators	0	1	2

LFn	DTPA-LFn	
MW (Da)	30393	30892
no. chelators	0	1

Figure 4.1 Chromatograms of purification step following bioconjugation reaction of LT components and chelators

Size exclusion chromatography was used to remove free unreacted chelator molecules after anthrax lethal toxin components bioconjugation. (A) Representative chromatograms after reactions based on isothiocyanate chemistry or (B) on maleimide chemistry. Pooled fractions indicated as a green dot were analysed by intact protein mass-spectrometry after liquid chromatography (LC-MS). Green table below chromatograms indicates the molecular weight (MW) corresponded to the major peaks of the LC-MS spectra and the correspondent number of chelators expected for each specimen of bioconjugated molecule.

4.2.2. ^{111}In-radiolabelling of LT components

Subsequently, bioconjugates described above were radiolabelled using ^{111}In chloride ($^{111}InCl_3$). To evaluate the purity of radioconjugates, instant Thin Layer Chromatography (iTLC) was performed as a quality control for all radiolabelled samples of LT.

To validate whether the differences in polarity and size of the radiolabelled LT components, and the polarity of the mobile and stationary phase were adequate to determine the level of radiochemical yield (RCY) or purity (RCP), control reactions were carried out in parallel as shown in Figure 4.2 and Figure 4.3. Importantly, $^{111}In^{3+}$ metal ions and free radiolabelled chelator molecules migrated with the solvent and presented (see Figure 4.2.A-B) completely distinct travelling patterns than LT radiolabelled components (see Figure 4.2.C-D). This demonstrates that both the stationary phase and the mobile phase were suitable to be used in quality control analysis of the radiolabelling reaction. In fact, free $^{111}In^{3+}$ migrated with the solvent front (S*f*), whereas chelators pre-radiolabelled with $^{111}InCl_3$ migrated less from the starting point (S*p*), when compared to free $^{111}In^{3+}$. The retention factor (R*f*) calculated for the radiolabelled chelators were different ([^{111}In]In-maleimide-DTPA, R*f* = 0.6, Figure 4.2.B; [^{111}In]In-*p*-SCN-Bn-DTPA, R*f* = 0.3, Figure 4.3.A) possibly due to differences in polarity between the molecules.

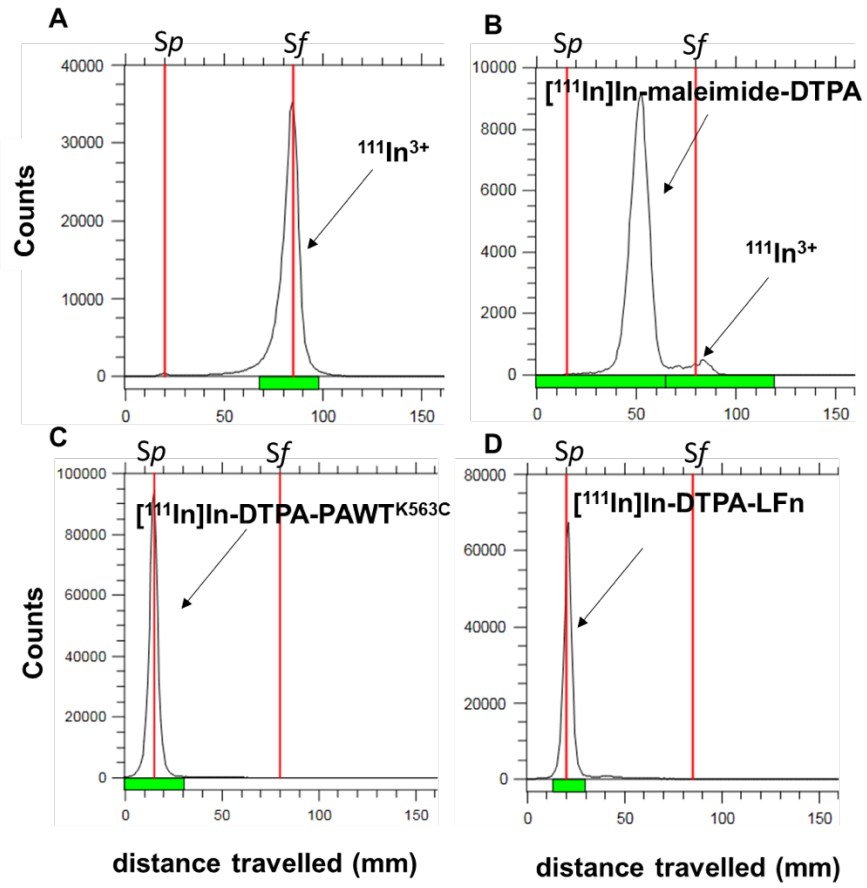

Figure 4.2 ^{111}In-radiolabelling of PAWT^{K563C} and LFn quality control

Representative iTLC chromatograms performed for different samples using citrate buffer (50 mM; pH 5.5) as the mobile phase and silica plates as the stationary phase. A) $^{111}In^{3+}$, B) [^{111}In]In-maleimide-DTPA, C) [^{111}In]In-DTPA-PAWT^{K563C} and D) [^{111}In]In-DTPA-LFn. Red lines correspond to the starting point (S*p*) where the sample was placed, and the solvent front (S*f*) respectively.

^{111}In-radiolabelled LT components stayed at the baseline of the iTLC (R*f* = 0). After optimisation, radiolabelling was achieved by addition of 20 MBq of $^{111}InCl_3$ to 20 µg of protein, with a RCY routinely above 99%, as demonstrated by iTLC (Figure 4.2.C-D and Figure 4.3.B). In the cases where RCY was below 99% (Figure 4.3.C), a purification step using size exclusion chromatography was performed (Figure 4.3.D). Each fraction eluted was evaluated by iTLC to ensure the collection of the fraction corresponded to radiolabelled LT presenting 100% of RCP.

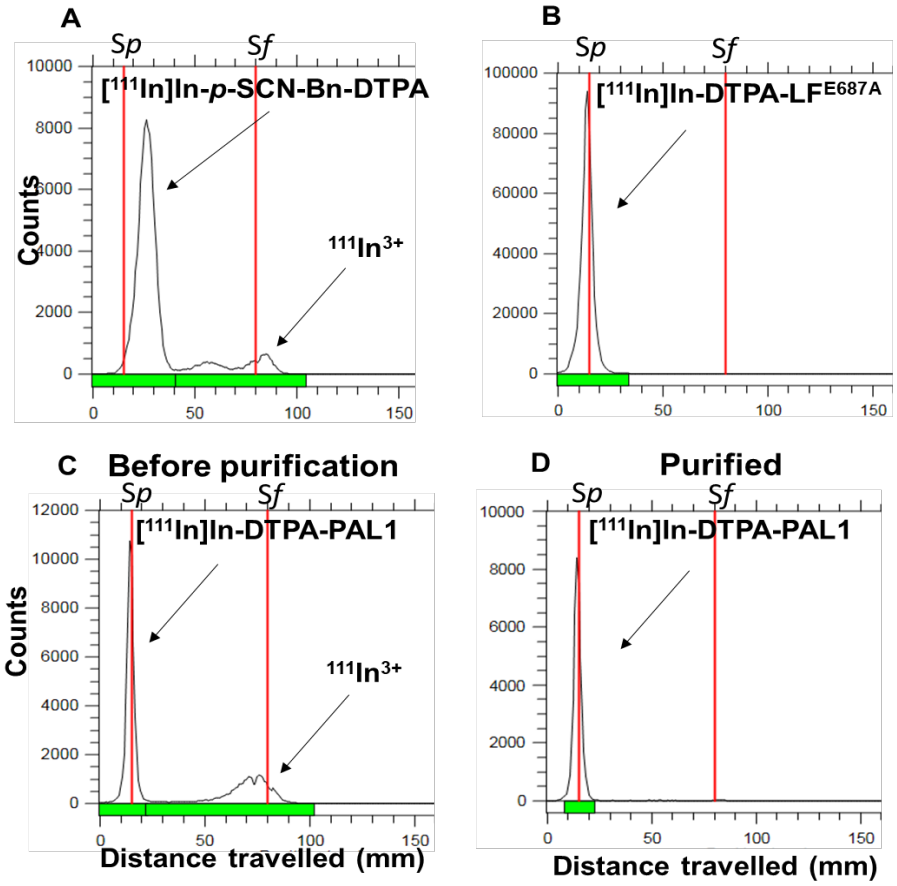

Figure 4.3 ^{111}In-radiolabelling of PAL1 and LF^{E687A} quality control

Representative iTLC chromatograms performed for different samples using citrate buffer (50 mM; pH 5.5) as the mobile phase and silica plates as the stationary phase. A) [^{111}In]In-*p*-SCN-Bn-DTPA and (B) [^{111}In]In-DTPA-LF^{E687A}. D) [^{111}In]In-DTPA-PAL1 before purification by size exclusion chromatography and (E) after purification step demonstrating > 99% RCP. Red lines correspond to the starting point (S*p*) where the sample was placed, and the solvent front (S*f*) respectively.

4.2.3. Interaction of radiolabelled PAs with cellular anthrax toxin receptors

Saturation binding assays were performed using ^{111}In-radiolabelled PAWT^{K563C} to characterise the cancer cell lines studied here. The resultant data allowed the determination of PA apparent binding affinity (K_D) and the maximum number of binding sites (B_{MAX}) that was considered as the total density of anthrax toxin receptors on the cell surface [262]. If compared with Western blot analysis, this assay was considered a more direct way to determine the number of anthrax toxin receptors available to engage with PAs on the cell

surface, and also to distinguish between the receptors TEM8 and CMG2. To calculate K_D specifically to either CMG2 or TEM8 receptors, CHO cell lines presenting different phenotypic status for anthrax toxin receptors, kindly provided by our collaborators, were also included in the saturation binding assay [200]. PA receptor-deficient CHO cell line CHO-PR230 (CMG2 $^{-/-}$ TEM8 $^{-/-}$), was stably transfected with vectors to encode either CMG2 or TEM8 receptors resulting in the cell lines CHO-CMG2 (TEM8 $^{-/-}$) and CHO-TEM8 (CMG2$^{-/-}$).

Saturation binding assays were performed in pre-fixed cells to remove the influence of MMP activity, and internalisation of PA /receptor complexes. After cell incubation with increasing concentrations of radiolabelled PA, unbound radiolabelled compound was removed and cells were washed prior to lysis with sodium hydroxide solution (NaOH). The radioactivity associated with the cell lysate was measured by gamma-counting and normalised by cell number.

The simplest model to describe the experimental data was a one-binding-site saturation model for all cancer cells (see Figure 4.4.A). This might be a result of the nonspecific binding component that was inferred from the shape of the total binding curve instead of being empirically measured. It is most likely that a direct measurement of the non-specific binding would have allowed discrimination between the two receptor populations on the cell surface. However, the levels of receptor density among the cells showed to be different for each cell line, ranging from approximately 5,000 to 60,000 molecules. Therefore, B_{MAX} values among the different cell lines could be described as CAPAN1>HT1080>MDA-MB-231>B8484>MCF7 (see Figure 4.4.C).

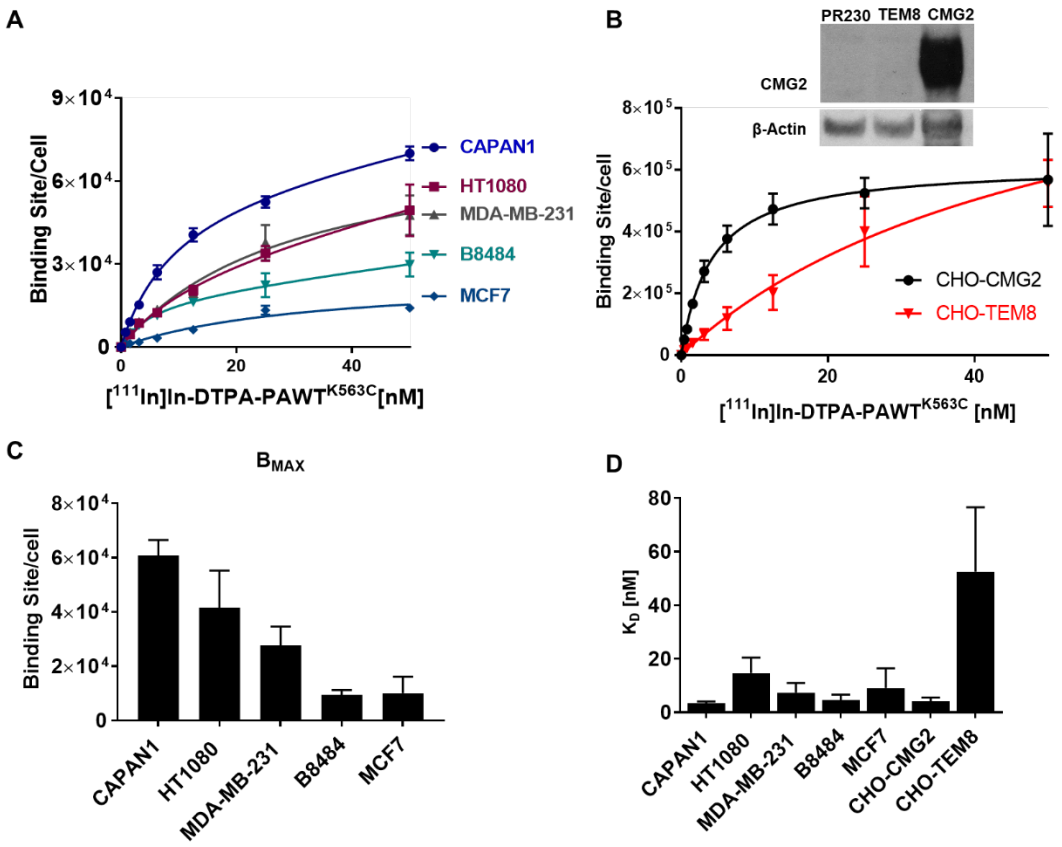

Figure 4.4 ^{111}In-radiolabelled PAWT^{K563C} interaction with anthrax toxin receptors in cancer cells

A-B) Saturation binding assay was performed by incubating increasing concentrations of [^{111}In]In-DTPA-PAWT^{K563C} to pre-fixed cells. After incubation for 2 h at room temperature, cells were lysed with NaOH and radioactivity associated was measured by gamma-counting. B) Graph inset is CMG2 expression evaluated in CHO cell lines by Western blot analysis confirming the differences in receptor expression. C) B_{MAX} and D) K_D values were calculated from the saturation binding curves for the different cell lines. The results reported here are a result of three independent experiments performed in triplicate.

Saturation binding assays with CHO-CMG2 and CHO-TEM8 were performed and analysed as described above for the other cell lines. One-binding-site saturation model was the simplest model describing the experimental data for both cell lines (see Figure 4.4.B). PA interaction with CMG2 receptors showed a K_D of 4.1 ± 1.5 nM, while a K_D of 52.6 ± 24.0 nM was determined for TEM8 receptors (see Figure 4.4.D). Interestingly, apart from HT1080 cells, all the other cancer cell lines tested here, presented a K_D equivalent to the one

established for CMG2 receptors in CHO-CMG2 cell lines. The K_D calculated for HT1080 (14.7 ± 5.8 nM) was statistically different (P = 0.003) from the one determined for CHO-CMG2, indicating the presence of TEM8 receptor on the HT1080 cell surface which can interact with PA molecules. For all the other cell lines, K_D values were not statistically different from CHO-CMG2 ($P \geq 0.57$). This result suggests that CMG2 might be the major receptor present in these cell lines which interact with PA molecules (see table below).

Table 4.1 Summary of the parameters calculated from saturation binding assays performed with ^{111}In-radiolabelled PAWT^{K563C}

Cell line	[1]B_{MAX} ($\times 10^3$)	[2]K_D (nM)	Anthrax Receptor status
CAPAN1	60.6 ± 5.8	3.4 ± 0.7	[3]CMG2
HT1080	41.6 ± 13.7	14.7 ± 5.8	CMG2 & [4]TEM8
MDA-MB-231	27.6 ± 7.0	7.5 ± 3.6	CMG2
B8484	9.5 ± 1.7	4.2 ± 2.0	CMG2
MCF7	10.0 ± 6.0	9.1 ± 7.4	CMG2
CHO-CMG2	617.8 ± 89.0	4.1 ± 1.5	CMG2
CHO-TEM8	1,159.5 ± 264.9	52.6 ± 24.0	TEM8

[1] Anthrax receptors density; [2] binding affinity concentration when half of the total binding sites are occupied; [3] Capillary morphogenesis gene 2; [4] Tumour endothelial marker 8

In another set of saturation binding experiments, [^{111}In]In-DTPA-PAL1 and [^{111}In]In-DTPA-PAWT^{K563C} binding affinity to anthrax receptors was compared. The curves describing the experimental data demonstrated that site-specific and non-site-specific radiolabelling of PAs does not significantly differ in the values calculated for K_D (P = 0.11) and B_{MAX} (P = 0.28) for [^{111}In]In-DTPA-PAL1 (2.0 ± 0.8 nM; 20.8 ± 3.4$\times 10^3$ binding sites/cell) and [^{111}In]In-DTPA-PAWT^{K563C} (5.9 ± 3.2 nM; 29.7 ± 9.2$\times 10^3$ binding sites/cell) (see Figure 4.5.A). To further evaluate specificity of the binding, a competition assay was performed using 5 nM of radiolabelled compound in the presence of an excess of 500 nM of unlabelled compound. In both cases blocking was 98 ± 0.3% effective, indicating good specificity of the radiolabelled Pas (see Figure 4.5.B).

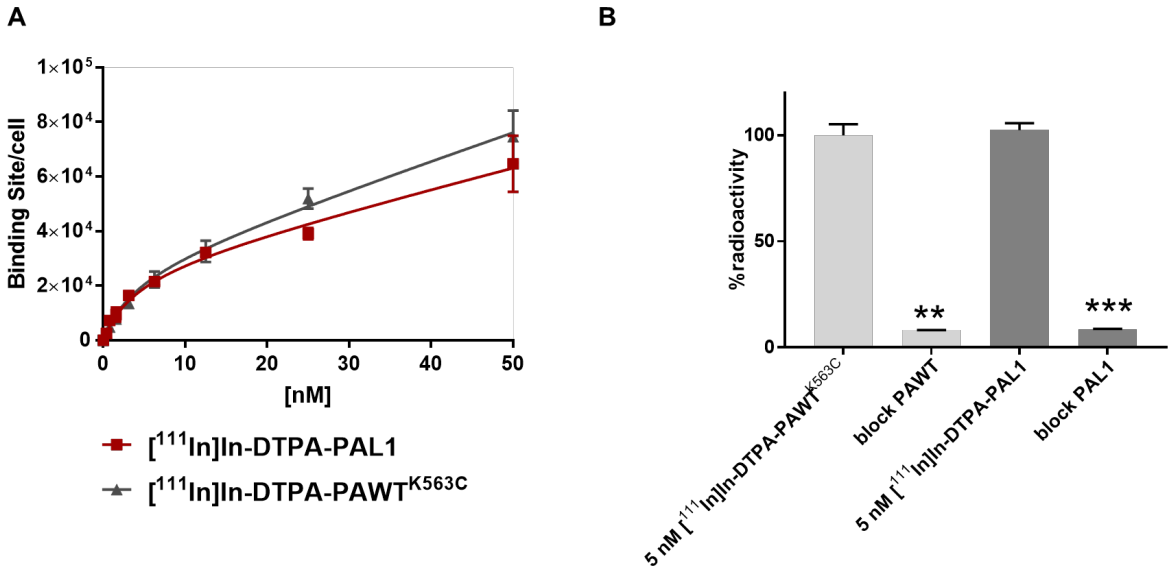

Figure 4.5 Comparison of site-specific and non-site-specific radiolabelling of PAs

A) Saturation binding assay of pre-fixed MDA-MB-231 cells with increasing concentrations of either [^{111}In]In-DTPA-PAL1 or [^{111}In]In-DTPA-PAWT^{K563C}. After incubation for 2 h at room temperature, cells were lysed with NaOH and radioactivity associated to cells was measured by gamma-counting. B) Competition binding assay with 500 nM of unlabelled PAs incubated 30 min prior to the addition of 5 nM of radiolabelled PAs. ** $P \leq 0.01$; *** $P \leq 0.001$. This experiment was repeated once more with similar results.

4.2.4. Delivery of ^{111}In-radiolabelled LF variants to cells by PA pre-pores

The delivery of either [^{111}In]In-DTPA-LF^{E687A} or [^{111}In]In-DTPA-LFn by PA pores was evaluated by cell uptake experiments. Notably, the internalisation of PA and LF by cells is described to be relatively slow, with a half-time of 30 min. Therefore, cells were incubated for 3 h at 37ºC in different treatment conditions to test the different components that are required by the LT delivery system (Table 4.2). Based on the experiments described above, the PA concentration used was 80 nM, which was considered to saturate all available receptors on the cell surface, while 25 nM of ^{111}In-radiolabelled LF was used because the binding stoichiometry of LF molecules for each PA pre-pore is 2-3 [167, 263]. Subsequently cells were washed with cold PBS and lysed using NaOH. Radioactivity associated with the

cell lysates was determined by gamma-counting. The total protein content was determined by BCA assay and the result was used to normalise the percentage of the total radioactivity added per mg of protein for the different cell lines.

Condition I, where PAL1 was added with ^{111}In-radiolabelled LF variants (10 MBq/nmol, at the moment of the experiment) to cells, was designed to test the delivery of radiolabelled LF^{E687A} or LFn by MMP activation of PAL1 pores. The specificity of the interaction of radiolabelled LFs with PAL1 pre-pores was tested in condition (II), using an excess of unlabelled LFn or LF^{E687A}. As a negative control, the uncleavable variant PAU7, (condition III) was used because it cannot form competent pre-pores to deliver the radiotracer. Additionally, condition IV was used as a another control, consisting of either [^{111}In]In-DTPA-LF^{E687A} or [^{111}In]In-DTPA-LFn only, to determine the degree of non-specific cell uptake. Condition V, was used to determine uptake of free ^{111}In, and to confirm that the radionuclide needs to be integrated to LFs in order to be delivered via PA pre-pores inside the cells. In condition VI, radiolabelled LFs were added in combination with PAWT, to gauge the delivery of radiolabelled compound depending on furin enzymatic activity.

Exposure of the panel of cancer cells to [^{111}In]In-DTPA-LF^{E687A}, demonstrated the selectivity and specificity of the LT system (see Figure 4.6). [^{111}In]In-DTPA-LF^{E687A} was taken up by CAPAN1, HT1080, MDA-MB-231 and B8484 cells when administered in combination with furin-cleavable PAWT or MMP-cleavable PAL1, but not in combination with vehicle control or non-activatable PAU7 ($P < 0.001$). Additionally, PAL1-mediated cell delivery of [^{111}In]In-DTPA-LF^{E687A} could be significantly reduced by blocking with a 10-fold excess of cold, unlabelled LF^{E678A}.

Table 4.2 Experimental conditions used for cell uptake. 25 nM of either ^{111}In-radiolabelled non-toxic LF variants (LF^{E687A} or LFn) were combined with

Condition	Co-treatment 80 nM [1]PA variants	Pre-incubation 30 min before	Function PA variant
I	PAL1	none	Forms pores upon [2]MMP cleavage and interacts with anthrax toxin receptors
II	PAL1	250 nM [3]LF^{E687A}/[4]LFn	Excess of unlabelled molecules blocks radiotracer interaction with PAL1 pre-pores
III	PAU7	none	Uncleavable thus does not form pre-pores
IV	none	none	Non-specifc uptake of radiotracer
V	^{111}In	none	Uptake of free ^{111}In in cells
VI	PAWT	none	Forms pre-pores upon furin cleavage and interacts with anthrax toxin receptors

[1]Protective Antigen; [2]Matrix metalloproteinases; [3] Lethal Factor variant presenting a defective catalytic domain; [4] Truncated Lethal factor variant corresponding to N-terminal translocation domain

No delivery of [^{111}In]In-DTPA-LF^{E687A} was observed in MCF7 cells under any of the conditions ($P > 0.05$). In condition VI, an uptake of 1.3 ± 0.3% radioactivity/mg was not significantly different ($P = 0.26$) from control treatment IV (1.13 ± 0.15% radioactivity/mg) suggesting that PAWT is not delivering radiolabelled LF^{E687A} to cells. Contrastingly, it was previously reported here (section 3.2.3) that MCF7 cells express furin and are sensitive to PAWT associated with a potent fusion toxin FP59 (LFn fused to Exotoxin A from Pseudomonas aeruginosa) [248]. Exotoxin A enzymatically modifies the eukaryotic Elongation Factor 2, impairing protein synthesis [249]. It was reported that two molecules of this toxin are enough to cause cell death. Therefore, the difference observed between the two types of experiments might be explained because the number of FP59 molecules,

delivered by PAWT pre-pores, is enough to cause cell death. Contrastingly, in the uptake experiments the number of [^{111}In]In-DTPA-LF^{E687A} are not enough to present differences to the control group.

Interestingly, in condition V, where only $^{111}InCl_3$ was added, B8484 and MCF7 cells presented associated radioactivity above the non-specific uptake of [^{111}In]In-DTPA-LF^{E687A} (condition IV). It is known that $^{111}In^{3+}$ can bind to transferrin and be endocytosed by transferrin cellular receptors [264]. Therefore, these results might indicate that there is a higher number of transferrin receptors in these two cell lines leading to higher uptake of $^{111}In^{3+}$.

In the case of cell uptake experiments performed with ^{111}In-radiolabelled N-terminal fragment of LF, [^{111}In]In-DTPA-LFn similar results were obtained with few exceptions (see Figure 4.7). Unexpectedly, CAPAN1 uptake of [^{111}In]In-DTPA-LFn combined with PAL1 (1.12 ± 0.3% radioactivity/mg), was not different from control conditions ($P > 0.05$). However, PAWT was able to promote cell uptake of [^{111}In]In-DTPA-LFn for this cell line (5.43 ± 0.58% radioactivity/mg) demonstrating that cells present the capacity to be intoxicated by LT system. For MDA-MB-231 cells, the blocking step did not completely stop the uptake of [^{111}In]In-DTPA-LFn and values were significantly above control condition IV where no PA is added (1.56 ± 0.17% radioactivity/mg; $P = 0.0018$).

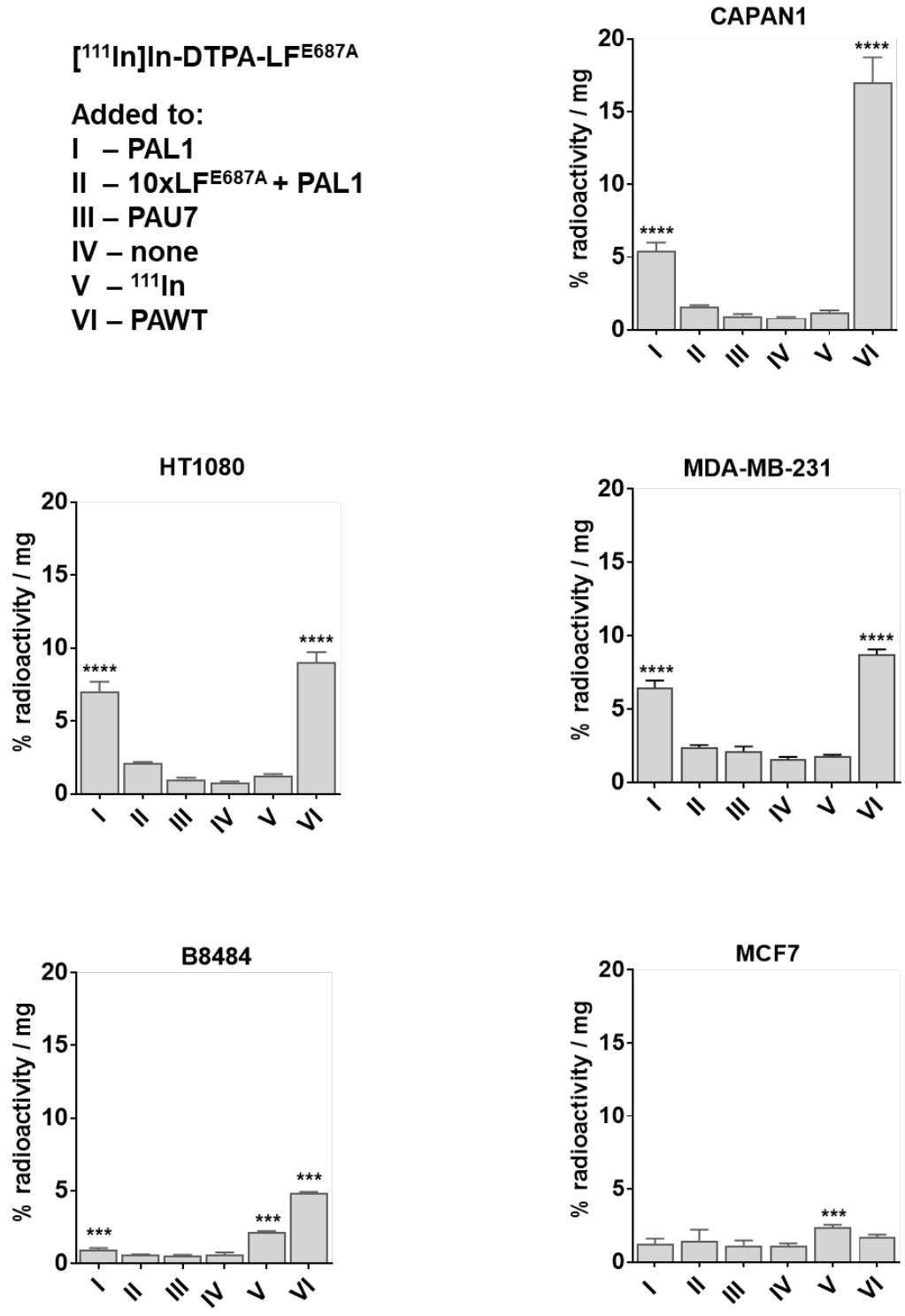

Figure 4.6 PAL1-mediated delivery of [^{111}In]In-DTPA-LF^{E687A} to cancer cells

Percentage of total radioactivity added to cells normalised by protein content in conditions I-VI. Cells were exposed to 25 nM of [^{111}In]In-DTPA-LF^{E687A} with or without PA proteins (80 nM) at 37°C for 3 h. The radioactivity associated with cell lysate were measured in counts per minute. ***$P \leq 0.001$; ****$P \leq 0.0001$. These experiments were repeated twice more with similar results.

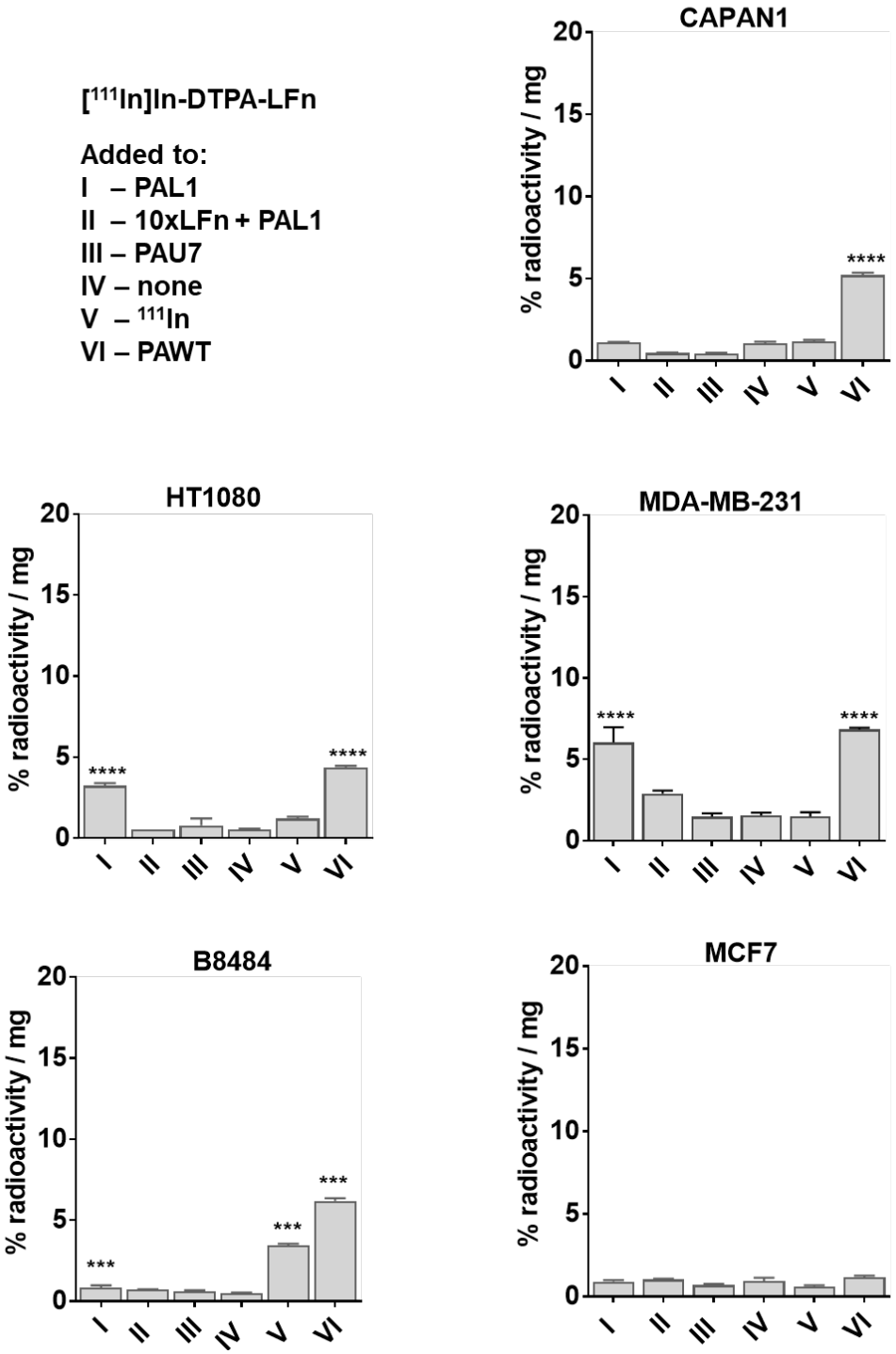

Figure 4.7 PAL1-mediated delivery of [^{111}In]In-DTPA-LFn to cancer cells

Percentage of total radioactivity added to cells normalised by protein content in conditions I-VI. Cells were exposed to 25 nM of [^{111}In]In-DTPA-LFn with or without PA proteins (80 nM) at 37°C for 3 h. The radioactivity associated with cell lysates were measured in counts per minute. ***$P \leq 0.001$; ****$P \leq 0.0001$. These experiments were repeated twice more with similar results.

4.2.1. PAL1 activation by MMPs and delivery of [^{111}In]In-DTPA-LF^{E687A}

To evaluate if MMP enzymatic activity was responsible for the PAL1-mediated delivery of ^{111}In-LF, cell uptake assays were performed treating MDA-MB-231 cells with a MMP broad spectrum inhibitor, GM6001. Briefly, 30 μM of GM6001 was added 30 min before exposing cells to 25 nM [^{111}In]In-DTPA-LF^{E687A} and 80 nM of different PAs (Figure 4.8). Subsequently the same experimental procedure described above (Section 4.3.1) was performed to obtain the amount of radioactivity associated with the MDA-MB-231 cellular fraction.

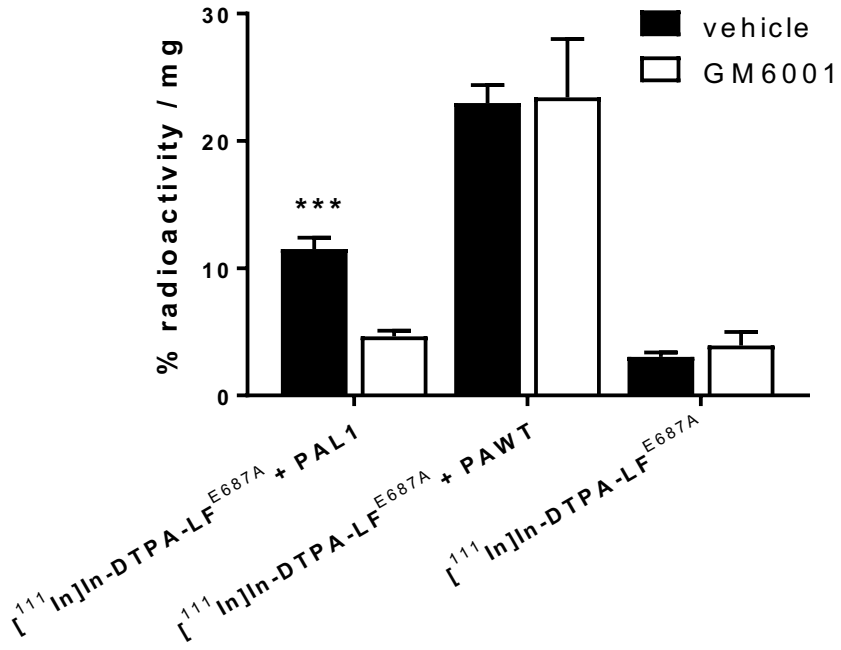

Figure 4.8 MMPs activate PAL1 pore formation

MDA-MB-231 cells were incubated with 25 nM of [^{111}In]In-DTPA-LF^{E687A} and 80 nM PAs for 3 h at 37ºC. Inhibited groups were pre-treated with 30 μM of MMP inhibitor GM6001. Data are plotted as percentage of total radioactivity added, associated to cells per mg of protein content. ***$P \leq 0.001$.

In the experimental condition where 80 nM of PAL1 and 25 nM [^{111}In]In-DTPA-LF^{E687A} was added, cell uptake corresponded to 11.51 ± 0.88% radioactivity/mg. This uptake was significantly reduced in the presence of the inhibitor, reaching an uptake value of 4.64 ±

0.46% radioactivity/mg (P = 0.0006) which corresponded to the value obtained for the experimental condition where no PA was added (3.94 ± 1.05% radioactivity/mg). As expected, the presence of GM6001 did not reduce the uptake of [^{111}In]In-DTPA-LF^{E687A} mediated by PAWT significantly (P = 0.59) since this molecule is activated by the furin enzyme and not MMPs. These results indicate that PAL1 requires the activity of MMPs in order to be cleaved, oligomerise into a competent pre-pore and expose the binding sites where [^{111}In]In-DTPA-LF^{E687A} can interact, thus allowing cell uptake.

4.2.2. Binding affinity of radiolabelled LF^{E687A} to PA pre-pores

For PA molecules to form a pre-pore on the cell surface, the N-terminal fragment (PA_{20}, 20 kDa) must be removed upon enzymatic cleavage. The remaining C-terminal fragment (PA_{63}, 63 kDa) can then oligomerise and form the binding sites, where LF molecules can interact with the PA_{63} pre-pore. To determine whether radiolabelling of LF^{E687A} molecules would be deleterious to its capacity to bind to PA pre-pores, the affinity of this interaction was determined in a cell-based assay. CHO-CMG2 cells were chosen for this assay because of its high receptor density. Cells were incubated with PA molecules for 24 h, at 4ºC to allow the formation of PA fragments with 63 kDa and also to prevent endocytosis. Cell lysates of CHO-CMG2 incubated with PAL1, PAWT or PAU7 were analysed by Western Blot to evaluate the presence of 63 kDa fragments (Figure 4.9.A). As expected cells incubated with PAL1 and PAWT resulted in the formation of cleaved PA whereas PAU7 molecules remained intact after cell incubation.

A saturation binding assay was performed with CHO-CMG2 cells exposed to PA molecules and washed with cold PBS, before being exposed to increasing concentrations of [^{111}In]In-DTPA-LF^{E687A} at 4ºC for an additional 2 h. The cells were then washed, solubilised, and examined for radioactive content by gamma counting. After subtracting nonspecific binding

using a control condition where cells were incubated with PAU7, the experimental data were fitted to a one-binding-site model (Figure 4.9.B). The K_D determined for [^{111}In]In-DTPA-LF^{E687A} to PAWT$_{63}$ pre-pores was 0.57 ± 0.06 nM, while a value of 0.98 ± 0.09 nM was determined for PAL1. Values previously determined for K_D by surface plasmon resonance for the interaction between PAWT$_{63}$ and LF was 2.8 ± 0.84 nM, which is statistically higher than the one determined here (P = 0.03) describing a weaker affinity. This might indicate that even though LF is not radiolabelled in this type of assay the artificial requirement to covalently fix PA molecules might at least in part disturb the interaction of PAWT$_{63}$ with LF molecules [265].

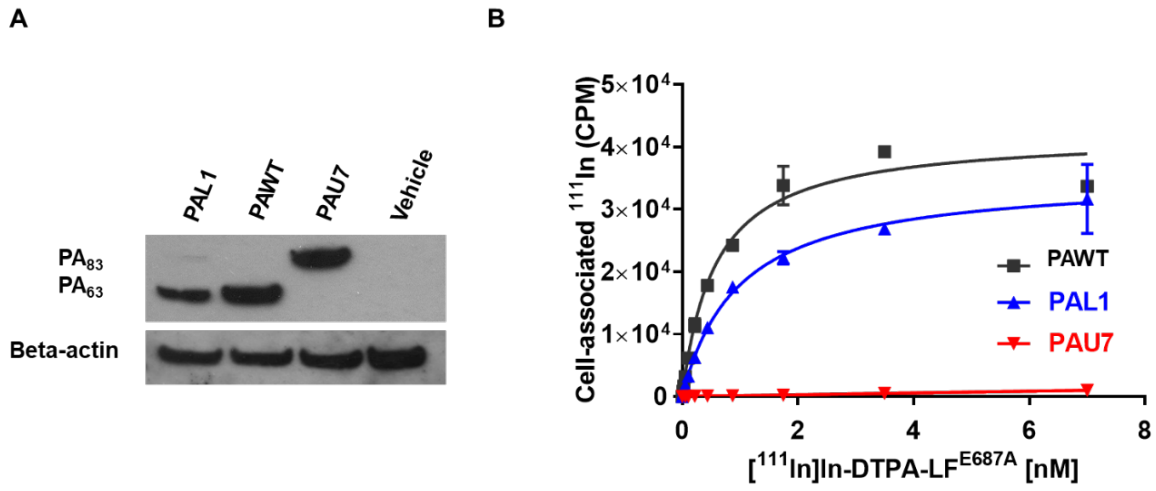

Figure 4.9 [^{111}In]In-DTPA-LF^{E687A} binding to PA pre-pores

CHO-CMG2 cells in culture were incubated with saturating amounts of PAs (80 nM) for 24 h, at 4°C. A) Western blot analysis was used to detect PA fragments in CHO-CMG2 lysates. Negative control condition was considered CHO-CMG2 cells only. B) Cells were incubated with various concentrations of [^{111}In]In-DTPA-LF^{E687A} at 4°C for 2 h, cells were washed with cold PBS, solubilised in NaOH, and examined for radioactive content by gamma counting (counts per minute, CPM).

4.2.3. Cytotoxicity of radiolabelled LF^{E687A} or truncated LFn to tumour cells

To evaluate if the cellular uptake of DTPA-LF^{E687A}, DTPA-LFn, [^{111}In]In-DTPA-LF^{E687A} or [^{111}In]In-DTPA-LFn has an effect on cell viability, the MTT colorimetric cell survival assay was used as previously described (section 3.2.3). The HT1080 cells were used in this assay because it presents high uptake for both ^{111}In-radiolabelled LF variants, and is also sensitive to the fusion toxin FP59 (section 3.2.3), in the presence of the different PA variants (see Figure 4.10). The experimental settings were based on the cytotoxic experiments previously demonstrated to cause cell cytotoxicity to HT1080 cells. The data of this assay confirmed that none of the conjugates or radiolabelled LF variants were toxic, alone or in combination with PAs.

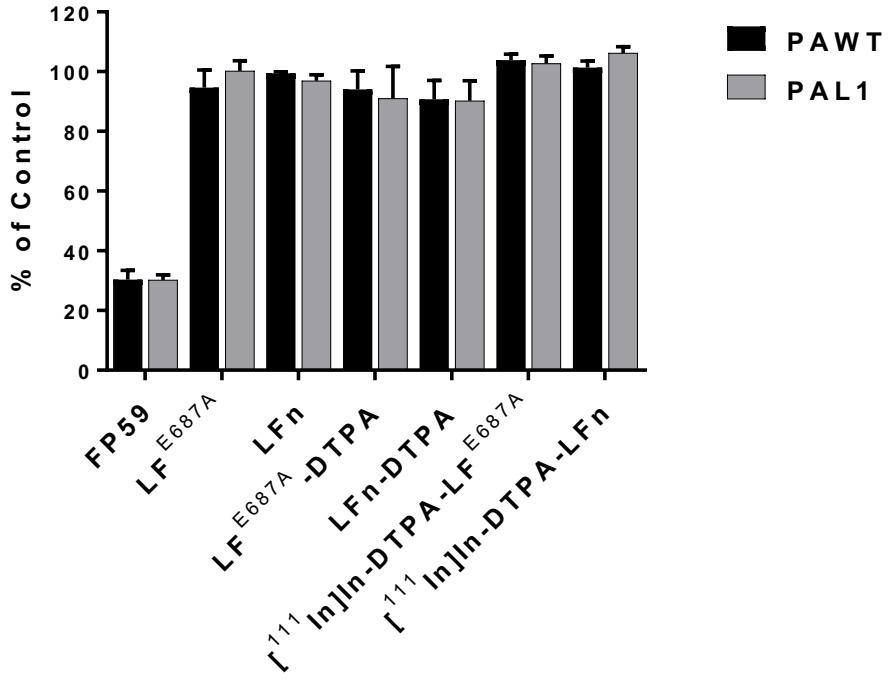

Figure 4.10 radiolabelled LT components are non-toxic to tumour cells

HT1080 tumour cells were treated with 3.5 nM of PAs in addition to 0.5 nM of molecules described in the X axis. Cells were incubated for 48 h prior to addition of MTT salt. Absorbance measured at 495 nm for the control group, treated with only vehicle, was considered 100% and the treated groups were normalised by the control group.

4.2.4. Stability of radiolabelled LT components in serum and PBS

The stability of the radiolabelled LT components in blood is essential for the use of this probe system in vivo. In an intravenous injection, a fraction of the radioactive metal can bind to a range of proteins present in the blood stream, a process known as transchelation, which can affect the tissue distribution and plasma clearance of radioactive drugs [266]. Therefore, serum stability assays were performed mimicking the in vivo condition by incubating radiolabelled LT components with mouse serum at 37ºC and analysing samples by SDS-PAGE gels, followed by phosphor imaging autoradiography. Data generated by this analysis, resulted in images such as the one presented in Figure 4.11.A (see Appendix, Figure A. 5, page175), which were analysed using ImageJ software (NIH, USA). The data was presented as a percentage of the signal intensity determined for the control condition, which corresponded to a sample of radiotracer that was not previously incubated in serum (see Figure 4.11.B).

For the intact [^{111}In]In-DTPA-LF^{E687A} compound, it was expected a band corresponding to 90 kDa size. After 10 min of its incubation, beside the intact radiotracer, a band with approximately >180 kDa corresponding to 5.5 ± 0.2% of the total intensity signal was detected, possibly indicating aggregation of radiolabelled LF^{E687A} molecules (see Figure 4.11.B). After one hour, fragments with 45-40 kDa corresponding to 5.5 ± 1.3% were observed, possibly indicating a transchelation process. After 3 h of incubation, the percentage of signal correspondent to the 45-40 kDa fragment significantly increased to 7.7 ± 1.0% (P = 0.02). Notably, in the subsequent time points (6 h, 8.6 ± 0.7%; P = 0.57 and 24 h, 7.9 ± 0.6%; P = 0.57) no change was observed. Intact [^{111}In]In-DTPA-LF^{E687A} with 90 kDa corresponded to 86.6 ± 0.2 % after 24 h of incubation.

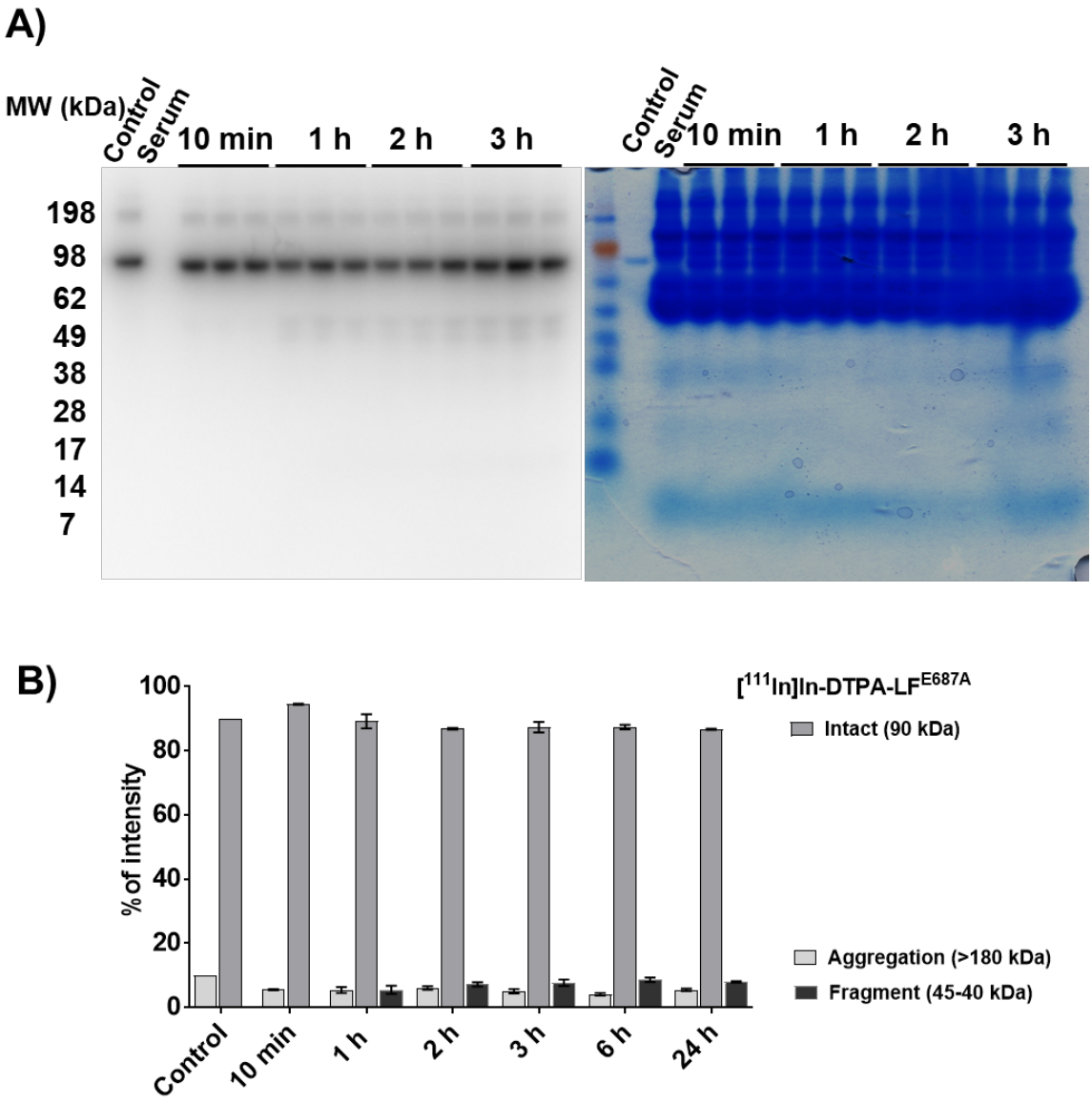

Figure 4.11 Serum stability of [^{111}In]In-DTPA-LF^{E687A}

A) [^{111}In]In-DTPA-LF^{E687A} samples were incubated with mouse serum at 37ºC. At different time points samples were collected and analysed by SDS-PAGE gel followed by autoradiography. B) Intensity signal analysis was performed for the autoradiographs.

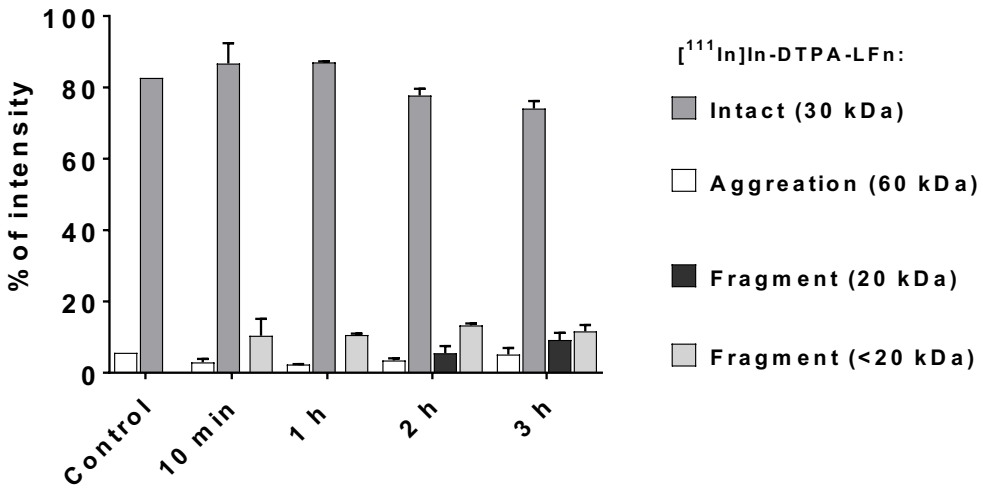

Figure 4.12 Serum stability of [^{111}In]In-DTPA-LFn

[^{111}In]In-DTPA-LFn samples were incubated with mouse serum at 37ºC. At different time points samples were collected and analysed by SDS-PAGE gel followed by autoradiography. Intensity signal analysis was performed for the autoradiographs.

In the case of [^{111}In]In-DTPA-LFn, 10 min after incubation in serum, autoradiography analysis of the SDS-PAGE (see Appendix, Figure A. 6, page 176) showed a band corresponding to the intact radiotracer with 30 kDa (86.7 ± 5.7%), and also another band with 60 kDa comprising 2.9 ± 1.0% of the total signal intensity (see Figure 4.12). Interestingly, smaller fragments bellow 20 kDa corresponding to 10.4 ± 4.7% were also observed at this time point. After 2 h, an additional fragment could be observed corresponding to a band of 20 kDa (5.5 ± 2.0%). At 3 h of incubation, 74.1 ± 2.1% of intact [^{111}In]In-DTPA-LFn compound was observed.

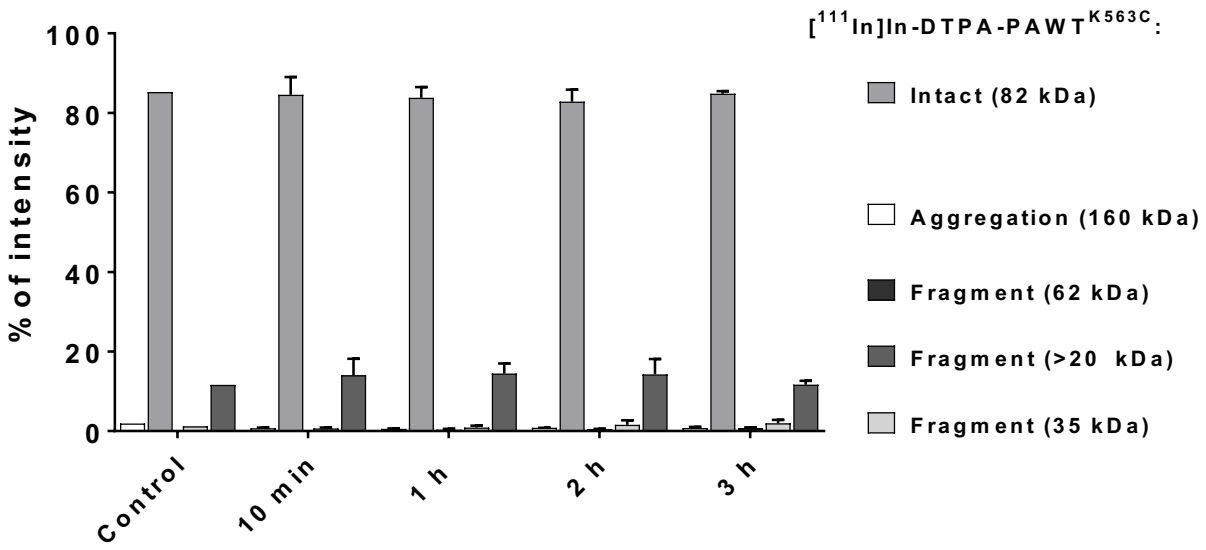

Figure 4.13 Serum stability of [^{111}In]In-DTPA-PAWT^{K563C}

[^{111}In]In-DTPA-PAWT^{K563C} samples were incubated with mouse serum at 37ºC. At different time points samples were collected and analysed by SDS-PAGE gel followed by autoradiography. Intensity signal analysis was performed for the autoradiographs.

Surprisingly, [^{111}In]In-DTPA-PAWT^{K563C} incubated in mouse serum displayed several bands (see Appendix, Figure A. 7,page 177). One band corresponded to the intact compound at 82 kDa (84.6 ± 4.4%), another band presenting >160 kDa (0.7 ± 0.2%), and a smaller band of 35 kDa (14.0 ± 4.1%) (see Figure 4.13). After 1 h, an additional fragment could be observed with 62 kDa (0.4 ± 0.2%). The percentage of these fragments did not increase with time, and at 3 h of incubation, 84.9 ± 0.6% of the intact [^{111}In]In-DTPA-PAWT^{K563C} could be still observed.

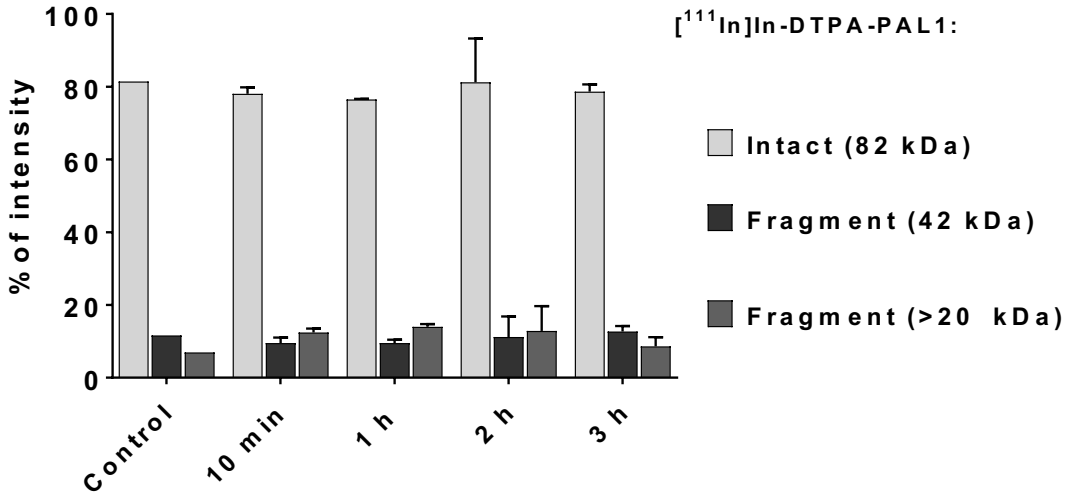

Figure 4.14 Serum stability of [^{111}In]In-DTPA-PAL1
[^{111}In]In-DTPA-PAL1 samples were incubated with mouse serum at 37ºC. At different time points samples were collected and analysed by SDS-PAGE gel followed by autoradiography. Intensity signal analysis was performed for the autoradiographs.

[^{111}In]In-DTPA-PAL1 incubated in mouse serum had a band corresponding to the monomer 82 kDa with 78.0 ± 1.8% (see Appendix, Figure A. 8, page 178). In addition, it also presented a band with 42 kDa corresponding to 9.5 ± 1.5% of the total intensity signal and a smaller band corresponding to fragments of 20 kDa (12.4 ± 1.1%) (see Figure 4.14). After 3 h, [^{111}In]In-DTPA-PAL1 intact compounds comprised 78.7 ± 1.97 % of the total sample.

4.3. Discussion

Imaging MMP activity in vivo non-invasively gives the opportunity to increase the understanding of these proteases in cancer [61]. One approach is to radiolabel an MMP-activatable imaging vector with ^{111}In. This can then be detected by SPECT imaging [122]. Here, we developed ^{111}In-radiolabelled components of an engineered variant of LT which targets MMP activity in cancer cells [223].

To radiolabel these proteins with ^{111}In, first they were modified with the acyclic chelator DTPA. The resulting conjugates were analysed using intact mass spectrometry (LC-MS)

which confirmed that PA variants (PAL1 and $PAWT^{K563C}$) and the LF variants (LF^{E687A} and LFn) were successfully modified with its respective chelators.

Although reactions using *p*-Bn-SCN-DTPA were performed under the same conditions, PAL1 presented 1 to 2 *p*-Bn-SCN-DTPA molecules covalently bound to its structure, whereas LF^{E687A} presented 4 to 8. This discrepancy may be attributed to differences between the two molecular structures. LF^{E687A} molecules present 66 solvent-accessible lysines, whereas PAL1 has 35, (data derived from PDB PISA [267]). For maleimide-DTPA, MS analysis demonstrated that one molecule of chelator is attached per molecule of engineered $PAWT^{K563C}$ and LFn, indicating the site-specific modification of these cysteine residues of these conjugates.

Saturation binding assays utilising either [^{111}In]In-DTPA-PAL1 or [^{111}In]In-DTPA-$PAWT^{K563C}$ resulted in comparable affinities of the radiolabelled PAs and anthrax toxin receptors, despite the differences of chelators used to modify these molecules. It is important to highlight that the position of the cysteine residue substitution in $PAWT^{K563C}$ is outside the small loop of domain 4 (amino acids 679 to 693) [178, 179]. Notably, this region contains the essential amino acids for PA binding to anthrax receptors, and has only 3 lysine residues which are exposed to the solvent. Therefore, in the case of ^{111}In-radiolabelled PAL1, where lysine modifications were utilised, the probability of altering specifically that region and reducing binding affinity is low, thus making comparable both site specific and non-site-specific conjugation of chelators to PAL1 or $PAWT^{K563C}$.

The PA affinity to CMG2 and TEM8 was determined as 4 nM and 52 nM respectively. These values are different from values calculated by cytotoxicity assays where the K_D was 0.9 nM and 10.9 nM between PA/CMG2 and PA/TEM8 complexes, respectively [201]. Other research from Wilgelsworth et al., using SPR analysis, has determined a binding affinity

between PA and CMG2 of 0.4 nM [263].This discrepancy might be explained by experimental differences, or possibly the radiolabelling process itself might reduce PA binding affinity towards CMG2 receptors [263]. Nevertheless, it remains clear that PA has a higher affinity to CMG2 when compared to TEM8. Notably, CMG2 is considered the major receptor of PA for both the anthrax pathology and for tumour therapy [201].

The abundance of anthrax receptors present on the membrane of the cancer cells studied here was considered a key piece of information for their characterisation. To this end, [^{111}In]In-DTPA-PAWT^{K563C} was used in saturation binding assays. Previously (Section 3.2.2) the level of CMG2 protein was determined by Western Blot analysis for the whole cell proteic content instead of specifically for the plasma membrane compartment. In addition to the isoforms 1and 2 of CMG2, which are capable of interacting with PA molecules, CMG2 isoform 3 is located in the endoplasmic reticulum [157]. Moreover, TEM8 expression levels were not determined by Western Blot successfully because of the lack of a validated antibody (Section 3.2.2). Therefore, data from the saturation binding assay better characterised the panel of cancer cells for the intended use of this project.

Interestingly, the cell lines which presented the highest number of anthrax receptors, CAPAN1, HT1080 and MDA-MB-231, also demonstrated a high uptake of [^{111}In]In-DTPA-LF^{E687A} in the presence of PAL1 or PAWT. In addition, based on the K_D between PA and its receptors it was established that CAPAN1 and MDA-MB-231 major receptor is CMG2 while HT1080 presents both TEM8 and CMG2 on its surface. Moreover, cell uptake experiments in the presence of a broad spectrum MMP inhibitor prevented the PAL1-mediated delivery of [^{111}In]In-DTPA-LF^{E687A} to tumour cells, confirming the specificity of the system developed here for MMP proteolytic activation. Additionally, both [^{111}In]In-DTPA-LF^{E687A} and [^{111}In]In-DTPA-LFn were non-toxic to cancer cells when combined with PAWT or PAL1, establishing this approach as an imaging tool for MMP activity in tumour

tissue. In addition, the affinity between ^{111}In-radiolabelled LF^{E687A} and PA pre-pores was calculated. For PAWT pre-pores, a K_D value of 0.57 nM was calculated, which is in accordance with a previous study performed in a cell-based assay with ^{125}I-radiolabelled (Iodine-125) LF (0.7 nM) [265]. The [^{111}In]In-DTPA-LF^{E687A} affinity with PAL1 pre-pores was weaker when compared to PAWT. This difference might be due to the presence of 4 (MLSQ) amino acids residues in the N-terminal of the PAL1$_{63}$ fragment which remains after PAL1 loses the 20 kDa fragment upon MMP cleavage [268].

Another important aspect to be tested in the development of a radiotracer is the stability of the probe under conditions that mimic the in vivo environment. All the radiotracers synthesized in the present work demonstrated satisfactory stability in mouse serum. However, a certain degree of radiotracer degradation and aggregation could be observed in practically all the radiotracers tested. These processes could be attributed to the release of ^{111}In, which can be transchelated to serum proteins such as transferrin or albumin resulting in the formation of new radiolabelled specimens [266]. Another explanation is the proteolytic activity of enzymes present in the serum that could be degrading the radiotracers and forming the fragmentation observed here. This may result in an altered *in vivo* behaviour or biodistribution [269].

4.4. Conclusion

The ^{111}In-radiolabelled versions of PA and LF developed here, allowed quantification of their interactions with the cancer cell panel. The affinity constants established between PA/receptor and LF/PA pre-pore complexes are in the nanomolar range and were considered to be suitable to be used in vivo. MMP14 and CMG2-positive cells (CAPAN1, HT1080 and MDA-MB-231) were considered to be the most promising cell lines to develop preclinical models for LF/PAL1 imaging system. Taken all together 111In-radiolabelled LT variants hold promise to image MMP activity non-invasively by SPECT in tumour tissue.

Chapter 5

5. Chapter 5: Evaluation of radiolabelled Lethal Toxin in tumour preclinical model

5.1. Introduction

The development of radioactive probes as clinical diagnostic imaging agents is dependent on the outcome of their evaluation in appropriate preclinical models [269]. High through-put tests are firstly performed using in vitro models, which can give valuable information about target specificity, cell uptake and cytotoxicity. Moreover, most of these radioactive probes are substrates of normal metabolic processes which happen in a living organism, and so the next step is the acquisition of preliminary information evaluating the delivery of a radioactive probes to its target tissue using preclinical in vivo models. As a non-invasive functional imaging modality, single photon emission computed tomography (SPECT) can be used to assess both pharmacokinetics and pharmacodynamic parameters of novel radiolabelled compounds. Importantly, due to the sensitivity of this imaging modality, radioactive probes can be administered at tracer amounts to avoid perturbing normal physiology.

In the current chapter, a modified version of Lethal Toxin (LT) produced by *Bacillus anthracis* bacteria was radiolabelled with indium-111 (^{111}In) with the aim of developing a radioactive probe for the molecular imaging of matrix metalloproteinase (MMP) activity in tumour models. In the previous chapter, radiolabelled LT components tested in cell-based assays demonstrated delivery to MMPs and capillary morphogenesis gene 2 (CMG2)-expressing cancer cells (CAPAN1, HT1080 and MDA-MB-231). These in vitro tests demonstrated that both radiolabelled Lethal Factor (LF) versions, one devoid of a functional catalytic domain (LF^{E687A}), and a truncated version of LF (LFn) were delivered to cancerous cells in the presence of the pore-forming molecule protective antigen (PA); either its wild

type variant furin-cleavable (PAWT) or an MMP-activatable variant (PAL1). In view of these positive in vitro results, in this chapter the study of ^{111}In-radiolabelled LT probes in tumour in vivo models are reported (Table 5.1). A combination of dynamic and static SPECT scans was acquired to assess the pharmacokinetics and biodistribution of radiolabelled LT proteins in vivo. Considering the complexity of the LT delivery system, extensively described (Section 1.8), its components were first studied in vivo separately to determine the best candidates to image MMP activity in tumour tissues.

Table 5.1 ^{111}In-radiolabelled *Bacillus anthracis* toxin-based probes

Lethal Toxin (LT)	Probes	Molecular weight (kDa)	Function
LFn	[^{111}In]In-DTPA-LFn	30	Translocates through PA pores. Smaller, non-toxic truncated version.
LF^{E687A}	[^{111}In]In-DTPA-LF^{E687A}	90	Translocates through PA pores. Full-length, non-toxic version.
PAL1	[^{111}In]In-DTPA-PAL1	82	Interacts with [1]CMG2 and forms pores upon [2]MMP cleavage.
$PAWT^{K563C}$	[^{111}In]In-DTPA-$PAWT^{K563C}$	82	Interacts with CMG2 and forms pores upon furin cleavage. Contain an engineered cysteine.

[1]Capillary morphogenesis gene 2; [2]Matrix metalloproteinase

5.1.1. Pharmacokinetics of radiolabelled LF versus LFn in tumour-naïve mice evaluated by dynamic SPECT/CT imaging

Since both [^{111}In]In-DTPA-LFn and [^{111}In]In-DTPA-LF^{E687A} effectively delivered radioactivity in cell uptake assays (section 4.2.4), next step was to evaluate whether the differences in molecular weight would result in different pharmacokinetic behaviour in vivo. Chest-gated dynamic SPECT scans were performed after intravenous bolus injection 0.1 nmol of either [^{111}In]In-DTPA-LFn or [^{111}In]In-DTPA-LF^{E687A}, with molar activities of 30 MBq/nmol and 50 MBq/nmol respectively at the time of injection, in healthy wild type mice as depicted in the diagram (see Figure 5.1.A).

To estimate the cardiac blood pool and the time activity curves (TACs) a sphere with a fixed volume (0,014 mL) was placed within the heart directly from the projections and considered the volume of interest (VOI). Imaging analysis data from dynamic SPECT scans revealed that LFn and LF^{E687A} present distinct pharmacokinetic profiles (see Figure 5.1.B). The blood clearance of [^{111}In]In-DTPA-LFn showed a biexponential signal decay with a rapid distribution phase resulting in a fast half-life of 2.0 ± 0.6 min (see Figure 5.1.C), and an elimination phase presenting a slower half-life of 6.1 ± 0.1 min. Sixty min after injection, negligible concentration of radiotracer in the blood pool was observed (0.54 ± 0.04%ID/mL).

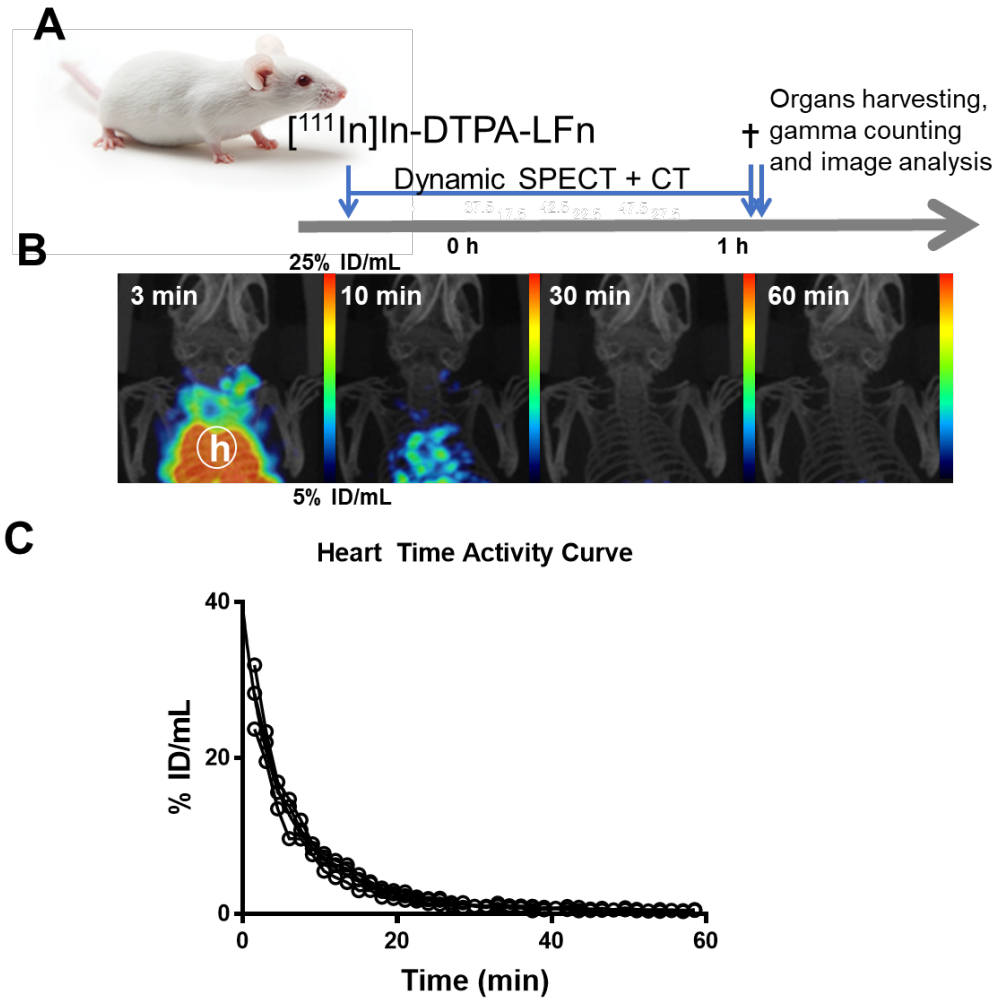

Figure 5.1 [^{111}In]In-DTPA-LFn pharmacokinetic in naïve Balb/C mice
A) Representative experimental design layout. B) Representative maximum intensity projections of chest-gated SPECT/CT scans at different time points. Heart volume of interest (VOI) = h. C) Blood time activity curves were determined by the percentage of injected dose per mL (%ID/mL) obtained from dynamic SPECT image analysis (n = 3).

Conversely, the radiolabelled full-length protein, [^{111}In]In-DTPA-LF^{E687A}, presented a significantly slower plasma clearance compared to the truncated protein (P = 0.0108), maintaining 60% of the starting concentration in the blood circulation 2 h post administration (Figure 5.2.A-B). In this case, a mono-exponential decay described the radiotracer pharmacokinetics with a blood half-life of 37 ± 18 min. As a result, the relative bioavailability of [^{111}In]In-DTPA-LF^{E687A} molecules was higher when compared to [^{111}In]In-DTPA-LFn.

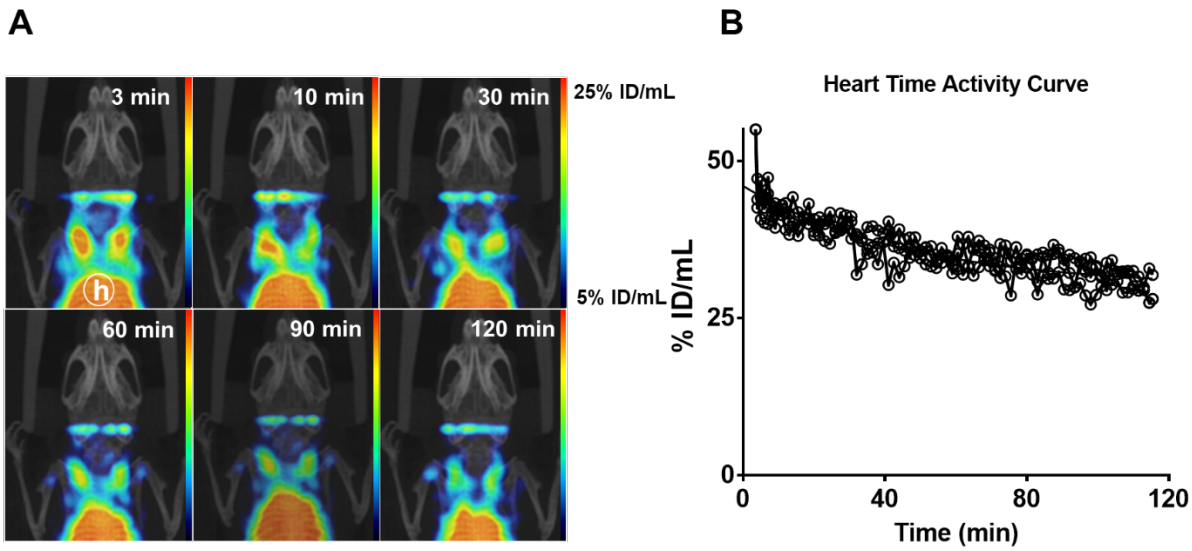

Figure 5.2 [^{111}In]In-DTPA-LF^{E687A} pharmacokinetic in naïve Balb/C mice

A) Representative maximum intensity projections of chest-gated SPECT/CT scans at different time points. Heart volume of interest (VOI) = h. B) Blood time activity curves were determined by the percentage of injected dose per mL (%ID/mL) obtained from dynamic SPECT image analysis (n = 3).

[^{111}In]In-DTPA-LFn ex vivo biodistribution 1 h post injection demonstrated high kidney uptake (25.95 ± 0.53%ID/g) (see Figure 5.3.A). Static whole-body SPECT/CT scans highlighted a high concentration of [^{111}In]In-DTPA-LFn accumulated in the cortex region of the kidneys and bladder, indicating fast renal clearance as depicted in Figure 5.3.B-C. This high kidney uptake was expected for [^{111}In]In-DTPA-LFn as its molecular weight falls below the protein glomerular filtration cut-off (67 kDa), and thus can be affected by renal proximal tubular endocytosis [270-272]. However, a less pronounced uptake was observed for the liver (5.43 ± 0.56%ID/g) and spleen (2.9 ± 0.1%ID/g) which may be associated with mononuclear phagocyte system clearance [269].

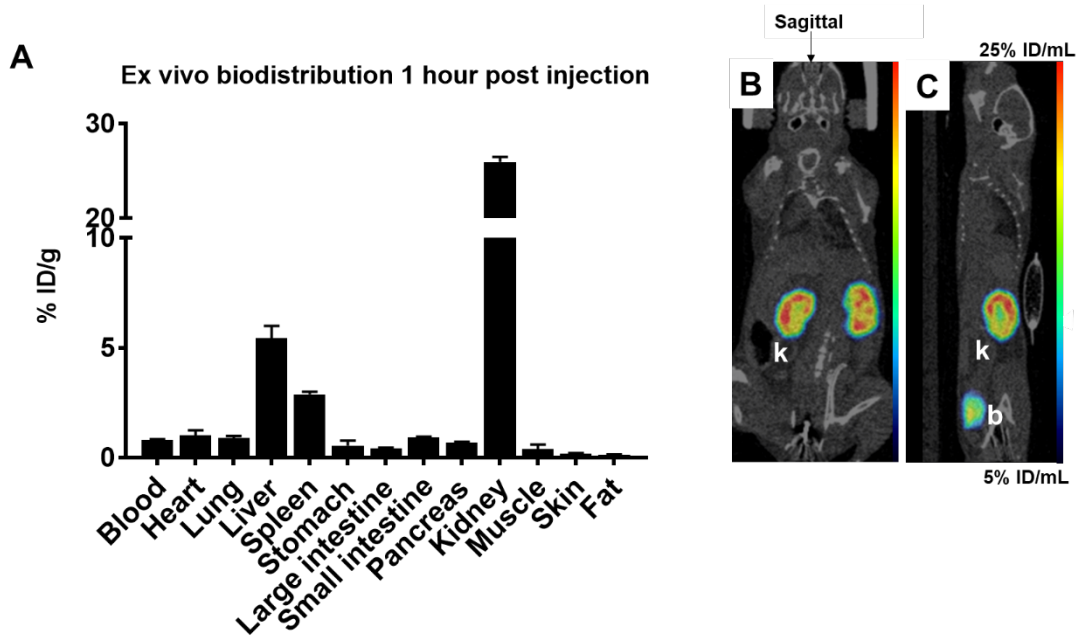

Figure 5.3 Biodistribution of [^{111}In]In-DTPA-LFn

A) Ex vivo biodistribution was determined 1 hour post injection of [^{111}In]In-DTPA-LFn in organs of interested. Representative SPECT/CT images: B) Coronal and C) Sagittal. k = kidneys; b= bladder.

In contrast, a high concentration of [^{111}In]In-DTPA-LF^{E687A} (25.7 ± 2.6%ID/g) remained in the blood and highly perfused organs, such as the liver (7.6 ± 1.7%ID/g), kidneys (9.9 ± 1.4%ID/g), lungs (10.1 ± 2.1%ID/g) and spleen (12.4 ± 2.9%ID/g) at 2 h post injection as determined by ex vivo tissue counting (see Figure 5.4.A). Hence, it is possible to infer that the higher molecular weight of LF^{E687A} increases its blood residence when compared to LFn. Since mouse blood was not completely removed before dissection by perfusion with a fixative solution, it is likely that a portion of the radioactivity found in highly perfused organs was due to the presence of [^{111}In]In-DTPA-LF^{E687A} in the blood pool. A representative maximum intensity projection image highlights the presence of [^{111}In]In-DTPA-LF^{E687A} in the blood 2 h post injection (see Figure 5.4.E).

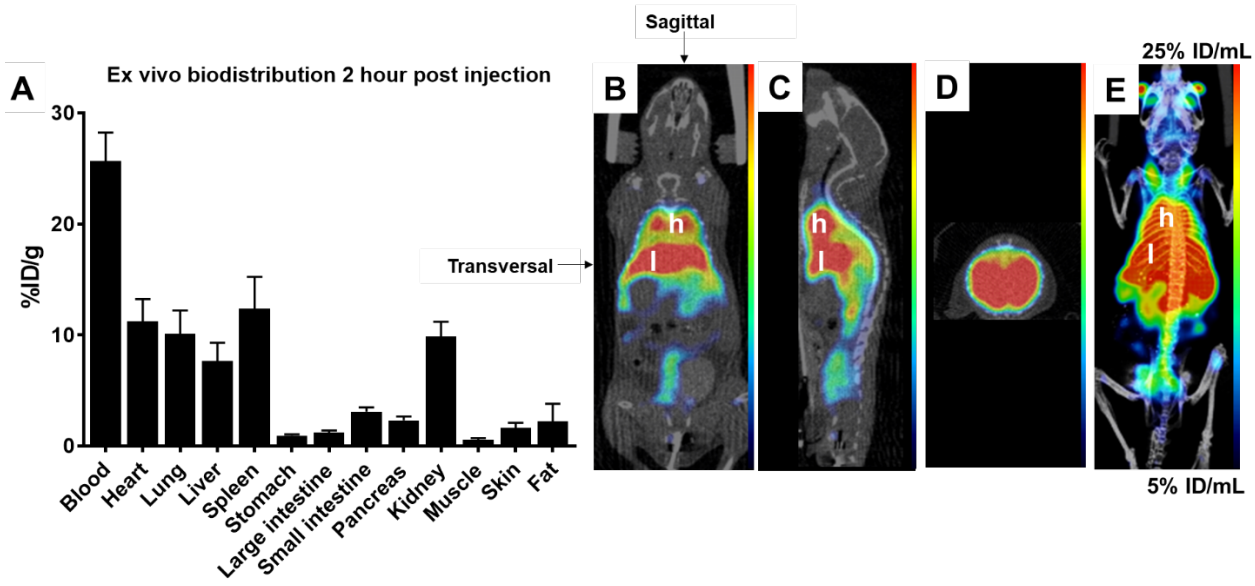

Figure 5.4 Biodistribution of [^{111}In]In-DTPA-LF^{E687A}

Ex vivo biodistribution was determined 2 h post intravenous injection of [^{111}In]In-DTPA-LF^{E687A}. At the same time point a representative SPECT/CT images: B) Coronal, C) Sagittal, D) Transversal slices and E) maximum intensity projection. h = heart; l = liver.

5.1.2. Pharmacokinetics of radiolabelled PAL1 versus PAWT in tumour bearing mice evaluated by dynamic SPECT/CT imaging

To select a suitable tumour model to test the LT delivery system in vivo, aspects concerning tumour growth and morphology were compared on a pilot experiment, where immunocompromised mice were inoculated with CAPAN1, HT1080 or MDA-MB-231 cells (see Appendix, Figure A. 9, page 179). MDA-MB-231 tumours demonstrated to have a medium-fast growth rate, and no visible ulceration within the time frame of the study was observed. HT1080 showed a fast-tumour growth presenting ulcerations within the first two weeks of experiment. Contrastingly, CAPAN1 showed a slow tumour development, requiring 8 weeks on average to reach a tumour volume adequate for in vivo imaging experiments. Therefore, MDA-MB-231 cell line was selected as the xenograft tumour model.

In vitro saturation assays using [^{111}In]In-DTPA-PAL1 or [^{111}In]In-DTPA-PAWT^{K563C} (see section 4.2.3) demonstrated that both radiotracers are able to bind to CMG2 receptors in MDA-MB-231 cells. To compare the pharmacokinetics and pharmacodynamics between the furin-cleavable PAWT^{K563C} and MMP-cleavable PAL1, MDA-MB-231 tumour bearing mice were injected with either radiotracer. For the purpose of this result chapter, "receptor" refers to all PA receptor/binding sites including the two currently identified (CMG2 and TEM8) and any potentially unidentified receptors. Whole-body dynamic SPECT scans were performed to compare blood clearance and tumour uptake of [^{111}In]In-DTPA-PAL1 or [^{111}In]In-DTPA-PAWT^{K563C} using mice bearing MDA-MB-231 tumours. VOI analysis of the dynamic SPECT images were used to determine TACs for blood (heart) and tumour (Figure 5.5.A-B).

A previous toxicological study, supported by assays based on immunodetection, demonstrated that 0.6 nmol of PAWT saturates its receptors in mice [273]. Hence, 0.2 nmol PA, with a molar activity of 50 MBq/nmol, at the time of injection, was intravenously injected in mice to avoid a decrease in target-to-background radioactivity ratios.

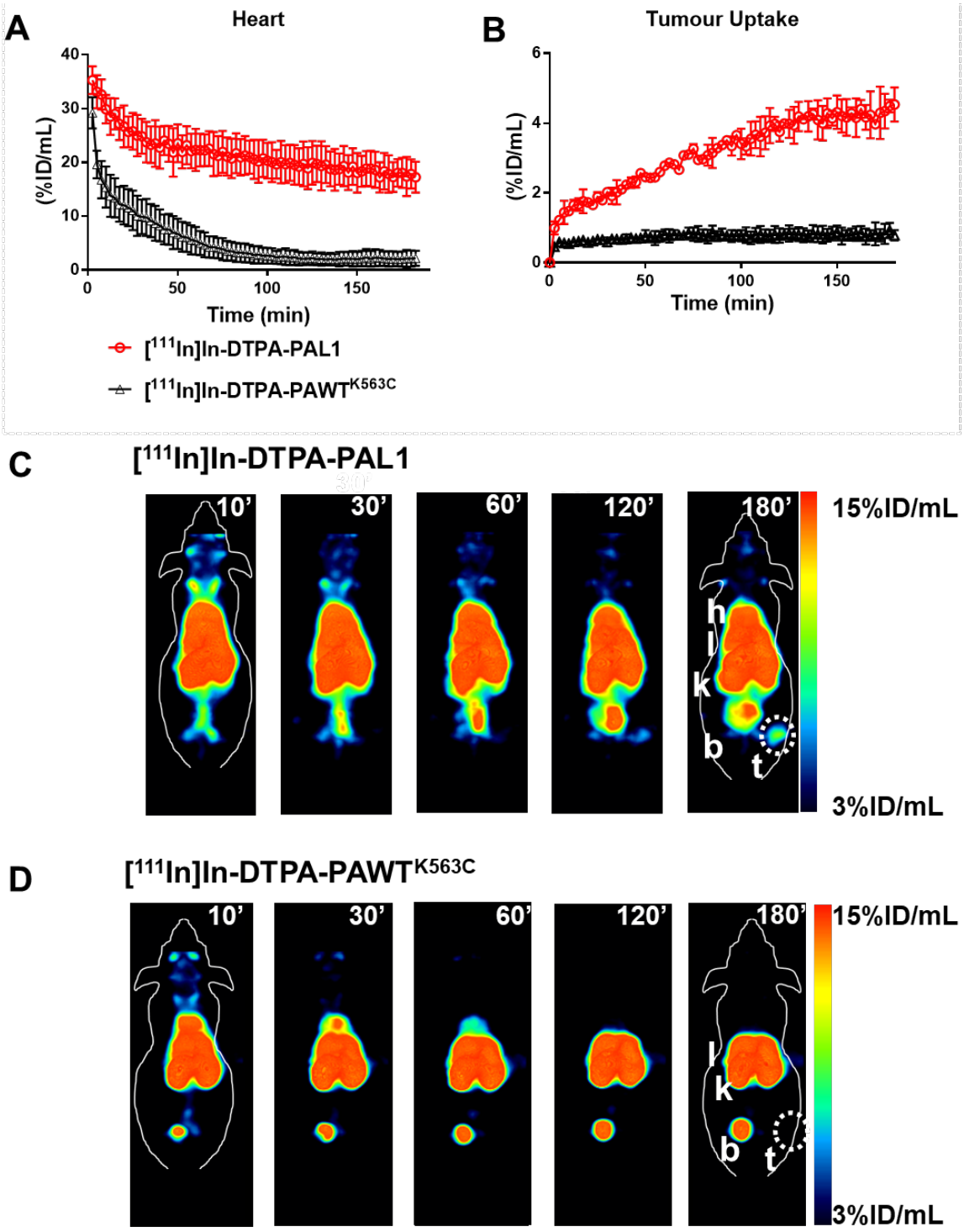

Figure 5.5 Pharmacokinetics of [^{111}In]In-DTPA-PAL1 and [^{111}In]In-DTPA-PAWT^{K563C} in MDA-MB-231 tumour bearing mice

A) Blood time activity curves were determined by the percentage of injected dose (%ID/mL) obtained from dynamic SPECT image analysis of VOI placed in the heart, and B) tumour. C) Representative coronal MIP SPECT images at different times (min) after administration of radiotracer. h=heart; l=liver; s=spleen; k=kidney, b=bladder; t= tumour. n=2 for [^{111}In]In-DTPA-PAL1 injected mice.

SPECT image analysis revealed a distinct pharmacokinetic profile for the two radiolabelled versions of PA as depicted in Figure 5.5.C-D. The parameters obtained from the model which presented the best experimental data fit are summarised in Table 5.2. Blood clearance of [^{111}In]In-DTPA-PAWT^{K563C} presented a mono-exponential decay with a blood half-life of 22.4 ± 2.3 min reaching low concentrations and a plateau of 1.8 ± 0.2%ID/g. In contrast, the blood clearance of [^{111}In]In-DTPA-PAL1 followed a biphasic pattern, with a fast half-life (55% fast clearance) and slow half-life (45% slow clearance) indicating a process of distribution and elimination of radiotracer.

Table 5.2 Parameters describing pharmacokinetic of [^{111}In]In-DTPA-PAWT^{K563C} or [^{111}In]In-DTPA-PAL1 in the blood

Radiotracer [^{111}In]In-DTPA-	Preferred model	Plateau (%ID/mL)	Half-life (min)	K Rate Constant (min^{-1})
PAWT^{K563C}	One phase	1.8 ± 0.2	22.4 ± 2.3	0.03
PAL1	Two phases	12.2 ± 5.0	Fast: 7.9 ± 1.0 Slow: 100.2 ± 5.0	Fast: 0.09 ± 0.2 Slow: 0.006 ± 0.005

At 3 h post administration of [^{111}In]In-DTPA-PAL1 more radioactivity could be observed in SPECT images and a different distribution pattern when compared with mice injected with [^{111}In]In-DTPA-PAWT^{K563C}. The significantly lower blood concentration of [^{111}In]In-DTPA-PAWT^{K563C} when compared to [^{111}In]In-DTPA-PAL1 (Figure 5.5.A) is in accordance with results previously described in the literature. Moayeri et al. described that after 2 h post administration of PAs, plasma concentrations of PAL1 were higher than PAWT molecules, reaching 20 fold difference at 6 h post administration [273]. In the same study, in vitro analyses using PAWT molecules and proteases inhibitors demonstrated that serine proteases present in the plasma catalyse PAWT degradation to a C-terminal 63 kDa fragment [273]. Considering that PAWT^{K563C} was radiolabelled site-specifically at the 563 amino acid position (cysteine residue), in the case of a proteolytic degradation by furin enzyme, the

63 kDa C-terminal fragment would still be seen. Hence, the biodistribution observed in mice injected with [^{111}In]In-DTPA-PAWT^{K563C} is either due to the fragment or to the complete molecule. The fast clearance, however, indicates that it is likely due to the cleaved PAWT^{K563C}, which is being cleared from the blood stream faster than it is interacting with its receptors.

Moreover, the difference in tumour uptake kinetics of [^{111}In]In-DTPA-PAWT^{K563C} versus [^{111}In]In-DTPA-PAL1 suggests that PAWT is being cleaved in the blood and cleared much faster than PAL1. Possibly, [^{111}In]In-DTPA-PAWT^{K563C} is been removed from the blood stream before molecules reach its receptors, accumulating significantly less in MDA-MB-231 tumours ($P = 0.02$) and other target organs, such as heart and liver (see Figure 5.5.C-D). The higher tumour accumulation of [^{111}In]In-DTPA-PAL1 over time compared to [^{111}In]In-DTPA-PAWT^{K563C} sheds light on previously reported results where these molecules were used for therapeutic purposes. In one study, Liu et al, observed that administrated LF combined with PAL1 presented an enhanced therapeutic advantage over PAWT/LF treatment in reducing the tumour burden in xenograft models indicating a higher delivery of LF molecules to tumour tissue [274]. The two possible explanations are (1) that both molecules present the same tumour uptake and that PAL1 is more effectively cleaved and activated into competent pre-pores, (2) or that more molecules of PAL1 are reaching the tumour site and delivering LF. Based on the higher uptake of [^{111}In]In-DTPA-PAL1 in the tumour tissue and slower blood clearance observed here, the second assumption is likely to be correct.

Maximum intensity projection images demonstrate a clear higher uptake of [^{111}In]In-DTPA-PAL1 in the tumour tissue when compared to [^{111}In]In-DTPA-PAWT^{K563C} at 3 h post administration of the radiotracer (see Figure 5.6.E-F). However, the long blood half-life of [^{111}In]In-DTPA-PAL1 when compared to [^{111}In]In-DTPA-PAWT^{K563C} could influence

tracer uptake as determined by ex vivo biodistribution analysis in highly perfused organs such as the kidney, liver and lungs, as well as the tumour (see Figure 5.6.A). In addition, tumour-to-blood ratios demonstrated a higher target-to-background signal for [^{111}In]In-DTPA-PAWT^{K563C} when compared to [^{111}In]In-DTPA-PAL1 (see Figure 5.6.B-D). Hence, the specificity of the radiotracer binding for anthrax receptors would require a blocking experiment with the use of cold PAWT/PAL1.

Ex vivo biodistribution performed in mice injected with [^{111}In]In-DTPA-PAWT^{K563C} demonstrated that the mainly targeted tissues were the heart (5.89 ± 1.33%ID/g), lungs (13.67 ± 3.09%ID/g), kidneys (143.71 ± 18.89%ID/g), spleen (35.98 ± 8.40%ID/g), liver (15.68 ± 4.41%ID/g) and small intestine (6.28 ± 0.38%ID/g) (see Figure 5.6.A). As expected, [^{111}In]In-DTPA-PAL1 biodistribution showed a similar global pattern albeit at significant higher concentration (P = 0.01) in all organs mentioned before but liver and spleen possibility due to fast saturation of anthrax receptors by radiotracer. Higher concentration can be due to higher blood values due to increased plasma stability of PAL1 molecules which are resistant to cleavage by proteinases present in the blood stream.

Previous work demonstrated that anthrax receptors are present in different human tissues at the transcriptional level [157] in the same organs which were target by radiolabelled PAs injected in mice here. These results indicate that even though both PAs might be targeting anthrax receptors, as mentioned before, in order to test the specificity of the binding, blocking experiments using excess of unlabelled PAs are necessary. Otherwise, the use of knock out mice models for the anthrax receptor could also further confirm the results reported here [275].

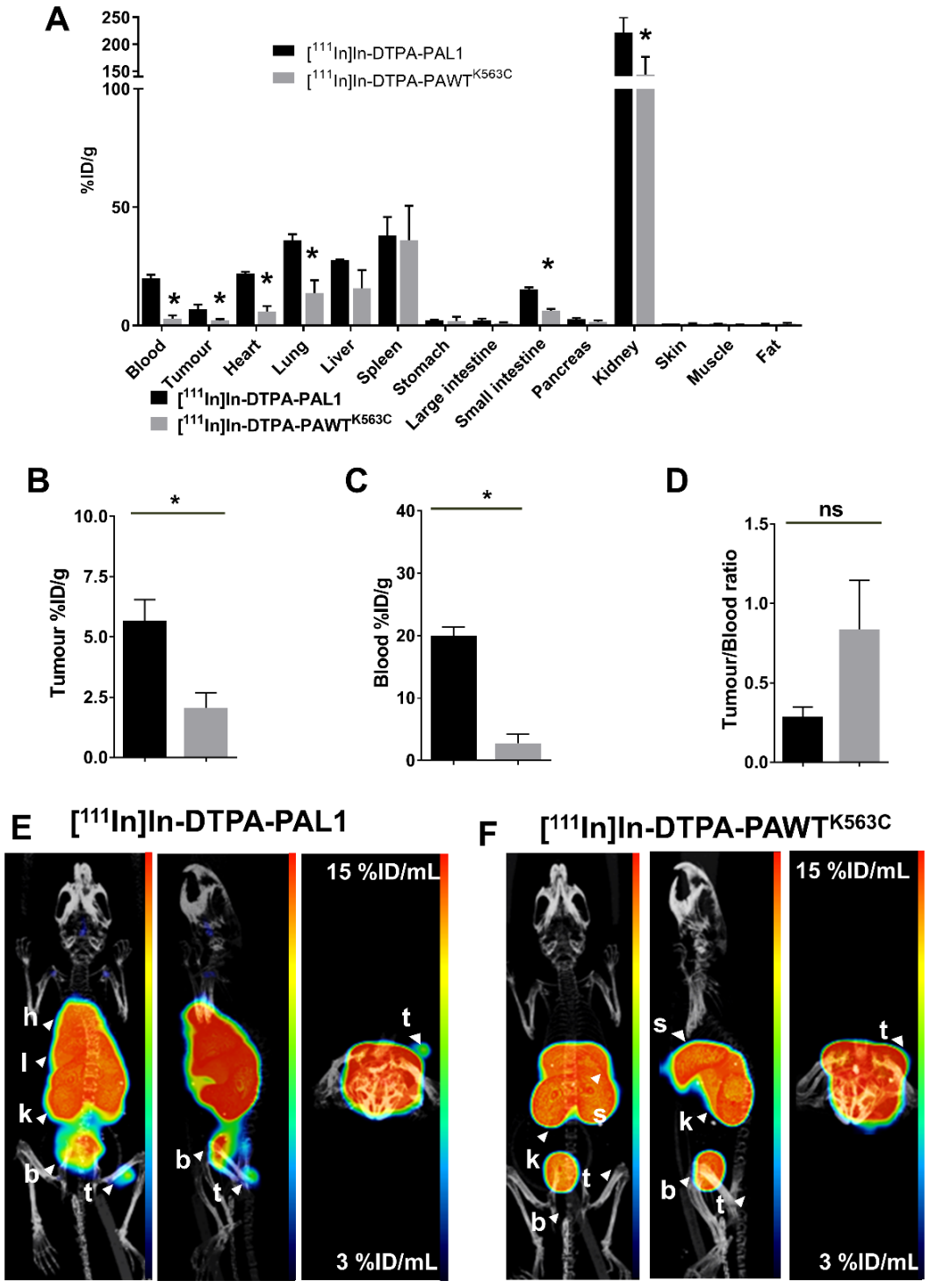

Figure 5.6 Biodistribution of [^{111}In]In-DTPA-PAL1 compared to [^{111}In]In-DTPA-PAWT^{K563C}

A) Ex vivo biodistribution of radiolabelled PAs in MDA-MB-231 tumour-bearing mice after gamma-counting represented by (%ID/g). B) Tumour and C) blood uptake at 3 h post administration of radiotracer. D) Ratio of radioactivity concentration in tumour tissue versus blood. E-F) SPECT representative maximum intensity projections at 3 h post intravenous administration. n=2 in [^{111}In]In-DTPA-PAL1 injected mice.

5.1.3. Ex vivo tumour autoradiography of ^{111}In-radiolabelled PAs

To further investigate the distribution of [^{111}In]In-DTPA-PAWT^{K563C} and [^{111}In]In-DTPA-PAL1 within MDA-MB-231 tumour tissue at higher resolution, tissue sections were imaged by autoradiography. Ex vivo autoradiographs reflected globally higher accumulation of [^{111}In]In-DTPA-PAL1 (Figure 5.7.A) in the tumour compared to [^{111}In]In-DTPA-PAWT^{K563C} (Figure 5.7.B), which is consistent with the SPECT imaging results (see Figure 5.7).

The same tumour sections imaged by autoradiography were stained for CMG2 by immunofluorescence, to evaluate if the presence of the receptor correlated with PA delivery on a microscopic level. CMG2 expression was observed throughout the tumour section, with noted membrane expression (inset Figure 5.7). Unexpectedly, the areas showing higher levels of radioactive compound did not correlate with those presenting higher CMG2 levels (Figure 5.7). It is possibly that the heterogeneity observed for radiotracer distribution might be correlated with the histological structure of tumour.

Haematoxylin and eosin staining (H&E) of adjacent tissue sections was performed to obtain structural information and to shed some light into the tracer's distribution. Comparing H&E staining with autoradiography images of tumour sections suggested that radiotracer concentrations are lower in areas characterised by reduced cellularity, characteristic of necrotic regions within the tissue (Figure 5.7) and, on the other hand, uptake is increased in areas of viable tumour cells. This might indicate the necessity of membrane and cell conservation in order for the radiotracer to have access to CMG2 receptors.

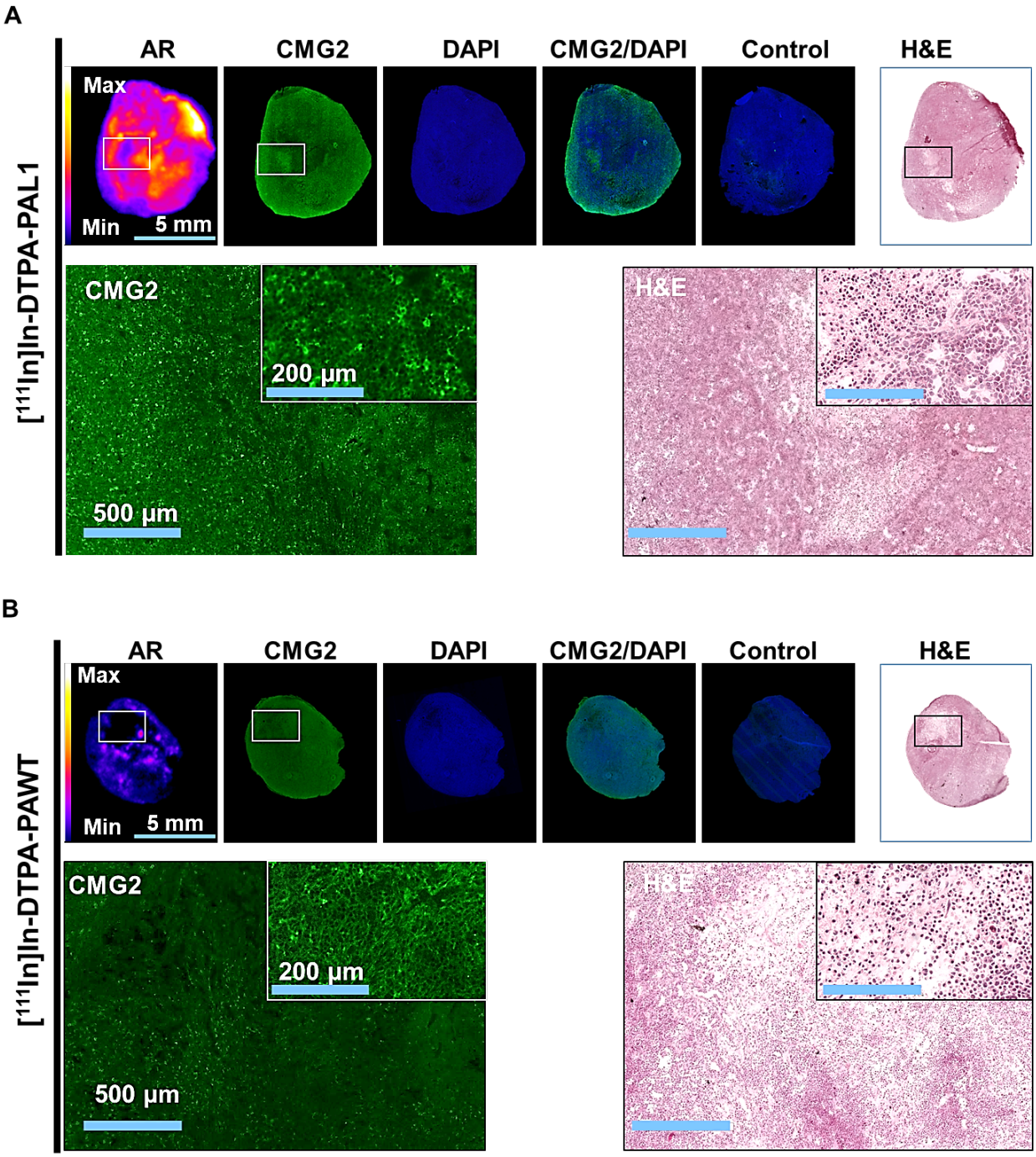

Figure 5.7 Differential accumulation of ^{111}In-radiolabelled PAs in CMG2 expressing tumours.

Ex vivo autoradiography (AR) from representative MDA-MB-231 tumour sections of mice sacrificed 3 h post administration of either (A) [^{111}In]In-DTPA-PAL1 or (B) [^{111}In]In-DTPA-PAWT^{K563C}. Immunofluorescence of the tumour tissue for CMG2 was performed, and for nuclear staining DAPI was used. Control demonstrates the specificity of CMG2 staining. Arrows indicate two correspondent areas from Haematoxylin and eosin (H&E) staining which correspond to reduction of radioactivity and a necrotic region.

5.2. Delivery of [^{111}In]In-DTPA-LF^{E687A} by PA pre-pores

Based on the pharmacokinetic profiles, [^{111}In]In-DTPA-LF^{E687A} was considered to be the best molecule to be delivered by PAL1 pre-pores to tumour tissues. The faster clearance of [^{111}In]In-DTPA-LFn would limit its delivery. In addition, the slow but steady increase in tumour uptake of PAL1 over time indicated that a co-injection of PAL1 with [^{111}In]In-DTPA-LF^{E687A} would be advantageous. Therefore, the next step was to inject MDA-MB-231 xenograft bearing mice with [^{111}In]In-DTPA-LF^{E687A}. The groups were designed to evaluate if the delivery of the radiotracer was mediated by MMP cleavage (see Table 5.3).

The design for the different experimental groups aimed to test different components which are required in the LT delivery system. Group I was designed to present MMP imaging in MDA-MB-231 tumour tissue, since 0.2 nmol PAL1 was co-injected with 0.1 nmol [^{111}In]In-DTPA-LF^{E687A} (100 MBq/nmol, specific activity at the time of experiment). All the other experimental groups were divided in two different categories: (1) presenting a blocking pre-injection (groups II and III) previous to [^{111}In]In-DTPA-LF^{E687A}/PAL1 co-injection, (2) or the radiotracer was co-injection with a different PA variant, either PAU7 (group IV) or PAWT (group V). In order to evaluate the non-specific uptake, group VI was considered the control group consisting of [^{111}In]In-DTPA-LF^{E687A} only.

Table 5.3 Experimental groups injected with [^{111}In]In-DTPA-LF^{E687A} for MMP imaging in MDA-MB-231 mouse bearing xenografts

Group	Protective Antigen co-injected	Pre-injection 1 h before	Function
I	PAL1	none	Forms pores upon [1]MMP cleavage and [2]CMG2 interaction.
II	PAL1	PAU7	Excess of PAU7 molecules block PAL1 interaction to CMG2 receptor.
III	PAL1	LF^{E687A}	Excess of unlabelled LF^{E687A} block radiotracer interaction with PAL1 pores.
IV	PAU7	none	It is not cleaved thus do not form pores but interacts with CMG2 receptors.
V	PAWT	none	Forms pores upon furin cleavage and interacts with CMG2 receptor.
VI	none	none	Non-specific uptake of radiotracer

[1]Matrix metalloproteinase; [2]Capillary morphogenesis gene 2

Due to the high blood concentration for [^{111}In]In-DTPA-PAL1 3 h post administration, imaging was performed 3 and 24 h post injection of the radiotracer (see Figure 5.8.A). After the last imaging time point, the animals were culled and organs and tissues of interest were excised and gamma-counted. VOI analysis of SPECT images demonstrated differential tumour uptake for group I (6.1 ± 0.6%ID/mL, $P < 0.05$), where PAL1 is combined with [^{111}In]In-DTPA-LF^{E687A}, at 24 h post administration of the radiotracers , but not at 3 h (see Figure 5.8.B-C). Interestingly, animals co-injected with [^{111}In]In-DTPA-LF^{E687A} and PAWT (group V) demonstrated a significantly lower tumour uptake if compared to the other groups (at 3h, $P < 0.05$ and at 24 h, $P \leq 0.001$).

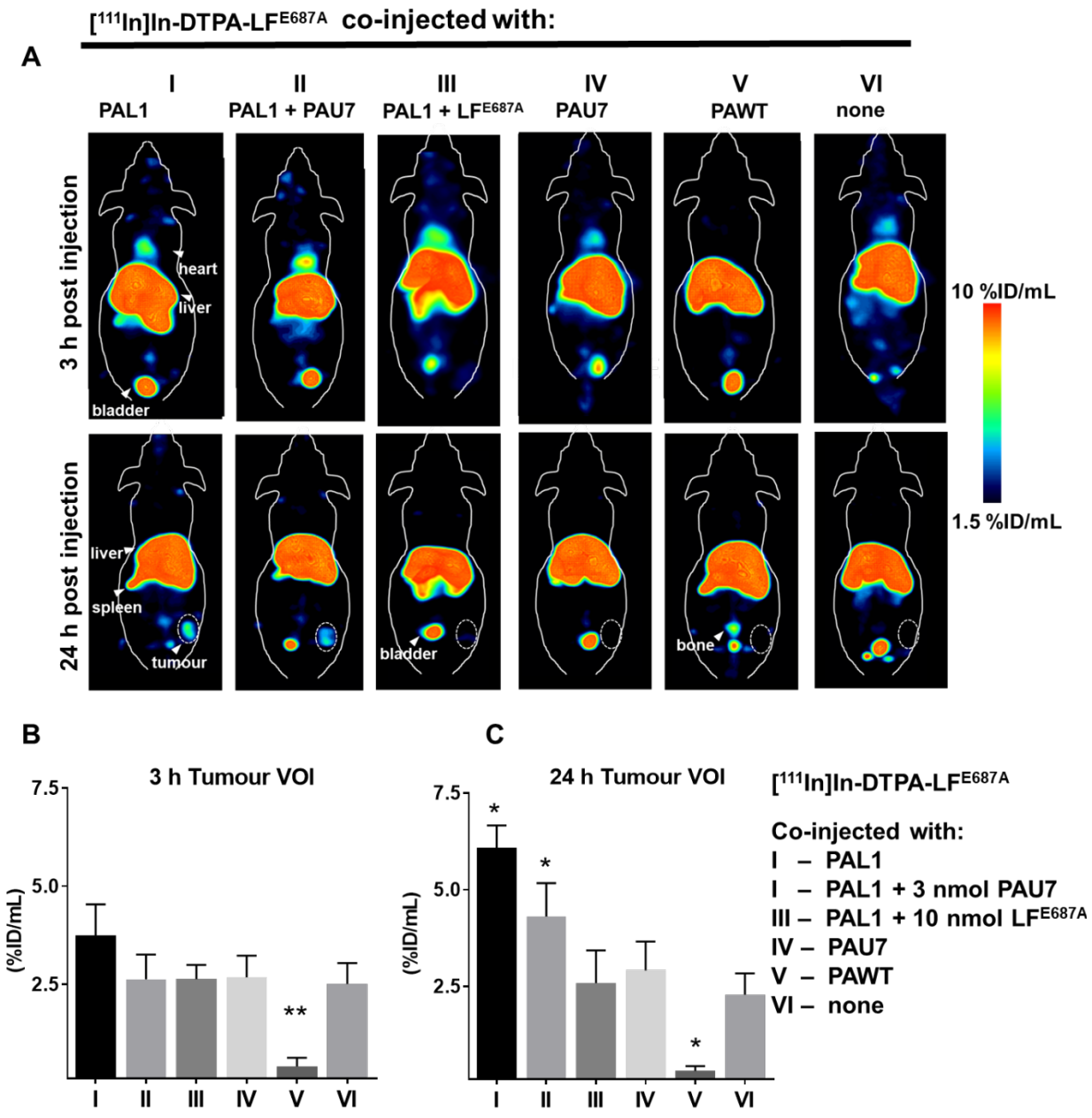

Figure 5.8 [^{111}In]In-DTPA-LF^{E687A} biodistribution by SPECT imaging in tumour bearing mice.

A) Representative MIP at 3 h and 24 h post intravenous co-injection of 0.1 nmol [^{111}In]In-DTPA-LF^{E687A} and 0.2 nmol PA variants (I-VI). B) VOI image analysis of MDA-MB-231 tumour uptake (%ID/mL). Statistically significant differences are indicated by *$P <$ 0.05; **$P \leq 0.001$.

Ex vivo biodistribution analysis of MDA-MB-231 tumours confirmed that in group I the uptake (6.0 ± 0.6%ID/g) was significantly higher than the uptake observed for groups III, IV, V and VI ($P \leq 0.001$) (see Figure 5.9.A). Surprisingly, group II, where an excess of PAU7 was pre-injected to prevent PAL1 interaction with CMG2, also a high tumour uptake was observed (5.4 ± 0.9%ID/g; $P \leq 0.001$) which was significantly different from groups III to VI. This result suggests that PAU7 does not efficiently block PAL1 interaction and subsequent activation by MMPs. PAL1 might replace PAU7 molecules, which are interacting with CMG2 receptors, be cleaved and oligomerise in stable PA pre-pores establishing a stronger interaction to the receptors than PAU7 molecules, which does not form a competent pore. Therefore, PAL1 interaction with the receptors is not an entirely reversible process. However, tumour to blood ratios demonstrate that group I presents a significantly higher signal-to-background ratio ($P < 0.0001$) when compared to all other groups (see Figure 5.9.B).

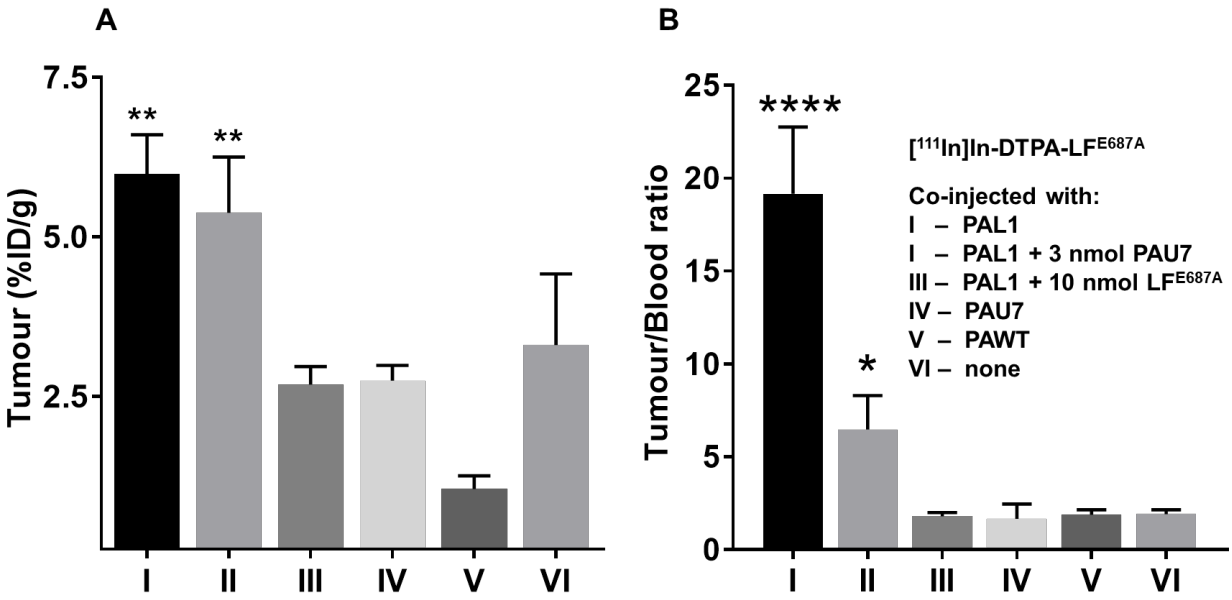

Figure 5.9 MDA-MB-231 tumour uptake of [^{111}In]In-DTPA-LF^{E687A}.

Ex vivo biodistribution of MDA-MB-231 tumours after gamma-counting 24 h post injection of 0.1 nmol [^{111}In]In-DTPA-LE^{E687A} combined with 0.2 nmol PA variants (I-VI). Uptake is represented by (%ID/g). B) Ratio of tumour and blood uptake. Statistically significant differences are indicated by *$P < 0.05$; **$P \leq 0.001$; ****$P < 0.0001$.

Control group VI, treated with just [^{111}In]In-DTPA-LF^{E687A}, presented a similar ex vivo biodistribution as group IV, where the tracer was co-injected with PAU7 (see Table 5.4). In both groups IV and VI, the organs with higher uptake were liver (48.0 ± 7.6%ID/g; 47.0 ± 2.3%ID/g), spleen (30.1 ± 4.7 %ID/g; 29.8 ± 16.1%ID/g) and kidneys (8.6 ± 3.6%ID/g; 10.8 ± 2.9%ID/g). The high uptake in these organs suggests that [^{111}In]In-DTPA-LF^{E687A} metabolism occurs via the liver and spleen with the mononuclear phagocyte system, and via the kidneys with endocytic receptors. Tumour uptake was not statistically different between these two groups (group IV 2.8 ± 0.2%ID/g and group VI 3.3± 1.1%ID/g, P = 0.85), indicating that the presence of [^{111}In]In-DTPA-LF^{E687A} observed is due to non-specific processes. In fact, enhanced permeability and retention (EPR) effect is specially observed in the abnormal tumour vasculature for macromolecules within the molecular weight range of LF^{E687A} [276].

The specificity of [^{111}In]In-DTPA-LF^{E687A} interaction with PAL1 competent pre-pores, was tested in group III, where mice were treated with a pre-injection of 100 fold excess of unlabelled LF^{E687A} (see Table 5.4). These mice presented a significantly reduction in tumour uptake when compared to group I and II (P < 0.001), reaching the same level as the non-specific uptake observed in control group VI (2.7 ± 0.3%ID/g, P = 0.79). Additionally, the reduction observed in liver uptake was significant when compared to group I (P < 0.0001) indicating that sites were blocked by increasing LF^{E687A} in the system [277]. Contrastingly, a significantly higher concentration was observed in the blood (1.6 ± 0.0%ID/g, P = 0.003), heart (3.0 ± 0.2%ID/g, P = 0.003) and kidneys (25.6 ± 4.0%ID/g P < 0.0001) when compared do group I (Table 5.4). This might be explained by the saturation of both non-specific and specific binding sites on the body by the pre-injection of unlabelled LF^{E687A} molecules, increasing the concentration of radiotracer in the blood stream and subsequently in the heart and kidneys.

In group V, where PAWT was co-injected with [^{111}In]In-DTPA-LF^{E687A}, tumour uptake was significantly lower ($P < 0.05$) when compared to all the other groups. However, concentrations of [^{111}In]In-DTPA-LF^{E687A} were significantly higher in the spleen ($P < 0.05$), lung ($P < 0.0001$) and liver ($P < 0.0001$). These results suggest that PAWT is interacting to its cellular receptors and forming competent pores after cleavage, resulting in delivery of [^{111}In]In-DTPA-LF^{E687A} to these organs. In fact, Liu et al., has demonstrated that hepatocytes are targeted by anthrax toxin, and the liver is considered a key tissue for anthrax toxin-induced-lethality in mice [275].

Table 5.4 Ex vivo biodistribution values (%ID/g) 24 h after radiotracer injection in MDA-MB-231 tumour bearing mice.

Group	I	II	III	IV	V	VI
[^{111}In]In-DTPA-LF^{E687A} +	PAL1	PAL1 + PAU7	PAL1 + LF^{E687A}	PAU7	PAWT	none
Blood	0.4 ± 0.1	0.9 ± 0.4	1.6 ± 0.0	1.3 ± 0.2	0.6 ± 0.1	1.7 ± 0.4
Tumour	6.0 ± 0.6	5.4 ± 0.9	2.7 ± 0.3	2.7 ± 0.2	1.1 ± 0.2	3.3 ± 1.1
Heart	1.8± 0.13	2.2 ± 0.7	3.0 ± 0.2	2.1 ± 0.4	1.0 ± 0.0	2.5 ± 0.8
Lung	2.3 ± 0.2	2.2 ± 0.3	3.2 ± 0.3	2.3 ± 0.2	6.2 ± 1.3	2.6 ± 0.8
Liver	53.8 ± 2.1	60.9 ± 7.5	24.9 ± 1.2	48.0 ± 7.6	62.5 ± 10.1	47.0 ± 2.3
Spleen	51.8 ± 20.3	62.8 ± 21.2	48.2 ± 2.8	30.9 ± 4.7	126 ± 42.8	29.8 ± 16.1
Stomach	0.7 ± 0.2	0.7 ± 0.2	0.8 ± 0.2	0.8 ± 0.4	0.7 ± 0.1	1.0 ± 0.2
Large intestine	2.6 ± 0.4	2.4 ± 0.4	3.2 ± 0.6	2.5 ± 0.2	2.8 ± 0.5	3.7 ± 0.4
Small intestine	2.8 ± 0.1	2.0 ± 0.2	2.0 ± 0.2	1.7 ± 0.3	1.2 ± 0.1	1.9 ± 0.4
Pancreas	0.7 ± 0.2	1.0 ± 0.3	1.2 ± 0.2	1.0 ± 0.3	0.3 ± 0.1	1.2 ± 0.3
Kidney	5.8 ± 1.8	5.4 ± 0.6	25.6 ± 4.0	8.6 ± 3.6	5.3 ± 0.7	10.8 ± 2.9
Skin	2.1 ± 1.9	1.8 ± 1.4	2.2 ± 0.6	1.6 ± 0.1	0.3 ± 0.0	1.4 ± 0.2
Muscle	0.4 ± 0.1	0.6 ± 0.1	0.5 ± 0.2	0.6 ± 0.1	0.12 ± 0.0	0.5 ± 0.2
Fat	0.8 ± 0.4	0.8 ± 0.2	1.6 ± 1.1	1.7 ± 0.7	0.5 ± 0.7	1.1 ± 0.4

5.2.1. Ex vivo tumour autoradiography of [^{111}In]In-DTPA-LF^{E687A} distribution compared to MMP14 and CMG2 expression

To investigate the microdistribution of [^{111}In]In-DTPA-LF^{E687A} within MDA-MB-231 tumour tissue, sections were analysed by phosphor imaging autoradiography and H&E staining, which gives the structural information of the tumour histology (see Figure 5.10). Adjacent tissue sections were stained for CMG2 and MMP14 by immunofluorescence (see Figure 5.11). Notably, ex vivo autoradiographs reflect globally higher accumulation of [^{111}In]In-DTPA-LF^{E687A} for tumours in group I and II – co-injected with PAL1 – as observed by SPECT images when compared to the other experimental groups. H&E staining demonstrates that radioactivity is mainly associated with viable tumour tissue in group I. In contrast, in group II a higher association of radioactivity was observed within the necrotic regions. In the other experimental groups (III-VI) the radioactivity is mainly associated with necrotic regions and capsule of the tumour, suggesting that tumour uptake in these groups is due to non-specific uptake possibly as a result of EPR effect since there is a higher back-ground-to-target effect in these groups.

The immunofluorescence staining of CMG2 and MMP14 revealed the codistribution of the two proteins mainly in areas where the tumour tissue was viable (see Figure 5.11). Similarly, the PAL1-mediated uptake of [^{111}In]In-DTPA-LF^{E687A} was concentrated in these regions of higher cellularity observed by H&E staining. Contrastingly, within the tumour necrotic centre less radiotracer was observed. However, the regions with higher uptake of [^{111}In]In-DTPA-LF^{E687A} was not related with higher expression of CMG2 or MMP14 indicating that other variables, which were not investigated here, such as, tumour vascularity, tissue viability at the molecular level, might be influencing the microdistribution of the tracer.

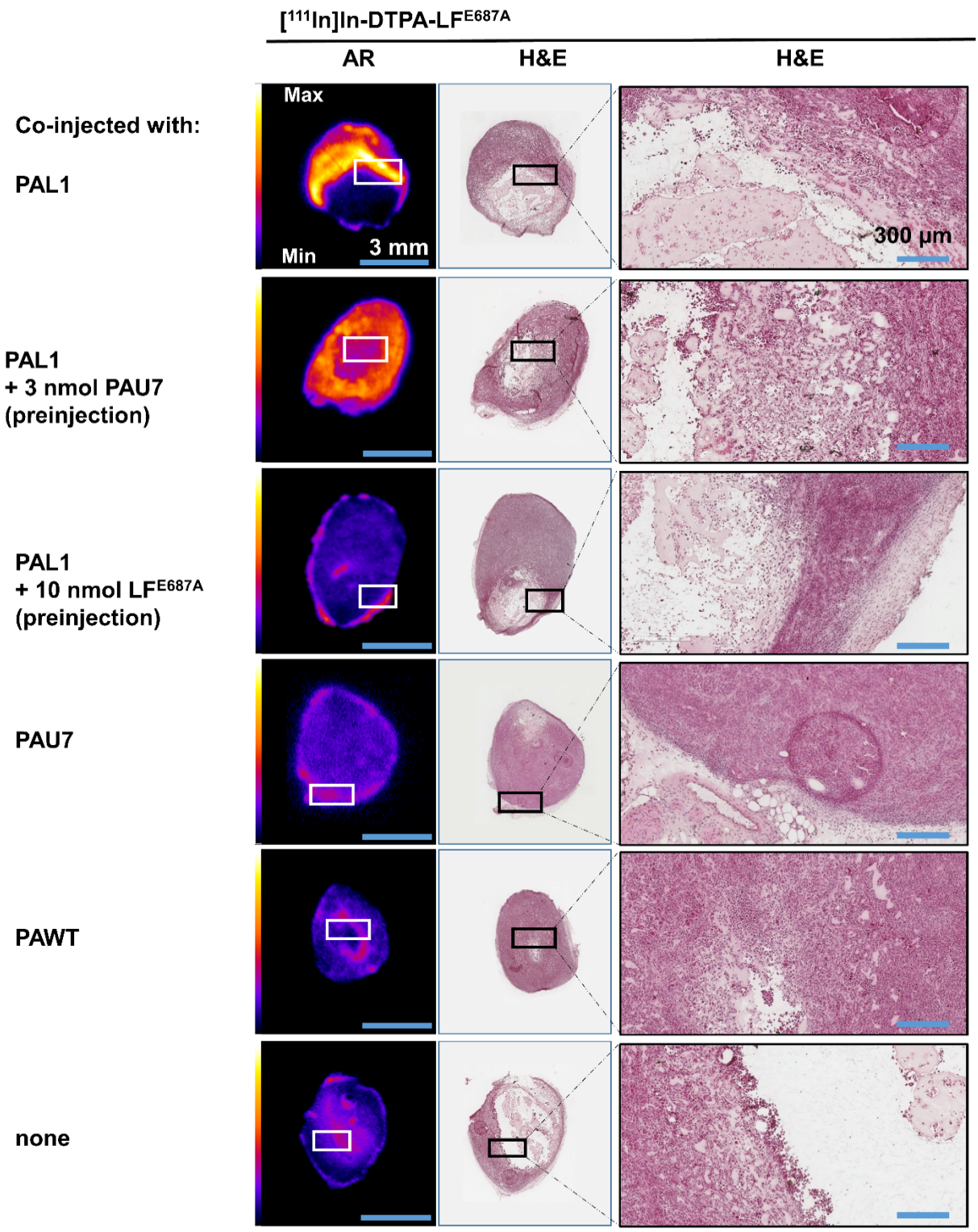

Figure 5.10 Specific delivery of [^{111}In]In-DTPA-LF^{E687A} to MDA-MB-231 tumour tissue in the presence of PAL1 pores.

Ex vivo autoradiographs (AR) from representative MDA-MB-231 tumour sections at 24 h post administration of [^{111}In]In-DTPA-LF^{E687A} co-injected with PAs. Haematoxylin and eosin (H&E) staining of MDA-MB-231 tumour section and magnification.

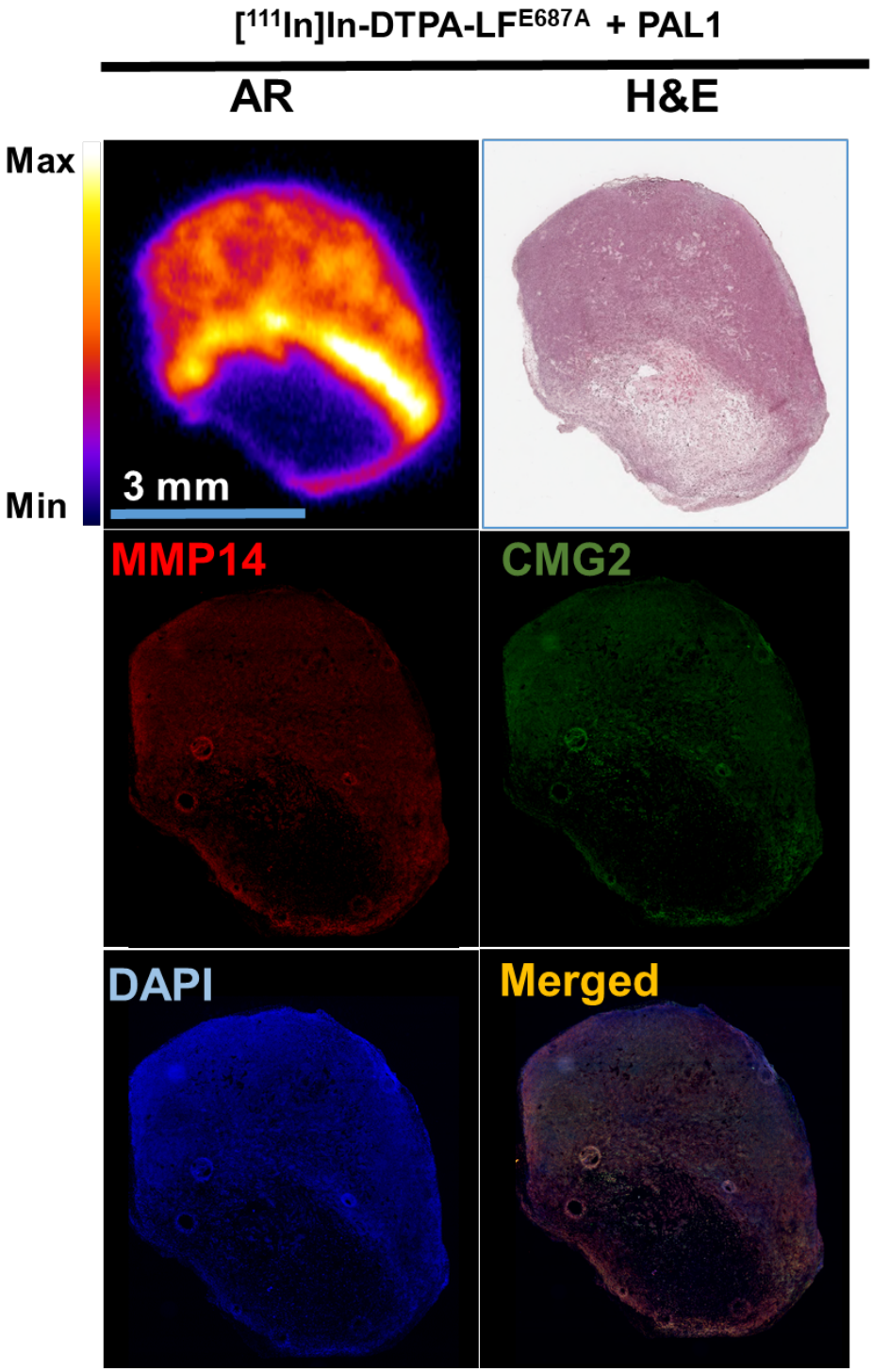

Figure 5.11 CMG2 and MMP14 expression in tissue sections codistributes with PAL1-mediated delivery of [^{111}In]In-DTPA-LF^{E687A}

Ex vivo autoradiographs (AR) from representative MDA-MB-231 tumour sections at 24 h post administration of [^{111}In]In-DTPA-LF^{E687A} co-injected with PAL1. Haematoxylin and eosin (H&E) staining of MDA-MB-231 tumour section. Immunofluorescence for MMP14 and CMG2 was performed in adjacent sections using DAPI for nuclear staining. Control staining was performed with secondary antibodies only.

5.3. Discussion

Growing evidence associates the role of MMP activity with changes in the microenvironment during tumour progression in different types of cancers [61, 68]. Molecular imaging is a promising method to visualise the clinical function of MMP activity in cancer. Here, a novel imaging agent was developed, using an MMP-activated pre-targeting approach, based on the *Bacillus anthracis* LT system. Previous work by Leppla et al. showed in detail that PAL1, an MMP-cleavable PA variant, allows for selective delivery of LF, to tumour tissue in vivo, for therapeutic gain [223, 225, 226, 256]. Here, this system is exploited to develop a molecular imaging agent using radiolabelled forms of LF.

In the current chapter four radiolabelled components of the LT system had their biodistribution and pharmacokinetic determined in mice models by SPECT imaging and ex vivo biodistribution analysis. At first, a comparison was performed between the two non-toxic variants of LF used in the current project; [^{111}In]In-DTPA-LFn and [^{111}In]In-DTPA-LF^{E687A}. The difference in molecular weight resulted in distinct pharmacokinetic profiles. [^{111}In]In-DTPA-LFn was rapidly cleared from blood with accumulation in the kidneys. On the other hand, [^{111}In]In-DTPA-LF^{E687A} presented a much higher blood residence time within the time of the study. The long blood circulation time observed for [^{111}In]In-DTPA-LF^{E687A} is in accordance with a toxicological study performed using Fischer rats injected with LT, reported in 1963 [278]. In that study, Molnar and Altenbern injected rats with PA or LF and then with PA, LF, or LT up to 24 h later. Injections of PA after LF caused death at all time intervals up to 20 h. This indicates that LF remains in the blood stream at toxic concentrations for up to 20 h. Similarly, 24 h after tail vein injections, [^{111}In]In-DTPA-LF^{E687A} was present in the blood (2.04 ± 0.5%ID/g).

Next, it was necessary to establish an in vivo tumour model compatible for the testing of LT MMP-activity imaging sistem. Previously, it was reported that [^{111}In]In-DTPA-LF^{E687A} delivers radioactivity to MMP14 and CMG2 expressing cells, CAPAN1, HT1080 and MDA-MB-231 in the presence of PAL1/PAWT (section 4.2.4). Based on the tumour growth behavior, MDA-MB-231 cell line was chosen for the development of the in vivo model (Appendix, Figure A. 9, page 179). We were discouraged from developing the negative cell line xenograft, MCF7, by our veterinary team due to the requirement of using an oestrogen supplementation [279]. However, since the LT-based probes are a pre-targeting system, it is possible to use different control groups in order to test the specificity of this approach to perform MMP activity imaging in MDA-MB-231 tumour bearing mice. Based on the pharmacokinetic characteristics of [^{111}In]In-DTPA-LF^{E687A} this molecule was selected to be used in assocition with PAL1 to target MMP activity associated with CMG2 receptors in MDA-MB-231 in tumour models.

After determining the pharmacokinetic behavior of the two radiolabelled LF variants, the pharmacokinetics and biodistribution of the two ^{111}In-radiolabelled PA variants were compared in MDA-MB-231 tumour bearing mice. SPECT image analysis demonstrated that few PAWT molecules reach the tumour site. This can be possibly attributed to the fast blood cleareance of [^{111}In]In-DTPA-PAWT^{K563C} as a result of proteases present in the blood stream which can recognise the motif, RKKR [161, 162, 280]. Hence, even though furin is upregulated in several cancers [221] and is actually required for MMP14 activation, the current study further confirms that PAWT is not suitable to deliver [^{111}In]In-DTPA-LF^{E687A} to tumours. In contrast, [^{111}In]In-DTPA-PAL1 molecules showed an increasing tumour uptake pattern within the 3 h of the study and also a high blood concentration. Since the only difference between PAWT and PAL1 is the labile sequence and their putative enzymes it was evident that PAL1 molecules are more stable in the blood stream. This encouraging

result has to be interpreted with caution since part of the accumulation of PAL1 molecules in the tumour site might be due to the EPR effect observed for macromolecules in the tumour tissue and to the blood fraction [276].

The biodistribution of [^{111}In]In-DTPA-PAWT^{K563C} was observed in organs where the presence of the CMG2 receptor has been previously described [157, 201]. However, its fast clearence from the blood pool, when compared to [^{111}In]In-DTPA-PAL1, indicates that part of the observed [^{111}In]In-DTPA-PAWT^{K563C} organ uptake, might rather correspond to metabolism of cleaved PA molecules than to the interaction with its receptors. Renal uptake of [^{111}In]In-DTPA-LF^{E687A} in animals also exposed to PAWT were similar to non-specific uptake levels. This may indicate that the uptake of PAWT observed in the kidneys is not due to competent PAWT pore formation. Conversely, mice treated with PAWT and [^{111}In]In-DTPA-LF^{E687A} presented higher liver, lung and spleen uptake of ^{111}In, suggesting higher levels of intoxication in these organs. These results suggest that PAWT is interacting with its cellular receptors and forming competent pores after being cleaved, resulting in delivery of [^{111}In]In-DTPA-LF^{E687A} to these tissues. Liu et al., has demonstrated that hepatocytes are targeted by anthrax toxin, and the liver is considered a key tissue for anthrax toxin-induced-lethality in mice [275]. Although this tool could be used to study LT intoxication, the delivery of labelled LF did not correlate with an earlier report by Liu et al. In this study, it was demonstrated in various cell-type specific CMG2-null mice, that the key tissues responsible for LT lethality are cardiomyocytes and smooth vasculature in the heart [243, 274, 275], indicating that targeting and toxicity of LT are not interchangeable for all organs.

Interestingly, the experimental group treated with [^{111}In]In-DTPA-LF^{E687A} and PAWT demonstrated the lowest tumour uptake compared to all other groups. This might indicate that [^{111}In]In-DTPA-LF^{E687A} might be delivered into cells by PAWT competent pores readily formed in its target organs which are better perfused than tumour tissue. Another possibility

is that [^{111}In]In-DTPA-LF^{E687A} interacts in the blood stream with cleaved PAWT [228, 281] molecules and the complex itself might interact with its receptors and deliver [^{111}In]In-DTPA-LF^{E687A} molecules. Studies demonstrated that this is a possible mode of action of LT intoxication mechanism, however, less effective than activation onto the cell surface before interaction with LF [282].

Similar to SPECT quantification, ex vivo autoradiography of MDA-MB-231 tumour sections demonstrated higher global accumulation of [^{111}In]In-DTPA-PAL1 than [^{111}In]In-DTPA-PAWT^{K563C}. Surprisingly, the distribution of both radiotracers did not correspond to the presence of CMG2 receptors within the tumour tissue. However, necrotic regions whithin the tumour showed lower concentration for both radiotracers autoradiography analysis. Possibly, the severe cellular damage in these necrotic regions might result in less availablity of CMG2 receptor to the radiotracers. To summarise, PAL1 demonstrated promissing distribution in tumour uptake and also pharmacokinetic compatible with LF^{E687A}.

Lastly, PAL1-mediated [^{111}In]In-DTPA-LF^{E687A} delivery to tumours was blockable with an excess of LF, or could be reduced by replacing PAL1 with PAU7, or vehicle only, indicating the PAL1 and thus MMP-depedendent cleavage of this interaction.Tumours were visualised by SPECT imaging performed 24 h after co-injection of [^{111}In]In-DTPA-LF^{E687A} and PAL1, whereas they could not be visualised in the others experimental groups. Ex vivo biodistribution and gamma-counting demonstrated tumour uptake of 6.0%ID/g for mice treated with [^{111}In]In-DTPA-LF^{E687A}/PAL1 and a tumour-to-blood ratio of approximately 20. Notably, for the other groups, an uptake of approximately 3%ID/g was observed which was mainly associated to necrotic regions of the tumour, which was confirmed by autoradiography analysis and H&E staining. In fact, a similar effect was reported by Heneweer et al., in a study where Zirconium-89 radiolabelled albumin molecules were injected in mice bearing prostate cancer. They have observed an uptake of 5%ID/g

considered to be non-specific because there are no receptors for albumin in this tumour tissue. Aditionally, the radiotracer concentrated mainly in necrotic regions of the tumour, as it observed here for the negative control group injected only with [^{111}In]In-DTPA-LF^{E687A} [283]. However, there are different variables that could have resulted in the heterogeneity of [^{111}In]In-DTPA-LF^{E687A} distribution observed. Here it was examined if CMG2 and MMP14 expression would determine the microdistribution of [^{111}In]In-DTPA-LF^{E687A} by PAL1 pre-pores to tumour tissues [284], but certain regions with higher radiotracer concentration did not correlated with higher expression of either MMP14 or CMG2. Therefore, other possible variables not tested here, such as vascularity network, vessel morphology, high interstitial pressure, and percolation of the macromolecule could explain this differential microdistribution of [^{111}In]In-DTPA-LF^{E687A} [285, 286].

5.4. Conclusion

The PAL1/LF system developed here is distinctly different from any previously reported MMP imaging methodology (section 1.7). Additionally, this system is advantageous because does not rely on binding to an extracellular, potentially non-permanent epitope, but rather depends on the build-up of radiolabelled [^{111}In]In-DTPA-LF^{E687A} within cells. Notably, the LT system has the distinct additional advantage that upon cleavage of PAL1 by MMPs, the PA pre-pore is capable of delivering multiple radiolabelled copies of [^{111}In]In-DTPA-LF^{E687A} to the cytoplasm of tumour cells. All these characteristics resulted in a specific high, MMP-activity targeting probe for SPECT imaging. Taken together, our results indicate that radiolabelled forms of mutated anthrax lethal toxin hold promise for non-invasive imaging of MMP activity in tumour tissue.

Chapter 6

6. Chapter 6: Summary and Future Perspectives

6.1. Introduction: Novel imaging agent for MMP activity in tumours

Matrix metalloproteinase (MMP) are a family of zinc-dependent proteases that can degrade most components of the extracellular matrix (ECM). MMP activity is essential for tumour growth, allowing cancer cells to invade surrounding tissues and metastasise, as well as interact with the local tumour immune environment [68, 287, 288]. The roles of MMPs include proteolytic degradation of the ECM, modification of cell-cell and cell-ECM interactions, stromal interactions, tumour cell migration, epithelial-to-mesenchymal transition, and angiogenesis. The structure, regulation and substrates of MMPs have been extensively reviewed elsewhere [289-291]. In particular, the gelatinases MMP2 and MMP9, as well as the membrane-anchored MMP14 have been strongly implicated in the above processes. Overexpression of these biomarkers correlates with a cancer's overall aggressiveness [59]. In addition to their role in cancer, MMPs are also implicated in cardiovascular diseases, neurodegenerative disorders such as Alzheimer's disease or Parkinson's disease, autoimmune diseases, and several pulmonary and oral pathologies [60]. Although early attempts to target MMPs using small molecule inhibitors for cancer therapy were largely unsuccessful in clinical trials [240, 292], MMPs remain a viable and highly desirable therapeutic target based on promising preclinical results and their role in disease progression [293].

A molecular imaging agent that allows non-invasive imaging of MMP activity and related proteins would allow in vivo visualisation of the processes outlined above, permitting early detection, prognosis, and measurement of therapy efficacy. A diverse range of molecular imaging agents have been developed over the past 20 years, summarised in the first chapter of this thesis (section 1.7). This range includes agents to be used with a wide variety of

molecular imaging modalities (SPECT, PET, MRI, and optical imaging). The agents are based on a variety of targeting vector systems, including labelled small molecule MMP inhibitors [294], antibodies targeting MMPs [295], or activatable, cleavable peptides [296]. With the exception of the latter, all of these imaging agents bind in a one-to-one fashion to mostly soluble MMP enzymes present in the blood fluids, and in addition to issues regarding pharmacokinetics and blood clearance, MMP specificity, and bioavailability, these compounds seldom reach sufficient tumour uptake to be useful as MMP imaging probes [287]. Notably, these imaging agents generally do not distinguish between the non-catalytically active pre-forms and the active forms of MMPs.

Here, a modified anthrax lethal toxin (LT) system was used to visualise MMP activity on the surface of tumour-cells [297]. *Bacillus anthracis* is a spore-forming bacterium that causes anthrax disease [298]. As a means of suppressing its host's immune response, the bacterium produces a set of toxins to promote its own survival: Protective Antigen (PA), Lethal Factor (LF), and Edema Factor (EF). After binding to the ubiquitous anthrax receptors (CMG2 and TEM8), full-length PA_{83} (83 kDa) is cleaved by furin or furin-like proteases to a 63 kDa C-terminal fragment (PA_{63}) [231]. Thus, the PA is activated to form a hepta- or octameric pre-pore on the cell-surface, creating a de novo binding site for LF and EF on the interface between cleaved PA_{63} monomers [299]. After clathrin-mediated endocytosis, LF is threaded through the oligo-PA pore, and is delivered to the cytoplasm, where it cleaves the N-terminal from several MEKs, thereby preventing the activation of downstream factors resulting in cytotoxic effects [300-302].

Liu et al. previously generated an engineered PA that requires cleavage-mediated activation by MMPs, by modifying the amino acid sequence that acts as a substrate for furin cleavage [233]. An MMP-cleavable version, PAL1, was generated by inserting an MMP-labile sequence, GPLGMLSQ, between amino acids ($_{164}$RKKR$_{167}$) of the original PA (PAWT).

PAL1 allows MMP-selective intoxication of tumour cells in vitro, as well as tumour xenografts grown in mice, combined with LF, incorporating the ADP-ribosylation domain of *Pseudomonas aeruginosa* exotoxin A (FP59) [248].

Here, the use of this MMP-activatable system was expanded to allow molecular imaging of MMP activity in mouse models of cancer, by SPECT imaging, using a radiolabelled catalytically inactive version of LF, LF^{E687A}, in combination with MMP-activatable PAL1. In this thesis, this novel pre-targeted imaging system demonstrated to be selective for MMP-expressing cancer cell lines in vitro, and showed selective, non-invasive, in vivo imaging in MMP-expressing tumours grown in mice. Below, the main results are summarised and certain aspects of this approach will be further discussed. In conclusion, I examine the potential role for the use of LT radiolabelled probes for cancer imaging and therapy.

6.2. Results and Discussion

6.2.1. PAL1 is cleaved and activated by MMPs

The validation of the enzymatic susceptibility for the different PA variants used here was considered a key aspect for the development of LT based imaging probes. Therefore, in a cell-free assay, the different PA molecules namely: furin-cleavable PAWT, MMP-cleavable PAL1 and uncleavable PAU7 variants were incubated with different enzymes (for further details section 3.2.1). Recombinant human MMP2 and MMP14, but not furin alone, were able to cleave PAL1. As expected, only furin was able to cleave PAWT, and neither MMPs nor furin were able to cleave PAU7. Cleavage of PAL1 by MMP2 and MMP14 at the intended site was further confirmed by mass spectrometry.

Previously, PAL1 susceptibility towards MMP9 activity was demonstrated by our collaborators [223], which together with MMP2 and 14, is linked with poor cancer

prognosis. However, it is likely that other MMPs might be able to cleave PAL1. This hypothesis is considered because of the methodology used for the sequence selection of PAL1 cleavable site. PAL1 was modelled after a reference peptide corresponding to one of the natural substrates for MMPs (1, 2, 8, 9, 12, 13 and 14 [303]), the α1 chain of type I collagen [304]. The PAL1 labile sequence was designed to be susceptible towards MMP2 and MMP9 cleavage. The residue substitution in PAL1 was chosen based on a previous systematic study where 50 variants of the reference peptide (GPQG*IAGQ - α1 chain of type I collagen) were submitted to cleavage by the gelatinases, but not MMP14. Nonetheless, the resulting PAL1 sequence was susceptible to MMP14 cleavage. This highlights the known overlap in MMP substrate preferences, and emphasises one of the challenges in designing peptidic sequences with susceptibility towards a specific MMP [305].

However, since the initial experiments performed to elucidate the cleavage signatures or physiological substrates for MMPs, bioinformatics and proteomic methods have evolved. High-throughput cleavage profiling technologies associated with tools for analysis have resulted in an increased testing space and improved sequence design [305]. This is well exemplified by a recent study developed by Ratnikov et al., where 64 million sequences were tested in a phage peptide substrate assay against 18 different MMPs using a multiplex analysis [12]. The data originated from this study was compiled on a data base called CleavPredict where proteolytic event predication for 11 different MMPs can be performed in silico [29]. Indeed, PAL1 analysis of the cleavage site indicated that possibly MMP8, 10, and all the membrane tethered MMPs could cleave its sequence. Based on these newer analyses and also on the established central role of MMP14 in cancer progression, new PA variants were design containing a different cleavable site aiming to increase the susceptibility towards MMP14.

6.2.2. PA variants designed for preferential MMP14 cleavage

In order to target MMP14 activity preferentially, four new variants of PA were designed replacing the furin recognition cleavage site for a new sequence. All variants were tested and compared to PAL1 and PAWT, as described below. Variant PANL12-I was designed based on a natural substrate for MMP14, pro-MMP2 (CPKESCN*LFVLKD) [306]. A second variant, named PAHL9-I, was based on the peptide sequence (CRPAH*LRDSG) recently developed by Ouyang et al., with the aim to create a cellular biosensor for MMP14 activity. This sequence was optimised by a phage substrate cleavage study and it was found to be susceptible to MMP14 but not to MMP2 or MMP9 [307]. Contrastingly, the two other variants used here, PAGL9 and PANL8, were designed by us using the MEROPS database, which concentrates the most common residues around the scissile bond of substrates cleaved by MMP14 described in the literature. In this particular case the number of cleavage events computed for MMP14 activity were 132 [308].

In the current work, Dr Leppla optimised the design for the four different primers to produce clones presenting the relevant cleavage site on the scaffold of the original PA molecule. All cysteine residues present in the original sequence were replaced to obtain a better charge balance and to reduce the possibility of post-translational modifications of the engineered protein (Figure 6.1.A). Dr Chen performed the mutagenesis work using Q5 Site-Directed Mutagenesis Kit (New England Biolabs, USA), resulting in four plasmids encoding the new PA variants. Dr Fattah was responsible for the expression and purification of the proteins which were kindly provided to us.

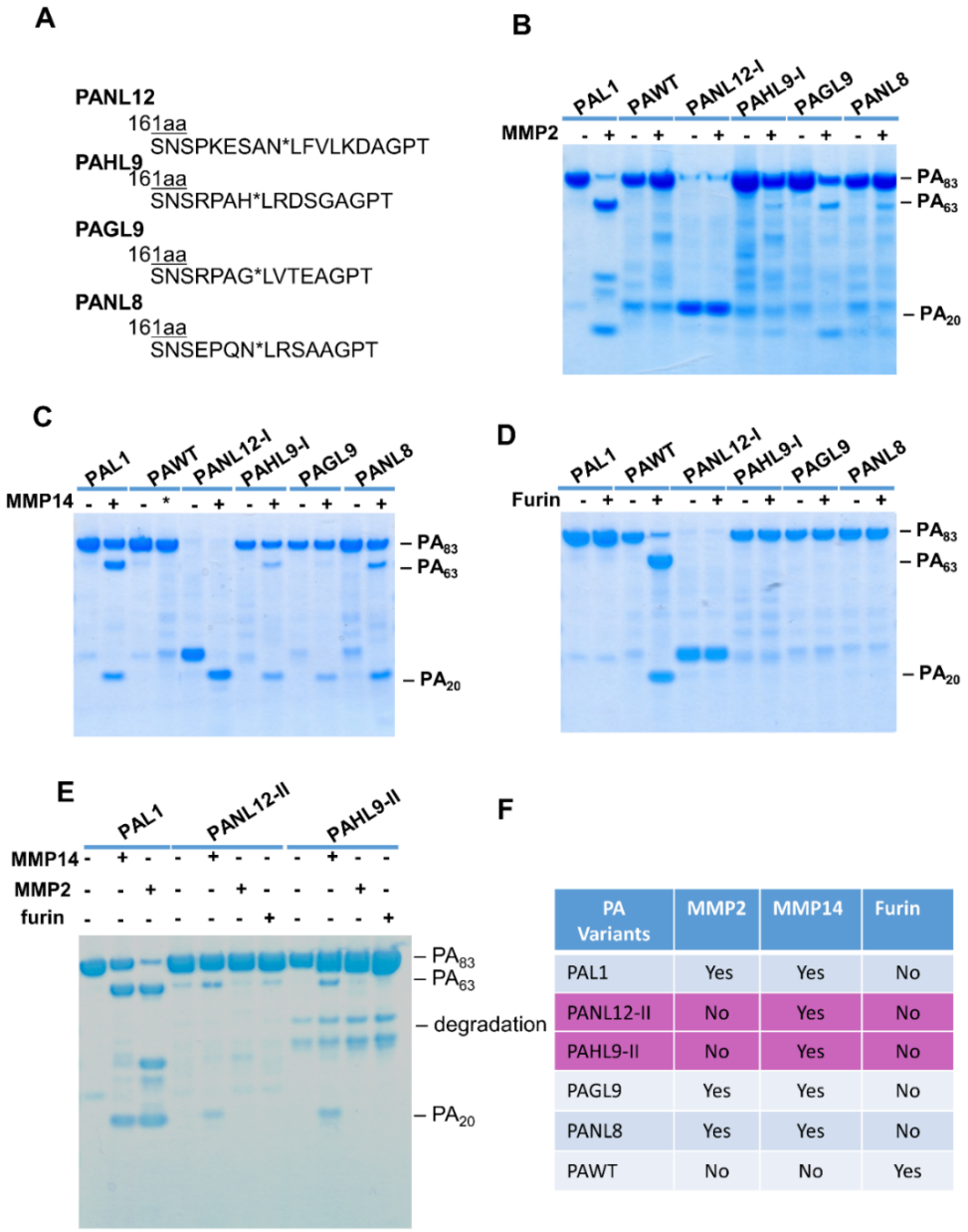

PA Variants	MMP2	MMP14	Furin
PAL1	Yes	Yes	No
PANL12-II	No	Yes	No
PAHL9-II	No	Yes	No
PAGL9	Yes	Yes	No
PANL8	Yes	Yes	No
PAWT	No	No	Yes

Figure 6.1 New PA variants and their susceptibility to MMP14

A) Engineered cleavage site of PA variants designed to be cleaved by MMP14. SDS-PAGE of PAs prepared in a cell-free assay after incubation for 16 h at 37ºC with B) MMP2, C) MMP14 or D) furin. (*) Corresponds to MMP14 not pre-activated with furin. E) New batch of PANL12-II and PAHL9-II. F) Data of cleavage patterns compiled for the different PA variants.

Firstly, the susceptibility of these new PA variants was tested against MMP2, MMP14 or furin enzymatic activity in a cell-free assay (Figure 6.1.B-C). Subsequent SDS-PAGE analysis showed that PAGL9 and PANL8 were susceptible to both MMP2 and MMP14,

demonstrating that these sequences does not outperform PAL1 in terms of specificity. Surprisingly, the PANL12-I variant was in fact an N-terminal truncated version with a mass of only 40 kDa (Figure 6.1.B-C). However, this truncated version still contained the cleavage site, which was cleaved by MMP14, but not by MMP2. Similarly, PAHL9 presented preferential susceptibility for MMP14 activity. However, some protein degradation was observed as bands between 20-60 kDa, which were also seen in the original sample. As expected, the new variants were not susceptible to furin proteolytic activity. Both PANL12-I and PAHL9-I were found to be the most promising samples regarding MMP14 specificity, therefore, the mutagenesis, cloning, protein expression and purification was repeated for these two variants. Consequently, full-length PANL12-II was confirmed to be preferentially cleaved by MMP14, when compared to MMP2 (Figure 6.1.E). Again, a yet unidentified degradation product (MW 55-50 kDa) in PAHL9-II was observed. Notably, PAL1 demonstrated a consistent higher conversion of $PAL1_{83}$ to fragments ($PAL1_{63}$ and $PAL1_{20}$) than any of the newly designed variants (Figure 6.1.F). However, this enzymatic cleavage assay can be considered an artificial setting when compared to a cell-based assay, thus further in vitro characterisation is warranted.

To test if the new variants would provide functional intoxication, cytotoxicity assays were performed with all four variants, using HT1080 cells. This cell line expresses both MMP2 and MMP14. Cells were treated for 48 h with new variants of PA in association with the fusion toxin (FP59). All treatments caused a significantly reduction in cell viability when compared to the control group ($P < 0.0001$). The extent of this reduction was comparable to PAL1. This result demonstrates that all the new PA variants were able to form a competent pre-pore to deliver FP59 to the cell cytoplasm, resulting in cell death (Figure 6.2).

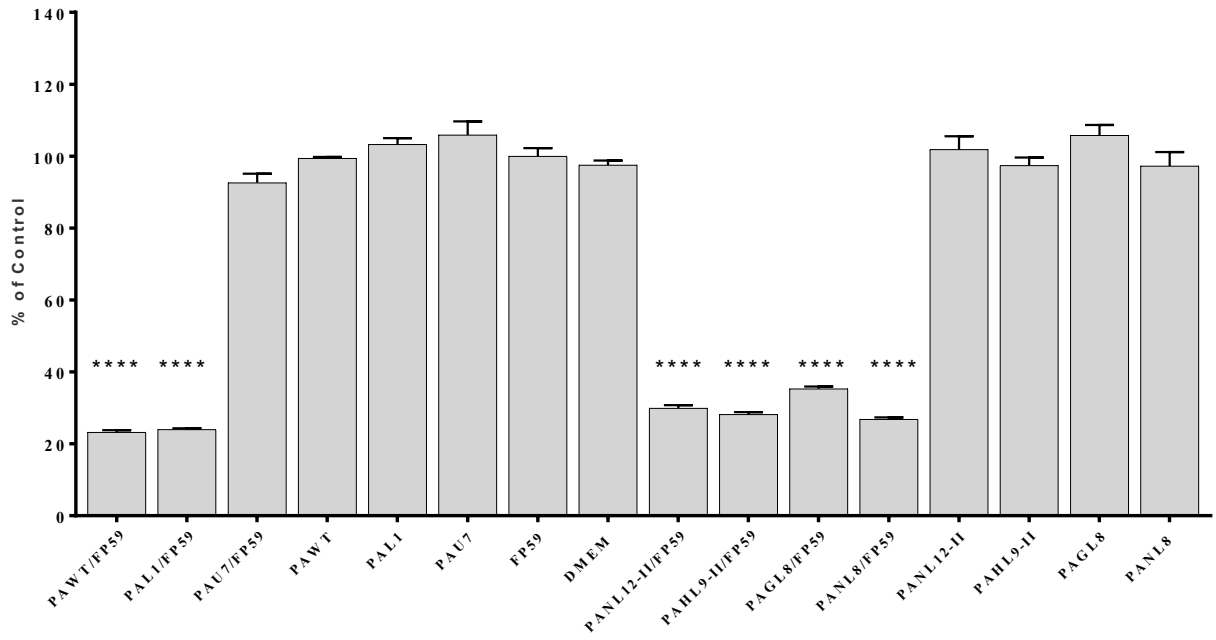

Figure 6.2 New PA variants deliver FP59 to MMP-expressing tumour cells

HT1080 cells were incubated with 3.5 nM PAs and fusion toxin 0.5 nM FP59 for 48 h prior to MTT salt addition. Absorbance was measured at 495 nm and the percentage of the control was considered as viability. Data are expressed as average ± standard deviation from experiments carried out in triplicate. This experiment was performed one more time with similar results. ****$P < 0.000$.

Considering both the cell-free and the cytotoxicity data, PANL12-II was elected as the most promising variant to preferentially target MMP14 activity. The next question to be answered, was if PANL12-II had the capacity to deliver radiolabelled LF^{E687A}, [^{111}In]In-DTPA-LF^{E687A}, to the same extent as PAL1 or PAWT to HT1080 cells. To answer that, cells were incubated with [^{111}In]In-DTPA-LF^{E687A} in the presence or not of PA variants for 3 h at 37°C prior to cell lysis and gamma-counting measurements (see Figure 6.3). Surprisingly, the amount of [^{111}In]In-DTPA-LF^{E687A} delivered by PANL12-II in cell uptake experiments was not statistically different ($P > 0.05$) from the other control conditions (II-IV). This result contradicted the cytotoxic experiment, however, it is important to remember that to cause cell death only few FP59 molecules are required [248]. In contrast, in the case of cell uptake assay, it is necessary an efficient association between PANL12-II and LF^{E687A} to result in

high cell uptake. It is likely that the modification of the cleavage sequence might have resulted in deviations of the binding site formed by PANL12-II, which might possibly have less affinity with radiolabelled LF molecules. However, other experiments should be performed in order to test this hypothesis. Therefore, to conclude, the PA variants designed here to be more susceptible towards MMP14 activity are not suitable for experiments in vivo and more optimisation and characterisation is required.

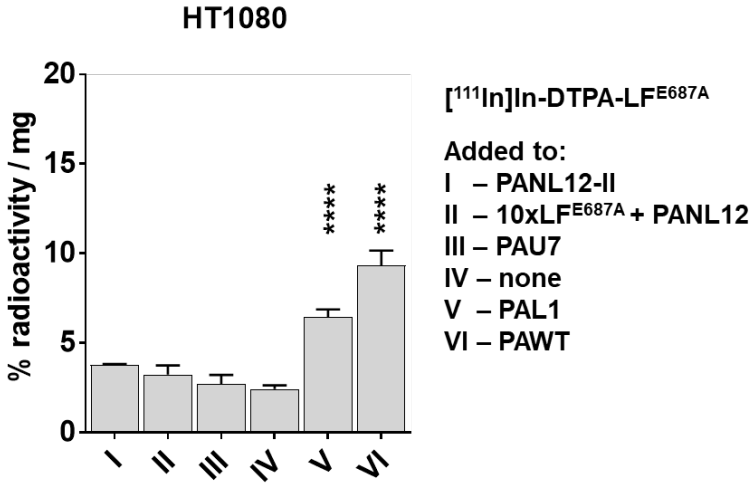

Figure 6.3 PANL12-II does not deliver [^{111}In]In-DTPA-LF^{E687A} to tumour cells

Percentage of total radioactivity added to cells normalised by protein content. Cells were exposed to 25 nM of [^{111}In]In-DTPA-LF^{E687A} with or without 80 nM PA proteins at 37°C for 3 h. The supernatant was discarded and cells were washed and lysed, then the radioactivity associated with cell lysate were measured in counts per minutes. ****$P < 0.0001$. This experiment was repeated once more presenting similar results.

6.2.3. MMP-mediated delivery by PAL1 of [^{111}In]In-DTPA-LF^{E678A}

The uptake experiments demonstrated that PAL1 was capable of delivering [^{111}In]In-DTPA-LF^{E687A} to cells and this interaction (PAL1/LF) was extensively characterised by other assays (section 4.2.4). In Chapter 5, it was described that the specific tumour uptake of [^{111}In]In-DTPA-LF^{E687A} only happened when mice were injected in combination with PAL1 (section

5.2). Together, these results demonstrated that the chelator conjugation chemistry to LF^{E687A} using lysine-directed via *p*-SCN-Bn-DTPA and radiolabelling allowed the quantification of its interaction with the cancer cells, both in vitro and in vivo. However, analysis by mass spectroscopy of the starting products revealed that LF^{E687A} was attached to 4-8 DTPA moieties resulting in a heterogeneous mixture of chelator-protein conjugates. Each subpopulation of this mixture can exhibit its own physicochemical, pharmacokinetic and, biological properties, which can reduce the accuracy of the characterisation of the radiotracer behaviour in vivo. Therefore, the radiolabelling reactions for LF^{E687A} could be further optimised with changes of the chemistry reactions used or with genetic engineering of these proteins [309, 310].

In fact, great effort has been invested in the development of site-specific labelling. However, these efforts mainly focus on antibodies although, the techniques can be applied to other proteins. An obvious approach would be to genetically engineer LF to present one cysteine as in $PAWT^{K563C}$ and LFn, creating the possibility to site-specifically modify the thiol lateral group using chelators presenting maleimide [311]. Secondly, replacing residues for a non-canonical amino acid such as selenocysteine and pyrrolysine, or non-natural amino acids via genetic engineering, could also create sites in LF^{E687A} which could be specifically modified by chelators [312-315].

Despite some of these limitations, ^{111}In-labelled LF^{E687A} was delivered to tumour tissue in vivo upon MMP activation of PAL1, enabling visualisation of MMP activity by SPECT imaging. Additionally, a detailed characterisation of the system was performed and it was demonstrated the selectivity for anthrax receptors, mainly CMG2. High affinity of radiolabelled LF^{E687A} for PAL1 pores in cells was also shown, specific delivery of [^{111}In]In-DTPA-LF^{E687A} to cancer cells in vitro and in vivo. PAL1-mediated [^{111}In]In-DTPA-LF^{E687A} delivery to tumours was blockable with an excess of LF, or could be reduced by replacing

PAL1 with PAU7, PAWT, or vehicle only, indicating the requirement of PAL1, and thus MMP-depedendent proteolytic activity in order to present significant tumour upatke of ^{111}In]In-DTPA-LF^{E687A}.

Despite the successful results reported in this thesis, one limitation of the [^{111}In]In-DTPA-LF^{E687A}/PAL1 system to visualise MMP activity is the inherent high uptake of [^{111}In]In-DTPA-LF^{E687A} in liver and spleen, possibly due to clearance of the tracer by the monocuclear phagocyte system preset in these organs. [^{111}In]In-DTPA-LF^{E687A} pharmacokinetics was also relatively slow, necessitating SPECT imaging 24 h after intravenous administration. Imaging at earlier time points, 3 h after injection did not show differences from the background values when compared to the longer interval. In contrast, [^{111}In]In-DTPA-LFn, presenting a smaller size (30 kDa), resulted in very fast renal clearance and therefore negligible liver uptake. Therefore, LF variants of intermediate size (80-60 kDa) may present a better balance for in vivo application by minimising the rapid, first-pass renal clearance observed for LFn while reducing the circulation time of full-lenth LF^{E687A} (90 kDa). Another possible advantage of an intermediate-sized LF variant would be increased tumour penetration, since the faster difusion rate through the vasculature network into tumours and through interstitial space is generally correlated with a smaller size of the radiotracer molecule [316]. For example, in vivo experiments comparing radiolabelled diabodies (60 kDa) to monomeric variable fragments from antibodies (scFv, 30 kDa) in xenograft tumour models show that diabodies have a significant advantage over monomoeric single chains [317]. In summary, the optimal consctruct-size and pharmacokinetics behavior result from a balance among multifactorial components, including, the speed of blood clearance associated with target affinity, the absolute tumour uptake and the tumour-to-background ratios [318, 319].

Another aspect that can influence the in vivo biodistribution of [^{111}In]In-DTPA-LF^{E687A} is the dose administered intravenously and its specific activity. In the current thesis a dose

escalation study to evaluate whether different ammounts of [^{111}In]In-DTPA-LF^{E687A} or PAL1 would result in increased tumour uptake and/or reduced non-specific uptake in off-target organs was not performed. Conversely, higher doses might increase homogeneity and overall tumour uptake of [^{111}In]In-DTPA-LF^{E687A} by the binding sites created by the PA pre-pore. Furtheremore, increasing the injected dose might result in increased non-specific uptake as observed for liver and spleen [320]. Given the low abundance of CMG2 receptors, and subsequent PA pre-pores (10^4) it is likely that lower injected amounts and higher specific activities of radiolabelled LF^{E687A} would result in an appropriate imaging signal and contrast. With the current specific activity of 100 MBq/nmol, 1 in every 20 unlabelled LF^{E687A} presents a ^{111}In atom, hence the majority of LF^{E687A} that are delivered by PAL1 pre-pores to cancer cells are not labelled.

Finally, to develop a radiotracer for oncological use some requirements are made as the use of high specific and selectivity, high plasma clearance and low plasma protein binding, enhanced elimination to reduce effective dose, and low toxicity is important. High non-specific binding as the one observed here for ^{111}In-radiolabelled LF^{E687A} is a common reason for the failure of a radiotracer to reach clinical studies [260]. In summary, we developed a non-invasive MMP-activity imaging probe based on the PAL1/LF system that is distinct from any previously reported MMP imaging methodology. However, to translate this system into the clinic optimisation, as discussed above, is required.

6.3. Therapeutic Perspectives of LF^{E687A}/PAL1 system

As previously mentioned, LF/PAL1 has been used therapeutically, demonstrating cytotoxicty mainly towards endothelial cells in solid tumours [224]. Interestingly, both of PA native receptors, TEM8 and CMG2, have been implicated in tumour angiogenesis and therefore have been considered themselves as potential targerts for cancer therapy [213,

321]. Notably, here it was demostrated that the distribution of CMG2 was mainly homogenous in the tumour tissue, in line with previous immunohistochemistry studies, showing that CMG2 expression is not just limited to tumour vasculature [244]. Moreover, autoradiography analysis confirmed that the distribution of [^{111}In]In-DTPA-LF^{E687A} by PAL1 pre-pores correlated with the presence of both CMG2 and MMP14 indicating that targeting and toxicity of LT are not interchangeable and lies beyond tumour vasculature. Previous work has reported that only cells that present a specific mutation in the B-Raf protein are sensitive to LF, and otherwise the cancer cell is resistant to LF/PAL1 treatment [243]. This indicates that other cells, inside the tumour lesion, where LF is deliverd by PAL1 pores, could be killed increasing the potency of the therapy.

A possible option would be to radiolabel LF^{E687A} with an radioisope that presents therapeutic as well as imaging properties. Lutetium-177 (^{177}Lu) has been used in the clinic [322]. ^{177}Lu emits β particels with an intermediate energy (βmax 490 keV) with a 0.7 mm as medium range in tissue which can cause cell death via DNA double strand breaks [323]. Therefore, ^{177}Lu-radiolabelled LF-based compounds could be delivered to cancer cells by PAL1 pre-pores causing cell death. Possibly, this approach would increase overall cell death due to targeted radiotherapy when compared to LF/PAL1. Another advantage about the physical properties of ^{177}Lu radionuclide is the emission of low-energy γ–rays at 208 and 113 keV that allows concurrent SPECT imaging and consequently the collection of information about tumour dosimetry.

Finally, the immunogenicity of DTPA-LF^{E687A} was not studied in the current work. However, it is known that non-modified LF and PA when injected in the blood stream induces formation of neutralising antibodies which results in protective immunity [324, 325]. Previous preclinical work has demonstrated that 6 doses of LF/PAL1 are required in order to promote tumour growth reduction. In fact, when mice are treated with a

immunosuppressive drug regimen, the anti-tumour effect of LF/PAL1 treatment was much more pronounced, demonstrating the influence of the immune system. Therefore, if a higher therapeutic potency would be achieve as a result from beta particle emittion originated from 177-Lu would be proven, possibly the ammount of injections to achieve therapeutic effect would be reduced and might facilitate the use of this strategy for cancer therapy [224]. To conclude, radiolabelled forms of mutated anthrax lethal toxin can be a platform compatible for targetted radiotherapy of cancer and it is a strategy that should be warrented.

References

1. Nagase, H., R. Visse, and G. Murphy, *Structure and function of matrix metalloproteinases and TIMPs.* Cardiovascular Research, 2006. **69**(3): p. 562-573.
2. J F Woessner, J., *Matrix metalloproteinases and their inhibitors in connective tissue remodeling.* The FASEB Journal, 1991. **5**(8): p. 2145-2154.
3. Van Wart, H.E. and H. Birkedal-Hansen, *The cysteine switch: a principle of regulation of metalloproteinase activity with potential applicability to the entire matrix metalloproteinase gene family.* Proceedings of the National Academy of Sciences, 1990. **87**(14): p. 5578-5582.
4. Piccard, H., P.E. Van den Steen, and G. Opdenakker, *Hemopexin domains as multifunctional liganding modules in matrix metalloproteinases and other proteins.* Journal of Leukocyte Biology, 2007. **81**(4): p. 870-892.
5. Murphy, G., et al., *The C-terminal domain of 72 kDa gelatinase A is not required for catalysis, but is essential for membrane activation and modulates interactions with tissue inhibitors of metalloproteinases.* The Biochemical journal, 1992. **283 (Pt 3)**(Pt 3): p. 637-641.
6. Murphy, G., et al., *Assessment of the role of the fibronectin-like domain of gelatinase A by analysis of a deletion mutant.* Journal of Biological Chemistry, 1994. **269**(9): p. 6632-6636.
7. Galea, C.A., et al., *Domain structure and function of matrix metalloprotease 23 (MMP23): role in potassium channel trafficking.* Cellular and Molecular Life Sciences, 2014. **71**(7): p. 1191-1210.
8. Hernandez-Barrantes, S., et al., *Regulation of membrane type-matrix metalloproteinases.* Seminars in Cancer Biology, 2002. **12**(2): p. 131-138.
9. Uekita, T., et al., *Cytoplasmic tail-dependent internalization of membrane-type 1 matrix metalloproteinase is important for its invasion-promoting activity.* The Journal of cell biology, 2001. **155**(7): p. 1345-1356.
10. Pei, D., T. Kang, and H. Qi, *Cysteine Array Matrix Metalloproteinase (CA-MMP)/MMP-23 Is a Type II Transmembrane Matrix Metalloproteinase Regulated by a Single Cleavage for Both Secretion and Activation.* Journal of Biological Chemistry, 2000. **275**(43): p. 33988-33997.
11. Jackson, B.C., D.W. Nebert, and V. Vasiliou, *Update of human and mouse matrix metalloproteinase families.* Human genomics, 2010. **4**(3): p. 194-201.
12. Ratnikov, B.I., et al., *Basis for substrate recognition and distinction by matrix metalloproteinases.* Proceedings of the National Academy of Sciences, 2014. **111**(40): p. E4148-E4155.
13. Andreini, C., et al., *Bioinformatic Comparison of Structures and Homology-Models of Matrix Metalloproteinases.* Journal of Proteome Research, 2004. **3**(1): p. 21-31.
14. Kukreja, M., et al., *High-Throughput Multiplexed Peptide-Centric Profiling Illustrates Both Substrate Cleavage Redundancy and Specificity in the MMP Family.* Chemistry & Biology, 2015. **22**(8): p. 1122-1133.
15. Nagase, H. and G.B. Fields, *Human matrix metalloproteinase specificity studies using collagen sequence-based synthetic peptides.* Peptide Science, 1996. **40**(4): p. 399-416.
16. Turk, B.E., et al., *The structural basis for substrate and inhibitor selectivity of the anthrax lethal factor.* Nature Structural & Molecular Biology, 2004. **11**(1): p. 60-66.

17. Smith, M.M., L. Shi, and M. Navre, *Rapid Identification of Highly Active and Selective Substrates for Stromelysin and Matrilysin Using Bacteriophage Peptide Display Libraries.* Journal of Biological Chemistry, 1995. **270**(12): p. 6440-6449.
18. Ohkubo, S., et al., *Identification of Substrate Sequences for Membrane Type-1 Matrix Metalloproteinase Using Bacteriophage Peptide Display Library.* Biochemical and Biophysical Research Communications, 1999. **266**(2): p. 308-313.
19. Kridel, S.J., et al., *Substrate Hydrolysis by Matrix Metalloproteinase-9*.* Journal of Biological Chemistry, 2001. **276**(23): p. 20572-20578.
20. Deng, S.-J., et al., *Substrate Specificity of Human Collagenase 3 Assessed Using a Phage-displayed Peptide Library.* Journal of Biological Chemistry, 2000. **275**(40): p. 31422-31427.
21. Eckhard, U., et al., *Active site specificity profiling of the matrix metalloproteinase family: Proteomic identification of 4300 cleavage sites by nine MMPs explored with structural and synthetic peptide cleavage analyses.* Matrix Biology, 2016. **49**: p. 37-60.
22. Schilling, O., et al., *Characterization of the prime and non-prime active site specificities of proteases by proteome-derived peptide libraries and tandem mass spectrometry.* Nature Protocols, 2011. **6**: p. 111.
23. Rawlings, N.D., A.J. Barrett, and R. Finn, *Twenty years of the MEROPS database of proteolytic enzymes, their substrates and inhibitors.* Nucleic Acids Research, 2016. **44**(D1): p. D343-D350.
24. Peri, S., et al., *Development of human protein reference database as an initial platform for approaching systems biology in humans.* Genome research, 2003. **13**(10): p. 2363-2371.
25. Apweiler, R., et al., *UniProt: the Universal Protein knowledgebase.* Nucleic Acids Research, 2004. **32**(suppl_1): p. D115-D119.
26. Holmbeck, K., et al., *MT1-MMP: A tethered collagenase.* Journal of Cellular Physiology, 2004. **200**(1): p. 11-19.
27. Page-McCaw, A., A.J. Ewald, and Z. Werb, *Matrix metalloproteinases and the regulation of tissue remodelling.* Nature Reviews Molecular Cell Biology, 2007. **8**: p. 221.
28. Löffek, S., O. Schilling, and C.-W. Franzke, *Biological role of matrix metalloproteinases: a critical balance.* European Respiratory Journal, 2011. **38**(1): p. 191-208.
29. Kumar, S., et al., *CleavPredict: A Platform for Reasoning about Matrix Metalloproteinases Proteolytic Events.* PLOS ONE, 2015. **10**(5): p. e0127877.
30. Minond, D., et al., *Differentiation of secreted and membrane-type matrix metalloproteinase activities based on substitutions and interruptions of triple-helical sequences.* Biochemistry, 2007. **46**(12): p. 3724-3733.
31. Tokmina-Roszyk, M. and G.B. Fields, *Dissecting MMP P10′ and P11′ subsite sequence preferences, utilizing a positional scanning, combinatorial triple-helical peptide library.* Journal of Biological Chemistry, 2018. **293**(43): p. 16661-16676.
32. Mott, J.D. and Z. Werb, *Regulation of matrix biology by matrix metalloproteinases.* Current opinion in cell biology, 2004. **16**(5): p. 558-564.
33. Chakraborti, S., et al., *Regulation of matrix metalloproteinases: An overview.* Molecular and Cellular Biochemistry, 2003. **253**(1): p. 269-285.
34. Yan, C. and D.D. Boyd, *Regulation of matrix metalloproteinase gene expression.* Journal of Cellular Physiology, 2007. **211**(1): p. 19-26.

35. Vincenti, M.P. and C.E. Brinckerhoff, *Signal transduction and cell-type specific regulation of matrix metalloproteinase gene expression: Can MMPs be good for you?* Journal of Cellular Physiology, 2007. **213**(2): p. 355-364.
36. Sato, H., et al., *A matrix metalloproteinase expressed on the surface of invasive tumour cells.* Nature, 1994. **370**: p. 61.
37. Morgunova, E., et al., *Structural insight into the complex formation of latent matrix metalloproteinase 2 with tissue inhibitor of metalloproteinase 2.* Proceedings of the National Academy of Sciences, 2002. **99**(11): p. 7414-7419.
38. Murphy, G., et al., *The N-terminal domain of tissue inhibitor of metalloproteinases retains metalloproteinase inhibitory activity.* 1991. **30**(33): p. 8097-102.
39. Grünwald, B., B. Schoeps, and A. Krüger, *Recognizing the Molecular Multifunctionality and Interactome of TIMP-1.* Trends in Cell Biology, 2019. **29**(1): p. 9-19.
40. Borth, W., *Alpha 2-macroglobulin, a multifunctional binding protein with targeting characteristics.* The FASEB Journal, 1992. **6**(15): p. 3345-3353.
41. Mazzieri, R., et al., *Control of type IV collagenase activity by components of the urokinase–plasmin system: a regulatory mechanism with cell-bound reactants.* The EMBO Journal, 1997. **16**(9): p. 2319-2332.
42. Rupp, P.A., et al., *Matrix Metalloproteinase 2-Integrin αvβ3 Binding Is Required for Mesenchymal Cell Invasive Activity but Not Epithelial Locomotion: A Computational Time-Lapse Study.* Molecular Biology of the Cell, 2008. **19**(12): p. 5529-5540.
43. Sabeh, F., R. Shimizu-Hirota, and S.J. Weiss, *Protease-dependent versus -independent cancer cell invasion programs: three-dimensional amoeboid movement revisited.* The Journal of Cell Biology, 2009. **185**(1): p. 11-19.
44. Redondo-Muñoz, J., et al., *α4β1 integrin and 190-kDa CD44v constitute a cell surface docking complex for gelatinase B/MMP-9 in chronic leukemic but not in normal B cells.* Blood, 2008. **112**(1): p. 169-178.
45. Redondo-Muñoz, J., et al., *MMP-9 in B-cell chronic lymphocytic leukemia is up-regulated by α4β1 integrin or CXCR4 engagement via distinct signaling pathways, localizes to podosomes, and is involved in cell invasion and migration.* Blood, 2006. **108**(9): p. 3143-3151.
46. Fanjul-Fernández, M., et al., *Matrix metalloproteinase Mmp-1a is dispensable for normal growth and fertility in mice and promotes lung cancer progression by modulating inflammatory responses.* Journal of Biological Chemistry, 2013. **288**(20): p. 14647-56.
47. Feinberg, T.Y., et al., *Functional roles of MMP14 and MMP15 in early postnatal mammary gland development.* Development (Cambridge, England), 2016. **143**(21): p. 3956-3968.
48. Martín-Alonso, M., et al., *Deficiency of MMP17/MT4-MMP Proteolytic Activity Predisposes to Aortic Aneurysm in Mice.* Circulation Research, 2015. **117**(2): p. e13-e26.
49. Soria-Valles, C., et al., *MMP-25 Metalloprotease Regulates Innate Immune Response through NF-κB Signaling.* The Journal of Immunology, 2016. **197**(1): p. 296-302.
50. Stickens, D., et al., *Altered endochondral bone development in matrix metalloproteinase 13-deficient mice.* Development, 2004. **131**(23): p. 5883-5895.
51. Triantafyllopoulou, A., et al., *Proliferative lesions and metalloproteinase activity in murine lupus nephritis mediated by type I interferons and macrophages.* Proceedings of the National Academy of Sciences, 2010. **107**(7): p. 3012-3017.

52. McClellan, S.A., et al., *Matrix Metalloproteinase-9 Amplifies the Immune Response to Pseudomonas aeruginosa Corneal Infection.* Investigative Ophthalmology & Visual Science, 2006. **47**(1): p. 256-264.
53. Holmbeck, K., et al., *MT1-MMP-Deficient Mice Develop Dwarfism, Osteopenia, Arthritis, and Connective Tissue Disease due to Inadequate Collagen Turnover.* Cell, 1999. **99**(1): p. 81-92.
54. Itoh, Y. and M. Seiki, *MT1-MMP: A potent modifier of pericellular microenvironment.* Journal of Cellular Physiology, 2006. **206**(1): p. 1-8.
55. Hiraoka, N., et al., *Matrix Metalloproteinases Regulate Neovascularization by Acting as Pericellular Fibrinolysins.* Cell, 1998. **95**(3): p. 365-377.
56. Itoh, T., et al., *Reduced Angiogenesis and Tumor Progression in Gelatinase A-deficient Mice.* Cancer Research, 1998. **58**(5): p. 1048-1051.
57. Mosig, R.A., et al., *Loss of MMP-2 disrupts skeletal and craniofacial development and results in decreased bone mineralization, joint erosion and defects in osteoblast and osteoclast growth.* Human Molecular Genetics, 2007. **16**(9): p. 1113-1123.
58. Oh, J., et al., *Mutations in two matrix metalloproteinase genes, MMP-2 and MT1-MMP, are synthetic lethal in mice.* Oncogene, 2004. **23**(29): p. 5041-8.
59. Roy, R., J. Yang, and M.A. Moses, *Matrix metalloproteinases as novel biomarkers and potential therapeutic targets in human cancer.* J Clin Oncol, 2009. **27**(31): p. 5287-97.
60. Lim, N.K., et al., *Investigation of matrix metalloproteinases, MMP-2 and MMP-9, in plasma reveals a decrease of MMP-2 in Alzheimer's disease.* J Alzheimers Dis, 2011. **26**(4): p. 779-86.
61. Kessenbrock, K., C.-Y. Wang, and Z. Werb, *Matrix metalloproteinases in stem cell regulation and cancer.* Matrix Biology, 2015. **44-46**: p. 184-190.
62. Atlas, T.H.P. *MMP9 prognostic summary*. 2018, November; Available from: https://www.proteinatlas.org/ENSG00000100985-MMP9/pathology.
63. Atlas, T.H.P. *MMP14 prognostic summary*. 2018, November; Available from: https://www.proteinatlas.org/ENSG00000157227-MMP14/pathology.
64. Liotta, L.A., et al., *Metastatic potential correlates with enzymatic degradation of basement membrane collagen.* Nature, 1980. **284**: p. 67-68.
65. Masson, V., et al., *Contribution of host MMP-2 and MMP-9 to promote tumor vascularization and invasion of malignant keratinocytes.* FASEB journal : official publication of the Federation of American Societies for Experimental Biology, 2005. **19**(2): p. 234-236.
66. López-Otín, C. and L.M. Matrisian, *Emerging roles of proteases in tumour suppression.* Nature Reviews Cancer, 2007. **7**(10): p. 800-8.
67. Hudson, L.G., N.M. Moss, and M.S. Stack, *EGF-receptor regulation of matrix metalloproteinases in epithelial ovarian carcinoma.* Future oncology (London, England), 2009. **5**(3): p. 323-338.
68. Kessenbrock, K., V. Plaks, and Z. Werb, *Matrix metalloproteinases: regulators of the tumor microenvironment.* Cell, 2010. **141**(1): p. 52-67.
69. Coussens, L.M., et al., *MMP-9 Supplied by Bone Marrow–Derived Cells Contributes to Skin Carcinogenesis.* Cell, 2000. **103**(3): p. 481-490.
70. Yu, Q. and I. Stamenkovic, *Cell surface-localized matrix metalloproteinase-9 proteolytically activates TGF-β and promotes tumor invasion and angiogenesis.* Genes & Development, 2000. **14**(2): p. 163-176.
71. Tatti, O., et al., *MT1-MMP releases latent TGF-β1 from endothelial cell extracellular matrix via proteolytic processing of LTBP-1.* Experimental Cell Research, 2008. **314**(13): p. 2501-2514.

72. Dallas, S.L., et al., *Proteolysis of Latent Transforming Growth Factor-β (TGF-β)-binding Protein-1 by Osteoclasts: A CELLULAR MECHANISM FOR RELEASE OF TGF-β FROM BONE MATRIX.* Journal of Biological Chemistry, 2002. **277**(24): p. 21352-21360.
73. Massagué, J., *TGFβ in Cancer.* Cell, 2008. **134**(2): p. 215-230.
74. Fiore, E., et al., *Matrix metalloproteinase 9 (MMP-9/gelatinase B) proteolytically cleaves ICAM-1 and participates in tumor cell resistance to natural killer cell-mediated cytotoxicity.* Oncogene, 2002. **21**(34): p. 5213-23.
75. Cowden Dahl, K.D., et al., *Matrix Metalloproteinase 9 Is a Mediator of Epidermal Growth Factor–Dependent E-Cadherin Loss in Ovarian Carcinoma Cells.* Cancer Research, 2008. **68**(12): p. 4606-4613.
76. Radisky, D.C., et al., *Rac1b and reactive oxygen species mediate MMP-3-induced EMT and genomic instability.* Nature, 2005. **436**: p. 123-127.
77. Nelson, C.M., et al., *Change in cell shape is required for matrix metalloproteinase-induced epithelial-mesenchymal transition of mammary epithelial cells.* Journal of cellular biochemistry, 2008. **105**(1): p. 25-33.
78. Sternlicht, M.D., et al., *The Stromal Proteinase MMP3/Stromelysin-1 Promotes Mammary Carcinogenesis.* Cell, 1999. **98**(2): p. 137-146.
79. Nakamura, E.S., et al., *Inhibition of lymphangiogenesis-related properties of murine lymphatic endothelial cells and lymph node metastasis of lung cancer by the matrix metalloproteinase inhibitor MMI270.* Cancer Science, 2004. **95**(1): p. 25-31.
80. Bergers, G., et al., *Matrix metalloproteinase-9 triggers the angiogenic switch during carcinogenesis.* Nature Cell Biology, 2000. **2**(10): p. 737-744.
81. Deryugina, E.I. and J.P. Quigley, *Tumor angiogenesis: MMP-mediated induction of intravasation- and metastasis-sustaining neovasculature.* Matrix biology : journal of the International Society for Matrix Biology, 2015. **44-46**: p. 94-112.
82. Sounni, N.E., et al., *Up-regulation of Vascular Endothelial Growth Factor-A by Active Membrane-type 1 Matrix Metalloproteinase through Activation of Src-Tyrosine Kinases.* Journal of Biological Chemistry, 2004. **279**(14): p. 13564-13574.
83. Ferreras, M., et al., *Generation and degradation of human endostatin proteins by various proteinases.* FEBS Letters, 2000. **486**(3): p. 247-251.
84. Bruyère, F., et al., *Modeling lymphangiogenesis in a three-dimensional culture system.* Nature Methods, 2008. **5**(5): p. 431-437.
85. Stacker, S.A., et al., *Lymphangiogenesis and cancer metastasis.* Nature Reviews Cancer, 2002. **2**(8): p. 573-583.
86. Wong, H.L.X., et al., *MT1-MMP sheds LYVE-1 on lymphatic endothelial cells and suppresses VEGF-C production to inhibit lymphangiogenesis.* Nature Communications, 2016. **7**: p. 10824.
87. Hanahan, D. and Robert A. Weinberg, *Hallmarks of Cancer: The Next Generation.* Cell, 2011. **144**(5): p. 646-674.
88. Hakulinen, J., et al., *Secretion of active membrane type 1 matrix metalloproteinase (MMP-14) into extracellular space in microvesicular exosomes.* Journal of Cellular Biochemistry, 2008. **105**(5): p. 1211-1218.
89. Dolo, V., et al., *Matrix-degrading proteinases are shed in membrane vesicles by ovarian cancer cells in vivo and in vitro.* Clinical & Experimental Metastasis, 1999. **17**(2): p. 131-140.
90. Shay, G., C.C. Lynch, and B. Fingleton, *Moving targets: Emerging roles for MMPs in Cancer Progression and Metastasis.* Matrix biology : journal of the International Society for Matrix Biology, 2015. **44-46**: p. 200-206.

91. Coussens, L.M., B. Fingleton, and L.M. Matrisian, *Matrix Metalloproteinase Inhibitors and Cancer—Trials and Tribulations.* Science, 2002. **295**(5564): p. 2387-2392.
92. Cathcart, J., A. Pulkoski-Gross, and J. Cao, *Targeting matrix metalloproteinases in cancer: Bringing new life to old ideas.* Genes & Diseases, 2015. **2**(1): p. 26-34.
93. Roy, R., J. Yang, and M.A. Moses, *Matrix Metalloproteinases As Novel Biomarker s and Potential Therapeutic Targets in Human Cancer.* Journal of Clinical Oncology, 2009. **27**(31): p. 5287-5297.
94. Hadler-Olsen, E., J.-O. Winberg, and L. Uhlin-Hansen, *Matrix metalloproteinases in cancer: their value as diagnostic and prognostic markers and therapeutic targets.* Tumor Biology, 2013. **34**(4): p. 2041-2051.
95. Shpitzer, T., et al., *Salivary analysis of oral cancer biomarkers.* British journal of cancer, 2009. **101**(7): p. 1194-1198.
96. Fernandez, C.A., et al., *The matrix metalloproteinase-9/neutrophil gelatinase-associated lipocalin complex plays a role in breast tumor growth and is present in the urine of breast cancer patients.* Clin Cancer Res, 2005. **11**(15): p. 5390-5.
97. INCORVAIA, L., et al., *MMP-2, MMP-9 and Activin A Blood Levels in Patients with Breast Cancer or Prostate Cancer Metastatic to the Bone.* Anticancer Research, 2007. **27**(3B): p. 1519-1525.
98. Hurst, N.G., et al., *Elevated serum matrix metalloproteinase 9 (MMP-9) concentration predicts the presence of colorectal neoplasia in symptomatic patients.* British journal of cancer, 2007. **97**(7): p. 971-977.
99. Wilson, S., et al., *Evaluation of the accuracy of serum MMP-9 as a test for colorectal cancer in a primary care population.* BMC cancer, 2006. **6**: p. 258-258.
100. Massoud, T.F. and S.S. Gambhir, *Molecular imaging in living subjects: seeing fundamental biological processes in a new light.* Genes & Development, 2003. **17**(5): p. 545-580.
101. Nathalie, M., et al., *Probes for Non-invasive Matrix Metalloproteinase-targeted Imaging with PET and SPECT.* Current Pharmaceutical Design, 2013. **19**(25): p. 4647-4672.
102. Reimann, C., et al., *Molecular imaging of the extracellular matrix in the context of atherosclerosis.* Advanced Drug Delivery Reviews, 2017. **113**: p. 49-60.
103. Lebel, R. and M. Lepage, *A comprehensive review on controls in molecular imaging: lessons from MMP-2 imaging.* Contrast Media & Molecular Imaging, 2014. **9**(3): p. 187-210.
104. Scherer, R.L., J.O. McIntyre, and L.M. Matrisian, *Imaging matrix metalloproteinases in cancer.* Cancer and Metastasis Reviews, 2008. **27**(4): p. 679.
105. Dhawan, A.P., B.D. Alessandro, and X. Fu, *Optical Imaging Modalities for Biomedical Applications.* IEEE Reviews in Biomedical Engineering, 2010. **3**: p. 69-92.
106. Sekar, R.B. and A. Periasamy, *Fluorescence resonance energy transfer (FRET) microscopy imaging of live cell protein localizations.* The Journal of cell biology, 2003. **160**(5): p. 629-633.
107. Bremer, C., C.-H. Tung, and R. Weissleder, *In vivo molecular target assessment of matrix metalloproteinase inhibition.* Nature Medicine, 2001. **7**: p. 743.
108. Kosaka, N., et al., *Clinical implications of near-infrared fluorescence imaging in cancer.* Future oncology (London, England), 2009. **5**(9): p. 1501-1511.
109. Shalinkky, D.R., et al., *Broad Antitumor and Antiangiogenic Activities of AG3340, a Potent and Selective MMP Inhibitor Undergoing Advanced Oncology Clinical Trials.* Annals of the New York Academy of Sciences, 1999. **878**(1): p. 236-270.

110. Aguilera, T.A., et al., *Systemic in vivo distribution of activatable cell penetrating peptides is superior to that of cell penetrating peptides.* Integrative biology : quantitative biosciences from nano to macro, 2009. **1**(5-6): p. 371-381.
111. Jiang, T., et al., *Tumor imaging by means of proteolytic activation of cell-penetrating peptides.* Proceedings of the National Academy of Sciences of the United States of America, 2004. **101**(51): p. 17867-17872.
112. Savariar, E.N., et al., *Real-time In Vivo Molecular Detection of Primary Tumors and Metastases with Ratiometric Activatable Cell-Penetrating Peptides.* Cancer Research, 2013. **73**(2): p. 855-864.
113. Zhu, L., et al., *In Vivo Optical Imaging of Membrane-Type Matrix Metalloproteinase (MT-MMP) Activity.* Molecular Pharmaceutics, 2011. **8**(6): p. 2331-2338.
114. Akers, W.J., et al., *Detection of MMP-2 and MMP-9 activity in vivo with a triple-helical peptide optical probe.* Bioconjugate Chemistry, 2012. **23**(3): p. 656-663.
115. Panth, K.M., et al., *In vivo optical imaging of MMP2 immuno protein antibody: tumor uptake is associated with MMP2 activity.* Scientific reports, 2016. **6**: p. 22198-22198.
116. Scherer, R.L., et al., *Optical imaging of matrix metalloproteinase-7 activity in vivo using a proteolytic nanobeacon.* Molecular imaging, 2008. **7**(3): p. 118-131.
117. Keereweer, S., et al., *Optical image-guided surgery - where do we stand?* Molecular imaging and biology : MIB : the official publication of the Academy of Molecular Imaging, 2011. **13**(2): p. 199-207.
118. Ahrens, E.T. and J.W.M. Bulte, *Tracking immune cells in vivo using magnetic resonance imaging.* Nature Reviews Immunology, 2013. **13**(10): p. 755-763.
119. Lebel, R., et al., *Novel solubility-switchable MRI agent allows the noninvasive detection of matrix metalloproteinase-2 activity in vivo in a mouse model.* Magnetic Resonance in Medicine, 2008. **60**(5): p. 1056-1065.
120. Gallo, J., et al., *CXCR4-targeted and MMP-responsive iron oxide nanoparticles for enhanced magnetic resonance imaging.* Angewandte Chemie (International ed. in English), 2014. **53**(36): p. 9550-9554.
121. Anani, T., P. Panizzi, and A.E. David, *Nanoparticle-based probes to enable noninvasive imaging of proteolytic activity for cancer diagnosis.* Nanomedicine (London, England), 2016. **11**(15): p. 2007-2022.
122. Wadas, T.J., et al., *Coordinating Radiometals of Copper, Gallium, Indium, Yttrium and Zirconium for PET and SPECT Imaging of Disease.* Chemical reviews, 2010. **110**(5): p. 2858-2902.
123. Whittaker, M., et al., *Design and Therapeutic Application of Matrix Metalloproteinase Inhibitors.* Chemical Reviews, 1999. **99**(9): p. 2735-2776.
124. Bloomston, M., E.E. Zervos, and A.S.R. Ii, *Matrix metalloproteinases and their role in pancreatic cancer: A review of preclinical studies and clinical trials.* Annals of Surgical Oncology, 2002. **9**(7): p. 668-674.
125. auf dem Keller, U., et al., *Novel MMP inhibitor [^{18}F]-Marimastat-aryltrifluoroborate as a probe for in vivo PET imaging in cancer.* Cancer Research, 2010. **70**(19): p. 7562.
126. Gatto, C., et al., *BAY 12-9566, A Novel Inhibitor of Matrix Metalloproteinases with Antiangiogenic Activity.* Clinical Cancer Research, 1999. **5**(11): p. 3603.
127. Tamura, Y., et al., *Highly Selective and Orally Active Inhibitors of Type IV Collagenase (MMP-9 and MMP-2): N-Sulfonylamino Acid Derivatives.* Journal of Medicinal Chemistry, 1998. **41**(4): p. 640-649.

128. Furumoto, S., R. Iwata, and T. Ido, *Design and synthesis of fluorine-18 labeled matrix metalloproteinase inhibitors for cancer imaging.* Journal of Labelled Compounds and Radiopharmaceuticals, 2002. **45**(11): p. 975-986.
129. Furumoto, S., et al., *Tumor detection using 18F-labeled matrix metalloproteinase-2 inhibitor.* Nuclear Medicine and Biology, 2003. **30**(2): p. 119-125.
130. Koivunen, E., et al., *Tumor targeting with a selective gelatinase inhibitor.* Nature Biotechnology, 1999. **17**: p. 768-774.
131. Liu, Q., et al., *Targeting of MMP2 activity in malignant tumors with a 68Ga-labeled gelatinase inhibitor cyclic peptide.* Nuclear Medicine and Biology, 2015. **42**(12): p. 939-944.
132. Liu, Q., et al., *Development of a Novel PET Tracer [18F]AlF-NOTA-C6 Targeting MMP2 for Tumor Imaging.* PLOS ONE, 2015. **10**(11): p. e0141668.
133. Giersing, B.K., et al., *Synthesis and Characterization of 111In−DTPA−N-TIMP-2: A Radiopharmaceutical for Imaging Matrix Metalloproteinase Expression.* Bioconjugate Chemistry, 2001. **12**(6): p. 964-971.
134. Kulasegaram, R., et al., *In vivo evaluation of 111In-DTPA-N-TIMP-2 in Kaposi sarcoma associated with HIV infection.* European Journal of Nuclear Medicine, 2001. **28**(6): p. 756-761.
135. Oltenfreiter, R., et al., *Synthesis, quality control and in vivo evaluation of [123I] rhTIMP-2, a potential tumour-imaging agent.* Journal of Labelled Compounds and Radiopharmaceuticals, 2005. **48**(5): p. 387-396.
136. Steenkiste, M.V., et al., *Membrane Type 1 Matrix Metalloproteinase Detection in Tumors, Using the Iodinated Endogenous [^{123}I]-Tissue Inhibitor 2 of Metalloproteinases as Imaging Agent.* Cancer Biotherapy and Radiopharmaceuticals, 2010. **25**(5): p. 511-520.
137. Temma, T., et al., *Development of a Radiolabeled Probe for Detecting Membrane Type-1 Matrix Metalloproteinase on Malignant Tumors.* Biological and Pharmaceutical Bulletin, 2009. **32**(7): p. 1272-1277.
138. Pfaffen, S., et al., *Tumour-targeting properties of antibodies specific to MMP-1A, MMP-2 and MMP-3.* European Journal of Nuclear Medicine and Molecular Imaging, 2010. **37**(8): p. 1559-1565.
139. Morcillo, M.Á., et al., *MT1-MMP as a PET Imaging Biomarker for Pancreas Cancer Management.* Contrast media & molecular imaging, 2018. **2018**: p. 13.
140. Duijnhoven, S.M.J.v., et al., *Tumor Targeting of MMP-2/9 Activatable Cell-Penetrating Imaging Probes Is Caused by Tumor-Independent Activation.* Journal of Nuclear Medicine, 2011. **52**(2): p. 279-286.
141. Chuang, C.-H., et al., *In Vivo Positron Emission Tomography Imaging of Protease Activity by Generation of a Hydrophobic Product from a Noninhibitory Protease Substrate.* Clinical Cancer Research, 2012. **18**(1): p. 238-247.
142. Ujula, T., et al., *Matrix Metalloproteinase 9 Targeting Peptides: Syntheses, 68Ga-labeling, and Preliminary Evaluation in a Rat Melanoma Xenograft Model.* Bioconjugate Chemistry, 2010. **21**(9): p. 1612-1621.
143. Goel, A.K., *Anthrax: A disease of biowarfare and public health importance.* World journal of clinical cases, 2015. **3**(1): p. 20-33.
144. Holty, J.C., et al., *Systematic review: A century of inhalational anthrax cases from 1900 to 2005.* Annals of Internal Medicine, 2006. **144**(4): p. 270-280.
145. Atlas, R.M., *Bioterrorism: From Threat to Reality.* Annual Review of Microbiology, 2002. **56**(1): p. 167-185.

146. John, A.J., et al., *Bioterrorism-Related Inhalational Anthrax: The First 10 Cases Reported in the United States.* Emerging Infectious Disease journal, 2001. **7**(6): p. 933.
147. Uchida, I., K. Hashimoto, and N. Terakado, *Virulence and Immunogenicity in Experimental Animals of Bacillus anthracis Strains Harbouring or Lacking 110 MDa and 60 MDa Plasmids.* Microbiology, 1986. **132**(2): p. 557-559.
148. Green, B.D., et al., *Demonstration of a capsule plasmid in Bacillus anthracis.* Infection and Immunity, 1985. **49**(2): p. 291-297.
149. Makino, S., et al., *Molecular characterization and protein analysis of the cap region, which is essential for encapsulation in Bacillus anthracis.* Journal of bacteriology, 1989. **171**(2): p. 722-730.
150. Smith, H. and J. Keppie, *Observations on Experimental Anthrax: Demonstration of a Specific Lethal Factor produced in vivo by Bacillus anthracis.* Nature, 1954. **173**: p. 869.
151. Klein, F., et al., *Anthrax Toxin: Causative Agent in the Death of Rhesus Monkeys.* Science, 1962. **138**(3547): p. 1331-1333.
152. Stanley, J.L., et al., *Purification of Factor I and Recognition of a Third Factor of the Anthrax Toxin.* Microbiology, 1961. **26**(1): p. 49-66.
153. Barth, H., et al., *Binary bacterial toxins: biochemistry, biology, and applications of common Clostridium and Bacillus proteins.* Microbiology and molecular biology reviews : MMBR, 2004. **68**(3): p. 373-402.
154. Stanley, J.L., *Purification of the Third Factor of Anthrax Toxin* Journal of genetic microbiology 1962. **29**: p. 517-521.
155. Ezzell, J.W., B.E. Ivins, and S.H. Leppla, *Immunoelectrophoretic analysis, toxicity, and kinetics of in vitro production of the protective antigen and lethal factor components of Bacillus anthracis toxin.* Infection and immunity, 1984. **45**(3): p. 761-767.
156. Bradley, K.A., et al., *Identification of the cellular receptor for anthrax toxin.* Nature, 2001. **414**(6860): p. 225-229.
157. Scobie, H.M., et al., *Human capillary morphogenesis protein 2 functions as an anthrax toxin receptor.* Proceedings of the National Academy of Sciences, 2003. **100**(9): p. 5170-5174.
158. Gladstone, G.P., *Immunity to anthrax: protective antigen present in cell-free culture filtrates.* British journal of experimental pathology, 1946. **27**(6): p. 394-418.
159. Young, J.A.T. and R.J. Collier, *Anthrax Toxin: Receptor Binding, Internalization, Pore Formation, and Translocation.* Annual Review of Biochemistry, 2007. **76**(1): p. 243-265.
160. Petosa, C., et al., *Crystal structure of the anthrax toxin protective antigen.* Nature, 1997. **385**(6619): p. 833-838.
161. Klimpel, K.R., et al., *Anthrax toxin protective antigen is activated by a cell surface protease with the sequence specificity and catalytic properties of furin.* Proceedings of the National Academy of Sciences of the United States of America, 1992. **89**(21): p. 10277-10281.
162. Gordon, V.M., et al., *Proteolytic activation of bacterial toxins by eukaryotic cells is performed by furin and by additional cellular proteases.* Infection and Immunity, 1995. **63**(1): p. 82-87.
163. Cunningham, K., et al., *Mapping the lethal factor and edema factor binding sites on oligomeric anthrax protective antigen.* Proceedings of the National Academy of Sciences, 2002. **99**(10): p. 7049-7053.

164. Mogridge, J., et al., *The lethal and edema factors of anthrax toxin bind only to oligomeric forms of the protective antigen.* Proceedings of the National Academy of Sciences, 2002. **99**(10): p. 7045-7048.
165. Milne, J.C., et al., *Anthrax protective antigen forms oligomers during intoxication of mammalian cells.* Journal of Biological Chemistry, 1994. **269**(32): p. 20607-12.
166. Krantz, B.A., et al., *A Phenylalanine Clamp Catalyzes Protein Translocation Through the Anthrax Toxin Pore.* Science, 2005. **309**(5735): p. 777-781.
167. Krantz, B.A., *Anthrax lethal toxin co-complexes are stabilized by contacts between adjacent lethal factors.* The Journal of general physiology, 2016. **148**(4): p. 273-275.
168. Beauregard, K.E., R.J. Collier, and J.A. Swanson, *Proteolytic activation of receptor-bound anthrax protective antigen on macrophages promotes its internalization.* Cellular Microbiology, 2000. **2**(3): p. 251-258.
169. Abrami, L., et al., *Anthrax toxin triggers endocytosis of its receptor via a lipid raft–mediated clathrin-dependent process.* The Journal of Cell Biology, 2003. **160**(3): p. 321-328.
170. Abrami, L., et al., *Membrane insertion of anthrax protective antigen and cytoplasmic delivery of lethal factor occur at different stages of the endocytic pathway.* The Journal of Cell Biology, 2004. **166**(5): p. 645-651.
171. Ménard, A., et al., *The vacuolar ATPase proton pump is required for the cytotoxicity of Bacillus anthracis lethal toxin.* FEBS Letters, 1996. **386**(2-3): p. 161-164.
172. Nassi, S., R.J. Collier, and A. Finkelstein, *PA63 Channel of Anthrax Toxin: An Extended β-Barrel.* Biochemistry, 2002. **41**(5): p. 1445-1450.
173. Miller, C.J., J.L. Elliott, and R.J. Collier, *Anthrax Protective Antigen: Prepore-to-Pore Conversion.* Biochemistry, 1999. **38**(32): p. 10432-10441.
174. Katayama, H., et al., *Three-dimensional structure of the anthrax toxin pore inserted into lipid nanodiscs and lipid vesicles.* Proceedings of the National Academy of Sciences, 2010. **107**(8): p. 3453-3457.
175. Wesche, J., et al., *Characterization of Membrane Translocation by Anthrax Protective Antigen.* Biochemistry, 1998. **37**(45): p. 15737-15746.
176. Mogridge, J., M. Mourez, and R.J. Collier, *Involvement of Domain 3 in Oligomerization by the Protective Antigen Moiety of Anthrax Toxin.* Journal of Bacteriology, 2001. **183**(6): p. 2111-2116.
177. Little, S.F., et al., *Characterization of Lethal Factor Binding and Cell Receptor Binding Domains of Protective Antigen of Bacillus anthracis using Monoclonal Antibodies.* Microbiology, 1996. **142**(3): p. 707-715.
178. Varughese, M., et al., *Identification of a Receptor-Binding Region within Domain 4 of the Protective Antigen Component of Anthrax Toxin.* Infection and Immunity, 1999. **67**(4): p. 1860-1865.
179. Rosovitz, M.J., et al., *Alanine-scanning Mutations in Domain 4 of Anthrax Toxin Protective Antigen Reveal Residues Important for Binding to the Cellular Receptor and to a Neutralizing Monoclonal Antibody.* Journal of Biological Chemistry, 2003. **278**(33): p. 30936-30944.
180. Arora, N. and S.H. Leppla, *Residues 1-254 of anthrax toxin lethal factor are sufficient to cause cellular uptake of fused polypeptides.* Journal of Biological Chemistry, 1993. **268**(5): p. 3334-3341.
181. Drum, C.L., et al., *Structural basis for the activation of anthrax adenylyl cyclase exotoxin by calmodulin.* Nature, 2002. **415**: p. 396-402.
182. Leppla, S.H., *Anthrax toxin edema factor: a bacterial adenylate cyclase that increases cyclic AMP concentrations of eukaryotic cells.* Proceedings of the National Academy of Sciences, 1982. **79**(10): p. 3162-3166.

183. Kumar, P., N. Ahuja, and R. Bhatnagar, *Anthrax Edema Toxin Requires Influx of Calcium for Inducing Cyclic AMP Toxicity in Target Cells.* Infection and Immunity, 2002. **70**(9): p. 4997-5007.
184. Ahuja, N., P. Kumar, and R. Bhatnagar, *The Adenylate Cyclase Toxins.* Critical Reviews in Microbiology, 2004. **30**(3): p. 187-196.
185. Pezard, C., P. Berche, and M. Mock, *Contribution of individual toxin components to virulence of Bacillus anthracis.* Infection and Immunity, 1991. **59**(10): p. 3472-3477.
186. Friedlander, A.M., *Macrophages are sensitive to anthrax lethal toxin through an acid-dependent process.* Journal of Biological Chemistry, 1986. **261**(16): p. 7123-7126.
187. Hanna, P.C., et al., *Role of macrophage oxidative burst in the action of anthrax lethal toxin.* Molecular medicine (Cambridge, Mass.), 1994. **1**(1): p. 7-18.
188. Klimpel, K.R., N. Arora, and S.H. Leppla, *Anthrax toxin lethal factor contains a zinc metalloprotease consensus sequence which is required for lethal toxin activity.* Molecular Microbiology, 1994. **13**(6): p. 1093-1100.
189. Duesbery, N.S., et al., *Proteolytic Inactivation of MAP-Kinase-Kinase by Anthrax Lethal Factor.* Science, 1998. **280**(5364): p. 734-737.
190. Vitale, G., et al., *Anthrax Lethal Factor Cleaves the N-Terminus of MAPKKs and Induces Tyrosine/Threonine Phosphorylation of MAPKs in Cultured Macrophages.* Biochemical and Biophysical Research Communications, 1998. **248**(3): p. 706-711.
191. Duesbery, N.S., et al., *Suppression of ras-mediated transformation and inhibition of tumor growth and angiogenesis by anthrax lethal factor, a proteolytic inhibitor of multiple MEK pathways.* Proceedings of the National Academy of Sciences, 2001. **98**(7): p. 4089-4094.
192. Agrawal, A., et al., *Impairment of dendritic cells and adaptive immunity by anthrax lethal toxin.* Nature, 2003. **424**: p. 329.
193. Pellizzari, R., et al., *Anthrax lethal factor cleaves MKK3 in macrophages and inhibits the LPS/IFNγ-induced release of NO and TNFα.* FEBS Letters, 1999. **462**(1): p. 199-204.
194. Erwin, J.L., et al., *Macrophage-Derived Cell Lines Do Not Express Proinflammatory Cytokines after Exposure to Bacillus anthracis Lethal Toxin.* Infection and Immunity, 2001. **69**(2): p. 1175-1177.
195. Santelli, E., et al., *Crystal structure of a complex between anthrax toxin and its host cell receptor.* Nature, 2004. **430**: p. 905-908.
196. Scobie, H.M., et al., *A Soluble Receptor Decoy Protects Rats against Anthrax Lethal Toxin Challenge.* The Journal of Infectious Diseases, 2005. **192**(6): p. 1047-1051.
197. Bonuccelli, G., et al., *ATR/TEM8 is highly expressed in epithelial cells lining Bacillus anthracis' three sites of entry: implications for the pathogenesis of anthrax infection.* American Journal of Physiology-Cell Physiology, 2005. **288**(6): p. C1402-C1410.
198. Friebe, S., J. Deuquet, and F.G. van der Goot, *Differential Dependence on N-Glycosylation of Anthrax Toxin Receptors CMG2 and TEM8.* PLOS ONE, 2015. **10**(3): p. e0119864.
199. Vargas, M., et al., *Broad Expression Analysis of Human ANTXR1/TEM8 Transcripts Reveals Differential Expression and Novel Splizce Variants.* PLOS ONE, 2012. **7**(8): p. e43174.
200. Chen, K.-H., et al., *Anthrax Toxin Protective Antigen Variants That Selectively Utilize either the CMG2 or TEM8 Receptors for Cellular Uptake and Tumor Targeting.* Journal of Biological Chemistry, 2016. **291**(42): p. 22021-22029.

201. Liu, S., et al., *Capillary morphogenesis protein-2 is the major receptor mediating lethality of anthrax toxin in vivo.* Proceedings of the National Academy of Sciences, 2009. **106**(30): p. 12424-12429.
202. Abrami, L., S.H. Leppla, and F.G. van der Goot, *Receptor palmitoylation and ubiquitination regulate anthrax toxin endocytosis.* The Journal of cell biology, 2006. **172**(2): p. 309-320.
203. Abrami, L., B. Kunz, and F. Gisou van der Goot, *Anthrax toxin triggers the activation of src-like kinases to mediate its own uptake.* Proceedings of the National Academy of Sciences, 2010. **107**(4): p. 1420-1424.
204. Hotchkiss, K.A., et al., *TEM8 expression stimulates endothelial cell adhesion and migration by regulating cell–matrix interactions on collagen.* Experimental Cell Research, 2005. **305**(1): p. 133-144.
205. Bell, S.E., et al., *Differential gene expression during capillary morphogenesis in 3D collagen matrices.* regulated expression of genes involved in basement membrane matrix assembly, cell cycle progression, cellular differentiation and G-protein signaling, 2001. **114**(15): p. 2755-2773.
206. Bürgi, J., et al., *CMG2/ANTXR2 regulates extracellular collagen VI which accumulates in hyaline fibromatosis syndrome.* Nature Communications, 2017. **8**: p. 15861.
207. Nanda, A., et al., *TEM8 Interacts with the Cleaved C5 Domain of Collagen α3(VI).* Cancer Research, 2004. **64**(3): p. 817-820.
208. Besschetnova, T.Y., et al., *Regulatory mechanisms of anthrax toxin receptor 1-dependent vascular and connective tissue homeostasis.* Matrix biology : journal of the International Society for Matrix Biology, 2015. **42**: p. 56-73.
209. Hu, K., B.R. Olsen, and T.Y. Besschetnova, *Cell autonomous ANTXR1-mediated regulation of extracellular matrix components in primary fibroblasts.* Matrix Biology, 2017. **62**: p. 105-114.
210. Stránecký, V., et al., *Mutations in ANTXR1 Cause GAPO Syndrome.* The American Journal of Human Genetics, 2013. **92**(5): p. 792-799.
211. Croix, B.S., et al., *Genes Expressed in Human Tumor Endothelium.* Science, 2000. **289**(5482): p. 1197-1202.
212. Høye, A.M., et al., *Tumor endothelial marker 8 promotes cancer progression and metastasis.* Oncotarget, 2018. **9**(53): p. 30173-30188.
213. Cryan, L.M. and M.S. Rogers, *Targeting the anthrax receptors, TEM-8 and CMG-2, for anti-angiogenic therapy.* Frontiers in bioscience : a journal and virtual library, 2011. **16**: p. 1574-1588.
214. Atlas, T.H.P. *ANTXR1-TEM8 prognostic summary*. 2018, November; Available from: https://www.proteinatlas.org/ENSG00000169604-ANTXR1/pathology.
215. Gong, Q., et al., *Effect of silencing TEM8 gene on proliferation, apoptosis, migration and invasion of XWLC-05 lung cancer cells.* Molecular Medicine Reports, 2018. **17**(1): p. 911-917.
216. Chaudhary, A., et al., *TEM8/ANTXR1 Blockade Inhibits Pathological Angiogenesis and Potentiates Tumoricidal Responses against Multiple Cancer Types.* Cancer Cell, 2012. **21**(2): p. 212-226.
217. Duan, H.-F., et al., *Antitumor Activities of TEM8-Fc: An Engineered Antibody-like Molecule Targeting Tumor Endothelial Marker 8.* JNCI: Journal of the National Cancer Institute, 2007. **99**(20): p. 1551-1555.
218. Rogers, M.S., et al., *Mutant Anthrax Toxin B Moiety (Protective Antigen) Inhibits Angiogenesis and Tumor Growth.* Cancer Research, 2007. **67**(20): p. 9980-9985.

219. Ji, C., et al., *Capillary morphogenesis gene 2 maintains gastric cancer stem-like cell phenotype by activating a Wnt/β-catenin pathway.* Oncogene, 2018. **37**(29): p. 3953-3966.
220. Abrami, L., et al., *Functional interactions between anthrax toxin receptors and the WNT signalling protein LRP6.* Cellular Microbiology, 2008. **10**(12): p. 2509-2519.
221. Thomas, G., *Furin at the cutting edge: From protein traffic to embryogenesis and disease.* Nature Reviews Molecular Cell Biology, 2002. **3**(10): p. 753-766.
222. Netzel-Arnett, S., et al., *Comparative sequence specificities of human 72- and 92-kDa gelatinases (type IV collagenases) and PUMP (matrilysin).* Biochemistry, 1993. **32**(25): p. 6427-6432.
223. Liu, S., et al., *Tumor Cell-selective Cytotoxicity of Matrix Metalloproteinase-activated Anthrax Toxin.* Cancer Research, 2000. **60**(21): p. 6061-6067.
224. Liu, S., et al., *Solid tumor therapy by selectively targeting stromal endothelial cells.* Proceedings of the National Academy of Sciences, 2016. **113**(28): p. E4079-E4087.
225. Alfano, R.W., et al., *Inhibition of tumor angiogenesis by the matrix metalloproteinase-activated anthrax lethal toxin in an orthotopic model of anaplastic thyroid carcinoma.* Molecular Cancer Therapeutics, 2010. **9**(1): p. 190-201.
226. Liu, S., et al., *Matrix Metalloproteinase-activated Anthrax Lethal Toxin Demonstrates High Potency in Targeting Tumor Vasculature.* Journal of Biological Chemistry, 2008. **283**(1): p. 529-540.
227. Alfano, R.W., et al., *Matrix metalloproteinase-activated anthrax lethal toxin inhibits endothelial invasion and neovasculature formation during in vitro morphogenesis.* Molecular cancer research : MCR, 2009. **7**(4): p. 452-461.
228. Goldman, D.L., et al., *Serum-Mediated Cleavage of Bacillus anthracis Protective Antigen Is a Two-Step Process That Involves a Serum Carboxypeptidase.* mSphere, 2018. **3**(3): p. e00091-18.
229. Pomerantsev, A.P., et al., *Genome engineering in Bacillus anthracis using tyrosine site-specific recombinases.* PLoS One, 2017. **12**(8): p. e0183346.
230. Liu, S., et al., *Solid tumor therapy by selectively targeting stromal endothelial cells.* Proc Natl Acad Sci U S A, 2016. **113**(28): p. E4079-87.
231. Molloy, S.S., et al., *Human furin is a calcium-dependent serine endoprotease that recognizes the sequence Arg-X-X-Arg and efficiently cleaves anthrax toxin protective antigen.* J Biol Chem, 1992. **267**(23): p. 16396-402.
232. Kintzer, A.F., et al., *Anthrax toxin receptor drives protective antigen oligomerization and stabilizes the heptameric and octameric oligomer by a similar mechanism.* PLoS One, 2010. **5**(11): p. e13888.
233. Liu, S., et al., *Tumor cell-selective cytotoxicity of matrix metalloproteinase-activated anthrax toxin.* Cancer Res, 2000. **60**(21): p. 6061-7.
234. Liu, S., T.H. Bugge, and S.H. Leppla, *Targeting of tumor cells by cell surface urokinase plasminogen activator-dependent anthrax toxin.* J Biol Chem, 2001. **276**(21): p. 17976-84.
235. Ballard, J.D., R.J. Collier, and M.N. Starnbach, *Anthrax Toxin as a Molecular Tool for Stimulation of Cytotoxic T Lymphocytes: Disulfide-Linked Epitopes, Multiple Injections, and Role of CD4+ Cells.* Infection and Immunity, 1998. **66**(10): p. 4696-4699.
236. Vitale, G., et al., *Anthrax lethal factor cleaves the N-terminus of MAPKKs and induces tyrosine/threonine phosphorylation of MAPKs in cultured macrophages.* Biochem Biophys Res Commun, 1998. **248**(3): p. 706-11.

237. Hamilton, G., et al., *AKT regulates NPM dependent ARF localization and p53(mut) stability in tumors.* Oncotarget, 2014. **5**(15): p. 6142-6167.
238. Varughese, M., et al., *Internalization of a Bacillus anthracis protective antigen-c-Myc fusion protein mediated by cell surface anti-c-Myc antibodies.* Mol Med, 1998. **4**(2): p. 87-95.
239. Gialeli, C., A.D. Theocharis, and N.K. Karamanos, *Roles of matrix metalloproteinases in cancer progression and their pharmacological targeting.* The FEBS Journal, 2011. **278**(1): p. 16-27.
240. Egeblad, M. and Z. Werb, *New functions for the matrix metalloproteinases in cancer progression.* Nature Reviews Cancer, 2002. **2**(3): p. 161-174.
241. SOUNNI, N.E., et al., *MT1-MMP expression promotes tumor growth and angiogenesis through an up-regulation of vascular endothelial growth factor expression.* The FASEB Journal, 2002. **16**(6): p. 555-564.
242. Benjamin, M.M. and R.A. Khalil, *Matrix metalloproteinase inhibitors as investigative tools in the pathogenesis and management of vascular disease.* EXS, 2012. **103**: p. 209-279.
243. Abi-Habib, R.J., et al., *BRAF status and mitogen-activated protein/extracellular signal-regulated kinase kinase 1/2 activity indicate sensitivity of melanoma cells to anthrax lethal toxin.* Molecular Cancer Therapeutics, 2005. **4**(9): p. 1303-1310.
244. Reeves, C.V., et al., *Anthrax toxin receptor 2 is expressed in murine and tumor vasculature and functions in endothelial proliferation and morphogenesis.* Oncogene, 2009. **29**: p. 789.
245. Reeves, C.V., et al., *Anthrax Toxin Receptor 2 Functions in ECM Homeostasis of the Murine Reproductive Tract and Promotes MMP Activity.* PLoS ONE, 2012. **7**(4): p. e34862.
246. Liu, S., T.H. Bugge, and S.H. Leppla, *Targeting of Tumor Cells by Cell Surface Urokinase Plasminogen Activator-dependent Anthrax Toxin.* Journal of Biological Chemistry, 2001. **276**(21): p. 17976-17984.
247. Ludwig, T., et al., *The cytoplasmic tail dileucine motif LL572 determines the glycosylation pattern of membrane-type 1 matrix metalloproteinase.* The Journal of biological chemistry, 2008. **283**(51): p. 35410-35418.
248. Arora, N., et al., *Fusions of anthrax toxin lethal factor to the ADP-ribosylation domain of Pseudomonas exotoxin A are potent cytotoxins which are translocated to the cytosol of mammalian cells.* Journal of Biological Chemistry, 1992. **267**(22): p. 15542-15548.
249. Dever, T.E. and R. Green, *The elongation, termination, and recycling phases of translation in eukaryotes.* Cold Spring Harbor perspectives in biology. **4**(7): p. a013706-a013706.
250. Hopkins, C.R., et al., *Movement of internalized ligand–receptor complexes along a continuous endosomal reticulum.* Nature, 1990. **346**: p. 335.
251. Watts, C., *Rapid endocytosis of the transferrin receptor in the absence of bound transferrin.* The Journal of Cell Biology, 1985. **100**(2): p. 633-637.
252. Racoosin, E.L. and J.A. Swanson, *M-CSF-induced macropinocytosis increases solute endocytosis but not receptor-mediated endocytosis in mouse macrophages.* Journal of Cell Science, 1992. **102**(4): p. 867-880.
253. Görlich, D. and U. Kutay, *Transport between the cell nucleus and the cytoplasm.* Annual Review of Cell and Developmental Biology, 1999. **15**: p. 607-660.
254. Kruth, H.S., et al., *Macropinocytosis Is the Endocytic Pathway That Mediates Macrophage Foam Cell Formation with Native Low Density Lipoprotein.* Journal of Biological Chemistry, 2005. **280**(3): p. 2352-2360.

255. Dunn, K.W., M.M. Kamocka, and J.H. McDonald, *A practical guide to evaluating colocalization in biological microscopy.* American journal of physiology. Cell physiology, 2011. **300**(4): p. C723-C742.
256. Alfano, R.W., et al., *Matrix metalloproteinase-activated anthrax lethal toxin inhibits endothelial invasion and neovasculature formation during in vitro morphogenesis.* Molecular cancer research: MCR, 2009. **7**(4): p. 452-461.
257. Sugiura, G., et al., *Radiolabeling Strategies for Tumor-Targeting Proteinaceous Drugs.* Molecules, 2014. **19**(2): p. 2135-2165.
258. Brom, M., et al., *Improved labelling of DTPA- and DOTA-conjugated peptides and antibodies with (111)In in HEPES and MES buffer.* EJNMMI Research, 2012. **2**: p. 4-4.
259. Dong, C., Z. Liu, and F. Wang, *Radioligand saturation binding for quantitative analysis of ligand-receptor interactions.* Biophysics Reports, 2015. **1**(3): p. 148-155.
260. Sharma, R. and E. Aboagye, *Development of radiotracers for oncology--the interface with pharmacology.* British journal of pharmacology, 2011. **163**(8): p. 1565-1585.
261. Hnatowich, D.J., F. Virzi, and P.W. Doherty, *DTPA-Coupled Antibodies Labeled with Yttrium-90.* Journal of Nuclear Medicine, 1985. **26**(5): p. 503-509.
262. Hulme, E.C. and M.A. Trevethick, *Ligand binding assays at equilibrium: validation and interpretation.* British Journal of Pharmacology, 2010. **161**(6): p. 1219-1237.
263. Wigelsworth, D.J., et al., *Binding Stoichiometry and Kinetics of the Interaction of a Human Anthrax Toxin Receptor, CMG2, with Protective Antigen.* Journal of Biological Chemistry, 2004. **279**(22): p. 23349-23356.
264. Qian, Z.M., et al., *Targeted Drug Delivery via the Transferrin Receptor-Mediated Endocytosis Pathway.* Pharmacological Reviews, 2002. **54**(4): p. 561-587.
265. Elliott, J.L., J. Mogridge, and R.J. Collier, *A Quantitative Study of the Interactions of Bacillus anthracis Edema Factor and Lethal Factor with Activated Protective Antigen.* Biochemistry, 2000. **39**(22): p. 6706-6713.
266. Meares, C.F., et al., *Covalent attachment of metal chelates to proteins:the stability in vivo and in vitro of the conjugate of albumin with a chelate of 111indium.* Proceedings of the National Academy of Sciences of the United States of America, 1976. **73**(11): p. 3803-3806.
267. Bank, P.D. and i. Europe. *PDBePISA (Proteins, Interfaces, Structures and Assemblies)*. 2018; Available from: http://www.ebi.ac.uk/msd-srv/prot_int/cgi-bin/piserver.
268. Feld, G.K., et al., *Structural basis for the unfolding of anthrax lethal factor by protective antigen oligomers.* Nature Structural &Amp; Molecular Biology, 2010. **17**(11): p. 1383-90.
269. Vallabhajosula, S., R.P. Killeen, and J.R. Osborne, *Altered Biodistribution of Radiopharmaceuticals: Role of Radiochemical/Pharmaceutical Purity, Physiological, and Pharmacologic Factors.* Seminars in Nuclear Medicine, 2010. **40**(4): p. 220-241.
270. Vegt, E., et al., *Renal uptake of different radiolabelled peptides is mediated by megalin: SPECT and biodistribution studies in megalin-deficient mice.* European Journal of Nuclear Medicine and Molecular Imaging, 2011. **38**(4): p. 623-632.
271. Behr, T.M., D.M. Goldenberg, and W. Becker, *Reducing the renal uptake of radiolabeled antibody fragments and peptides for diagnosis and therapy: present status, future prospects and limitations.* European Journal of Nuclear Medicine, 1998. **25**(2): p. 201-212.
272. Behr, T.M., et al., *Overcoming the nephrotoxicity of radiometal-labeled immunoconjugates.* Cancer, 1997. **80**(12): p. 2591-2610.

273. Moayeri, M., J.F. Wiggins, and S.H. Leppla, *Anthrax Protective Antigen Cleavage and Clearance from the Blood of Mice and Rats.* Infection and Immunity, 2007. **75**(11): p. 5175-5184.
274. Liu, S., et al., *Matrix metalloproteinase-activated anthrax lethal toxin demonstrates high potency in targeting tumor vasculature.* The Journal of Biological Chemistry, 2008. **283**(1): p. 529-540.
275. Liu, S., et al., *Key tissue targets responsible for anthrax toxin-induced-lethality.* Nature, 2013. **501**(7465): p. 63-68.
276. Maeda, H., *The enhanced permeability and retention (EPR) effect in tumor vasculature: the key role of tumor-selective macromolecular drug targeting.* Advances in Enzyme Regulation, 2001. **41**(1): p. 189-207.
277. Kung, M.-P. and H.F. Kung, *Mass effect of injected dose in small rodent imaging by SPECT and PET.* Nuclear Medicine and Biology, 2005. **32**(7): p. 673-678.
278. Molnar, D.M. and R.A. Altenbern, *Alterations in the Biological Activity of Protective Antigen of Bacillus anthracis Toxin.* Proceedings of the Society for Experimental Biology and Medicine, 1963. **114**(2): p. 294-297.
279. Dall, G., et al., *Low Dose, Low Cost Estradiol Pellets Can Support MCF-7 Tumour Growth in Nude Mice without Bladder Symptoms.* Journal of Cancer, 2015. **6**(12): p. 1331-1336.
280. Molloy, S.S., et al., *Human furin is a calcium-dependent serine endoprotease that recognizes the sequence Arg-X-X-Arg and efficiently cleaves anthrax toxin protective antigen.* Journal of Biological Chemistry, 1992. **267**(23): p. 16396-16402.
281. Jr, E.J., *Serum Protease cleavage of Bacillus anthracis protective antigen.* J Gen Microbiology, 1992. **138**(3): p. 543-9.
282. Panchal, R.G., et al., *Purified Bacillus anthracis Lethal Toxin Complex Formed in Vitro and during Infection Exhibits Functional and Biological Activity.* Journal of Biological Chemistry, 2005. **280**(11): p. 10834-10839.
283. Heneweer, C., et al., *Magnitude of Enhanced Permeability and Retention Effect in Tumors with Different Phenotypes: 89Zr-Albumin as a Model System.* Journal of Nuclear Medicine, 2011. **52**(4): p. 625-633.
284. Hand, P.H., et al., *Definition of Antigenic Heterogeneity and Modulation among Human Mammary Carcinoma Cell Populations Using Monoclonal Antibodies to Tumor-associated Antigens.* Cancer Research, 1983. **43**(2): p. 728-735.
285. Jain, R.K., *Transport of molecules across tumor vasculature.* Cancer and Metastasis Reviews, 1987. **6**(4): p. 559-593.
286. Fujimori, K., et al., *Modeling Analysis of the Global and Microscopic Distribution of Immunoglobulin G, F(ab')2, and Fab in Tumors.* Cancer Research, 1989. **49**(20): p. 5656-5663.
287. Lebel, R. and M. Lepage, *A comprehensive review on controls in molecular imaging: lessons from MMP-2 imaging.* Contrast Media Mol Imaging, 2014. **9**(3): p. 187-210.
288. McCawley, L.J. and L.M. Matrisian, *Matrix metalloproteinases: multifunctional contributors to tumor progression.* Mol Med Today, 2000. **6**(4): p. 149-56.
289. Fanjul-Fernandez, M., et al., *Matrix metalloproteinases: evolution, gene regulation and functional analysis in mouse models.* Biochim Biophys Acta, 2010. **1803**(1): p. 3-19.
290. Hadler-Olsen, E., et al., *Regulation of matrix metalloproteinase activity in health and disease.* FEBS J, 2011. **278**(1): p. 28-45.
291. Visse, R. and H. Nagase, *Matrix metalloproteinases and tissue inhibitors of metalloproteinases: structure, function, and biochemistry.* Circ Res, 2003. **92**(8): p. 827-39.

292. Coussens, L.M., B. Fingleton, and L.M. Matrisian, *Matrix metalloproteinase inhibitors and cancer: trials and tribulations.* Science, 2002. **295**(5564): p. 2387-92.
293. Cathcart, J., A. Pulkoski-Gross, and J. Cao, *Targeting Matrix Metalloproteinases in Cancer: Bringing New Life to Old Ideas.* Genes Dis, 2015. **2**(`1): p. 26-34.
294. Oltenfreiter, R., et al., *Valine-based biphenylsulphonamide matrix metalloproteinase inhibitors as tumor imaging agents.* Appl Radiat Isot, 2006. **64**(6): p. 677-85.
295. Temma, T., et al., *Development of a radiolabeled probe for detecting membrane type-1 matrix metalloproteinase on malignant tumors.* Biol Pharm Bull, 2009. **32**(7): p. 1272-7.
296. Jiang, T., et al., *Tumor imaging by means of proteolytic activation of cell-penetrating peptides.* Proc Natl Acad Sci U S A, 2004. **101**(51): p. 17867-72.
297. Altai, M., et al., *Pretargeted Imaging and Therapy.* J Nucl Med, 2017. **58**(10): p. 1553-1559.
298. Mock, M. and A. Fouet, *Anthrax.* Annu Rev Microbiol, 2001. **55**: p. 647-71.
299. Lowe, D.E. and I.J. Glomski, *Cellular and physiological effects of anthrax exotoxin and its relevance to disease.* Front Cell Infect Microbiol, 2012. **2**: p. 76.
300. Duesbery, N.S., et al., *Proteolytic inactivation of MAP-kinase-kinase by anthrax lethal factor.* Science, 1998. **280**(5364): p. 734-7.
301. Pellizzari, R., et al., *Anthrax lethal factor cleaves MKK3 in macrophages and inhibits the LPS/IFNgamma-induced release of NO and TNFalpha.* FEBS Lett, 1999. **462**(1-2): p. 199-204.
302. Vitale, G., et al., *Susceptibility of mitogen-activated protein kinase kinase family members to proteolysis by anthrax lethal factor.* Biochem J, 2000. **352 Pt 3**: p. 739-45.
303. Fields, G.B., *Interstitial Collagen Catabolism.* Journal of Biological Chemistry, 2013. **288**(13): p. 8785-8793.
304. Netzel-Arnett, S., et al., *Sequence specificities of human fibroblast and neutrophil collagenases.* Journal of Biological Chemistry, 1991. **266**(11): p. 6747-55.
305. Vizovišek, M., et al., *Protease Specificity: Towards In Vivo Imaging Applications and Biomarker Discovery.* Trends in Biochemical Sciences, 2018. **43**(10): p. 829-844.
306. Ouyang, M., et al., *Visualization of Polarized Membrane Type 1 Matrix Metalloproteinase Activity in Live Cells by Fluorescence Resonance Energy Transfer Imaging.* Journal of Biological Chemistry, 2008. **283**(25): p. 17740-17748.
307. Ouyang, M., et al., *Simultaneous Visualization of Protumorigenic Src and MT1-MMP Activities with Fluorescence Resonance Energy Transfer.* Cancer Research, 2010. **70**(6): p. 2204-2212.
308. MEROPS. *Membrane-type matrix metallopeptidase-1*. 2017, January 17; Available from: https://www.ebi.ac.uk/merops/cgi-bin/pepsum?mid=M10.014.
309. Junutula, J.R., et al., *Site-specific conjugation of a cytotoxic drug to an antibody improves the therapeutic index.* Nature Biotechnology, 2008. **26**(8): p. 925-932.
310. Morais, M. and M.T. Ma, *Site-specific chelator-antibody conjugation for PET and SPECT imaging with radiometals.* Drug Discovery Today: Technologies, 2018. **30**: p. 91-104.
311. Adumeau, P., et al., *Site-Specifically Labeled Immunoconjugates for Molecular Imaging--Part 1: Cysteine Residues and Glycans.* Molecular imaging and biology : MIB : the official publication of the Academy of Molecular Imaging, 2016. **18**(1): p. 1-17.
312. Wang, L., J. Xie, and P.G. Schultz, *EXPANDING THE GENETIC CODE.* Annual Review of Biophysics and Biomolecular Structure, 2006. **35**(1): p. 225-249.

313. Ou, W., et al., *Site-specific protein modifications through pyrroline-carboxy-lysine residues.* Proceedings of the National Academy of Sciences, 2011. **108**(26): p. 10437-10442.
314. Nguyen, D.P., et al., *Genetic Encoding and Labeling of Aliphatic Azides and Alkynes in Recombinant Proteins via a Pyrrolysyl-tRNA Synthetase/tRNACUA Pair and Click Chemistry.* Journal of the American Chemical Society, 2009. **131**(25): p. 8720-8721.
315. Xie, J. and P.G. Schultz, *A chemical toolkit for proteins — an expanded genetic code.* Nature Reviews Molecular Cell Biology, 2006. **7**(10): p. 775-782.
316. Colcher, D., et al., *Effects of genetic engineering on the pharmacokinetics of antibodies.* The quarterly journal of nuclear medicine : official publication of the Italian Association of Nuclear Medicine (AIMN) [and] the International Association of Radiopharmacology (IAR), 1999. **43**(2): p. 132-9.
317. Wu, A.M., et al., *Tumor localization of anti-CEA single-chain Fvs: improved targeting by non-covalent dimers.* Immunotechnology, 1996. **2**(1): p. 21-36.
318. Olafsen, T., et al., *Covalent disulfide-linked anti-CEA diabody allows site-specific conjugation and radiolabeling for tumor targeting applications.* Protein Engineering, Design and Selection, 2004. **17**(1): p. 21-27.
319. Wittrup, K.D., et al., *Chapter ten - Practical Theoretic Guidance for the Design of Tumor-Targeting Agents*, in *Methods in Enzymology*, K.D. Wittrup and G.L. Verdine, Editors. 2012, Academic Press. p. 255-268.
320. Willekens, S.M.A., et al., *Characterization of ^{111}In-labeled Glucose-Dependent Insulinotropic Polypeptide as a Radiotracer for Neuroendocrine Tumors.* Scientific Reports, 2018. **8**(1): p. 2948.
321. Carson-Walter, E.B., et al., *Cell Surface Tumor Endothelial Markers Are Conserved in Mice and Humans.* Cancer Research, 2001. **61**(18): p. 6649-6655.
322. Stimmel, J.B. and F.C. Kull Jr, *Samarium-153 and Lutetium-177 Chelation Properties of Selected Macrocyclic and Acyclic Ligands.* Nuclear Medicine and Biology, 1998. **25**(2): p. 117-125.
323. Yong, K.J., et al., *Mechanisms of Cell Killing Response from Low Linear Energy Transfer (LET) Radiation Originating from (177)Lu Radioimmunotherapy Targeting Disseminated Intraperitoneal Tumor Xenografts.* International journal of molecular sciences, 2016. **17**(5): p. 736.
324. Li, Q., et al., *Anthrax LFn-PA Hybrid Antigens: Biochemistry, Immunogenicity, and Protection Against Lethal Ames Spore Challenge in Rabbits.* The open vaccine journal, 2009. **2**: p. 92-99.
325. Williamson, E.D., et al., *Immunogenicity of Recombinant Protective Antigen and Efficacy against Aerosol Challenge with Anthrax.* Infection and Immunity, 2005. **73**(9): p. 5978-5987.

Appendix

A1. Lethal Toxin variants characterisation

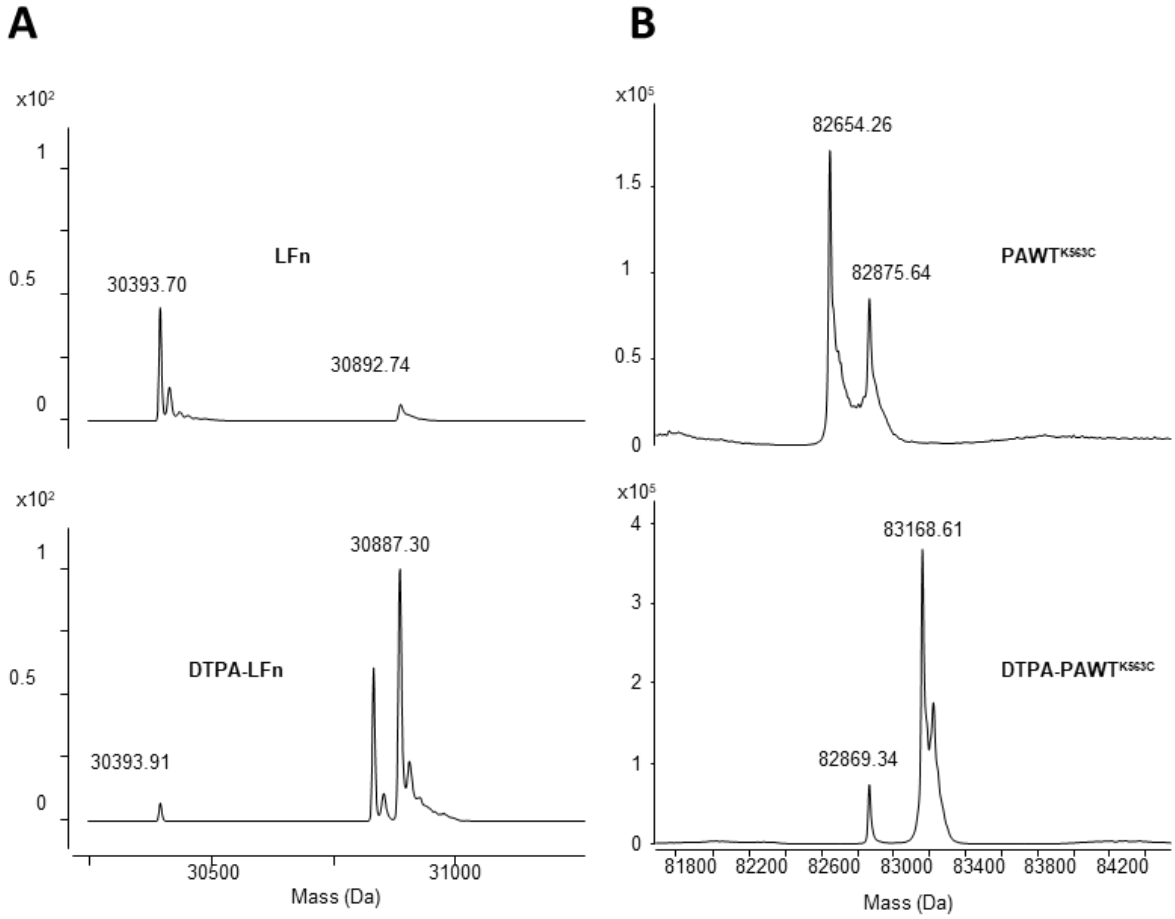

Figure A. 1 Variants presenting engineered cysteine residue and DTPA conjugates

Spectra obtained from intact protein LC-MS for the different maleimide-DTPA-conjugates.

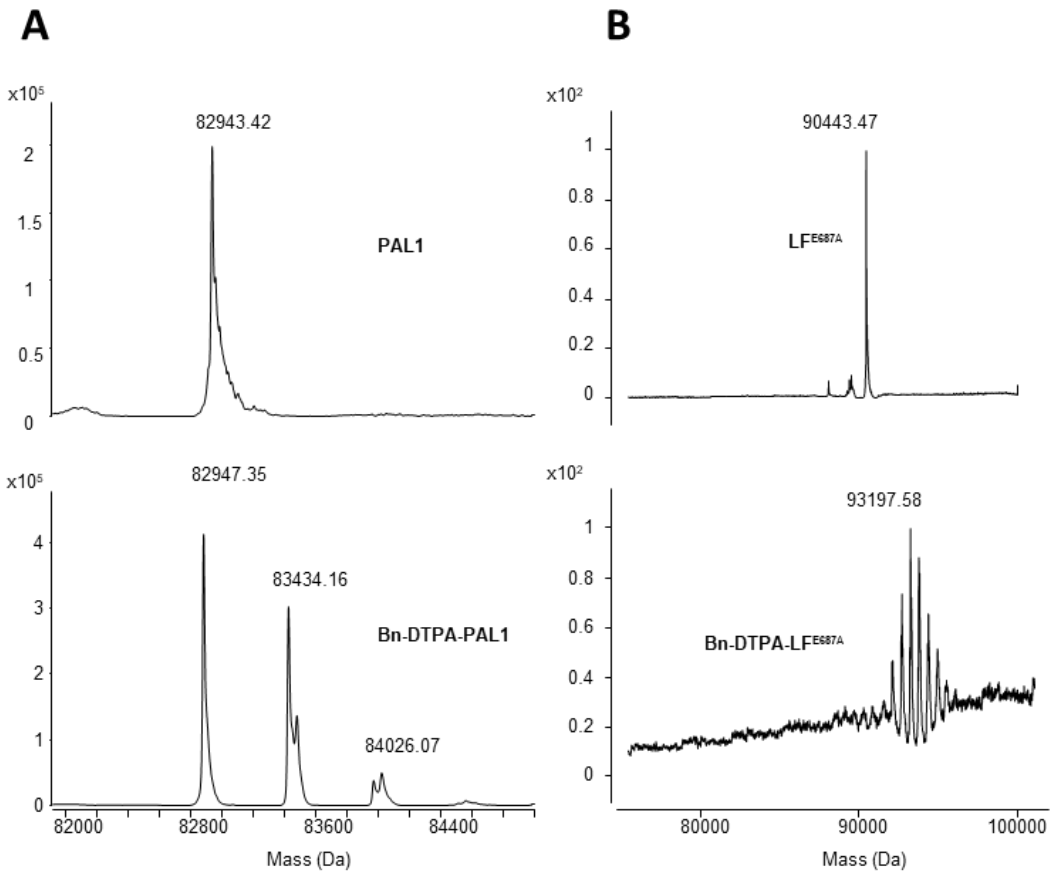

Figure A. 2 Variants presenting no engineered cysteine residue and DTPA conjugates

Spectra obtained from intact protein LC-MS for the different maleimide-DTPA-conjugates.

A2. Cleaved PAL1 and PAU7

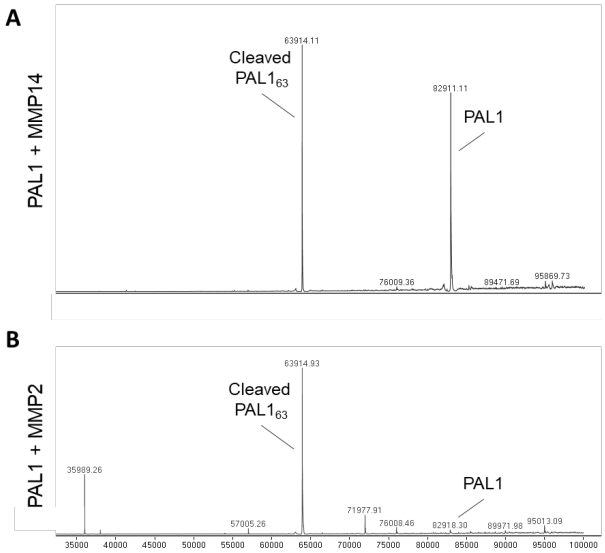

Figure A. 3 Fragments of PAL1 after MMP cleavage

Spectra of $PAL1_{83}$ (83 kDa) samples submitted to MMP cleavage analysed by Liquid Chromatography-Mass Spectrometry. PAL1 was exposed to MMP2 or MMP14. $PAL1_{63}$ (63 kDa) fragments presented adducts corresponding to an addition of 6.4 Da, probably a substitution of arginine to a tyrosine residue.

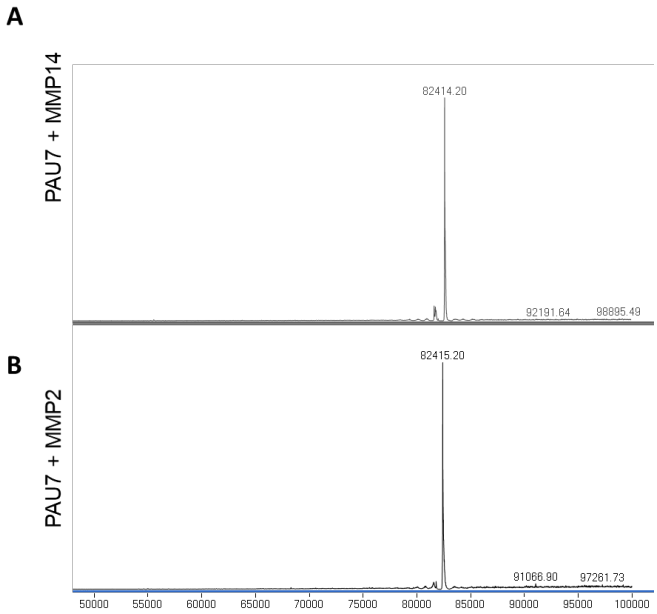

Figure A. 4 Full-length PAU7 after MMP treatment

Spectra of $PAU7_{83}$ (83 kDa) samples submitted to MMP cleavage analysed by Liquid Chromatography-Mass Spectrometry. PAU7 was exposed to MMP2 or MMP14. However, the starting mass presented a difference of 50.6 Da indicating that a possible substitution from one serine to a histidine amino acid might have happened.

A3. Raw data for Serum stability assay

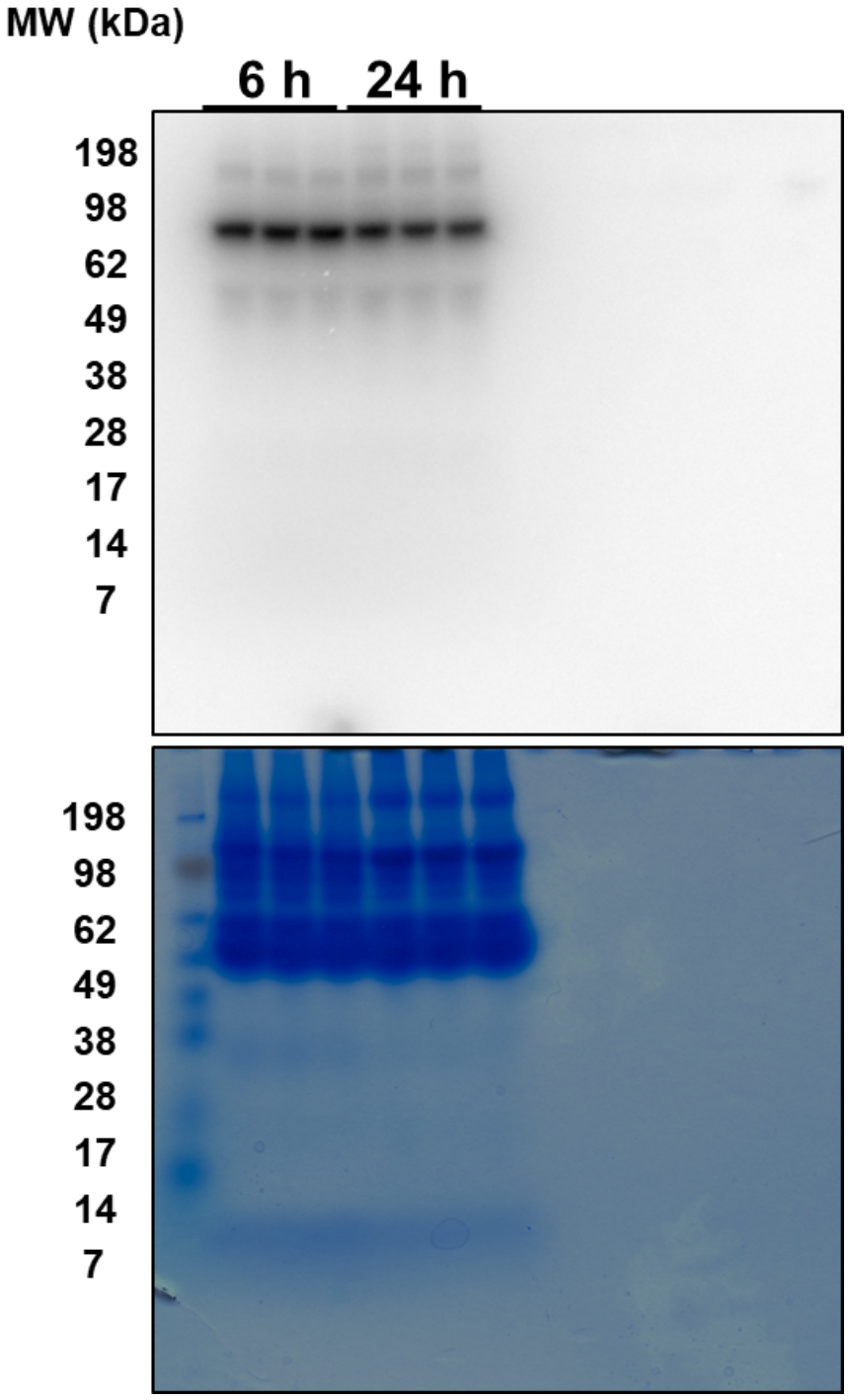

Figure A. 5 Serum stability of [^{111}In]In-DTPA-LF^{E687A}

Samples were incubated with mouse serum at 37ºC under agitation. At different time points samples were collected and analysed by SDS-PAGE gel followed by autoradiography.

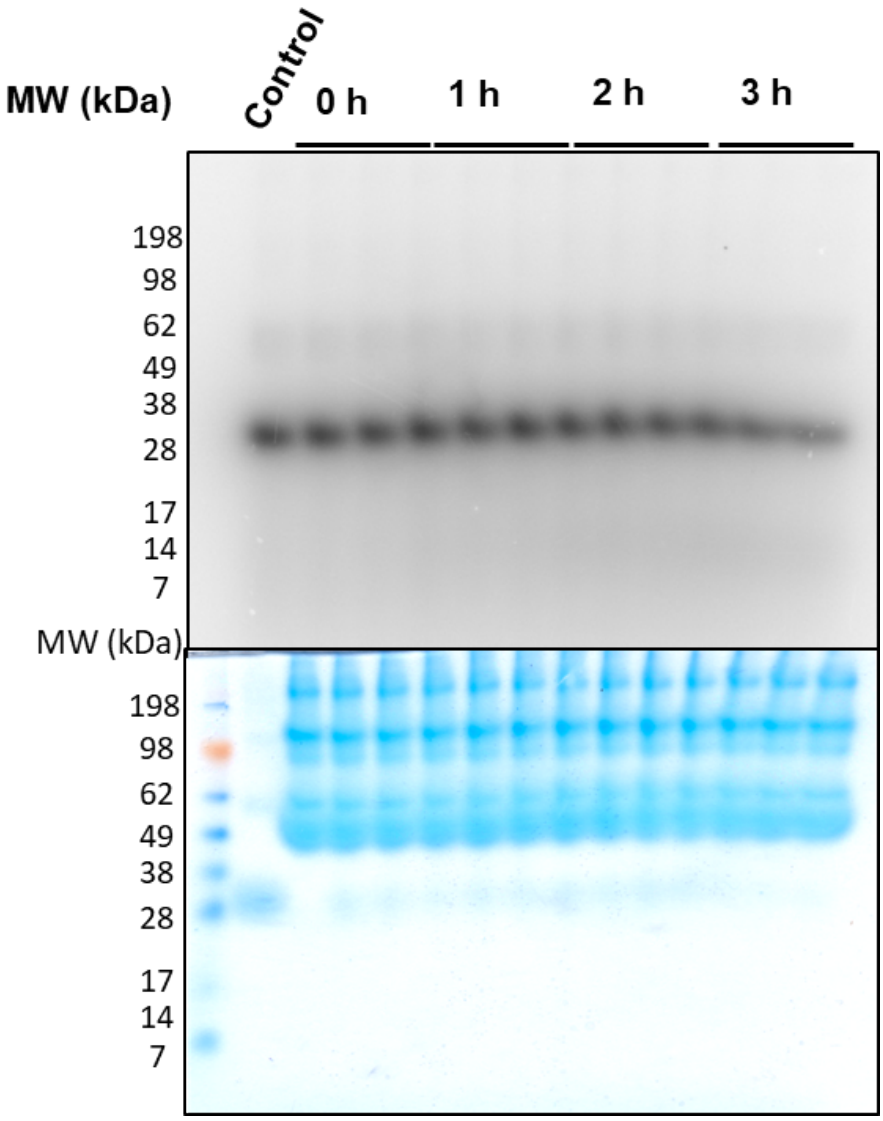

Figure A. 6 Serum stability of [^{111}In]In-DTPA-LFn

Samples were incubated with mouse serum at 37ºC under agitation. At different time points samples were collected and analysed by SDS-PAGE gel followed by autoradiograms.

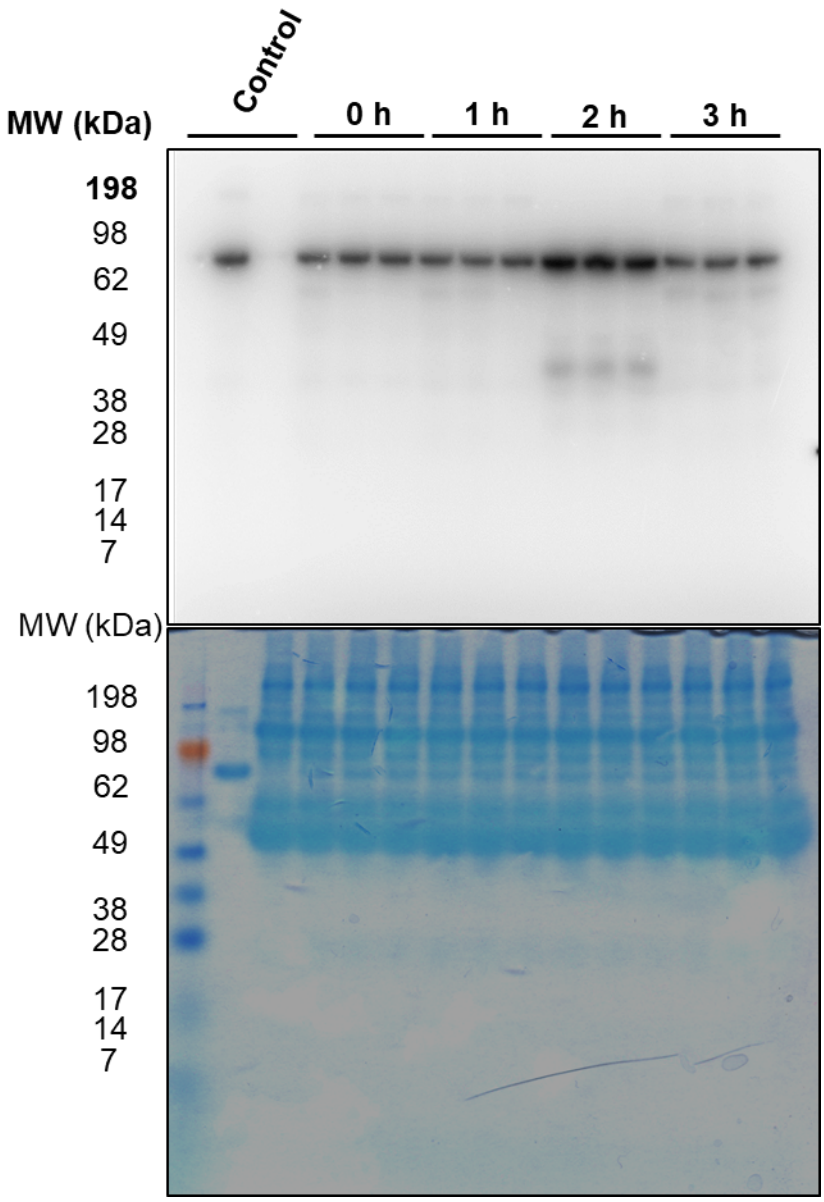

Figure A. 7 Serum stability of [^{111}In]In-DTPA-PAWT^{K563C}

Samples were incubated with mouse serum at 37ºC under agitation. At different time points samples were collected and analysed by SDS-PAGE gel followed by autoradiograms.

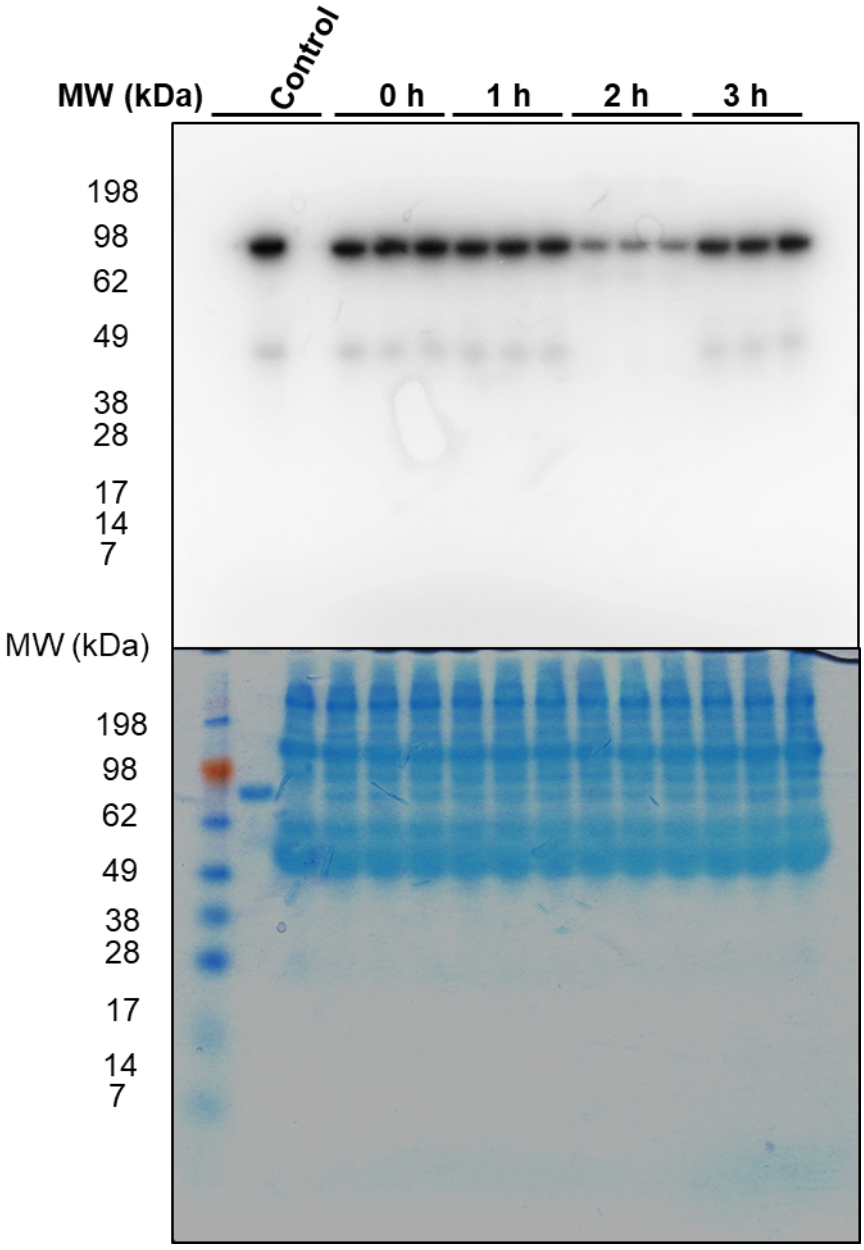

Figure A. 8 Serum stability of [^{111}In]In-DTPA-PAL1

Samples were incubated with mouse serum at 37ºC under agitation. At different time points samples were collected and analysed by SDS-PAGE gel followed by autoradiograms.

A.4 Tumour growth curves

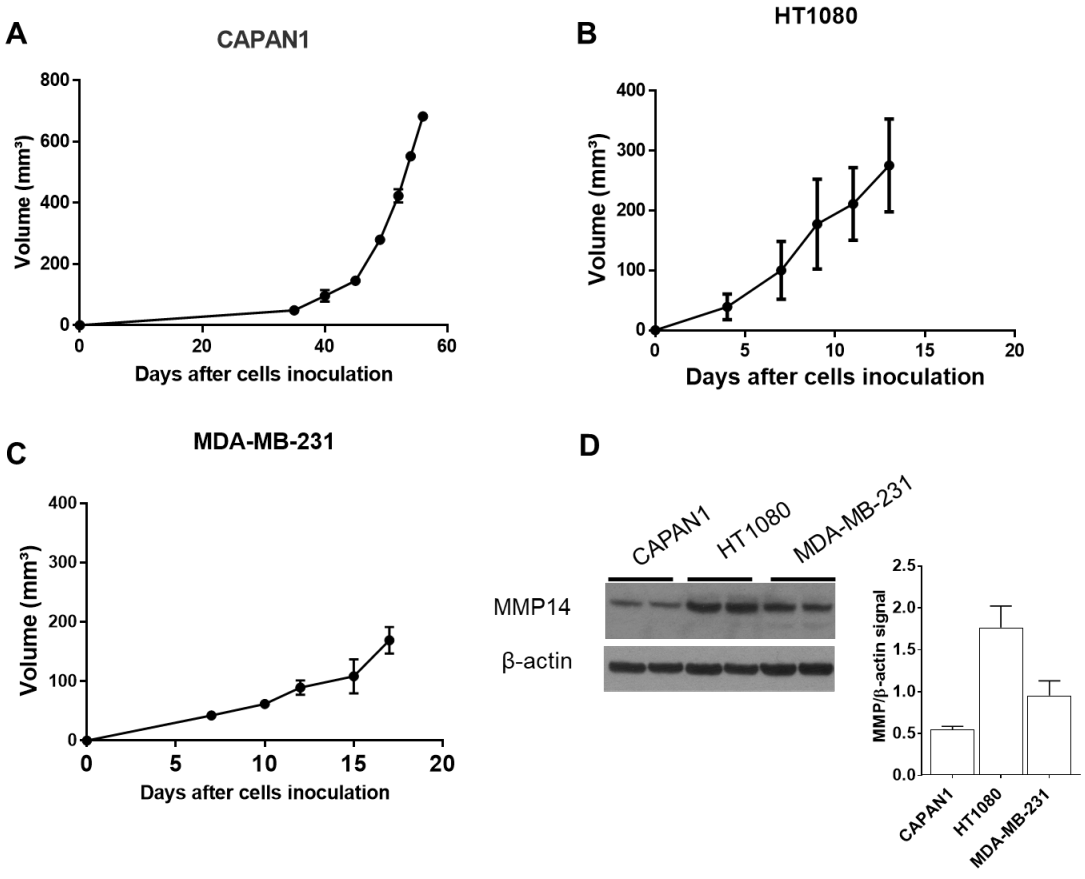

Figure A. 9 Tumour growth and MMP14 expression for different cell lines

Growth curves of different cell types inoculated in mice (A-C). D) MMP14 expression levels in tumour tissue were analysed by Western Blot (n=2) and optical density plotted against the loading control (β-actin).